Applicability of Catalytic *in situ* Olefin Polymerization in Wood Technology

Dissertation

with the aim of achieving a doctoral degree at the

Institute of Wood Science

Department of Biology

&

Institute of Technical and Macromolecular Chemistry

Department of Chemistry

Faculty of Mathematics, Informatics and Natural Sciences

Universität Hamburg

Submitted by

Julius Gurr

Hamburg

2020

1st Supervisor: **Prof. Dr. Andreas Krause**
Universität Hamburg
Fachbereich Biologie
Institut für Holzwissenschaften
Leuschnerstraße 91c
21031 Hamburg

2nd Supervisor: **Prof. Dr. Gerrit A. Luinstra**
Universität Hamburg
Fachbereich Chemie
Institut für Technische und Makromolekulare Chemie
Bundesstraße 45
20146 Hamburg

Submission: 21.12.2020
Disputation: 04.05.2021

Dedicated to my family

Acknowledgement

The study at hand is the result of a collaboration between the Institute of Wood Sciences and the Institute of Technical and Macromolecular Chemistry, both of the University of Hamburg.

First of all I would like to thank my doctoral advisor Prof. Dr. Andreas Krause for his encouragement to stay on as a doctoral student, the enormous freedom he gave me, as well as his kindness and trust. I have learned a great deal from him and it has been an invaluable experience to me. I would also like to thank my second thesis examiner Prof. Dr. Gerrit A. Luinstra for the opportunity to perform my studies at his facilities as well as for his support and scientific advice.

Prof. Dr. Bodo Saake and Prof. Dr. Elizabeth Magel not only agreed to be part of my defense commission, but accompanied me during my undergrad and postgrad studies as highly dedicated and valued teachers. I would like to express my gratitude for all their effort, not only towards me but all wood science students.

I would like to thank the "Östad-Gang" Dr. Oliver Mertens, Dr. Goran Schmidt und Dr. Martin Nopens for their friendship, moral support and great time. I would like to thank my TMC office fellows Sebastian Eller, Daniel Griebe and Dirk de Boer for their friendship, endless support and patience.

Special thanks go to my friends, colleagues and supporters Sylvia Diestel, Bettina Steffen, Dr. Julien Navarro and Yannick Wencke. I would also like to thank my student assistants Adriana Molina Benitez and Dominik Radsziwill for their help with the lab work.

I consider myself extremely lucky for having had the opportunity of working alongside a long list of admirable colleagues.

From the Institute of Wood Sciences and the Thuenen Institute for Wood Research I would like to thank Johannes Beruda, Dörte Bielenberg, Stephanie Warsow, Daniela Nissen, Regina Schröter, Sergej Kaschuro, Tanja Potsch and Gabrielle Circelli for their years of help and support. I would also like to thank all of them for their pleasant company and the enjoyable time we spent together. A special thanks goes to the library team, namely Astrid Stilke and Sandra Jacobi, who have wielded their magic in finding lost treasures of literature countless times.

From the Institute of Technical and Macromolecular Chemistry I would like to thank Dr. Robert Meyer, Dr. Felix Scheliger, Dr. Werner Pauer, Kathleen Pruntsch, Peter Harry, Stefan Bleck, Ansgar Weidner and Josef. Further members of the Chemistry Department that have my sincere gratitude are Claudia Wackendorff, Dr. Ulrich Riederer and Andreas Kornowski.

Special thanks go to Sophie Füchtner from the University of Copenhagen for her friendship and her support in Raman microscopy. I would also like to thank her whole team for the kind reception and atmosphere.

From the Zoology of the University of Hamburg I would like to thank Renate Walter, Sabine Gaude and Dr. Frank Friederich for their support in electron microscopy.

From the Heinrich-Pette-Institute Hamburg I would like to thank Dr. Rudolph Reimer for his support in cryo-ultra-microtome sectioning.

Furthermore, I would like to express my sincere gratitude to Prof. Dr. Jörg B. Ressel and Prof. Dr. Udo Mantau for the decades of dedication they have put into the education of Wood Science students. I have been fortunate to have had such excellent teachers and they have my deepest appreciation.

Many more people have been involved, have supported me or have been companions along the way. They all have my deepest gratitude.

Last but not least, I would like to thank my family and my wife for their continuous moral support, encouragement and love. Without them I would not be where or who I am today. I will be forever grateful.

Hamburg, December 2020

Abstract

This study investigates the introduction of metallocene olefin polymerization methods into the field of wood science. For the first time, catalytic ethylene polymerization was applied to bulk wood, in order to perform lumen filling as measure of physical preservation. This represents, in addition, the first demonstration of successful catalytic olefin polymerization within macro-porous solids. In addition, this study represents the most comprehensive discussion to date on catalytic olefin polymerization in combination with wood or cellulose. The utilized, highly specialized catalytic system consisted of a metallocene catalyst and aluminum alkyl cocatalyst.

Using wood bound water in combination with trimethylaluminum as a more economical substitute for prefabricated methylaluminoxane in metallocene catalysis in the production of wood polyethylene composites has been proven highly successful and recommendable. Precise moisture management has been shown to be paramount for the successful and repeatable *in situ* synthesis of an active aluminoxane species. Vacuum drying experiments and subsequent coulometric Karl Fischer Titration showed that the moisture management of pine wood flour, beech wood flour and microcrystalline cellulose is feasible. By varying the drying time, temperature and pressure, the moisture content may be fine-tuned. Gas titration experiments revealed that the degree of hydrolysis of trimethylaluminum with wood bound water can be fine-tuned by moisture management. The formation of a catalytically active aluminoxane species by partial hydrolysis of trimethylaluminum with wood bound water was proven by successful polymerization experiments. Catalytic activities were comparable to those of prefabricated methylaluminoxane. Moisture management was shown to influence catalytic activities. The utilization of wood flour containing residual moisture was shown to lead to enhanced filler encapsulation. Material characterization showed that molecular weights of the resultant polymers increased, offering the opportunity to produce higher molecular weight polyethylene at lower temperatures. Results also suggest that the single-site character of the catalyst is preserved and that the molecular structure of the resultant polymer remains relatively similar.

Proof of concept of the macro-confined metallocene catalyzed polymerization of ethylene has been demonstrated successfully. The impregnation of solid wood samples with a catalyst was investigated by energy dispersive X-ray spectroscopy. Soaking samples in pure liquid trimethylaluminum as well as alternating pressure impregnation led to the most homogeneous distribution. A variety of microscopic techniques were employed to investigate successful polymerization within the macro-confinement of the wood cell lumen. Clusters of cells with lumen entirely filled were observed repeatedly. The polyethylene nature of the materials filling the lumen were proven with energy dispersive X-ray spectroscopy and Raman-microscopy.

Promising areas of future research regarding basic research questions, potential alternative processes as well as novel material concepts and applications are outlined.

Kurzfassung

Diese Studie untersucht die Anwendbarkeit von Metallocen-Olefin-Polymerisationsverfahren im Bereich der Holzforschung. Erstmals wurde die katalytische Ethylenpolymerisation auf Vollholz angewandt, um eine neuartige Lumenfüllung als Maßnahme des physikalischen Holzschutzes durchzuführen. Diese Studie stellt somit den ersten Nachweis erfolgreicher katalytischer Olefinpolymerisation innerhalb makro-poröser Feststoffe dar. Darüber hinaus beinhaltet diese Studie die bisher umfassendste Diskussion über die Heterogenisierung von Polymerisationskatalysatoren auf Cellulosesubstraten zur anschließenden Mischpolymerisation von Olefin-basierten Verbundmaterialien. Das eingesetzte, hochspezialisierte Katalysatorsystem bestand aus einem Metallocen-Katalysator und einem Aluminiumalkyl-Cokatalysator.

Die Verwendung von holzgebundenem Wasser in Kombination mit Trimethylaluminium als kostengünstiger Ersatz für vorgefertigtes Methylaluminoxan in der Metallocenkatalyse bei der Herstellung von Holz-Polyethylen-Verbundwerkstoffen hat sich als sehr erfolgreich und empfehlenswert erwiesen. Es hat sich herausgestellt, dass ein präzises Management der Holzfeuchte für die erfolgreiche und wiederholbare *in situ* Synthese einer katalytisch aktiven Aluminoxan-Spezies von entscheidender Bedeutung ist. Vakuumtrocknungsversuche mit anschließender coulometrischer Karl-Fischer-Titration zeigten, dass die präzise Regulierung der Materialfeuchten von Kiefernholzmehl, Buchenholzmehl und mikrokristalliner Cellulose möglich ist. Die Variation von Trocknungszeit, Temperatur und Druck ermöglichen die Kontrolle über Feuchtigkeitsgehalte in den katalytisch relevanten Bereichen. Gastitrationsexperimente zeigten, dass der Grad der Hydrolyse von Trimethylaluminium durch Reaktion mit holzgebundenem Wasser ebenfalls durch Holzfeuchtemanagement kontrolliert werden kann. Die Bildung einer katalytisch aktiven Aluminoxan-Spezies durch partielle Hydrolyse von Trimethylaluminium mit holzgebundenem Wasser wurde durch erfolgreiche Polymerisationsversuche nachgewiesen. Die katalytischen Aktivitäten waren vergleichbar mit denen von vorgefertigtem Methylaluminoxan. Es konnte gezeigt werden, dass das Holzfeuchtemanagement die katalytischen Aktivitäten beeinflusst. Im Vergleich zu darrgetrocknetem Holzmehl, führte die Verwendung von Holzmehl mit Restfeuchte zu einer verbesserten Einkapselung des Füllstoffs. Die Materialcharakterisierung zeigte, dass die Molekulargewichte der resultierenden Polymere zunahmen. Letzteres bietet die Möglichkeit, Polyethylen mit höherem Molekulargewicht bei niedrigeren Temperaturen herzustellen. Die Ergebnisse deuten auch darauf hin, dass der selektive Charakter des aktiven Zentrums des Katalysators und die Molekularstruktur der resultierenden Polymere weitestgehend erhalten bleiben.

Die Machbarkeit der Metallocen-katalysierten Polymerisation von Ethylen in den makroskopischen Zelllumen von Holz wurde erfolgreich demonstriert. Die Imprägnierung von Massivholzproben mit den Katalysatorkomponenten wurde mit energiedispersiver Röntgenspektroskopie untersucht. Das Tränken der Proben in reinem flüssigem Trimethylaluminium als auch die Druck-Vakuumimprägnierung mit Katalysatorlösungen führten zu den homogensten Verteilungen der untersuchten Katalysatoren. Das Maß der Wechsel-

wirkungen zwischen Holzsubstrat und Katalysatorkomponente scheint die Güte der Imprägnierung zu beeinflussen. Eine Vielzahl mikroskopischer Verfahren wurde eingesetzt, um die erfolgreiche Polymerisation in den makroskopischen Hohlräumen des Holzes zu untersuchen. Es wurden wiederholt Cluster von Zellen mit vollständig gefüllten Lumen beobachtet. Der Nachweis, dass es sich bei dem Lumen-füllenden Material um Polyethylen handelt, wurde mit energiedispersiver Röntgenspektroskopie und Raman-Mikroskopie erbracht.

Vielversprechende Fragestellungen zukünftiger Grundlagenforschung, mögliche alternative Prozesse sowie neuartige Materialkonzepte und Anwendungen werden skizziert.

List of Contents

List of Figures

List of Tables

1 Introduction

The roots of macromolecular chemistry and wood science are very much intertwined. Celluloid, which is based on cellulose and was patented by the British Alexander Parkes in 1855 (Worden 1911), is considered to be the first manmade polymer (Thielen 2018). The chemist Herman Staudinger (1881 - 1965) introduced the term "macromolecule" in 1922 (Staudinger and Fritschi 1922) and is seen to be among the most influential founders in the field of polymer chemistry. For his discoveries in the field of macromolecular chemistry he was awarded the Nobel Prize for chemistry in 1953. The chemists Kurt H. Meyer (1883 - 1952) and Hermann F. Mark (1895 - 1992) performed X-ray crystallography and ultra-microscopy on polymeric materials. The latter three, among others, made important contributions to the structural clarification of natural and manmade polymers such as cellulose, chitin, starch, natural rubber and polystyrene (Faix 2004).

The economic success stories of wood- and polymer-derived materials have common origins as regards their abundance, utility and high economic value.

Cellulose, lignin and chitin are often cited as the most abundant biopolymers with the highest annual growth rates on earth. However, the variation of abundance and annual growth rates provided in the literature is very high. The annual growth rates of cellulose and lignin are given in broad ranges of 100 – 1,000 billion tonnes and 200 – 3,600 billion tonnes respectively (Krässig 1993; Argyropoulos and Menachem 1998; Gilbert and Kadla 1998; Koch 2006; Gellerstedt and Henriksson 2008, Sonnewald 2014). The above ground biomass in forests worldwide in 2015 was specified at 419.1 billion tonnes (FAO 2016), representing a large source of cellulose and lignin in the form of wood that is easily accessible for harvest.

Bulk chemicals for the synthesis of polymers such as ethylene and propylene are predominantly derived from fossil hydrocarbon resources such as oil, natural gas or black coal (Geyer et al. 2017). The total proven world reserves of oil, natural gas and coal are figured at 244.1 billion tonnes, 169.3 billion tonnes (oil equivalent) and 1,054.8 billion tonnes (oil equivalent) respectively (BP p.l.c. 2019). About 130 and 85 million tonnes of ethylene and propylene respectively were produced worldwide in 2013, with major shares going into the production of polyethylene and polypropylene (Ceresana ek 2014a, 2014b). The world’s total polymer production amounted to 359 million tonnes in 2018 (PlasticsEurope AISBL 2019).

It is evident that with their abundance, no other natural material is as likely to substitute finite fossil resources as cellulose and lignin. Furthermore, large quantities of above ground lignocellulosic biomass are highly accessible. Wood in particular, providing a large supply of raw material with relative seasonal independence, is destined to be the backbone of a future bio-based economy.

Wood and plastics have many beneficial properties, but one property in particular is drawing a lot of attention: biodegradability. Wood, as a natural material, is biodegradable, whereas none of the high volume commodity plastics are. Only around 1 % of the plastics produced annually are labelled as biodegradable. More than half of the primary plastics produced between 1950 and 2015 of 8,300 million tonnes were discarded after use

(Geyer et al. 2017). Its accumulation in terrestrial environments, in the open oceans, on remote shorelines and in the deep sea is causing one of the most ubiquitous and long-lasting recent anthropogenous changes to the surface of this planet. Plastic debris is posing a considerable threat by harming wildlife, distributing non-native organisms around the globe, absorbing and distributing toxic chemicals in the marine environment as well as degrading into ingestible micro-plastics (Barnes et al. 2009). It seems obvious that biodegradability is a desirable feature. In some applications where recycling is an unlikely option, such as single-use tableware or plastic mulch in agricultural landscaping, biodegradability delivers additional value. Contradictorily though, in the majority of applications the persistence of plastics is one of their major features and strengths, oftentimes making them unsubstitutable (Thielen 2018). Hence, the persistence of plastics is origin of both, its market success and the environmental challenges caused by it.

Next to their accumulation in the environment, plastics also pose health risks that are challenging to assess. Whereas many polymers in their pure form are considered non-toxic (Vasile and Pascu 2005), plastic products generally comprise a diverse mix of polymers and fillers, containing a complex supplement of additives, many of which are unknown compounds. A majority of the consumer plastic products investigated have been found to exhibit high *in vitro* baseline toxicity (Zimmermann et al. 2019). Plastic products marketed as bio-based or biodegradable containing complex compositions of chemicals have been shown to be just as toxic. Their raw materials were found to exhibit a lower baseline toxicity (Zimmermann et al. 2020). Achieving the desired product properties without excessive utilization of additives would potentially reduce associated health and environmental risks.

Wood on the other hand, owes part of its good reputation to the fact that it is a natural material, biodegradable and non-toxic. However, the penetration of certain markets by wood products is often hindered by its susceptibility to biological decay, changes in its aesthetic appearance when exposed to weathering and its dimensional changes due to its hygroscopic nature (Hill 2006). The biodegradability of wood is origin of its environmental agreeableness but also restricts its potential to successfully substitute plastics in some market areas.

The desire to make wood more resistant to biodegradation by microorganisms and insects is centuries old. To achieve this, two approaches in particular have been of interest in decades past, the incorporation of lignocellulosic biomass into plastics (Klyosov 2007; Oksman Niska and Sain 2008) and the modification of solid wood (Hill 2006).

In summary, fossil resources as well as lignocellulosic biomass are – as of now – abundant. Wood and other bio-resources offer environmentally friendly options, but are limited in their potential to substitute plastics due to their property profile. Plastics threaten the environment but offer unique and almost unsubstitutable features. Bio-plastics offer a compelling bridge between these two material classes, but come with their own issues, such as toxicity, limited biodegradability and high cost.

2 Objectives of this Study

This thesis represents a crossover between macromolecular chemistry and wood science and aims to transfer knowledge and technology between these two fields. To marry the beneficiary properties of man-made polymers and wood, new approaches of combining solid wood and polyethylene are investigated.

Filling solid wood with neat hydrophobic polymers would yield a product that is potentially water repellent, features enhanced mechanical properties and poses less health and environmental risks than their neat polymer counterparts. Their water repellency would likely make them usable in applications with short-term moisture exposure, accompanied by an improved resistant to biodegradation. Favorably such materials would gain much of their basic strength properties from their parent wood, whose structure remains unimpaired. In addition, the filling of the porous wood structure with polymers would potentially yield improvements, e.g. in hardness, abrasiveness and impact resistance. The beneficial combination of these two material classes would potentially eliminate the need for the excessive use of additives and thereby mitigate health and environmental hazards. The combination of wood filled with a suitable neat thermoplastic would also offer a realistic and sound “cascade” utilization scenario, i.e. serving as basic material for the production of Wood Plastic Composites, enabling a sequential circular economic pathway.

This study aims to deliver proof of concept of the polymerization of polyethylene within the macro-confinement of the porous wood structure and to provide the basis for future research and development, by identifying and outlining important process parameters and influencing factors. In order to do so, the topics of wood moisture management, catalyst-wood interaction, polymerization in the immediate proximity to wood flour as well as the polymerization within the porous wood structure are investigated.

The anticipated reader will likely come from either macromolecular chemistry or wood science. The fundamental knowledge section describes relevant topics in detail to provide the foundation for the research chapters. The research chapters will revert to the content of these fundamental knowledge chapters.

3 Fundamental Knowledge

3.1 Wood

Wood is one of the oldest materials utilized by mankind. For thousands of years it has been used in tools, as a building material, fuel and much more. (Schulz 1993). Today it remains a very important raw material for many industries serving in a large variety of applications (Mantau et al. 2018).

Wood is a complex biomaterial, having a variety of properties. It may be defined as a porous three dimensional, hygroscopic, viscoelastic, anisotropic biopolymer composite made up of an interconnected matrix of cellulose, hemicellulose and lignin with minor amounts of inorganic elements and organic extractives (Rowell 2016). Figure 1 displays a holistic schematic illustration based on Hoffmann (2003) of the hierarchical structure of wood. In order to understand wood as a raw material, it is necessary to familiarize oneself with its microscopic structure as well as its molecular structure.

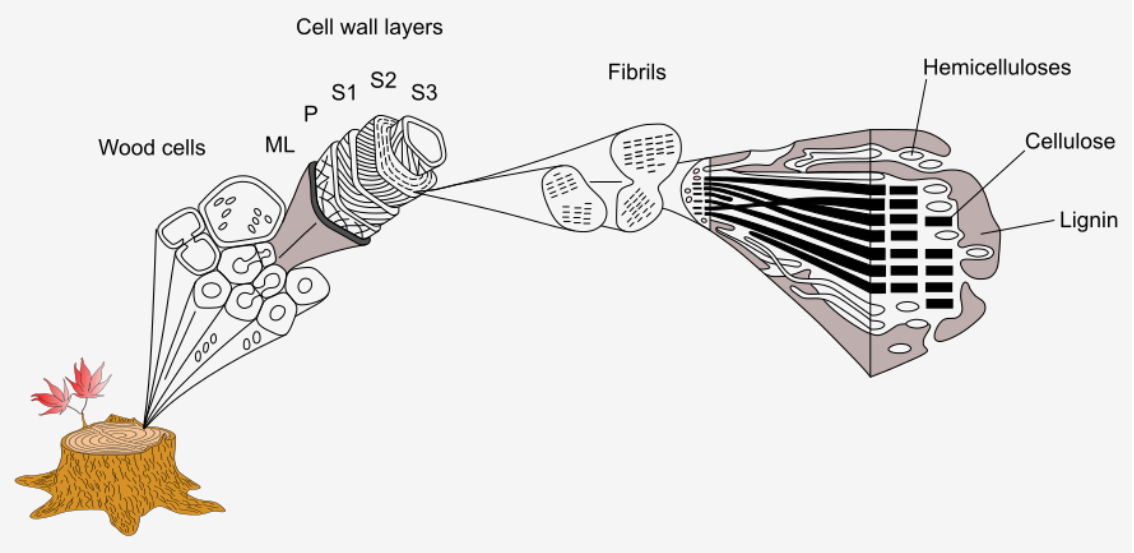

Figure 1: Exploded-view illustration of the hierarchical structure of wood
(ML) Middle lamella; (P) Primary wall; (S1-S3) Secondary walls

The defining differentiation of wooden materials from other cellulosic plant materials is the lignification of the cell wall, i.e. the incorporation of the macromolecule lignin into the cell wall matrix. This is why the hypernym **lignocellulosic** materials is often used. This wider definition includes dicotyledons, such as trees, as well as monocotyledons, such as bamboos or palms. Differently from trees, monocotyledons do not show secondary lateral growth but rather attain their final radius during primary growth. It is important to acknowledge that the cellular assembly of their structural tissue is vastly different.

The term **wood** more specifically refers to the structural tissue of tree trunks, roots and branches, which thicken over time. This secondary lateral growth of gymnosperms and dicotyledons originates from their vascular cambium, continues throughout the entire life

of the tree and strongly influences its microscopic structure. In geographical zones with a seasonal climate, this ongoing growth manifests itself in so called annual rings, which are visible to the naked eye and are made up of early wood and late wood. At the beginning of each season, a tree forms early wood, lateral rows of cells with thin walls and large pores that mainly serve the transport of fluids. Towards the end of each season, a tree forms latewood, lateral rows of cells with thick walls and smaller pores that serve as mechanical reinforcement. As mainly pine sapwood was used in this work, the following explanations will focus on wood from conifers and will emphasize on properties that are deemed important in the context of this work.

The **macro- and microscopic structure of wood** may be thought of as a natural fiber reinforced composite, which is constituted of plant cells, i.e. individual physiological units. During growth and until the cells have fully differentiated themselves into their designated form of function, they are alive. However, a major portion of cells in trees die once differentiated, a process called apoptosis, thus ending up hollow. These dead cells may be roughly differentiated into a scaffold of solid cell wall tissue and an empty pore encased by the former. The cell wall faces and edges are interconnected to the cell walls of adjacent cells. The mostly macroscopic cell pores are referred to as lumen. Within the realm of cellular solids, wood would be defined as three-dimensional foam with semi-closed cells (Gibson and Ashby 1999). The bulk density of wood ranges from about 0.2 g/cm^3 for balsa to about 1.3 g/cm^3 for ironwood. The true density of the wooden cell wall is found to be relatively uniform throughout all tree species at around 1.5 g/cm^3 (Kollmann 1951).

Cell types, distribution and orientation constitute the anisotropic nature of wood. The largest part of fibers are oriented longitudinal to the stems axis, exploiting anisotropy to increase mechanical efficiency (Gibson et al. 2010). The wood of conifers is comprised 90 – 95 % of tracheid cells (Figure 2). The remaining part is made up of parenchyma and epithelial cells, which are short and brick-like. Tracheids are elongated tapered fibers, which contribute to the tree's fluid transport system as well as provide for structural strength of the tree. Their length in European conifers is commonly around 3 to 4 mm and their diameter revolves around 40 to 50 µm, corresponding to a length to width ratio of 60 to 100 (Kollmann 1951; Sixta 2006). Measurements conducted on scanning electron microscopy (SEM) micrographs of the pine sapwood used in this study revealed slightly smaller diameters. The cell diameter range of early wood and late wood was 20.3 … 33.4 … 46.0 µm and 7.0 ... 17.8 … 32.6 µm respectively. These measurements are in good agreement with specific literature values for pine wood tracheid dimensions (Ilvessalo-Pfäffli 1995; Wagenführ 2006).

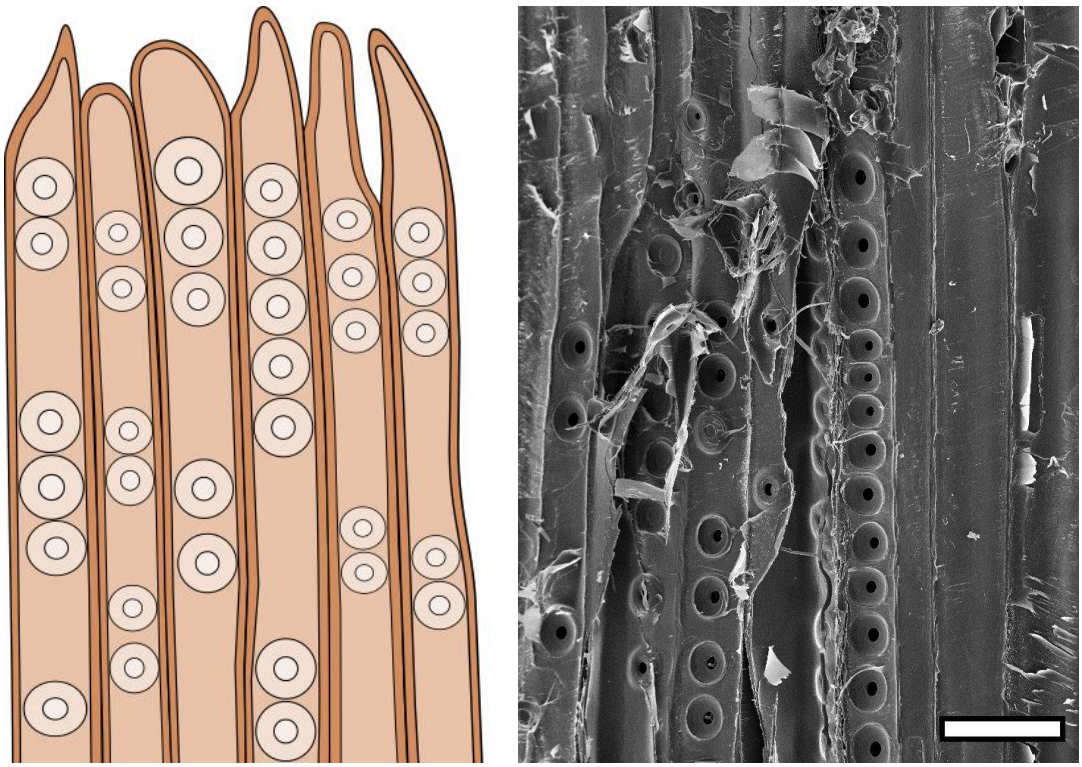

Figure 2: Comparative depictions of softwood tracheid cells.
Left: Schematic illustration based on Grosser 1977; Right: Scanning electron micrograph of pine sapwood used in this study; Scale bar 50 µm.

Individual cell lumen are interconnected by pits – openings in cell walls, through which adjacent cells can communicate or exchange fluids. Early wood tracheids of Pinus sylvestris exhibit large single-row bordered pit pairs with a pit membrane on their radial faces (Figure 2) and large cross-field window pits (not displayed) between adjacent parenchyma and tracheid cells (Grosser 1977). The configuration of the pits of a wood species is important to consider, as it defines the freedom of movement of fluids within. This in turn defines the suitability of a wood species for technical processes, whose efficiency depend on its accessibility for treatment agents; among others impregnation with preservatives, pulping and wood modification (Lebow 2010). The general makeup of a bordered pit pair is displayed in Figure 3. The pit membrane regulates the pits functions and consists of a torus surrounded by an annular margo. The flexible margo is composed of microfibrilar strands with openings between them, which permit fluid flow. The torus is mostly solid and serves as a plug, able to close off either side of the pit. The flow of liquids between two cells is inhibited, if a torus of a pit pair is in the aspirated position, i.e. closing off one of the pori. Microscopic measurements and indirect determinations from gas flow as well as capillary pressure measurements, indicate that softwood pit openings have effective diameters between 0.02 and 8.00 µm. It is indicated that these values are a presentation of pit aperture size rather than the openings in the margo (Siau 1995). Measurements conducted on SEM micrographs of the pine sapwood used here, revealed a range of pit apertures of 3.0 … 4.5 … 6.3 µm and a range of margo opening diameters of 0.1 … 0.8 … 1.9 µm.

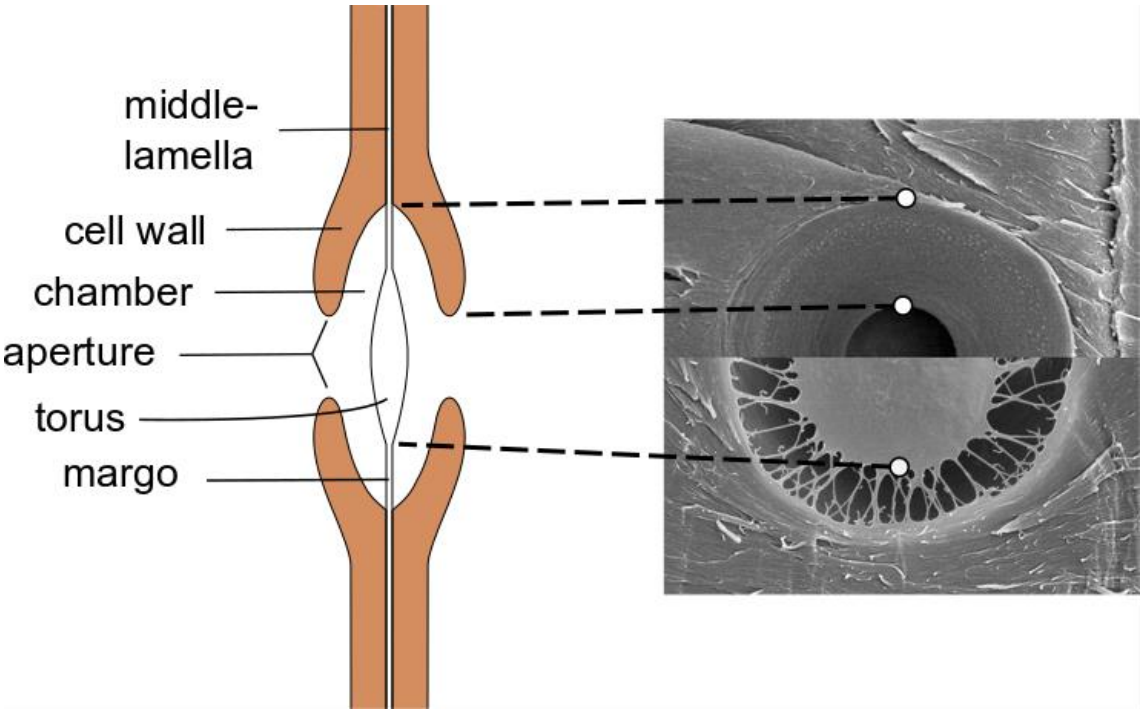

Figure 3: Comparative depictions of softwood bordered pit pairs.
Left: Schematic cross section of a softwood bordered pit pair; Right: Composite micrograph showing the internal makeup of a bordered pit of the pine sapwood used in this study

The **molecular structure** of wooden cell walls can be described as a complex three-dimensional fiber-reinforced biopolymer composite which consists of an interconnected network of three main structural components, lignin, cellulose and hemicelluloses. The common perception is that, lignin is the matrix polymer, cellulose is the fiber reinforcement and the hemicelluloses serve as coupling agents between them. The cell wall in its native state can be considered an integer compound (Gruber 2006), absent of mesopores (Nopens et al. 2020). However, compatible fluids may penetrate the cell wall, where they are held in solid solution (Stamm 1967a). The cell wall commonly differentiated into different layers, the middle lamella (ML), the primary wall (P) and the three secondary walls (S1 - S3), as depicted in Figure 1, that differ in their molecular structure and their chemical composition (Fengel and Wegener 1989; Gandini and Naceur Belgacem 2008).

The **chemical composition** of the structural components of wood comprises of cellulose, hemicelluloses and lignin. Figure 4 depicts their exemplary macromolecular structures. Softwood contains around 40 % cellulose, 30 % hemicelluloses and 30 % lignin. Cellulose is a linear semi-crystalline homopolymer consisting of repeating units of β-1,4-D-glucose. Wood derived cellulose can have a degree of crystallinity of up to 65 %. Hemicelluloses have a chemical structure that consists of branched and amorphous heteropolysaccharides. These two categories of polysaccharides, often summarized by the term holocelluloses, are rich in hydroxyl groups. The strong intermolecular forces between cellulose molecules, i.e. hydrogen bonds, lead to relatively high glass transition temperatures of 230 °C for dry cellulose and an estimated melting point of 450 °C (Nordin

et al. 1974), the latter being higher than its degradation temperature. Nevertheless, melting cellulose using an infrared laser has already been claimed by Schroeter and Felix (2005). Lignin is an amorphous cross-linked aromatic polymer, mainly consisting of a complex three-dimensional network of phenyl propane units (Rowell et al. 2005; Sixta 2006; Menges et al. 2011). However, according to contemporary research, lignin is more linear than was originally assumed (Ralph et al. 2019). The softening temperature of lignin is influenced by a variety of factors, such as the presence of low molecular contaminants – including water and solvents – molecular weight, thermal history, cross-linking and pressure. Therefore, a specific T_g value for any particular lignin cannot be accurately recorded (Hatakeyama 1992). Date compiled from a literature review revealed that lignin in water-saturated wood softens at temperatures around 60 °C, whereas lignin in dry wood softens at temperatures around 100 °C. Hemicelluloses from a dry to water-saturated state soften at temperatures around 120 to 20 °C respectively (Engelund et al. 2013).

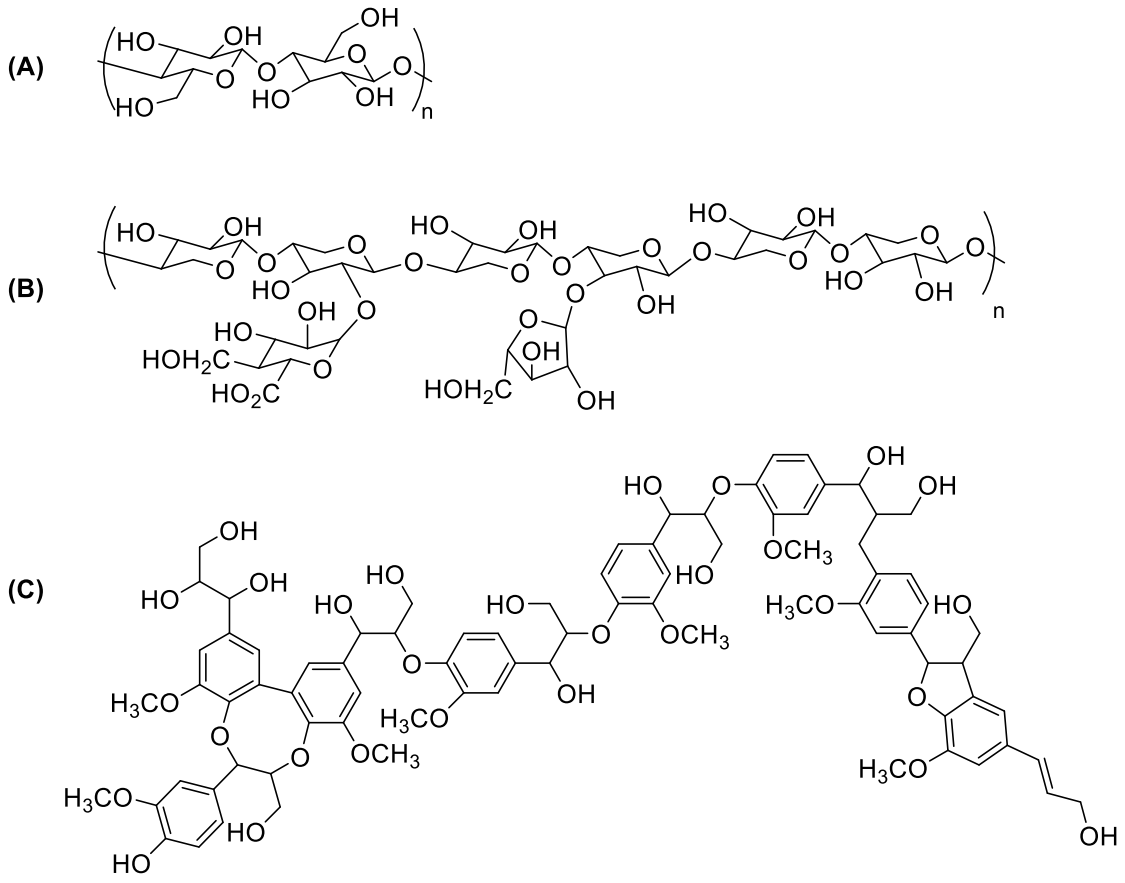

Figure 4: Exemplary macromolecular structures of cellulose, hemicellulose and lignin. (A) Cellulose unit; (B) Hemicellulose unit; (C) Lignin fraction.

The chemical composition of the cell wall constituents, particularly of the polysaccharides, is the cause of the hygroscopic nature of wood, which in turn directly influences properties such as dimensional stability, i.e. swelling and shrinking as well as resistance to biological attack (Kollmann 1951). Cellulose and hemicelluloses are rich in hydroxyl

groups, have a high propensity to form hydrogen bonds and a great affinity towards water. Lignin, on the other hand, contains less hydroxyls. These polysaccharides and lignin are often considered to be hydrophilic and hydrophobic respectively (Rowell 1984; Ross 2010). Therefore, wood as a whole, has to be considered to be amphiphilic. This is emphasized by the amphiphilic attributes of the lignin-carbohydrate complex (Koshijima et al. 1989; Uraki et al. 2006). Furthermore, cellulose itself shows amphiphilic behavior, which is explained by steric effects and has attracted attention in recent literature (Lindman et al. 2010; Jiang and Hsieh 2014).

In wood, moisture exists either as free water or bound water. Free water may occur in the form of liquid or vapor in both lumen and cavities. Bound water is held by intermolecular attraction on the surface and within the bulk of the cell wall. The gravimetric **moisture content** (MC) of wood is defined as the mass of water held by a sample divided by its dry mass. The maximum water binding capacity of lignified cell walls is regularly stated to approximate to a MC of 30 %. This point of so called *fiber saturation* (MC_{FS}) may be defined by the complete saturation of the cell wall by water and no occurrence of free water in the pore volume (Tiemann 1906). Although today this definition of MC_{FS} is thought to be an unsatisfactory oversimplification (Engelund et al. 2013), for the purposes of this study it is believed to suffice. The sorption and desorption of water vapor ranges from complete dryness up to the MC_{FS} (Kollmann 1951; Ross 2010) and causes a simultaneous change of wood mass and dimension, also referred to as swelling and shrinking (Nopens et al. 2019). Comprehensive books have been written on this topic (Siau 1984; Skaar 1988; Siau 1995). The hygroscopic behavior is object of interest and discussed in more detail in Chapter 4.

3.2 Wood Preservation

The decay of wood in its natural environment, which may be caused by UV radiation, insects, fungi or other microorganisms, is all but inevitable. The so called natural durability of wood, which may vary from species to species, is simply an indication of the rate of decay. However, decay in wood in service may be – in practical terms – prolonged to near infinity by adapted preservation processes (Richardson 2001).

To meet the ever growing demand for wood, the worldwide area of planted forests for wood production has increased considerably in the past decades. However, fast grown wood from plantations is often of inferior quality, exhibiting reduced durability and lower mechanical properties, than slow grown wood (Hill 2006). As demand rises and wood with adequate natural durability grows ever more scarce, it becomes necessary to adopt preservative processes (Richardson 2001).

In recent history, tropical hardwoods, which are less susceptive to biological attack, were popular in exterior applications until deforestation became a widespread public concern and supply diminished. To substitute for tropical hardwoods, manufacturers had to turn to less durable softwoods. In order to increase their longevity in exposed applications, biocidal preservatives, such as chromated copper arsenate (CCA), had become common to prevent biological attack. However, in spite of CCA being an extremely effective

preservative, health and environmental issues regarding the release of arsenic and chromium into the biosphere during disposal of CCA treated wood, lead to a widespread ban of these toxic metal-based preservatives. Further legislative restrictions have since been placed on safe disposal of treated timber, consequently increasing their overall cost. Because of these restrictions, the preservative measures today are selected not simply on the basis of efficacy and initial cost, but also environmental impact during service and under the consideration of an end-of-life scenario (Hill 2006). The challenges the industry faces are to design products for better durability and recyclability, as well as to improve waste management processes and market uptake of recycled post-consumer wood (Heräjärvi et al. 2020). It is here where the need for further wood preservation research originates from today.

Preservation treatments are thought to have existed almost as long as the utilization of wood itself (Richardson 2001). Systematic research dates back to the first half of the 20th century, where Alfred J. Stamm and colleagues pioneered the field (Kollmann 1972). Most efforts are aimed at improving the dimensional stability, the resistance to biological degradation, the reduction of the effect of weathering on the appearance of wood (Hill 2006) and to reduce its inflammability (Merk et al. 2015).

Wood preservation methods may be roughly classified into constructive precautionary measures, as well as physical and chemical treatments and modifications. The aim of constructive wood protection is to limit the exposure of the wood to degrading factors by effective building design (Rijckaert et al. 2001). Physical preservation of wood comprises among others the impregnation with hydrophobic agents (Scholz et al. 2010c) and protective coating systems (Rijckaert et al. 2001), all without altering the molecular consistency of the cell wall. In chemical wood modification the cell wall polymers are chemically modified to change their properties and improve the woods performance (Rowell 2005).

In this work, the catalytic ethylene polymerization does potentially lead to the filling of the cell lumen with hydrophobic polyethylene. Furthermore, the chemical agents utilized potentially undergo chemical reaction with the cell wall. Hence, impregnation of wood with hydrophobic agents and the chemical modification of wood will be described in more detail in the following.

Methods of **physical** and **chemical wood preservation** may be classified into three main categories, lumen filling, modification of the inner cell surface and modification of the cell wall at molecular level (Norimoto and Gril 1993). Figure 5 displays cross sections of single model cells. (A) represents an untreated cell. The dashed outline indicates that it is not swollen to its maximum. In lumen filling (B) the cell wall remains untreated, whilst the lumen is filled partially or entirely by a resin, wax, oil or another desirable reagent. In inner surface coating (C) the bulk of the cell wall remains untreated, whilst a resin or another reagent is deposited on the internal face of the cell wall. This may include or exclude chemical reaction. In cell wall filling (D) the cell wall substrate is impregnated by a resin or another reagent, which may or may not include chemical reaction. The impregnation of the cell wall generally leads to bulking. Combinations of these three categories are possible.

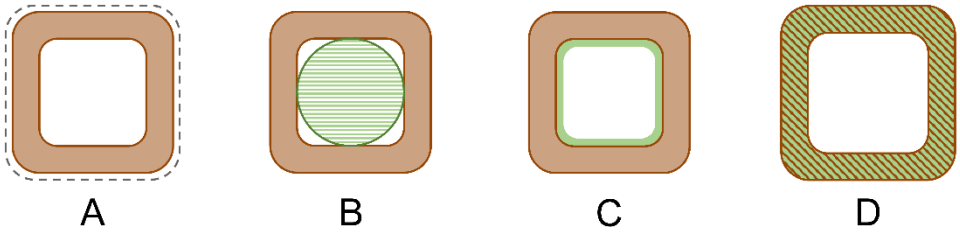

Figure 5: Models of wood modification at cellular level.
Brown rounded rectangles represent the wood substrate; Green color represents reagent
(A) Untreated cell; (B) Lumen filling; (C) Inner surface coating; (D) Cell wall filling

The filling of lumen with hydrophobic agents, as a measure of **physical preservation,** reduces capillary water uptake and may also improve water repellency, if hydrophobic agents are used (Sell 1977; Scholz et al. 2012). Furthermore, lumen filling has been reported to improve the strength properties of solid wood, most notably hardness and compressive strength, and can be used to consolidate degraded wood (Unger et al. 2001; Scholz et al. 2010b, 2012).

Chemical modification processes aim to alter the amount or accessibility of wood hydroxyl groups through selective chemical reaction at the molecular cell wall level, i.e. they aim to alter the wood-water relationship, in order to increase the dimensional stability and durability of wood (Sandberg et al. 2017).

Modifications at the cell wall level can be differentiated as follows: Figure 6 displays a model of the free volume between two cell wall fragments. In its native state (a), the cell wall molecules with their hydroxyl groups are in close proximity, able to form hydrogen bonds or to attract water. In bulking (b), the cell walls volume is increased by a reagent, which is able to penetrate into the cell wall but does not form chemical bonds with the lignocellulosic constituents. The resultant more or less permanent bulking means that the dimensional stability of the wood is increased, making it more suitable for large area applications such as planking. Actual chemical modification at the molecular level is represented by the following examples. In bonding (c), a reagent forms a single covalent bond with a hydroxyl group of the wood polymers. In cross-linking (d), a reagent forms multiple covalent bonds with the adjacent hydroxyl groups. In degradation (e), the amount of hydroxyl groups is reduced by e.g. thermal treatment (Norimoto and Gril 1993; Sandberg et al. 2017). It is worth noting that the thermal modification of wood can be seen as a physical modification, as generally no chemicals are necessary in the treatment; or as chemical modification due to the cell wall substrate undergoing molecular changes.

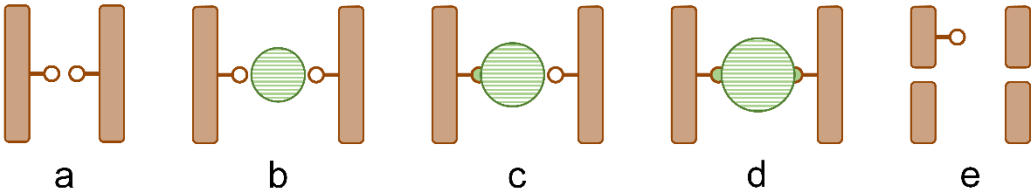

Figure 6: Models of wood modification at the cell wall level.
Brown bars represent the wood substrate; Small brown circles represent hydroxyl groups; Large green circles represent reagents
(a) Native state; (b) Bulking; (c) Bonding; (d) Cross-linking; (e) Degradation

Overall, the systematization of the wood modification methods is inconsistent. In contrast to the aforementioned classification, Norimoto and Gril (1993) differentiated between heat treatments, formalization, esterification, etherification, treatment with resins, deposition of inorganic compounds, impregnation with polyethylene glycol or waxes as well as wood plastic composites – where vinyl monomers are impregnated and polymerized *in situ*. Mehl (1977) refers to the latter as "*Polymerholz*", which is German and translates to polymer wood.

The processes for physical wood preservations have been successfully commercialized in the past. The treatment of wood with oils and waxes, in order to make it more water repellent, has been well documented since ancient times, and today, these products are abundantly available (Scholz et al. 2010c). The opportunity to improve the mechanical properties by resin impregnation and densification are also known (Mehl 1977) and products for this established themselves in specialty markets decades ago.

Only a few processes of chemical wood modification have been successfully commercialized and market growth is slow, in spite of the amount of scientific and patent literature that has accumulated over time. High investment costs for specialized production equipment, as well as the marketing necessary for these new, unknown products make modified wood often more expensive than untreated or biocide-treated wood. Thermal modification has advanced the most commercially speaking. Other processes that have seen commercialization are e.g. acetylation, furfurylation and the modification with 1,3-Bis(hydroxymethyl)-4,5-dihydroxyimidazolidine-2-on (DMDHEU) (Hill 2006, 2011; Sandberg et al. 2017).

In spite of these hindrances, the scientific community has grown over time with regards to wood modification and is today, larger than ever (Militz 2020). New strategies for specific and multi-step functionalization have seen a surge of interest within the same said community (Ermeydan et al. 2012; Li et al. 2012; YongFeng et al. 2013; Cabane et al. 2014; Ermeydan et al. 2014a; Ermeydan et al. 2014b; Keplinger et al. 2015; Grosse et al. 2016). Herein, dimensional stability and durability are not the sole driving motivators; rather, wood is seen as a hierarchical large-scale bio-template with significant potential for creating novel, functionalized materials (Burgert et al. 2015). In order to differentiate this field of research from traditional wood modification, the term wood nanotechnology

was promoted (Berglund and Burgert 2018), with the first “Wood Nanotechnology Conference” being held in 2018 in Ascona, Switzerland.

3.3 Wood Polymer Composites

Wood Polymer Composites (WPC) and Natural Fiber Composites (NFC) have attracted the attention of both the wood and the plastics industry. The general objective of composite materials is to achieve a synergistic combination of matrix and filler properties. In general, a vast number of natural materials may be combined with either thermosetting or thermoplastic polymers. The terms WPC and NFC, in a wider sense, refer to any composites that contain bio-material particles or fibers within a thermoset or thermoplastic matrix. NFC commonly contain cellulosic or lignocellulosic fibers, i.e. featuring a high length to width ratio, acting as reinforcement in a thermosetting or thermoplastic matrix. WPC refers to, in most cases, thermoplastic polymers filled with wood flour (WF) (Clemons 2002), which is the applied definition in this study.

The addition of wood filler to a polymer leads to enhanced mechanical properties such as stiffness, strength and heat deflection temperature. Wood is a low-cost resource and, compared to various mineral fillers, also a low density material. The introduction of wood filler into plastics combines their respective advantages but also yields disadvantages. The ductility and impact resistance are generally lower than of the corresponding neat polymer. The wood filler introduces hygroscopy into the composite, increasing not only water uptake and swelling but also the susceptibility towards fungi (Klyosov 2007; Oksman Niska and Sain 2008).

The prerequisites for the reinforcement of a matrix material by a filler are, (1) the filler features higher strength than the matrix, (2) the filler features higher stiffness than the matrix and (3) the matrix should not fail before the filler (Ehrenstein 2006). In a particle filled composite under load, the particles restrain the matrix deformation. Thereby a fraction of the stress is transferred from the matrix onto the particle. The degree of reinforcement or improvement of mechanical properties, i.e. the ability of stress transfer, depends on the adhesion at the particle-matrix interface (Callister, Jr. 2007).

The manufacture of WPC is based on the production technologies of the polymer industry. Compared to other wood based products, this offers a far greater freedom in product shapes and dimensions. Independent of the processing equipment the manufacture may be divided into the basic steps of blending, compounding and forming. The blending of the ingredients may be done as a standalone process, common in polyvinyl chloride processing, in which the temperature stays below the melting point of the matrix polymer and a homogeneous granular dry blend is produced. The blending may also be integrated into the next processing step, the compounding, which is common in polyolefin processing. During compounding the polymer is exposed to heat and shear and thereby plasticized. The fillers and additives are dispersed to achieve a homogeneous melt, which is called compound. The compounding step also serves to remove moisture and gases from the compound, which is particularly critical in the case of WPC. After compounding, the material may immediately be formed into products or pelletized for later processing (Stark et al. 2010; Mertens et al. 2017).

Because of the low thermal stability of wood, it may only be combined with plastics whose processing temperature is sufficiently low. Non-reversible chemical changes start to occur with hemicelluloses and lignin at temperatures of around 150 – 160 °C. Degradation accelerates with rising temperatures but is only minor until temperatures reach 200 °C (Rowell and LeVan-Green 2005). The thermal degradation of wood is also dependent on the time of exposure and atmosphere. Decomposition starts to occur at 200 °C, and from 220 °C onwards lignin and cellulose start to degrade rapidly (Fengel and Wegener 1989). As regards the production of WPC, the time the wood is exposed to high heat is relatively short, so only temperatures resulting in rapid degradation are relevant here. Because of this, WF is usually only used as the filler material in plastics that are processed at temperatures of 200 °C or lower (Klyosov 2007; Oksman Niska and Sain 2008).

The development of the WPC market in the European Union has been dynamic in the past decades. In 2012, WPC and NFC made up 15 % of Europe's composite market. WPC accounted for almost 11 % with a production volume of 260,000 tonnes. The main fields of application are decking and automotive. Nevertheless, WPC is increasingly used in other fields of application such as furniture, technical parts, consumer goods and household electronics. Due to increasing polymer prices and incentives for bio-based products, the market growth is expected to continue over the next decades at two-digit rates. An especially strong growth has been predicted in the specific areas siding, fencing, technical applications, consumer goods and furniture strong growth was predicted (Carus et al. 2015a).

The three most common matrix polymers used for WPC are polyethylene, polypropylene and polyvinyl chloride. In the US in 2003, polyethylene was the main matrix polymer utilized in the WPC market. It accounted for approx. 70 % of the production volumes, followed by polypropylene with 17 % and polyvinyl chloride with 13 % (WRAP 2003). In 2005 in Germany, polypropylene was used in 82 % of the total WPC production. Polyethylene and polyvinyl chloride accounted for 10 % and 8 % respectively (Vogt et al. 2006). In Asia, polyvinyl chloride is the main matrix polymer used in WPC production. The share of polyvinyl chloride based WPC is steadily growing in all markets (Carus et al. 2015b). Next to these commodity plastics, thermoplastic elastomers such as styrenic-block-copolymers and thermoplastic-polyurethanes as well as bio-polymers such as bio-polyethylene and polylactic acid are gaining interest in the industry (Diestel and Krause 2018; Carus and Partanen 2018).

3.4 Polyethylene

Polyethylenes (PE) are considered part of polyolefins, a family of polymers which are produced from olefins, acyclic and cyclic hydrocarbons (alkenes, cycloalkanes and polyenes) with one or more double bonds. The most prominent representative of which are the semi-crystalline commodity thermoplastics PE and polypropylene.

PE was synthesized as a by-product for the first time in 1898 by Hans von Pechmann during the investigation of diazomethane (Pechmann 1898). The analysis of this white by-product was postponed. His colleagues Eugen Bamberger and Friedrich Tschirner later characterized the waxy substance and recognized that it contained long CH_2-

chains. PE received attention once again when Reginald Oswald Gibson and Eric Fawcett rediscovered it in 1933 (Domininghaus et al. 2012). In 1935, the British chemist Michael Willcox Perrin developed the first reproducible high-pressure synthesis and by that induced the industrialization of PE (Cathcart 2004).

In general, polyethylenes feature low water sorption, low water vapor permeability and a high resistance towards chemicals. Their basic properties are governed by the size and shape of the hydrocarbon chains, i.e. degree of branching, degree of polymerization, mean molecular weight and molecular weight distribution (dispersity). They are distinguished into different types in respect to production process, degree of branching and properties; all of which are interdependent. The more common ones are low-density polyethylene (LDPE), linear-low density polyethylene (LLDPE) and high-density polyethylene (HDPE).

LDPE (Figure 7 above) is produced by free-radical polymerization at temperatures and pressures of 1500 – 3000 bar and 170 – 320 °C respectively. Oxygen or organic peroxides serve as the radical initiators. LDPE has a high degree of short- and long-chain branching. As a result of this, the polymer chains are unable to organize into highly ordered and tightly packed domains. Their degree of crystallinity (X_c), density and melting temperatures (Tm) are low compared to other types of polyethylene.

HDPE (Figure 7 below) is produced in catalytic processes, which are discussed in more detail in the following Chapter 3.5. They are produced at pressures ranging from ambient to 50 bar and at temperatures ranging from ambient to 180 °C. HDPE contains long linear main chains with a low degree of short-chain branching. As a result, of which the polymer chains are able to organize into highly ordered and tightly packed domains. Their degree of crystallinity, density and melting temperatures are high compared to other types of polyethylene.

LLDPE, (Figure 7 middle) similar to HDPE, is produced in catalytic processes under the addition of alpha-olefins such as 1-butene, 1-hexene or 1-octene. This results in long linear main chains with regular, short side chain branching. LLDPE exhibits low density but relatively high melting points. They feature some enhanced product properties, but also demand more intense processing (Domininghaus et al. 2012).

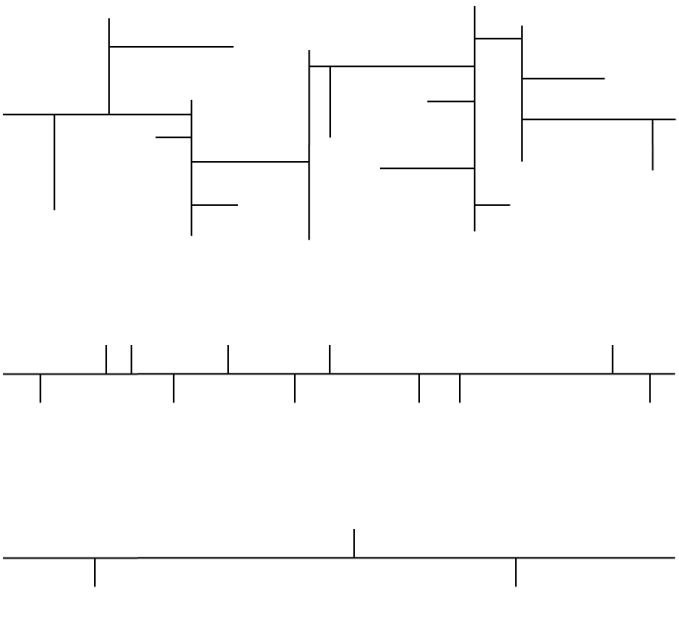

LDPE
Density: 0.915 – 0.935 g/cm³
T_m: 105 – 115 °C
X_c: 40 – 50 %

LLDPE
Density: 0.900 – 0.930 g/cm³
T_m: ca. 120 – 130 °C
X_c: 10 – 50 %

HDPE
Density: 0.940 – 0.970 g/cm³
T_m: ca. 128 – 145 °C
X_c: 60 – 80 %

Figure 7: Schematic illustration of the polymolecular structure and basic properties of the more common types of polyethylene: LDPE, LLDPE and HDPE.
(T_m) Melting temperature; (X_c) Crystallinity (Carraher 2003; Franck et al. 2011; Domininghaus et al. 2012)

PE is in general a linear polymer but may contain, as mentioned, a certain degree of branching. This has a large influence on the properties of PE. The main chains of LDPE may contain 20 – 40 side methyl groups and 0.5 – 5 long chains per 1000 C-atoms. These long side chains may be of a similar length to the main chain. HDPE in comparison, only contains around 2 side methyl groups per 1000 C-atoms. These morphological features influence the ability of the polymer to crystallize upon cooling. Regular polymer chains are able to align to one another and form crystals more easily, leading to higher degrees of crystallinity. Branching interferes with the alignment of polymer chains, leading to lower degrees of crystallinity with weaker intermolecular forces and higher amorphous portions (Carraher 2003; Franck et al. 2011; Domininghaus et al. 2012).

Because of the symmetric morphology of its hydrocarbon chain, PE has a high propensity to form crystals. The degree of crystallinity is dependent on the degree of branching. Highly branched PE may have crystallinities as low as 40 %, whereas linear PE may have crystallinities of up to 80 %. However, the cooling rate at which PE is consolidated also affects its crystallinity. If molten PE is cooled rapidly, the hydrocarbon chains loose mobility at a rate which inhibits the formation of crystals, locking them in a glassy state (Franck et al. 2011). Certain nucleating agents and microscale particles may also influence the crystallization behavior and resultant crystal morphology (Huang et al. 2007).

The molecular weight is another parameter that governs polymer properties. The avg. molecular weight of PEs can range from 6,000 to 4,000,000 g/mol. Below 10,000 g/mol they exhibit waxy properties. Customary PE plastics range in the 100,000s whereas molecular weights of 500,000 – 4,000,000 g/mol are considered to be high to ultra-high and are utilized in special applications (Franck et al. 2011).

3.5 Catalytic Olefin Polymerization

Before 1950, the only ethylene polymer available was a highly branched, low-density PE from radical polymerization at high temperatures and very high pressures. Around the 1950s, John P. Hogan and Robert L. Banks discovered the so-called Phillips catalysts, a solid-state catalyst consisting of chromium oxide supported on silica gel, and were able to produce linear PE for the first time (Hogan and Banks 1956). In the early 1950s, Karl W. Ziegler and Giulio Natta produced HDPE and crystalline polypropylene using a mixture of triethylaluminum ($AlEt_3$) and titanium tetrachloride ($TiCl_4$). Today, these catalysts are known as Ziegler-Natta catalysts. These catalytic polymerization methods may be performed at low pressures and ambient temperatures (Carraher 2003; Domininghaus et al. 2012). To date Phillips and Ziegler-Natta belong to the two most commercially employed catalysts (McDaniel 2010).

Ziegler-Natta catalysts are a combination of a transition metal compound from groups 4 to 8 and an organometallic compound from the groups 1, 2 and 13 of the periodic table. In fact, many early and late transition metal catalysts are indeed precursors that require activation to achieve the desired polymerization. In combination with suitable catalyst activators, these catalyst precursors undergo a chemical transformation that converts them to their active form. These precursors and activators are also referred to as precatalyst and cocatalyst (Ittel et al. 2000; Carraher 2003).

Heterogeneous catalysis, utilizing insoluble solid-state catalysts, suffers from a few drawbacks. The activity in gram polymer per gram metal catalyst was rather low. This is because a large portion of the metal, e.g. titanium, remains within the center of the insoluble titanium-chloride particles excluded from the catalytic reaction on the particle surfaces. Because high titanium residues within the product polymer can catalyze photochemical degradation reactions, elaborate washing steps for purification were necessary. Today, it is customary to immobilize titanium catalysts on solid supports (discussed in more detail in Chapter 3.6), in order to enhance their activity per gram of catalyst, so much so that purification steps are no longer necessary (Koltzenburg et al. 2014). Furthermore, the actual polymer properties produced by solid-state catalysts are often lower than the theoretical upper limits. This is attributed to the solid state character of the catalyst restricting the motion of the growing polymer chain. Additionally, many of these catalysts offer several polymerization sites, each with a different structure, leading to wider polymer property distributions (Carraher 2003). In addition, the high content of corrosive halogens, such as chlorine, calls for expensive corrosion-resistant equipment (Kaminsky 1980). On the other hand, heterogeneous catalysts provide a reliably control over grain size, bulk weight and particle morphology and lead to less reactor fouling (Mädler 1987; Müller 2003; Koltzenburg et al. 2014).

Research on homogeneous catalysis utilizing soluble catalysts, derived much of its impetus from the desire to model the reaction mechanisms and kinetics of heterogeneous polymerization catalysts (Mädler 1987; Brintzinger et al. 1995). Special attention was given to metallocenes. Catalytic systems based on titanocenes and aluminum alkyl compounds, showed short-lived active olefin polymerization, which generally came to a halt very quickly (Patat and Sinn 1958; Long 1959; Henrici-Olivé and Olivé 1967). Long

(1959) stated that titanocene dichloride (Cp_2TiCl_2) catalysts are rapidly reduced by $AlEt_3$ and diethylaluminum chloride ($AlEt_2Cl$), from an active tetravalent titanium to a less active trivalent state. Mentioned complexes revealed to be more stable in combination with methylaluminum compounds. It was later proposed by Henrici-Olivé and Olivé (1967) that Ti(IV) is the catalytically active form, while Ti(III) is inactive. Analogous zirconocene systems showed no such activity (Andresen et al. 1976). As the deactivation of the titanocene catalysts continued to be unsolved, metallocenes were bound to remain the exclusive subject of interest in the science community.

Simultaneously to early research on soluble catalysts, the positive effect of oxygen on the performance of homogeneous catalysts was investigated and verified by Breslow and Newburg (1959). In their experiments with Cp_2TiCl_2 / $AlEt_3$ or $AlEt_2Cl$ catalysts, traces of oxygen were introduced along with the ethylene gas, leading to increased polymerization. The mechanism of partial hydrolysis of aluminum alkyls and the resultant product structure was investigated by Sakharovskaya et al. (1964). They concluded that the reaction between aluminum alkyls and water has an intermediate stage, where monohydroxydialkylaluminum is formed, before further hydrolysis occurs. The basic structure of aluminoxanes of $[\text{-AlR-O-}]_n$ was proposed. Figure 8 depicts the reaction scheme between trimethylaluminum ($AlMe_3$) and H_2O in forming methylaluminoxane (MAO), accompanied by the elimination of methane. Reichert and Meyer (1973) mentioned the known influence of water and presented their own results, where an increasing H_2O content leads to increasing ethylene polymerization rate of a $Cp_2TiEtCl$ / $AlEtCl_2$ catalyst. The highest Al to H_2O ratio of 20:1 investigated also showed the highest activity. The influence of water was also the subject of interest in investigations conducted by Long and Breslow (1975). They noticed that the activity of titanocenes decreases with the increasing effort to exclude water from the reaction, leading to the suspicion that these systems may in fact be entirely inactive without water. Furthermore they conducted experiments with $AlMe_3$ and water, but only reported moderate activities.

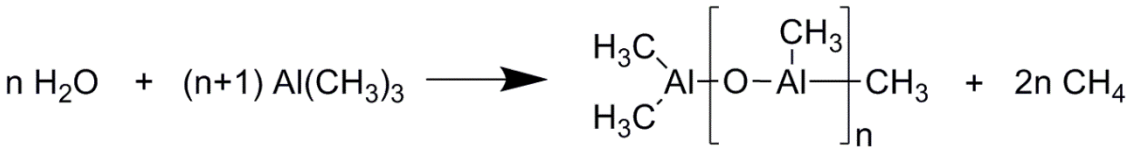

Figure 8: "Equimolar" reaction scheme between $AlMe_3$ and water to methylaluminoxane (MAO) and methane.

The development gathered momentum when Mottweiler (1975) investigated the complexation reactions between Cp_2Ti-compounds with aluminum alkyls. Surprisingly, he observed high and long lasting ethylene polymerization activity from the combination of dimethyl titanocene (Cp_2TiMe_2) and $AlMe_3$. At the time, the formation of Ti-Al-complexes was seen as a necessity for catalytic activity. The aforementioned pair did not show complexation in NMR-spectroscopy, nor did earlier results via UV-spectroscopy (Sinn 1963), and was therefore thought to be entirely inactive. In conjunction with the findings of Meyer and Reichert (1970) it is proposed that a coordinative, covalent interaction in

dynamic equilibrium between the titanocene and the aluminum alkyl, opposed to the assumption of complexation, may in fact be the polymerization “active species”. Mottweiler’s work was followed up by Merck (1976) and Herwig (1976), who were able to show that in fact, water was responsible for the high activities observed by Mottweiler.

Derived from the aforementioned theses, the role of aluminoxanes in homogeneous ethylene polymerization was investigated further. It was shown by Andresen et al. (1976) that chlorine free systems such as Cp_2TiMe_2 and otherwise inactive zirconocenes, exhibit very high polymerization activities in combination with $AlMe_3$ previously treated with water. Maximum activities of 430,000 g(PE)/g(Ti)*h were reached at Al to H_2O ratios of 2:1 to 5:1. Activity disappeared when the ratio dropped below 1:3, i.e. all alkyl groups were hydrolyzed. These findings were substantiated by Cihlář et al. (1978), showing an analogous effect of water on systems containing chlorine.

The invention of MAO as a cocatalyst for ethylene and propylene polymerization and copolymerization was patented by Sinn et al. (1980b). Sinn et al. (1980a) reported the necessity of providing the cocatalyst in larger quantities than the catalyst. According to their findings, the reaction rate in zirconocene / MAO systems is a linear function of the Zr-concentration but a quadratic function of the MAO-concentration.

MAO has been shown to exhibit higher activities than its ethyl- and isobutyl- counterparts (Kaminsky et al. 1983; Kaminsky and Steiger 1988). It was also shown that Cp_2TiMe_2 / MAO catalyze propylene homo-polymerization as well as ethylene-propylene copolymerization. MAO is also active with a variety of other transition-metal compound catalysts (Herwig and Kaminsky 1983). The use of separately produced MAO together with Cp_2TiMe_2 further increased the activity by a factor of 100 compared to the system of Cp_2TiMe_2 / $AlMe_3$ / H_2O (Herwig and Kaminsky 1983; cited in Kaminsky and Sinn 2013; cited publication does not contain the recited statements). MAO may separately be produced by – among other pathways – the reaction of $AlMe_3$ with water-ice or inorganic salts, containing relatively consistent amounts of crystallization water (Zijlstra and Harder 2015).

To date, the structure of MAO has not conclusively been established. The possible structural features of MAO were summarized by Chen and Marks (2000) and are displayed in Figure 9. It is believed that a cage like structure, complexing $AlMe_3$ within itself, is the catalyst activating species (Sinn 1995; Alt and Köppl 2000). It has been reported that the degree of oligomerization has a strong effect, i.e. higher degrees of oligomerization lead to higher and longer lasting activities (Sinn et al. 1980a; Kaminsky 1981).

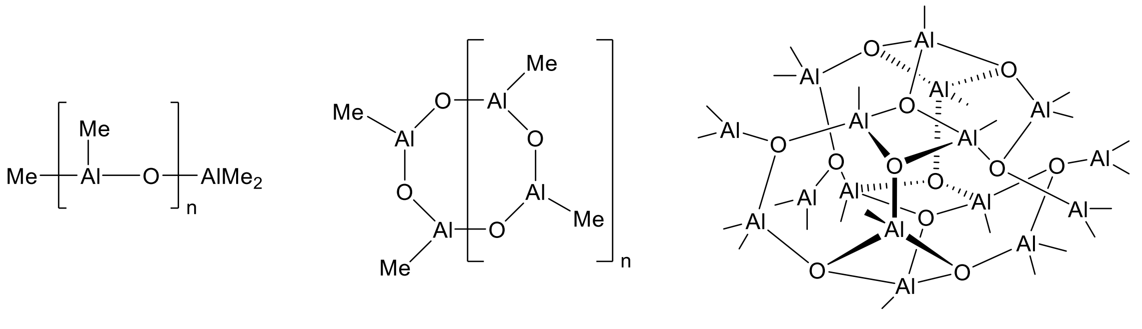

Figure 9: Proposed oligomeric structures of MAO.

Homogeneous catalysis, utilizing soluble metallocenes and MAO for vinyl polymerization, gathered more and more interest in the 1990s, as they solved a few of the aforementioned problems inherent to heterogeneous Ziegler-Natta systems. They are less prone to be encapsulated by polymer and therefore preserve their high accessibility and activity over time. Their relatively stable activity leads to narrow molecular weight distributions and their solubility leads to polymers containing little or no catalytic agents, making elaborate purification steps unnecessary. Additionally, their single active site is uniform, allowing the synthesis of polymers with well-defined and predictable molecular properties (Breslow and Newburg 1959; Henrici-Olivé and Olivé 1967; Carraher 2003).

These soluble catalysts require three features: a metal atom (active) site, a cocatalyst and a ligand system. Among the successfully used metal centers are Zirconium, Titanium, Hafnium, Scandium and rare earths. Cyclopentadienyls (Cp) have been the most commonly used ligands, but a number of others have been successfully employed, such as substituted Cp and bridged Cp. The most commonly used metal-ligand grouping is zirconium-dichloride (Carraher 2003). Figure 10 displays examples of the possible ligand configurations of metallocenes.

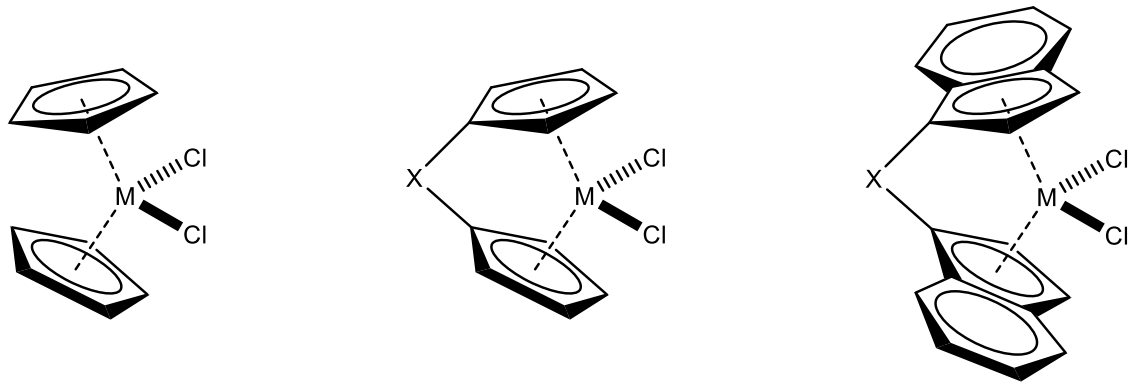

Figure 10: Exemplary types of metallocenes.
Left: Metallocene dichloride; Middle: Bridged ansa-metallocene dichloride; Right: Ansa-indenyl-metallocene dichloride.

The structure of soluble catalyst complexes controls activity, stereoselectivity, and selectivity towards monomers. Their single-site character allows for the production of polymers with narrow molecular weight distributions. They are able to produce PE with less branching than Ziegler-Nata catalysts. The summation of these effects is the production of polymers with increased strength and tensile properties (Carraher 2003). Next to polyolefins, it is possible to polymerize a number of other materials with metallocene catalysts, e.g. polystyrene, elastomers, copolymerizates from longer α-olefins and polymerizates from cycloolefins (Kaminsky 1996).

The cocatalyst is believed to serve the following functions: It maintains the catalyst complex as a cation but without strongly coordinating the active site. It also alkylates the metallocene chloride, replacing one of the chloride atoms with an alkyl group and removing the second chlorine, thus creating a coordinately unsaturated cation complex

(Cp_2MR^+). Furthermore, as the catalyst structure is sensitive to Lewis bases such as water and hydroxyls, the cocatalyst often serves as a scavenger to avoid the inactivation, often referred to as poisoning, of the catalyst (Carraher 2003).

The activation of a metallocene catalyst takes place in several steps (Figure 11). In the first step, the metallocene is coordinated in the vicinity of MAO and a methylation – i.e. a chlorine atom is exchanged for a methyl group – takes place. When larger quantities of MAO are available, both chlorine ligands may be exchanged and a dimethyl complex may be formed. In the second step, one ligand is abstracted and the complex $[Cp_2Zr(Ch_3)]^+$ cation is formed. The MAO anion stabilizes the complex cation, which features the active site for olefin polymerization. It has been suggested that in fact $AlMe_3$ contained within MAO is essential for this process (Kaminsky and Steiger 1988; Cam and Giannini 1992; Sishta et al. 1992; Babushkin et al. 2006).

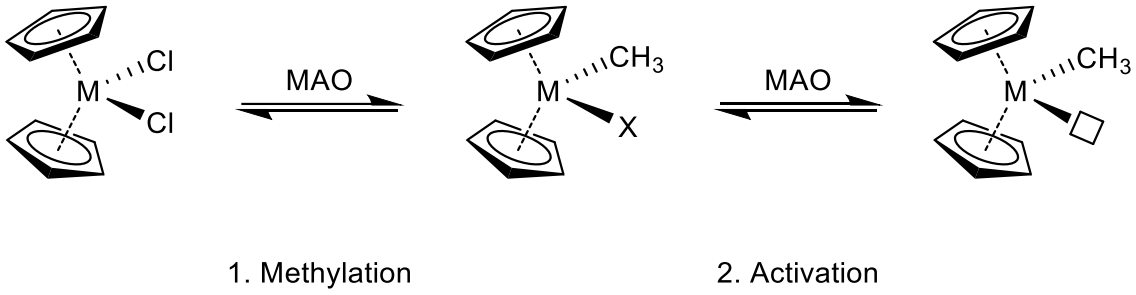

Figure 11: Activation of metallocene catalysts by MAO.
(M) Metal atom; (X) Cl or CH_3; (Box) Active site.

The understanding of the polymerization mechanisms brought forward by Arlman and Cossee (Arlman 1964; Arlman and Cossee 1964; Cossee 1964, 1966) is considered to be among the most comprehensive (Brintzinger et al. 1995). Further advancements by Brookhart and Green on the aforementioned insertion mechanism involve α-agostic interaction (Brookhart and Green 1983).

A polymerization scheme involving agostic interactions is displayed in Figure 12. In the first step, the olefin monomer is coordinated at the free coordination site of the metallocene complex cation. In the second step, a 1,2-insertion takes place, where the monomer is inserted in between the metal-center and the coordinated methyl group or growing polymer chain. Agostic interactions, referring specifically to 3-center-2-electron bonds involving M-H-C groups, facilitate 1,2-insertion by reducing the steric inhibition to the carbon-carbon bond forming step. However, the question whether agostic interactions are in fact an absolute necessity for active polymerization or, if polymerization also occurs on occasion in the absence of these interactions, remains unanswered (Brintzinger et al. 1995; Grubbs and Coates 1996; Brookhart et al. 2007).

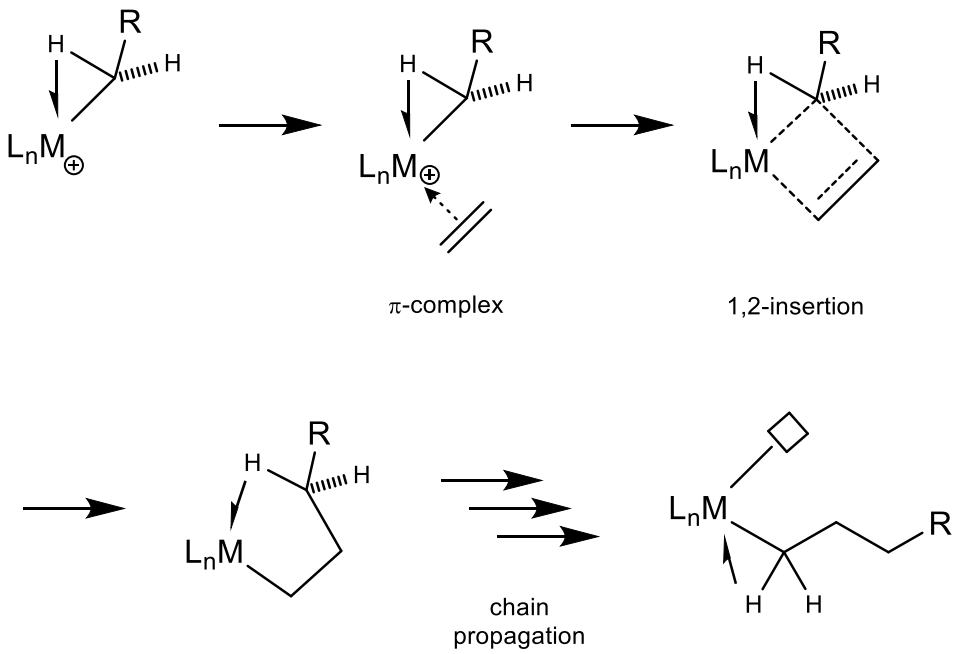

Figure 12: Polymerization mechanism according to Brookhart and Green. (L_n) Ligands; (M) Metal atom; (R) Propagating polymer chain; (Box) Active site.

Apart from chain propagation, chain termination and transfer mechanisms influence polymer properties to a great extent. The so called β-hydride transfer is the main termination pathway in the case of metallocene catalysts. A β-positioned hydrogen of the growing polymer chain is transferred to the metal center of the catalyst and a terminal olefin function at the end of the polymer chain is produced. This α-polyolefin can either be split-off or can participate in the following coordination steps. Long chain branching is the result of the latter. The degree of the β-hydride transfer reactions depends on the nature of the catalyst but may also be initiated on purpose by the addition of molecular hydrogen. The hydrogen atoms compete with the olefins for the free coordination sites of the catalyst. By coordination onto the metal center, the growing polymer chain is saturated by a hydrogen atom and split off, thereby producing a new coordination site. The newly formed metal-hydrogen center with one free coordination site allows for further olefin insertion. The addition of hydrogen thereby increases catalyst activity and decreases the molecular weight of the resultant polymer. In addition to the β-H elimination mechanisms, chain transfer to aluminum and to the monomer can also occur (Alt and Köppl 2000; Böhm 2003).

3.6 *in situ* Polymerization of Wood-Olefin-Composites

The conventional process of thermoplastic polymer composite manufacture involves melt compounding, which may be done with internal mixers or extruders. During melt compounding the thermoplastic is fused and additives and fillers are dispersed within the polymer melt by kneading (Koltzenburg et al. 2014; Mertens et al. 2017) (see also Chapter 3.3).

Another approach to form composites is the coating of each individual filler particle with polymer during polymer synthesis. Dubois et al. (1998) differentiated between "*in situ* polymerization" (ISP) and "polymerization filling technique" (PFT). The ISP describes methods where a polymerization process is carried out in the presence of filler particles, thereby encapsulating these particles by chance. In other words, in ISP, the polymerization occurs detached from but in close proximity to the filler entities. The term PFT describes the polymerization from catalysts anchored on the filler surfaces, thereby encapsulating these particles specifically. In other words, in PFT, only the filler surface is catalytically active and polymerization occurs on these surfaces exclusively. In practice, graded hybrids between these two categories are common. This is caused by phenomena such as catalyst leaching, where anchored catalysts detach during polymerization.

The incentive for ISP and PFT originates in the desire to improve on composite performance. By individually encapsulating single particles or fibers with polymer, they are dispersed more homogeneously in the final product. This is especially interesting in the case of nano-sized fillers that tend to agglomerate. Increased interfacial adhesion is also claimed (Kaminsky et al. 2008). Furthermore, the combination of a ductile matrix and a non-ductile filler can lead to a concentration of stress at their interface under load, ultimately leading to failure. This can be mitigated by encapsulating individual filler particles with a polymer of intermediate modulus, acting as a transition layer to prevent such concentrations (Dubois et al. 1998).

It should be noted that in common industrial practice, the predominant incentive for heterogenization, i.e. the immobilization of homogeneous catalysts on solid supports, originates from the advantages concerning processing and product handling (see also Chapter 3.5). Homogeneous catalysts that are soluble in the reaction media lead to the so-called reactor fouling, i.e. the polymerization of ultra-fine polymer particles that tend to adhere and agglomerate onto reactor surfaces, demanding high maintenance. In addition, handling ultra-fine polymer powders is elaborate. By adhering catalysts to solid, insoluble supports, the particle size of the polymerizate is increased. The morphology of polymer grains may be controlled to a certain extend by the choice of support to which the catalyst is anchored to (Müller 2003). Thereby, reactor fouling may be avoided and polymerizate with, for example, free-flowing behavior and high bulk density may be achieved. The preferred particle size for supports ranges between 10 and 100 µm. It is desired that the supports fragment into smaller particles during polymerization, in order for them not to interfere with product quality (Fink et al. 2000). In addition, many existing production plants are optimized to handle solid catalysts. To increase the likelihood of commercial viability, new catalyst systems need to be adapted to operate in existing production processes. By immobilizing homogeneous catalysts on solid supports, they can be utilized in existing production plants without the need for expensive refitting (Severn et al. 2005).

The anchoring of catalysts on solid surfaces can be achieved by physisorption (Park and Choi 2009) or by chemical bonding with surface functional groups (Orsino et al. 1959; Hendren et al. 2020). Furthermore, metallocenes can be heterogenized directly or indirectly. Metallocenes, which are heterogenized by immobilizing them directly onto solid

supports, are described to produce different polymers to their homogeneous counterparts. The interaction between the catalyst and the support slightly affect the catalyst, changing the nature of its active center and thereby the properties of the resultant polymer. Their activity is generally lower and the molecular weight and the molecular weight distribution are higher (Kaminsky 1996). Metallocenes can also be heterogenized indirectly. In such processes the cocatalyst – commonly MAO – is tethered onto the surfaces of the solid supports first. The subsequently added metallocene is thought to adhere to such MAO-treated surfaces by physisorption (Alexandre et al. 2000; Kaminsky et al. 2008; Rosehr and Luinstra 2017). MAO-immobilized metallocenes are described to produce very similar polymers to their homogeneous counterparts. The singles-site nature of the catalyst is preserved. However, one side of the catalyst is blocked, leading to generally lower activities (Kaminsky 1996).

The latter approach is depicted in Figure 13 and represents the method investigated in this study. The linkage between MAO and the oxygen atoms of the filler are displayed as dotted lines, in order to indicate that the nature of the bond, i.e. adsorption or covalent bond, remains in many cases inconclusive (Stürzel et al. 2013).

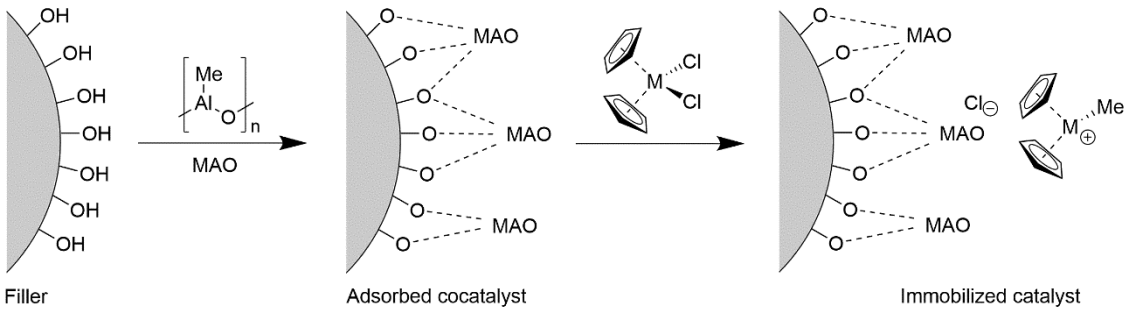

Figure 13: Immobilization of metallocene / MAO catalysts on solid supports containing hydroxyl groups.

A vast variety of materials have been investigated as supports for metallocene / MAO systems, such as kaolinite (Dubois et al. 1998), silica (Kaminsky 1996; Santos et al. 1999; Kaminsky 2014; Käselau et al. 2019), metal powders (Dutschke 1985; Kaminsky and Zielonka 1993; Kaminsky 1996; Käselau et al. 2019) and carbon nanotubes (Bonduel et al. 2005; Kaminsky et al. 2008; Rosehr 2012; Kaminsky 2014; Rosehr and Luinstra 2017).

The immobilization of Ziegler-Natta, metallocene and bisiminopyridine catalysts on biomaterials such as cellulose, starch, wood, chitosan and other carbohydrates is mentioned in the literature several times. Table 1 summarizes the corresponding literature. The use of lignin as support is also mentioned (Kaminsky 1980, 1983; Köppl et al. 1997), but no original research is cited. Mädler (1987) cites Spiehl (1984) who in turn cites Dutschke (1985), but there is no original research concerning lignin in either work.

Dyachkovskii (1988) cites Akelah and Sherrington (1982) who state that natural polymers containing hydroxyl groups such as cellulose are used as support for polymerization catalysts. However, Akelah and Sherrington do not report on polymerization catalysts but rather the immobilization of phase transfer catalysts. Dyachkovskii does not present or cite any further research.

In all early records, up until the 1970s, Ziegler-Natta catalysts were used. From the beginning of the 1980s onwards, the main share of publications concerns MAO based systems, most of which utilized metallocenes. This reflects the history of catalytic olefin polymerization and the discovery of MAO as a highly active cocatalyst in the middle and late 1970s, which is described in more detail in Chapter 3.5.

Only one record of propylene polymerization, using Ziegler-Natta catalysts supported on cellulose was found (Dankovics et al., 1969). Another record reports the copolymerization of ethylene and propylene using metallocene / MAO catalysts immobilized on starch and cellulose (Mädler, 1981). In another record still, the polymerization of ethylene as well as styrene using metallocene / MAO catalysts immobilized on cyclodextrins is reported (Lee and Yoon, 1995). All other records listed in the table below concern the synthesis of PE only.

Table 1: Overview on the different bio-supports and catalysts used in the cited literature.

Reference	Type	Cellulose	Starch	Wood	Other*
Orsino et al. 1959	Patent	A			
Herman and Dunlap 1965	Journal	A			
Herman et al. 1965	Journal	A			
Yanulis 1965	Journal	A			
Kruse 1967	Patent	A			
Chanzy et al. 1968	Journal	A			
Dankovics et al. 1969	Journal	A			
Prahl and Hart 1970	Patent		A		
Chanzy and Revol 1973	Journal		A		
Chanzy et al. 1973	Journal		A		
Chanzy et al. 1974	Journal		A		
Chanzy and Revol 1974	Journal		A		
Fisa and Marchessault 1974	Journal	A			
Chanzy et al. 1975	Journal	A		A	
Kaminsky 1980	Patent	B	B		
Mende 1981	Diploma		B		
Mädler 1981	Diploma	B	B		
Kaminsky 1982	Patent		B		
Kaminsky 1983	Journal	B	B		
Spiehl 1984	Diploma			B	
Dutschke 1985	Diss.		B		
Mädler 1987	Diss.	B	B		B
Marchessault et al. 1989	Journal	A			
Pettijohn 1989	Patent		A		
Lee and Yoon 1995	Journal				B
Köppl et al. 1997	Patent	**	**		**
Minh Hoang et al. 1999	Patent	B			
Belelli et al. 2000	Journal	B			B
Eberhardt et al. 2001	Journal	B	B		B
Minh Hoang et al. 2001	Patent	B			
Francq 2002	Poster	B			
Karmarkar 2011	Poster	B			
Cornelius et al. 2014	Patent			C	
Hees et al. 2017	Journal	C			
Hendren et al. 2020	Journal	B			
Spottog pending	Diss.	B		B	

(A) Ziegler-Natta; (B) Metallocene/MAO; (C) Bisiminopyridine/MAO

* Other carbohydrates; ** Claims extend across multiple bio- and inorganic materials but examples only speak of flour

Early works utilizing **Ziegler-Natta catalysts** were mostly concerned with applications in the pulp and paper industry and concentrated on cellulose as support.

The earliest record of cellulose being used as support for Ziegler-Natta catalysts is the US Patent by Orsino et al. (1959). The patented claims extend over various pathways

for the slurry ISP of ethylene, with catalysts supported on cellulosic fibers and are described in detail. Catalyst combinations of titanium tetrachloride ($TiCl_4$), zirconium tetrachloride ($ZrCl_4$), vanadium trichloride (VCl_3) and chromium trichloride ($CrCl_3$) with methylmagnesium bromide (CH_3MgBr), triisobutylaluminum ($Al(i\text{-}Bu)_3$) and triethylaluminum ($AlEt_3$) are described. The importance of treating the filler with one component before the other is stated. If the cocatalyst and the precatalyst are mixed together beforehand, polymerization occurs randomly, adjacent to the cellulose filler. On the other hand, if the cellulosic filler is treated with one of the catalyst components before the other is added, polymerization takes place at the surface of that filler. The order in which the filler is treated is not essential. The one percent of moisture retained within the cellulose is claimed not to interfere with the reaction and in fact, have a beneficial effect. The manufacture of PE paper and porous materials by dissolving the cellulose part with sulphuric acid or cuprammonium solution is described. In associated publications (Herman et al. 1965; Herman and Dunlap 1965) these claims are scientifically described. They come to the conclusion that: the polymer is not grafted onto the cellulose that the polymer does not penetrate into the cellulose and that, for the most part, the polymer and cellulose are not in direct contact to one another.

The encapsulation of woven cellulose fabrics and yarns with PE by analogous methods is reported. Yanulis (1965) investigated a variety of forming processes and resultant composite properties. The immobilization of $TiCl_4$ / $AlEt_3$ on paper sheets and subsequent polymerization were investigated by Fisa and Marchessault (1974). A continuous process of catalyst immobilization and subsequent polymerization on a continuous paper web was presented by Marchessault et al. (1989).

The encapsulation of starch by the immobilization of Ziegler-Natta catalysts and subsequent ethylene polymerization was also patented (Prahl and Hart 1970; Pettijohn 1989).

In addition to this, the encapsulation of cellulose and potato starch with PE utilizing VCl_4 was thoroughly investigated by Chanzy and his coworkers (Chanzy et al. 1968; Chanzy and Revol 1973, 1974). VCl_4 was immobilized on the dried carbohydrates by refluxing. $AlEt_3$ and ethylene were added in succession, in order to start polymerization. They reported that the exclusion of residual moisture is paramount for good polymerization activity. The importance of choosing an appropriate stirring speed at the beginning of the polymerization is emphasized. The initial layers of PE are sticky and cause the starch granules to form agglomerates if stirred to slowly. However, if initial stirring is too intensive, catalysts may be brushed off of the starch grains. After a time, the stirring speed becomes less critical and may be increased. The nascent morphology of PE as a function of polymerization conditions was investigated with catalysts immobilized on starch grains (Chanzy et al. 1973; Chanzy et al. 1974). The vapor phase deposition of catalysts onto pulp paper sheets and subsequent polymerization therefrom was also investigated (Chanzy et al. 1975).

Only two records of the immobilization of Ziegler-Natta catalysts onto wood or other lignocellulosic substrates were found. Kruse (1967) patented the encapsulation of individual lignocellulosic substrates by slurry ISP of ethylene using VCl_4 / $AlEt_3$. However, the given examples only refer to cellulose. Results were compared to $TiCl_4$ / $AlEt_3$. It was

claimed that the vanadium system leads to more uniform encapsulation, reaches considerably higher activities and is less sensitive to moisture than other contemporary systems. Lignin containing groundwood pulp was encapsulated by Chanzy et al. (1975) using $TiCl_4$ / $AlEt_3$ and applying the methodology described elsewhere (Chanzy et al. 1967). The encapsulated pulp was used to form paper sheets and the properties of the received sheets were determined.

Later works utilizing **Metallocene catalysts**, mostly regarded the technical feasibility of ISP or PFT processes utilizing bio-materials as supports and fillers. Most publications do not address resultant composite properties or applications.

The first record of ethylene polymerization using metallocene catalysts in combination with aluminum-alkyls supported on carbohydrates, is a German patent by Kaminsky (1980) and its corresponding US patent (Kaminsky 1982). Starch was used as support, but the claims are also extended to cellulose, lignin and saw dust. In the most successful example presented, starch was dried by azeotropic distillation in toluene and subsequently treated with $AlMe_3$ at a ratio of approx. 10 mmol/g for 40 min at 40 °C. 0.05 mmol of Cp_2TiMe_2 is added and ethylene is applied at 9 bar. The resultant compound contained 1.5 g of PE per 1 g of starch. In the following years Kaminsky (1981, 1983) briefly mentioned the advantages of composites produced by the polymerization of PE with metallocene / MAO catalysts immobilized on starch grains and cellulose. It appears that the German Maizena GmbH, trading in starch derived foods, promoted some of the starch-focused research in the polymer chemistry department in Hamburg (Woelk 1981); four related theses were conducted regarding starch, cellulose and wood.

As regards the diploma thesis by Mende (1981), $AlMe_3$ and MAO were used in combination with Cp_2ZrMe_2 to investigate the ISP of ethylene in the presence of undried and thoroughly dried starch. It was shown that $AlMe_3$ only forms an active MAO-species in the presence of moist starch and the compound starch-O-$AlMe_2$ does not function as active cocatalyst. Overall, prefabricated MAO showed considerably higher activity compared to the MAO-species formed *in situ*. Polymerization activities were subject to high variation and it is reported that polymer and starch were easily separable by extraction with decalin.

Simultaneously to Mende, Mädler (1981) performed further investigations in the scope of his diploma thesis, regarding the ISP of ethylene and copolymerization of ethylene and propylene in the presence of starch or microcrystalline cellulose (MCC). Mädler came to very similar conclusions. $AlMe_3$ only formed an active MAO-species in the presence of a bio-filler containing residual water. The performance of prefabricated MAO was generally higher, but suffered from residual water. The reproducibility was generally low, but improved with higher MAO to carbohydrate ratios. No chemical bonds between the polymer and the carbohydrate are formed, as they were easily separable by decalin extraction.

In another diploma thesis, Spiehl (1984) investigated the ISP of ethylene in the presence of wood with Cp_2ZrCl_2 / MAO. Spruce wood particles were sieved with a mesh size of 250 µm, extracted with toluene and pre-dried at 60 °C. They were vacuum dried again within an autoclave at 95 °C. Similarly to the two prior theses and in spite of the thorough

pre-processing performed here, variations remained high and rendered it impossible to evaluate the polymerization kinetics. Microscopic images were presented, proving – at least in part – successful encapsulation of particles. The polymer coating was easily removed from the wood filler by dissolving it in decalin at a high temperature.

In his dissertation, Dutschke (1985) observed a temperature dependence for the fixation of catalyst components on supports. First, starch and calcium carbonate were vacuum dried at 105 °C for 24 h. The fillers were then suspended in toluene and treated with MAO or Cp_2ZrCl_2. The temperature and duration of these treatments were varied. Secondly, he filtered the suspension; after which the solid residues as well as the filtrate were tested for their polymerization activity. In the case of MAO treated starch, the solid residue did not exhibit any ethylene polymerization activity. In the case of zirconocene treated starch, the catalytic activity exhibited a clear dependency on the treatment temperature and duration. Catalytic activities were considerably higher when treated at 30 °C compared to 70 °C and peaked after 1 h of pretreatment. Dutschke concludes that the observed attachments are based on physisorption rather than on chemical reaction. It is also shown that it is possible to treat biomass with metallocenes before MAO and still achieve active catalysis.

In his comprehensive dissertation, Mädler (1987) elaborated on the work of Mende (1981) and investigated the *in situ* formation of MAO-like structures by utilizing the residual moisture of different types of starch as well as MCC to partially hydrolyze $AlMe_3$. The MC of native starch was varied, in order to investigate its effect on the degree of oligomerization and the morphology of the resultant MAO. The amount of reaction between $AlMe_3$ and starch was determined by gas titration experiments, where the methane development was recorded. Relatively dry native corn starch showed very low gas development. The different bio-materials with their varying EMCs exhibited very different reaction rates. It was shown that not all bound water was available for reaction with $AlMe_3$ and that this amount differed heavily depending on the carbohydrate material. It was concluded that the optimum ratio between $AlMe_3$ to H_2O was more dependent on the water available for the reaction than the absolute amount of water. In all cases, prefabricated MAO showed higher polymerization activities than the *in situ* formed derivative. Mädler also investigated a variety of monomeric polyols, to see whether they would form active cocatalysts in combination with $AlMe_3$. The polyols sorbitol, glucose and erythritol were shown to form complexes with $AlMe_3$ without producing methane. However, they surprisingly led to active polymerization. The polyols dianhydrosorbitol, monoanhydrosorbitol and anhydroerythritol were shown to react with $AlMe_3$ under the development of methane. They form aluminoxane-like structures that show cocatalytic activity. The acidity of hydroxyl groups is thought to be the factor determining reaction with $AlMe_3$.

Kamnisky – who supervised the aforementioned theses – presents corresponding content several times again. It is mentioned that natural substances such as starch, cellulose and lignin can, due to their residual water content, form aluminoxane analogous structures when treated with $AlMe_3$. A variety of micrographs are presented (Kaminsky et al. 1988; Kaminsky and Steiger 1988; Kaminsky 1996, 2004).

Lee and Yoon (1995) successfully investigated the immobilization of $AlMe_3$ and MAO on cyclodextrins for subsequent ethylene and styrene polymerization using Cp_2ZrCl_2 or $CpTiCl_3$ catalysts. The cyclodextrins were thoroughly vacuum dried at 120 °C and stored over calcinated silica before use.

In another US patent (Köppl et al. 1997), unspecified flour was used as support for $AlMe_3$. In the first example, wet nitrogen was guided through a slurry containing $AlMe_3$ before adding the flour. In another example, the flour was treated with $AlMe_3$ before water was introduced via nitrogen stream. Cp_2ZrCl_2 was used as catalyst for successful ethylene polymerization. It is not mentioned if the flour was dried beforehand and the yield was quite low. The claims extend over a vast amount of cocatalysts, catalysts and support materials.

In further US patents (Minh Hoang et al. 1999, 2001) it is claimed that the pretreatment of MAO with dried carbohydrates, in order to remove residual aluminum alkyls, increases polymerization activity. The insoluble parts of carbohydrates were removed prior to polymerization. Two examples were presented in which MAO pretreated with cellulose showed higher activity than MAO pretreated with silica.

A variety of carbohydrate-supports were comprehensively investigated by another group (Belelli et al. 2000; Eberhardt et al. 2001). Cellulose, starch and two types of chitosan, the latter differing in the degree of de-acetylation, were used in conjunction with Cp_2ZrCl_2 / MAO to catalyze ethylene polymerization. Filler materials were not dried nor were their MCs determined. Parameters such as specific surface area were found to have no effect. In experiments where the filler was treated with the zirconocene before the MAO, no active polymerization was observed. The successful pathway was treating the filler with MAO first followed by the zirconocene. The ethylene was applied at atmospheric pressure and polymerizations were conducted at 45 °C for 30 and 60 min. The highly deacetylated chitosan showed the highest activities, followed by the cellulose, starch and less deacetylated chitosan. The authors concluded that the low activity of the starch is caused by residual moisture. Furthermore, they state that the acetyl groups sterically hinder the MAO from reacting with all hydroxyl- and amino groups, which may in turn still be existent and cause catalyst poisoning. The PE received from the supported catalysts yielded higher molecular weight than the PE received by analogous homogeneous polymerization. These findings imply the importance of moisture management when dealing with hygroscopic support materials.

A poster, originating from the master thesis written by Francq (2002) at the Université de Mons – Hainaut in Belgium, discusses the ethylene polymerization filling with $Cp^*_2ZrCl_2$ / MAO immobilized on MCC. Homogeneous polymerization, ISP and PFT are compared in terms of activity. Interestingly, the immobilization on cellulose lead to increased stability of the catalyst and increased long term productivity. No further publications have been written and no further research has been performed on that subject by the corresponding research team (Dubois 2020).

Karmarkar (2011) presented a poster in the course of the 11th International Conference on Wood & Biofiber Plastic Composites. He treated cellulose fibers with MAO and

Cp_2ZrCl_2 for subsequent ethylene polymerization. He reported successful polymerization and the absence of reactor fouling.

Hendren et al. (2020) comprehensively explored another approach: using cellulose nanocrystal aerogels as catalyst support. Instead of impregnating the carbohydrate surface with aluminoxane, 1,1'-bis(bromodimethylsilyl)zirconocene dibromide was anchored onto said surface first. A modified MAO species containing a small share of octane units (MMAO-12) was then added to activate the catalyst for ethylene polymerization. Satisfactory yields and composite properties were achieved. The nanoscale filler was shown to be well dispersed. This approach trades the freedom to vary catalysts for the freedom to vary cocatalysts, which may be favorable in some specific cases. The CNC/metallocene supported catalyst was found to be less susceptible to oxygen and moisture than its CNC/aluminoxane counterpart, making handling less cumbersome. Foils produced from received materials were translucent. The e-modulus of received materials were elevated, but other mechanical properties were comparable to the control neat polyethylene.

Spottog (pending) investigated the ISP of LLDPE in the presence of a variety of cellulose based filler materials, most of which contained lignin. She used (n-BuCp)$_2ZrCl_2$ / MAO, the same catalytic system utilized in the study at hand. By the addition of 1-octene, LLDPE was formed. In her standard procedure, the filler was pre-dried at 100 °C until a constant weight was reached. After placing the dried filler into the reactor, the whole chamber was vacuum dried for 2 h at 85 °C. Toluene, co-monomer and MAO were added. Ethylene partial pressure was applied at 2 bar in a semi-batch process and the suspension was stirred for 1 h. The polymerization was then started by the addition of the catalyst. As a result of her studies and analogous to Mädler (1981), she found that the speed of polymerization depended on the amount of MAO available to the catalyst. The latter in turn depended on the amount of filler added, as the functional groups of that filler presumably adsorb MAO and make it in part unsuitable to act as co-catalyst. Overall, catalytic activities comparable to homogeneous polymerization were achieved in the presence of cellulosic fillers if the MAO dosage was increased, in order to compensate for the losses due to its scavenging function. Specimens prepared from the *in situ* polymerized compound did not exhibit superior mechanical properties compared to the compound that was produced conventionally by mixing. The moisture uptake of the specimens from the *in situ* compound was elevated.

Two records are known of, which immobilize **Late Transition Metal Catalysts** and MAO on bio-material supports.

Cornelius et al. (2014) patented the utilization of alkylaluminoxanes in combination with α-diimine- and bisiminopyridine- late transition metal catalysts for the ISP of lignocellulosic composites. In the most successful example presented, 10 g of WF is pre-dried for 2 d at 100 °C before being transferred to an autoclave, where it is dried again for 1 h at 85 °C. After cooling down to 50 °C, 300 ml of toluene and 4 ml of 10%-MAO solution are added. The slurry is saturated with ethylene gas at 3 bar and polymerization is initiated by the addition of 0.95 µmol 2,6-bis[1-(2,6-Dichlorphenylimino)ethyl]pyridine iron, being terminated after 10 min. The resultant compound contained 3.1 g of PE per 1 g of WF.

Hees et al. (2017) comprehensively explored a new pathway to use nanocellulose as catalyst support, in order to produce nanocellulose-polyethylene composites. It is well known that nanocellulose tends to irreversibly aggregate upon drying (Sandquist 2013). To circumvent this issue, nanocellulose aerogels were formed via freeze drying, which were then cryo-milled. The obtained flour was treated with MAO before adding the bis(imino)pyridine iron dichloride catalyst. Polymerization was carried out in a steel reactor with n-heptane as solvent and triisobutylaluminum as scavenger for Lewis bases such as water and hydroxyls. The prepared catalyst was dispersed in n-heptane and transferred to the autoclave. Ethylene polymerization was carried out at 3 and 5 bar. In the most successful example presented, the resultant compound contained 41.1 g of PE per 150 mg of nanocellulose. They discovered that the ISP with nanocellulose leads to the formation of “shish-kebab” structures and stated that the utilized catalyst does not usually produce these structures. The mechanical properties of nanocellulose and mesoporous silica-containing composites were compared. Specimens containing a similar filler content exhibited comparable e-moduli. Specimens containing nanocellulose exhibited inferior tensile strength but preserved elongation at break better than the silica filled specimens.

This literature review demonstrated that, whereas the general process of polymerization of ethylene by catalysts immobilized on bio-filler materials appears well researched, verification of the advantages arising from ISP or PFT, i.e. improved product properties and performance, is lacking. The papers by Hees et al. (2017) and Hendren et al. (2020) represent the only published reviewed articles where the mechanical properties of materials containing nanoscale cellulose fillers were investigated. Spottog (pending) investigated the material properties of microscale lignocellulose filled composites, but no reviewed publications incorporated her results regarding the properties of composites containing such microscale fillers are known. The results of these three records do not show clear advantages of compounds produced by ISP or PFT.

4 Dynamic Desorption of Lignocellulosic and Cellulosic Substrates during Vacuum Drying

4.1 Introduction

Water plays a key role in wood science, wood processing and service life of a product, since it affects all relevant material properties of wood (Thybring et al. 2018). Wood-water interactions have been the subject of investigation for at least the past century. One might think that this would have been solved by now and is absent of any inconsistencies. However, the fact that wood-water interactions are still the subject of contemporary research, are a testimony to their complexity. Many seemingly established facts and theories are now increasingly considered to be inadequate (Engelund et al. 2013; Nopens 2019; Zelinka et al. 2020).

As can be concluded from the fundamental knowledge presented in Chapter 3, it is clear that the consideration of the moisture content (MC) of hygroscopic biomaterials is of the utmost importance, when they are to be used in processes in conjunction with catalysts that are prone to react with protonic groups and water. This remains true for *in situ* Polymerization as well as for the Polymerization Filling Technique processes in general, but is even more critical in procedures where either the biomaterial itself or the moisture it contains are meant to play an active part in the catalysis.

Pilot experiments performed in the scope of this study confirmed the importance of precise moisture management. No active polymerization was observed when either very dry or relatively moist wood was used in combination with $AlMe_3$ as cocatalyst. Furthermore, polymerization success and activity were subject to considerable variation, even when procedures were kept seemingly constant, which coincides with earlier studies (Mende 1981; Mädler 1981; Spiehl 1984). As the polymerization equipment utilized in this study employed a vacuum as its means of drying, the extent to which the MC of wood could be managed with the given polymerization equipment was investigated. Karl-Fischer titration (KFT) has long been recognized of being one of the most suitable methods for reliably determining wood MCs (Kollmann and Höckele 1962). The indirect oven mode of the coulometric KFT (cKFT) is especially suitable for measuring low MCs of substrates that only release water slowly and at high temperatures, such as wood. It was therefore seen as suitable for the purposes of this study.

Moisture management is and always has played a key role in wood processing and related industries. Drying of bulk wood, wood chips, particles or fibers is all necessary and common practice in sawmill and wood-based panel industries, as is the dewatering and drying of pulp and paper. Both, the consideration of the materials' form and the anticipated purpose of the resultant product, pose their own requirements and optimization challenges on the drying process. In many cases, cost efficiency conflicts with other requirements, such as product quality and safety (Holik 2006; Trübswetter 2006). The desired MC of wood depends heavily on the type of intended processing or on its designated use case, but is commonly in the range between 4 and 14 % (Skaar 1988).

There are a number of procedures utilized for timber drying, such as natural air drying, kiln drying and vacuum drying. The most prevalent industrial process is kiln drying (Brunner 1987).

Vacuum drying of wood, even though it has been around since the beginning of the last century, is limited to specific applications, such as drying of very thick lumber (Espinoza and Bond 2016). In the sawmill industry, it is commonly used for high quality commodities and wood species that are otherwise challenging to dry using conventional processes. The basic advantage is that by lowering the pressure below the boiling point of water at a given temperature, the wood moisture begins to evaporate more evenly throughout an entire bulk cross section, making for fast and gentle drying at low temperatures (Brunner 1987). Though, it has been noted that in the case of bulk wood, a vacuum only accelerates drying at MCs below MC_{FS}. Additionally, the pressure within bulk wood remains higher than the ambient pressure during vacuum drying (Neumann et al. 1993). In industrial practice, absolute pressures during vacuum drying can range between 500 and 80 mbar (Trübswetter 2006), which corresponds to boiling temperatures of water ranging between 60.1 and 41.5 °C (Grigull 1988). The vapor pressure of cell wall bound water is lower than that of liquid free water (Skaar 1988). Desorption plots of wood exhibit power law functionality, i.e. initial desorption is very fast and slows down over time (Nopens et al. 2019). This means, with an ongoing drying time and a decreasing MC, the drying speed is hypothesized to slow down.

Independent of the applied drying process, the mechanisms by which fluids may move within wood can be differentiated into fluid flow and diffusion. Diffusion in wood may further be divided into diffusion of a solute through the solvent saturated continuous pore volume, diffusion of a gas or vapor through the continuous pore volume and lastly, diffusion of a fluids through the cell walls (Stamm 1967a, 1967b). In vacuum drying processes, where heat transfer is controlled, bound water diffusion and pressure driven bulk vapor flow are considered to be the predominant mass-transfer mechanisms for bulk wood MCs below fiber saturation (Koumoutsakos et al. 2001). In a study concerning the lignocellulosic fibers, diffusion is believed to be the dominant form of moisture transport for MCs below 2.5 % (Watt and Kabir 1975). As the materials investigated in this chapter were below FS and, on average, of smaller particle size than individual physiological cells, bound water diffusion is hypothesized as the main mechanism of moisture transport here.

It is well known that, under atmospheric conditions, the equilibrium moisture content (EMC) depends primarily on relative humidity (RH) and temperature. However, Chen and Lamb (2002) studied the theoretical dependency between vacuum drying conditions and the resultant EMC, under the assumption that the amount of air present in a vacuum may be considered negligible and that the predominate portion of the absolute pressure is represented by water vapor pressure. A view that is shared by others (Fohr et al. 1995). This led to their hypothesis that EMC in a vacuum is solely dependent on absolute pressure and temperature. Concluding from mathematical calculations, they proposed a direct positive relationship between pressure and EMC at constant temperature and an inverse relationship between temperature and EMC at constant pressure. Yi et al. (2008)

validated the general conclusions made by Chen and Lamb experimentally, though results deviated considerably. Contradictorily to the former researchers, Liu et al. (2010a, 2010b) considered the RH and temperature to be the relevant factors influencing EMC under vacuum conditions. Surprisingly, their results show that, when RH and temperature are kept constant, the EMC increases with decreasing pressure. In another paper by Liu et al. (2015), EMC charts for vacuum conditions and a modified Hailwood-Horrobin model were published. It is evident that these contradicting results are in need of further verification. Also, all research cited in this paragraph was performed on solid wood samples and may not be directly applicable to wood particles as used in this study.

In the specific case of this study, very low amounts of residual moisture are of interest. It is well known that wood may retain varying low quantities of water even after intensive drying, depending more on the materials precondition rather than drying time or temperature (Kollmann and Höckele 1962). Differences of the retained MC between a first and a second drying cycle were reported by Hill et al. (2015) and the term “trapped water” was introduced. Hergt and Christensen (1965) investigated the water retention of wood and cellulose. Samples were subjected to a high vacuum of 0.13×10^{-3} mbar at 27 °C for a minimum of 24 h. A variety of preconditioning procedures, initial MCs and drying procedures were tested. They noted that up to 1 % MC may be retained, even after prolonged drying. Higher drying temperatures only slightly decreased water retention. Reproducible minimum MCs are obtained when samples are rapidly dried from a state of fiber saturation. Hence, they concluded that the amount of water retained depends on the vapor pressure or MC prior to drying. Analogous effects were found in the case of jute fibers (Watt and Kabir 1975) and protein-based biopolymers such as wool (Watt and Kennett 1960). The proposed dependency of the retained water as a function of prior storage conditions, could provide an explanation for the inconsistent polymerization activities in the presence of biomaterials of earlier polymerization studies (Mende 1981; Mädler 1981; Spiehl 1984). Furthermore, it underlines the importance of controlling the sorption history of biomaterials in scientific experiments.

Sorption dynamics are influenced by, among other factors, the sorption history. The longer a sample was held at a constant EMC, the slower a following rate of sorption is, which was found to be true for wood (Christensen and Hergt 1969) as well as for jute fibers (Watt and Kabir 1975). Heat transfer into the to-be-dried material may also be a drying rate governing factor (Koumoutsakos et al. 2001). In drying experiments performed under continuous vacuum at room temperature, constant drying rates instead of the expected power law functionality were observed. The heat supply was deemed the determining factor for the drying rate (Chen 1997). This may very well be a relevant factor in this study, since the polymerization equipment used in this study is not designed to precisely control the heat transfer into solids.

Cellulosic materials, such as chemical pulps derived from wood, normally show lower EMCs than their lignified source material (Christensen and Kelsey 1959). They have higher shares of cellulose and lower shares of lignin and hemicelluloses. In other words, the portion of amorphous material is lowered and the share of cellulose crystals is thereby increased. Even more so, microcrystalline cellulose (MCC) is deprived of a large share of the amorphous cellulose, leading to high crystallinities of up to 80 %. These

crystalline regions are thought to be inaccessible for water. The decreased gravimetric share of water-accessible material is the cause of the overall lower EMCs exhibited by cellulosic materials (Trache et al. 2016).

It is difficult to compare results across studies due to differences in wood species, sample mass, geometry as well as the inherent general inhomogeneity of wood. Furthermore, a wide variation of equipment and procedures were used in prior studies. In order to answer the question as to what extend the MC can be managed within given polymerization equipment by means of applying vacuum drying, it was necessary to produce specific results upon which further investigations could be based. In order to account for the heterogeneity between wood species, pine and beech flours were investigated. Wood as well as wood derived cellulose may be considered as viable filler materials in polymerization processes. Highly standardized MCC was investigated as a representative of cellulosic materials.

4.2 Experimental

4.2.1 Materials

4.2.1.1 Cellulosic Materials

Pine sapwood flour, beech wood flour and **microcrystalline cellulose** were used, in order to investigate their residual MC after vacuum drying. The WF was produced from commercially kiln-dried pine sapwood and beech wood with a rotary mill (SLf 90 S/4 T, Retsch GmbH, DE). After fractioning, their main share particle diameter lay 1 – 4 mm. “MCC012” (ProUmid GmbH & Co. KG, DE) was used as MCC, which is a certified reference material for humidity validation procedures in sorption measurements.

4.2.1.2 Chemicals

The **titration reagents** “HYDRANAL-Coulomat AG-Oven” as well as “Fluka Hydranal Coulomat AG” were used for coulometric Karl-Fischer-Titration. The cKFT setup was verified using the **lactose monohydrate standard** “HYDRANAL-Water Standard KF-Oven, 140-160°C” (all sourced from Honeywell International Inc., US).

4.2.1.3 Gases

Grade 5.0 **Nitrogen** 99.999 % (Linde GmbH, DE) was used as inert gas.

4.2.2 Methods

4.2.2.1 1l-Autoclave

Samples were vacuum dried in 1l-autoclave glass reactors (Büchi Glas Uster AG, CH); the schematics thereof are displayed in Figure 14. As regards temperature control, the autoclave featured a jacketed glass shell, in order to accommodate the flow of heat exchange liquids. Thermostats (EH heating circulators, JULABO GmbH, DE) were used for active heating. In all cases where temperatures well below 100 °C were needed, demineralized water was used as heat exchange liquid. In cases where higher temperatures

were needed, polyethylene glycol 300 (Rotipuran, Carl Roth GmbH + Co. KG, DE) was used instead of water. The temperature within the autoclave was monitored via a thermocouple. The pressure was monitored simultaneously with both an analog and a digital pressure gauge.

The autoclaves were equipped with several in- and outlets, which enabled the direct addition of monomer, toluene, nitrogen, vacuum and the manual dosing of other chemicals. For the direct application of nitrogen and vacuum, the autoclave was connected to a vacuum gas manifold (Schlenk line), which in turn was connected to the central nitrogen supply and the laboratory-shared main rotary vane pump.

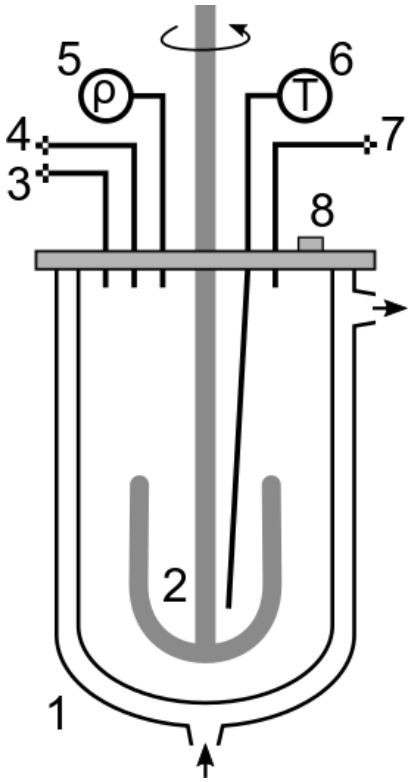

Figure 14: 1l-Autoclave polymerization glass reactor schematics.
(1) Jacketed glass shell; (2) Anchor stirrer; (3) Inert gas and vacuum; (4) Ethylene; (5) Pressure gauge; (6) Thermometer; (7) Toluene; (8) Manual access with septum).

4.2.2.2 Coulometric Karl Fischer Titration

In order to assess the residual moisture of pine wood, beech wood and MCC after varying vacuum drying procedures, coulometric Karl-Fischer titration (cKFT), using the indirect oven mode, was performed. According to the equipment manufacturer, the indirect oven mode of cKFT is especially suitable for measuring small MCs of substrates that only release water slowly and at high temperatures. The equipment used was the “831 KF Coulometer” in combination with the “860 KF Thermoprep” and the “Tiamo” Software (all Metrohm GmbH & Co. KG, DE) for data analysis. 6 ml sample vials and aluminum septum caps were used (Metrohm GmbH & Co. KG, DE).

The standard indirect oven method is as follows: Samples are weighed and then sealed within the vials. The oven temperature as well as the flow rate of the dry carrier gas are preset to the desired values. A sample vial is placed into the oven. The hollow two-way needle is lowered through the septum into the vial (Figure 15, left). Dry carrier gas flows through the inner part of the needle into the vial chamber and exits again through the outer part of the needle. The gas, now carrying the moisture released from the sample, is then led into the coulometric titration unit (Figure 15, right) where the amount of water is determined electrochemically.

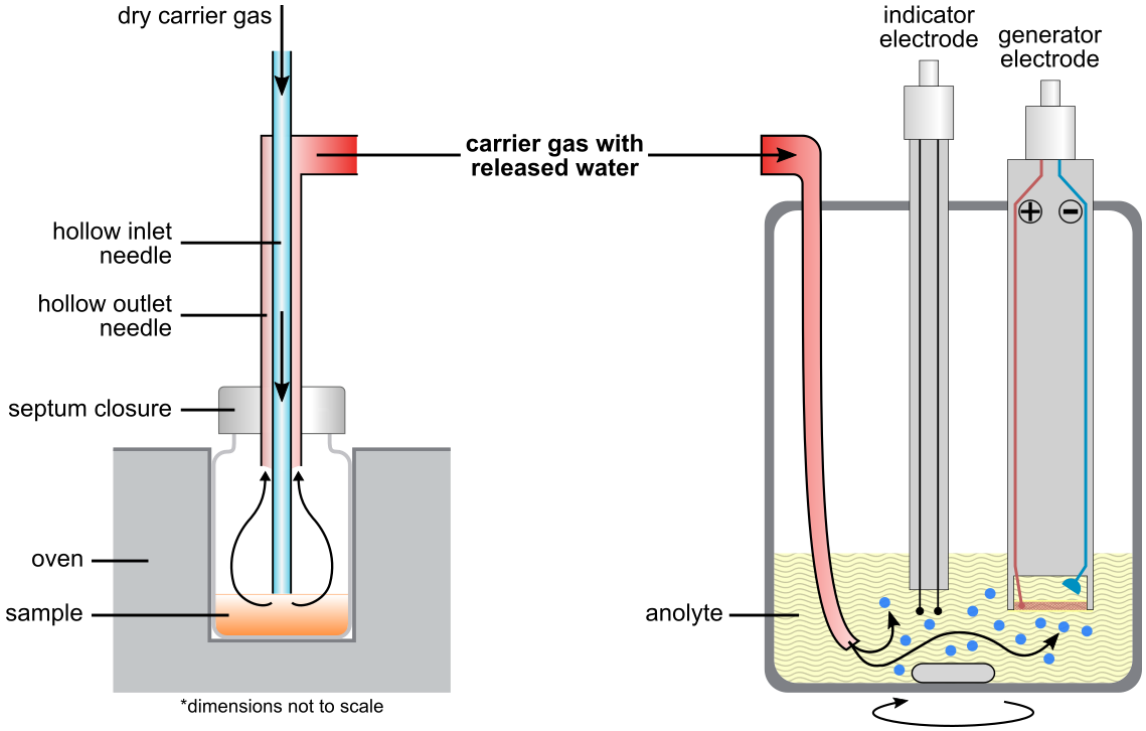

Figure 15: Schematic illustration of coulometric Karl Fischer Titration in oven mode. Left: Oven unit containing a vial with specimens; Right: Coulometric titration unit.

4.2.2.3 Design of Experiments

The design of experiments (DoE) software “Design-Expert Version 11” (Stat-Ease Inc., US) was used to design and analyze the experiments, in the matter of the residual moisture of wood and wood derived cellulose after vacuum drying. DoE software was used to aid the evaluation of possible dependencies between factors, reduce the overall experimental scope and provide detailed statistical analysis. For a more detailed description please refer to the mentioned chapter.

4.2.3 Procedure

The residual MCs of the WFs and MCC after vacuum drying were investigated, for which the Design of Experiment software was used. The flour materials were dried within the same 1l-autoclaves, which were later used in the polymerization experiments described in Chapter 6. The MC was measured with coulometric Karl Fischer titration.

The **design of experiments** was used to reduce the number of combinations of a full factorial design and to facilitate the evaluation. The influence and 2-factor-interactions of four different factors were investigated: (1) temperature, (2) time, (3) pressure and (4) material (Table 2). A randomized response surface methodology study type was selected to explore the influence and interactions of several explanatory variables on one or more response variables. The design scope was 34 runs. An unblocked I-optimal design type was used to set up the initial design and a coordinate exchange algorithm was used to improve the selection of model points. The extreme values were derived from the preliminary results. The range of levels for the numeric factors was chosen to represent a reasonable but also maximized design space. The minimum temperature of 30 °C was chosen, as it was above room temperature and the given equipment was only able to regulate the temperature by heating. The upper limit of 103 °C was chosen in conjunction with the *German Industry Standard* for oven drying wood (Deutsches Institut für Normung DIN EN 13183-1:2002-07). The minimum and maximum drying duration of 10 and 1440 min (24 h) were chosen as a reasonable compromise between consistent manageability and economic feasibility. Discrete values within 360 and 900 min were chosen, in order to facilitate a normal working day schedule. The categorical factors of pressure, i.e. medium and high vacuum, were chosen with regards to the available equipment. The medium vacuum represented a pressure of 150 mbar, while the high vacuum represented a pressure range of 1.0 to 0.1 mbar.

Table 2: Factors and levels used in design model for vacuum drying experiments.

				Values		
Factors	**Code**	**Type**	**Levels**	**Low "-1"**		**High "1"**
Temp. [°C]	A	Numeric	10	30.00		103.00
Duration [min.]	B	Numeric, discrete	4	10.00		1440.00
Pressure [mbar]	C	Categorical, ordinal	2	Medium*		High**
Material	D	Categorical, nominal	3	Pine	Beech	MCC

* Pump with vacuum controller set to 150 mbar; ** Pump without controller achieved pressure between 1.0 and 0.1 mbar

The vapor pressure (p_0) may be calculated with equation (1), provided by Siau (1995) for temperatures between 273.15 K and 433.15 K, i.e. 0 and 160 °C. Figure 16 displays the vapor pressure in the temperature range investigated in this study. According to this, the saturated vapor pressures at 30 °C and at 103 °C are equal to 42.5 mbar and 1131.1 mbar respectively. At 150 mbar, the water boiling point is approximately 54 °C. It is clear that the medium pressure series of this study comprised experiments below and above boiling temperature. In contrast thereto, the absolute pressures of all high vacuum drying experiments were below the vapor pressure.

$$p_0\,[mbar] = 0.01\,\exp(53.421\ - 6{,}516.3/T - \ 4.125\ln T) \qquad (1)$$

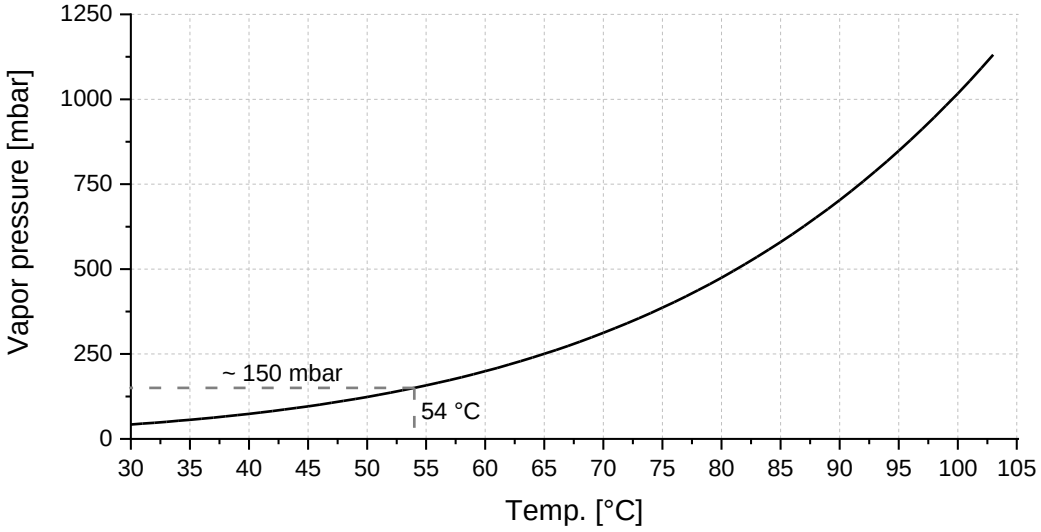

Figure 16: Water vapor pressure as function of temperature in the range of 30 to 103 °C.

The **specimen preparation** was performed as follows: All flour materials were stored until equilibrium at the standard climate of 20 °C and 65 % RH in accordance with the *German Industry Standard* for the determination of wood bulk-density (Deutsches Institut für Normung DIN 52182:1976-09) was reached. Approximately 50 mg of the specimen flours were weighed under standard climate, placed into cKFT vials and sealed.

Vacuum drying was performed inside the 1l-autoclave, which was also used in polymerization experiments. Polyethylene glycol 300 was used as heat exchange liquid instead of water, in order to be able to achieve temperatures above 100 °C. The rotary vane pump connected straight to the 1l-autocalve produced pressures between 1.0 and 0.1 mbar. This pressure range represented the “high” vacuum value in this study. In order to produce the “medium” vacuum value of 150 mbar the rotary vane pump connected to the 1l-autoclave was equipped with the vacuum-controller CVC 3000 and a VV 6C valve (Vacuubrand GmbH + Co KG, DE). The fourth factor comprised the materials pine, beech and MCC in the form of powders. The factor combinations were selected randomly by the software. The autoclave as well as the vacuum pumps were left to heat up prior to testing. To allow for gas exchange, syringes (Sterican, inner diameter 0.65 mm, outer diameter 0.90 mm, length 40 mm) were pierced into the septum of the vials just before the vials were placed into the autoclave. The autoclave was tightly sealed and the vacuum was applied. After the drying time had elapsed, three purge-and-refill cycles were applied using nitrogen. The autoclave was opened while at nitrogen atmospheric pressure, the vials were removed and their syringes pulled out as quickly as possible.

By equalizing the pressure inside the vials and by swift removal of the syringe after drying, the gas exchange with the ambient atmosphere was minimized. Pretrials had revealed that this method was preferable to sealing the vials after drying, as the latter yielded control over the initial MC and exposed samples to the ambient atmosphere after drying. However, the puncture in the septum left by the syringe was not entirely airtight. Sealing of the punctured septa with “Parafilm” showed no effect. It was therefore necessary to determine the residual MC directly after drying.

Moisture measurement was performed using cKFT. The Thermoprep oven was set to 103 °C with a dried airflow of 100 ml/min. Each variation comprised three blank and three specimen vials, which were all part of the same drying run. First, the blank vials were tested for remaining moisture. Blank measurements lasted 188 s. Subsequently, the three specimen vials were tested. The duration of the single measurements depended on the MC of the specimens and ranged from 188 s for low MCs up to 794 s for high MCs. The average blank values were subtracted from the specimen values. Furthermore, all measurements were automatically drift corrected by the software. In some cases, where there were very low MCs, the blank value subtraction and drift correction resulted in the artefact of negative moisture measurements. The mean MCs of the three samples per run were calculated and used for statistical evaluation.

The **statistics** were evaluated at a 0.05 level of significance. The DoE software was used to calculate the effects of all possible model terms using multiple regression analysis. In order to compare the different models, they were assessed for p-values, lack of fit, adjusted and predicted R^2. The following selection criteria were applied: The p-value had to be significant ($p < 0.05$), while the lack of fit had to be insignificant ($p > 0.05$). The adjusted and predicted R^2 were preferred to be high, i.e. as close to 1 as possible, and should not differ by more than 0.2. By the application of these criteria a 2-factor-interaction (2FI) model was suggested. For the results of the ANOVA analysis please refer to the Annex (Table 27).

4.3 Results

The raw data from the vacuum drying experiments can be found in the Annex (Table 26).

The coded factor equation (2) was computed by Design Expert and rounded down to two decimal places. The actual factors are converted into equivalents in a design space ranging from -1 to +1, representing the lowest and highest actual value respectively. A coded equation is useful for identifying the relative impact of different factors by comparing their coefficients. They can be used to make predictions about the response for given levels of each factor. However, coded factor equations are not able to predict actual response values.

$$\begin{aligned} MC\ [\%] = {} & 4.00 - 1.69[A] - 1.49[B] - 3.36[C] + 0.9667[D1] + 0.3138[D2] \\ & + 1.10[AC] - 0.1628[AD1] - 0.5654[AD2] + 0.5730[BC] \\ & - 0.7302[CD1] - 0.4857[CD2] \end{aligned} \quad (2)$$

According to these results, the categorical factor **pressure [C]** exerts the overall largest influence on the MC. Medium vacuum is coded for by -1 and high vacuum is coded for by +1. The second largest single influence was exerted by factor **temperature [A]**. In both cases, it may be concluded from the negative value of these two factors that higher vacuum and temperature lead to lower MCs. The quantitative **[AC] interaction** reflects that the influence of temperature at medium vacuum is larger than at high vacuum. Temperature determines partial vapor pressure and the rate of evaporation is dependent on relative vapor pressure. In the medium vacuum of 150 mbar, the vapor pressure surpasses the absolute pressure within the temperature range investigated, leading to the high temperature influence. In the high vacuum of ≤ 1 mbar, the vapor pressure is at all times well above the absolute pressure, reducing the temperature influence.

The **duration [B]** exhibits the overall third largest single influence on the drying rate during vacuum drying. The duration does not influence any evaporation rate governing mechanisms. It is therefore conceivable that interactions with temperature and material were computed as insignificant. The quantitative **[BC] interaction** reflects the fact that the drying rate is different at medium and high vacuums for the aforementioned reasons. No more significant interactions with the duration were found. This is also reflected by the actual factor equations (Table 3), were the coefficient for the duration is constant within one pressure group. However, the pressure during the high vacuum was not entirely constant, ranging between 1.0 mbar at the beginning and 0.1 mbar towards the end of the drying process. This is not considered within the design model as the pressure was set as a categorical, i.e. constant, factor. In spite of the end-pressure being somewhat dependent on the drying time, the differences were minimal and are presumed to only exercise a negligible impact.

The **material** factor is split into **[D1]** and **[D2]** with different encoding. In [D1] pine, beech and MCC are coded for by 1, 0 and -1 respectively. In [D2] pine, beech and MCC are coded for by 0, 1 and -1 respectively. The coefficients are the difference between the average response data at a particular factor setting and the overall average. For example, in the case of pine, the coded factor [D1] is positive while the coded factor [D2] is zero, leading to a response above the overall average, corresponding to the coefficient of [D1]. In the case of beech, the coded factor [D1] is zero and the coded factor [D2] is positive, leading to a response above the overall average, corresponding to the coefficient of [D2]. In the case of MCC, both coded factors are multiplied by minus one and are therefore negative, leading to a response below the overall average, corresponding to the sum of coefficients [D1] and [D2].

Different wood species are known to show slight variations in their wood-water interactions. Furthermore, cellulosic materials derived from wood sources, such as the MCC used in this study, are known to exhibit lower EMCs than their parent wood. This is reflected by the results here, where beech and pine wood display only minor differences but MCC exhibits significantly lower MCs.

The quantitative **interaction** between **[AD1]** and **[AD2]** reflect the fact that a change in temperature influences the MC of the three tested materials differently. The MC of beech

wood reacts the most sensitively to higher temperatures with a negative [AD2] coefficient. Pine wood reacts less sensitively with a smaller negative [AD1] coefficient. MCC reacts the least sensitively with the multiplied positive coefficients of [AD1] and [AD2].

The quantitative **interaction** between **[CD1]** and **[CD2]** reflect the fact that a change in pressure influences the MC of the materials differently. In contrast to the [AD] interactions, this time the MC of pine wood reacts more sensitively to lower pressures than beech wood, with a negative [CD1] coefficient and a slightly smaller negative [CD2] coefficient respectively. Again, MCC reacts the least sensitively with the multiplied positive coefficients of [CD1] and [CD2].

In Table 3 the actual factor equations are displayed, which can be used to calculate the predicted response values. The levels should be specified in the original units for each factor. This equation should not be used to determine the relative impact of each factor as the coefficients are scaled to accommodate the units of each factor, additionally, the intercept is not at the center of the design space. The actual factor equations translate the relative impact into actual behaviors.

The general difference between the wood materials and the cellulose material is apparent again. The temperature [A] influences the MCs of all materials differently, but again, the two wood species stand apart from the cellulose. Only the influence of the duration [B] does not distinguish between the materials.

Table 3: Resultant actual factor equations for all tested materials and vacuum drying conditions.

Factors		Equation
C	**D**	**A [°C] B [min]**
Med.	Pine	$MC\ [\%] = 16.52023 - 0.080891A - 0.002879B$
Med.	Beech	$MC\ [\%] = 16.35625 - 0.091921A - 0.002879B$
Med.	MCC	$MC\ [\%] = 10.70348 - 0.056480A - 0.002879B$
High	Pine	$MC\ [\%] = 3.17441 - 0.020635A - 0.001276B$
High	Beech	$MC\ [\%] = 3.49945 - 0.031664A - 0.001276B$
High	MCC	$MC\ [\%] = 1.24989 + 0.003777A - 0.001276B$

(A) Temperature; (B) Duration; (C) Pressure; (D) Material; (MC) Moisture content as function of drying duration and temperature.

Deducted from the minimum and maximum MCs calculated by the actual factor equations (Table 4), it is evident that the behavior of the two WFs is highly similar at a low temperature and less resemplant at high temperature. The cellulosic materials general behaviour is similar to that of the wood materials, i.e. higher drying temperature and longer duration lead to lower MCs. However, the overall level of MC of the MCC is lower and the gradients are slightly flatter. These coherencies are valid in both the

medium and the high vacuum, although, the absolute differences are much smaller in the high vacuum.

The model does produce negative MCs in long duration, high vacuum conditions, which is obiously impossible. The Design Expert software did not offer a function to integrate boundary values into the statistical model. The tilting of the high-vacuum MCC plain towards higher MCs with increasing drying temperatures also seems peculiar.

Table 4: Outlining moisture contents calculated with actual factor equations for all tested materials and vacuum drying conditions.

Factors		A	30		103	
C	D	B	10	1440	10	1440
Med.	Pine		14.06	9.95	8.16	4.04
Med.	Beech		13.57	9.45	6.86	2.74
Med.	MCC		8.98	4.86	4.86	0.74
High	Pine		2.54	0.72	1.04	-0.79
High	Beech		2.54	0.71	0.23	-1.60
High	MCC		1.35	-0.47	1.63	-0.20

(A) Temperature [°C]; (B) Duration [min]; (C) Pressure; (D) Material.

The interaction graphs in Figure 17 are derived from the actual factor equations and display the quantitative **[CD1]** and **[CD2] interactions**.

It is apparent that the differences between the medium and high vacuum are the most pronounced at 30 °C and 10 min and the least at 103 °C and 1440 min. Furthermore, the **high vacuum** leads to overall low MCs and a low range thereof. All measured MCs are below 4 %, showing that a minimum of two-thirds of the original moisture is removed rapidly within the first 10 min of drying, regardless of the other factors. On the other hand, the **medium vacuum** leads to MCs that comprise the full range, from close-to original to very low MCs.

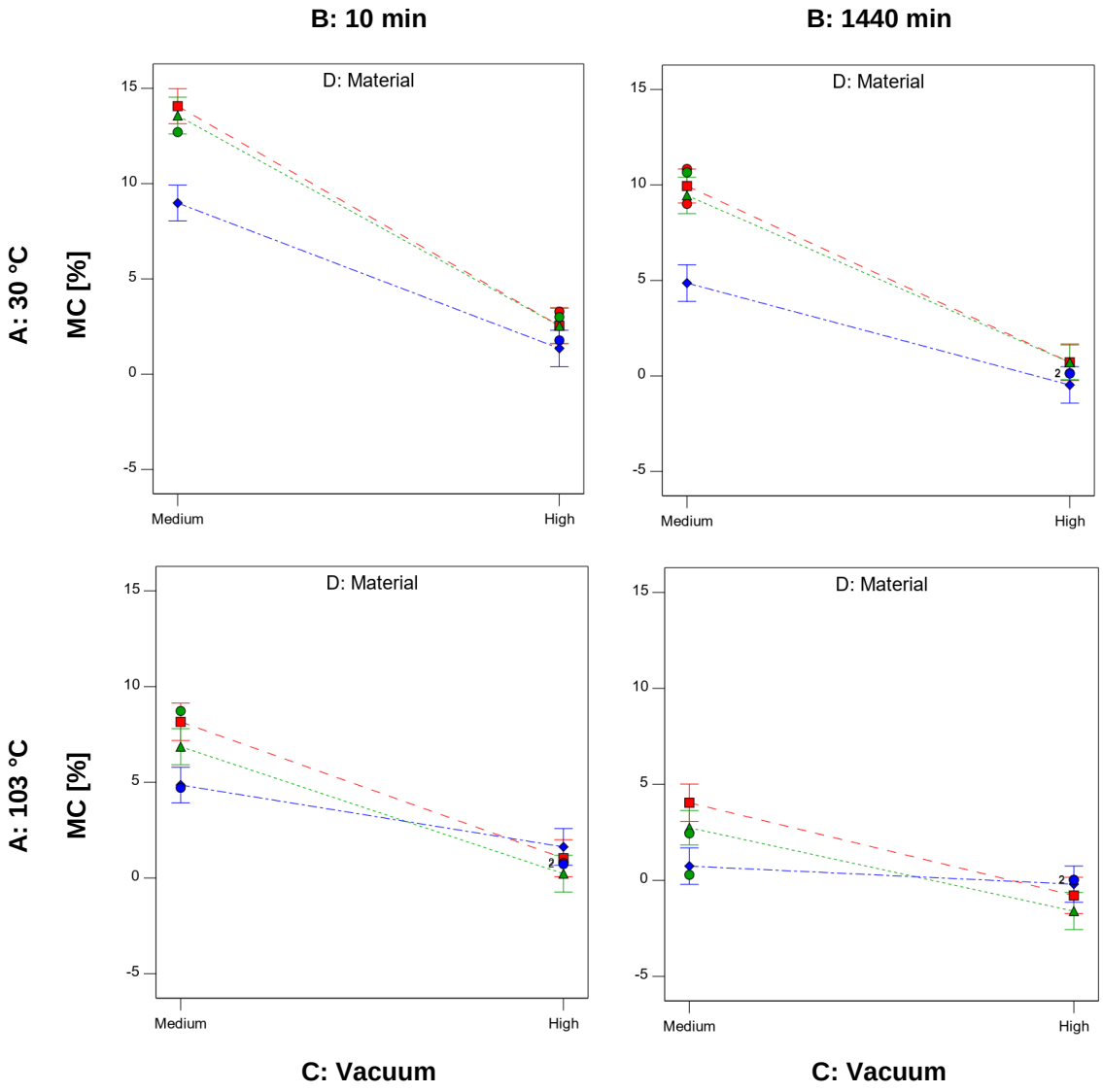

Figure 17: Moisture content as function of the interaction between pressure level and material as well as temperature and duration.

(■)Pine; (▲) Beech; (●) MCC.

Some results are ambiguous. Samples were preconditioned at 20 °C and 65 % RH until EMC was reached. These preconditioned materials were pre-tested, in order to determine their original MCs. They exhibited MCs lower than the highest values determined in the actual test series. The original MCs of pine, beech and MCC after conditioning were determined at 12.21 %, 11.70 % and 7.97 % respectively. The highest MC of pine in the test series was 13.29 % (med. vac.; 10 min; 30 °C), while beech showed a maximum MC of 12.70 % (med. Vac.; 10 min; 42.8 °C). MCC came in with the lowest maximum MC in the test series at 7.68 % (med. Vac.; 360 min; 30 °C). The MCs of beech and MCC may have been even higher if a medium vacuum test run of 10 min and 30 °C had been a part of the experiment.

4.4 Discussion

With respect to the former studies, the results of the vacuum drying experiments are somewhat surprising.

Short sessions of medium vacuum drying at a low temperature appeared to lead to no drying at all. During pre-tests pristine pine flour, which was preconditioned at 20 °C and 65 % RH until EMC, produced an avg. MC of 9.65 %. The highest measured MCs during the drying experiments were considerably higher, some reaching above 13 %. On the other hand, MCs were considerably lower than the EMCs ascertained by earlier studies (Chen 1997; Chen and Lamb 2002; Yi et al. 2008; Liu et al. 2010a, 2010b). For example, calculations by Chen and Lamb led to high theoretical EMCs close to MC_{FS}. In contrast to that, in medium vacuum drying experiments using conditions similar to this study, EMCs between 7 and 12 % were produced by Liu and others. There is no apparent explanation for these effects. Though it is important to note that the MCs determined in this study were most likely not at their equilibrium. With ongoing drying time, the measured MCs would be expected to reduce further.

Samples still contained considerable amounts of moisture after being medium vacuum dried at 103 °C for 1440 min. Absolute dryness of wood is – per definition – achieved with oven drying at 103 °C and atmospheric pressure until a sample's weight is constant, i.e. it changes less than 0.1 % per 2 h. Although this definition may be debated, the measured MCs of 5 – 10 % are far too high to be conceivable. Moreover, moisture that was not removed during vacuum drying at 103 °C, is removed from the samples during cKFT at 103 °C in a nitrogen stream of ambient pressure.

Bound water vapor pressure as well as bound water diffusion decrease along with decreasing MCs, which should lead to a changing drying rate over time. The drying rate is more linear than most reported drying curves. The specimens dried at an almost constant rate, whereas some kind of power law functionality would have been expected. A natural log transformation was suggested by the Design Expert software. In spite of sound statistical indicators suggesting a viable fit, the values produced by the model were not realistic. The calculated MCs that resulted from gentle drying conditions were considerably higher than the original MCs of the investigated materials. The natural log transformation was therefore dismissed.

It has been suggested by other authors (Chen 1997; Koumoutsakos et al. 2001) that the heat transfer to the sample may in fact be the governing factor as regards the drying rate. High amounts of water are expected to evaporate quickly at the beginning of the process, resulting in cooling. In the experiments conducted in this study, the contact surface between the autoclaves heated glass shell and the sample containing vials was often small and inconsistent. This was caused by the curved inner shell that did not allow for a flat consistent interface. Furthermore, the space within the autoclave was limited, making stacking of the vials necessary. The heat transfer from the glass shell, though the vacuum volume and the glass vial shell, into the sample under the conditions investigated are expected to be relatively constant over time and by that, may be the cause of the linearity of the observed drying rates. In addition, the irregular interface between the autoclaves shell and the sample vials may – to some degree – be the origin of the high

variability of the results. The direct transferability to material dried within the autoclave chamber in direct contact with the heated shell is thereby impaired.

Another possible explanation for the relatively constant drying rate is the scope of the design space that only includes measurements as early as 10 min into applying vacuum. This may have impeded the correct modelling of the drying function by natural log transformation, as was suggested by the Design Expert software. In the high vacuum drying process, high amounts of water are expected to be removed quickly at the beginning. The reduction of the drying rate would also be higher at the beginning, slowing down over time. It may be possible that this fast initial drying took place within the first minutes of drying and was not monitored by the experimental design. If this is true, the results only reflect the latter “slow” part of the drying process. This explanation is seen as less viable in the case of medium vacuum, as the corresponding samples included MCs as high or above the assumptive original.

It is also important to consider some basic gas flow mechanisms. Under high or normal pressure conditions, the mean free path of gas particles is usually much smaller than the dimensions of its confinement. By frequently colliding, the particles of that gas exchange momentum and energy. A flow is the result of a pressure gradient and is often referred to as viscous flow. In this case, a gas behaves as a continuum. The mean free path may be calculated by the following equation (3) provided by Jousten (2016):

$$\bar{l}p = \frac{kT}{\sqrt{2}\pi d_p^2} \tag{3}$$

$\bar{l}$ = Mean free path [m]
p = Pressure [Pa]
k = Boltzmann’s constant [J/K]
T = Temperature [K]
d_p = Diameter of gas particle [m]

As pressure reduces the mean free path of gas particles increases. This may continue to the point at which it is larger than the dimensions of its confinement. In that case, collisions between gas particles and the confinement wall become more frequent than particle-particle collisions. This may continue to the point where particle-particle collisions become negligible compared to particle-confinement collisions. The observable flow is referred to as molecular flow and is described by Knudsen diffusion. Knudsen numbers are dimensionless numbers, represented by the ratio of the mean free path and the dimensions of its confinement and may be calculated by equation (4) for tubular confinements. Knudsen numbers below 0.01 indicate viscous flow, whereas Knudsen numbers above 0.5 indicate molecular flow. Knudsen numbers between 0.01 and 0.5 indicate transitional flow behavior, i.e. a mixture of viscous and molecular flow.

$$Kn = \frac{\bar{l}}{d_c} \tag{4}$$

Kn = Knudsen number
$\bar{l}$ = Mean free path [m]
d_c = Diameter of confinement [m]

The vials containing the samples were pierced by a syringe with an inner diameter of 0.65 mm. The tube going from the autoclave to the vacuum pump had an inner diameter of 3 mm. Knudsen numbers were calculated with the utilized temperatures and pressures as well as a water molecule radius of d_p = 0.289 nm (Jousten 2016). The medium vacuum with a pressure of 150 mbar resulted in Knudsen numbers far below 0.01, indicating viscous flow. Yet within the syringe, the high vacuum with pressures of 1.0 and 0.1 mbar resulted in Knudsen numbers of 0.22 and 2.15, indicating either transitional or molecular flow behavior respectively. Within the tube, the high vacuum resulted in Knudsen numbers of 0.05 and 0.47, indicating transitional flow.

Molecular flow within a confinement is – within certain boundaries – independent of the surrounding ambient pressure changes. As during high vacuum experiments, transitional and molecular flow must have occurred, the effect of the pressure variations between 1.0 and 0.1 mbar are expected to be low. Furthermore, there must have been a slight pressure difference between the vials and autoclave chamber. The transferability of these results to a material dried within the autoclave chamber may thereby be impaired. The intent behind inert gas purging is to carry out remaining trapped gas molecules, which should have removed the remaining gaseous water. However, short duration purge cycles may not be sufficient for residual moisture to diffuse through the wood material, desorb and be removed.

4.5 Conclusion

It was successfully demonstrated that it is possible to govern the MC of WF and MCC within the investigated hygroscopic range, utilizing autoclave vacuum drying by controlling pressure, temperature and duration. Whereas the medium vacuum was more suitable in governing higher MCs, the high vacuum was more suitable in governing the lower end of MCs. The ranges of achievable MCs of the medium and high vacuum only overlapped in the case of MCC but not at all in the case of pine and beech. Reaching these intermediate MCs should be straight forward by applying pressures in between 1 and 150 mbar.

Drying times stay within a manageable range and can be adjusted with regards to temperature and pressure. This makes it possible and practical to manage the MCs in the full range between the initial MC and presumed dryness. The basic conclusion gathered here that higher temperature, longer duration and lower pressure lead to lower MCs is expected to be universally applicable.

The gathered results call into question some general practices concerning research of wood-water relations. Results clearly show that vacuum drying conditions and equipment

influence the drying process and resultant MCs. In order to archive very low MCs in a reasonable amount of time, high temperatures and high vacuum are a necessity. However, vacuum drying processes are often not described and considered sufficiently. The topic of heat transfer specifically appears to be widely neglected. In many cases, absolute dryness after 24 h of vacuum drying at low temperatures is just assumed. All the while, phenomena such as “trapped moisture” observed by other authors question customary definitions of “absolute dry” wood.

The precision of moisture management is somewhat restricted; as reported in earlier research, high statistical deviation was also recorded in this study. There are a number of possible reasons for this. The history of the specimen materials was highly controlled and kept constant as much as possible. Differences in sorption or treatment history are therefore deemed unlikely. Research on biomaterials has demonstrated again and again that their inherent inhomogeneity leads almost inevitably to a high deviation. The level of control that can be exerted over the MC of wood may therefore be less defined compared to some other materials such as salts.

cKFT in oven mode has shown that it is able to measure very small amounts of wood moisture. In investigations regarding applied questions or quality control, this method offers fast and reliable results. However, conditioning samples *in situ* and subsequent testing is not possible. Preconditioned samples need to be weighed and sealed. The necessity of sample handling between conditioning and vial sealing, potentially introduces irregularities and reduces control. Therefore, it should be performed preferably within an atmosphere analogous to the conditioning atmosphere or – if the former is impractical – the contact to the surrounding atmosphere should be minimized as far as possible. This is especially crucial when investigating low MCs, as dry wood and cellulose take in water vapor from the surrounding air very quickly.

In basic research, where measurements need to be repeatable with high precision, more suitable equipment should be utilized. With specialized equipment such as dynamic vacuum vapor and gas gravimetric sorption analyzers, it should be possible to further elucidate basic scientific questions, such as water retention, absolute dryness and vacuum drying dynamics. The question whether EMC during vacuum drying is dependent solely on absolute pressure or RH remains unanswered. The contradictory results from prior studies and the overall limited amount of research performed in this field make further investigations in this area necessary.

5 Reactions between $AlMe_3$ and Wood

5.1 Introduction

Metallocene based catalysts for olefin polymerization are known to only perform well and exhibit high activities in combination with oxygen containing aluminum alkyls such as MAO (see Chapter 3.5). However, the market penetration of MAO is hindered by its high cost. Efforts to develop highly active but economical alternatives have been strong in the past decades (Ittel et al. 2000; Severn et al. 2005). Aluminum alkyls such as $AlMe_3$ are more economical and may possess unexploited potentials.

The hygroscopic behavior of cellulosic materials makes them potential carriers of low amounts of water for the partial hydrolysis of $AlMe_3$, as regards the *in situ* synthesis of an active MAO-species for metallocene-catalyzed ethylene polymerization. Therefore, the suitability of WF as a low-cost water carrier for *in situ* MAO synthesis and subsequent catalyst immobilization for olefin polymerization was investigated.

Results from Chapter 4 show how the amount of residual water within cellulose and wood can be fine-tuned by the varying the vacuum drying parameters. The ratio of $AlMe_3$ to water is known to be critical for the formation of an active MAO species (see Chapter 3.5). However, knowledge of MC has been reported to not directly translate into its availability for reaction with $AlMe_3$. In addition, the functional groups of cellulosic materials allegedly offer suitable reaction sites for the immobilization of homogeneous catalysts but the depletion of catalytic agents, due to reactions with functional groups, also needs to be accounted for (see Chapter 3.6). The question of hydroxyl accessibility for reaction with $AlMe_3$ is more ambiguous than one might think and needs to be addressed. The complex nature of wood makes the consideration of the following factors necessary:

The wood constituents are rich in hydroxyl groups, but also contain considerable amounts of carbonyl, carboxyl, acetyl and methoxy groups (Lin and Dence 1992; Wagenführ 2006) that may participate in reactions. Cellulose makes up the largest portion of wood, i.e. up to 45 %, and contains one primary and two secondary hydroxyl groups, i.e. more hydroxyl groups per weight compared to lignin and hemicelluloses (Engelund et al. 2013). The reactivity of these three hydroxyl groups is not equal. Their involvement in hydrogen bonding and the dispersive forces caused by the proximity of neighboring atoms impart differences in reactivity. Additionally, the rotational freedom of the C-6 hydroxyl distinguishes it from the other two. It is important to note that cellulose and sugars do not behave equally in their types of reaction, which is ascribed to steric effects (Kalia et al. 2011). The research concerning cellulosic hydroxyl groups is ambiguous, reporting indiscriminate reactivity (Habibi 2014) as well as differences in reactivity of the three groups (Hebeish and Guthrie 1981; Faix 2004; Fox et al. 2011).

The reaction media also affects hydroxyl reactivity. Cellulose hydroxyls have been shown to be much more reactive in a solution as dissolution breaks apart the hydrogen bonding network, making more hydroxyls accessible for reaction (Fox et al. 2011). In homogeneous processes, a cell wall constituent is dissolved in a suitable solvent and reactions may occur uniformly along all individual glucose polymers (Hebeish and Guthrie 1981). In

contrast, cellulose dispersed in non-polar media not only tends to agglomerate, which reduces accessibility, but undergoes surface passivation, i.e. surface hydroxyl groups are less reactive (Johansson et al. 2011).

Additionally, the accessibility of functional groups on the surface is higher than in the bulk material, and within the bulk material is higher in amorphous regions than in crystalline regions (Hebeish and Guthrie 1981). The degree at which $AlMe_3$ is able to penetrate the wood substrate is unknown. Triethylamine as well as toluene was shown not to penetrate and swell the CW (Rowell 1984; Mantanis et al. 1994). It is reasonable to assume that $AlMe_3$, whether pure or in toluene solution, does not penetrate into the CW to a large extent and reactions are limited to the substrate surface.

The ambiguous behavior of wood upon drying adds to the already presented complexity. Conventional terms such as hornification and surface inactivation describe the fact that the reactivity and accessibility of wood are not constant but change with time and particularly depend on its treatment history. Hornification – a term used in the pulp and paper industry – is associated with the irreversible stiffening and loss of swelling capabilities of chemical pulps as result of drying, reducing the ability to form inter-fiber bonds (Laivins and Scallan 1996). This is often attributed to the collapse into hydrogen-bonded configurations that cannot be fully re-wetted by water, progressing crystallization as well as strong physical cross-linking between microfibrils. The degree of hornification is said to be dependent on the degree of lignin removal and hemicelluloses during pulping, i.e. a higher degree of removal increases the tendency to hornify (Minor 1994; Hult et al. 2001; Fernandes Diniz et al. 2004; Idström et al. 2013). Oddly, similar phenomena, namely the loss of hygroscopicity and the lowering of the EMC at a given RH upon first drying, are also well known in wood (Skaar 1988). The severity of this has been shown to be dependent on the drying and rewetting procedure (Hoffmeyer et al. 2011). The re-organization rate of amorphous cell wall constituents relative to the rate of drying, i.e. the mobility of amorphous polymers as a function of MC and temperature, is proposed to be one important factor. Controversially, vacuum saturation with liquid water was found to restore the hydroxyl accessibility to a degree equal to that of its native, never-dried state (Thybring et al. 2017), challenging the idea of cross-linking and irreversibility. The inactivation of wood surfaces – a phenomenon well known in the plywood and wood based panel industry – describes the reduced ability of adhesives to wet and penetrate wood surfaces, as well as to cure due to chemical and physical changes, often introduced by drying or aging (Ross 2010). Presumed causes are the diffusion of extractives to the surface, the reorientation of surface molecules turning their less polar side outwards, as well as oxidation and pyrolysis (Christiansen 1990, 1991; Sernek 2002; Frihart and Hunt 2010). The precipitation of airborne contaminants has also been observed (Johansson et al. 2011).

Carbohydrates have been used in *in situ* Polymerization and Polymerization Filling Technique processes analogous to the intended investigations of this study before and have been described in Chapter 3.6.

Gas development is often measured in chemistry or biology to give information on the conversion during chemical and biochemical processes (Dubois et al. 1998; Wegner

2009; Schimpf 2014; Rosehr and Luinstra 2017). $AlMe_3$ and MAO readily react with water as well as functional groups that contain oxygen, such as hydroxyl- and carboxyl-groups. As a product of these reactions, methane is eliminated (Scheel 2014; Rosehr 2019). The methane development provides stoichiometric information on the hydrolysis reaction (Collins et al. 1992).

Mende (1981) observed that gas generated by the reaction between $AlMe_3$ and starch was related to the MC of starch. The reaction with moist starch led to distinct gas development. In the case of dry starch, no methane development was observed. Mädler (1987) investigated the gas generated by the reaction between $AlMe_3$ and native corn starch, amorphous corn starch and MCC. At -10 °C and after 120 min, native starch with a MC of 3.65 % generated very low amounts of methane of 0.175 mol/mol of water. On the other hand, native starch with a MC of 13 % generated 1.1 mol/mol methane, approximately equal to the amount of contained water. Higher treatment temperatures led to more methane development over time. Amorphous starch with a MC of 6 % generated considerably higher methane than native starch with a MC of 13 %, showing that the molecular assembly influences the amount of reaction. The water molecules contained in amorphous biomolecules may be more mobile and available. In addition, the hydroxyls may be more reactive. MCC with a MC of 4.7 % was tested at -20 °C and was found to reach its peak gas generation after only 20 min, with a methane to water ratio of 1.3 mol/mol. Regarding MCC it is worth noting that, in dependence of source material and manufacturing process, the amount of amorphous cellulose surrounding the cellulose crystals is reduces. Thereby the degree of crystallinity of MCC is generally higher than of native cellulose and can be as high as 80 % (Trache et al. 2016). The crystalline regions of cellulose are thought to be impenetrable for water. It is therefore conceivable that water is largely contained on the outside of the MCC grains where it is accessible, facilitating fast turnover. These prior results indicate that dry carbohydrates do not react with $AlMe_3$ or MAO to a large degree; they further show that chemically, seemingly similar carbohydrates perform very differently. The conundrum as to whether these differences are due to more mobile and available moisture, to higher hydroxyl accessibility and reactivity or a mixture of both remains unresolved.

Furthermore, in filtration experiments it was observed that neither $AlMe_3$ nor MAO adhered to dry starch in large quantities (Mende 1981; Dutschke 1985). In ISP, using dry starch in combination with MAO, the encapsulation of the starch grains appeared less consistent and homogeneous polymerization occurred simultaneously (Mende 1981). This coincides with Spottog (pending) where polymerizate synthesized with MAO, which was presumably anchored to thoroughly dried WF, exhibited some segregation of wood and polymer fraction. This leads to the conclusion that only little reaction occurs between the hydroxyls of thoroughly dried starch or wood and the aluminum components. However, Spottog also observed no active polymerization when MAO in small amounts of 0.2 mmol/g were used in the presence of thoroughly dried WF. This in turn indicates the occurrence of some kind of interaction.

In light of the described phenomena, making credible predictions on the amount of reaction between $AlMe_3$ and wood based only on prior moisture measurements is hardly possible. Past research indicates low transferability of results. The author is not aware of

any prior research, where the reaction between wood and $AlMe_3$ has been regarded separately in more detail. To generate data more specific to the material and methods used in this study, independent experiments were needed. Here, gas titration experiments are intended to quantify the overall hydrolysis reaction taking place between $AlMe_3$ or MAO and wood as a function of wood filler drying pretreatment.

5.2 Experimental

5.2.1 Materials

5.2.1.1 Cellulosic Materials

The **wood flour** “Arbocel C100” (J. Rettenmaier & Söhne GmbH & Co. KG, DE) was used in the gas titration experiments. According to the producer, it features a particle size distribution between 70 µm and 150 µm and primarily cubical particle morphology. C100 is derived of varying proportions of spruce, pine and fir wood and contains lignin. The bulk density is between 140 – 200 kg/m³ and the true density is approximately 1.5 g/cm³.

The C100 was extracted prior to all further experiments. By extracting solvable components (refer to Chapter 3.1) from the WF utilized in the following experiments, it was intended to prevent these components from influencing the subsequent investigations in any way. The extractor utilized was of a Soxhlet design and the solvent used was xylene. The extraction was carried out for 4 h. According to Faix (2008), the extraction of wood with non-polar solvents such as petroleum ether or diethyl ether would remove fatty acids, fats, sterols, sterol esters, hydrocarbons and terpenes, as well as resin acids from softwood. As xylene is also non-polar, it is expected to remove analogous fractions.

5.2.1.2 Chemicals

Acetone 99 %, denatured **ethanol** 96 %, **isopropyl alcohol** 99 % (all from BCD Chemie GmbH, DE) and an isomeric mixture of **xylene** ≥97 % (Carl Roth GmbH und Co. KG, DE) were used for cleaning, quenching and extraction purposes.

Toluene 99 % (BCD Chemie GmbH, DE) was purified by distillation and passing through columns filled with a 4 Å molecular sieve as well as the PuriStar R3-11G catalyst (BASF SE, DE).

5.2.1.3 Cocatalysts

Trimethylaluminum was purchased in two forms, pure (Prod. No. 257222-100G, Sigma-Aldrich, subsidiary of Merck KGaA, DE) and as a 2 mol/l toluene solution (Prod. no. 198048, Sigma-Aldrich, subsidiary of Merck KGaA, DE).

Despite its name and its basic formula, trimethlyaluminum is actually arranged as the dimer Al_2Me_6, where both molecules are connected by two 3-center-2-electron bonds.

5.2.1.4 Gases

Grade 5.0 **Nitrogen** 99.999 % (Linde GmbH, DE) was used as inert gas.

5.2.2 Gas Titration

The gas titration apparatus (Figure 18) was adapted in close reference to the directive 4630 of *The Association of German Engineers* (Verein Deutscher Ingenieure e.V. VDI 4630), where apparatuses such as eudiometers and gas sampling tubes are described. It consisted of a single-neck Schlenk-flask, equipped with a pressure-equalizing dropping funnel hermetically connected to a gas collecting tube. The collecting tube contained a barrier liquid, in this case water, and was connected to an equalizing tank, both together acting as a liquid column. The Schlenk-flask contained a stir bar and was placed into an oil bath sitting on top of a magnetic stirrer.

The standard gas titration methods is as follows: The flask and the funnel each contain one of the reagents in liquid form, which take part in the gas developing reaction. The reaction is started by releasing the content of the funnel into the flask. The developing gas then extends and displaces the liquid column in the collecting tube. In due consideration of gas temperature and pressure, the volume of the displaced liquid can be used to calculate the chemical amount of gas that has developed.

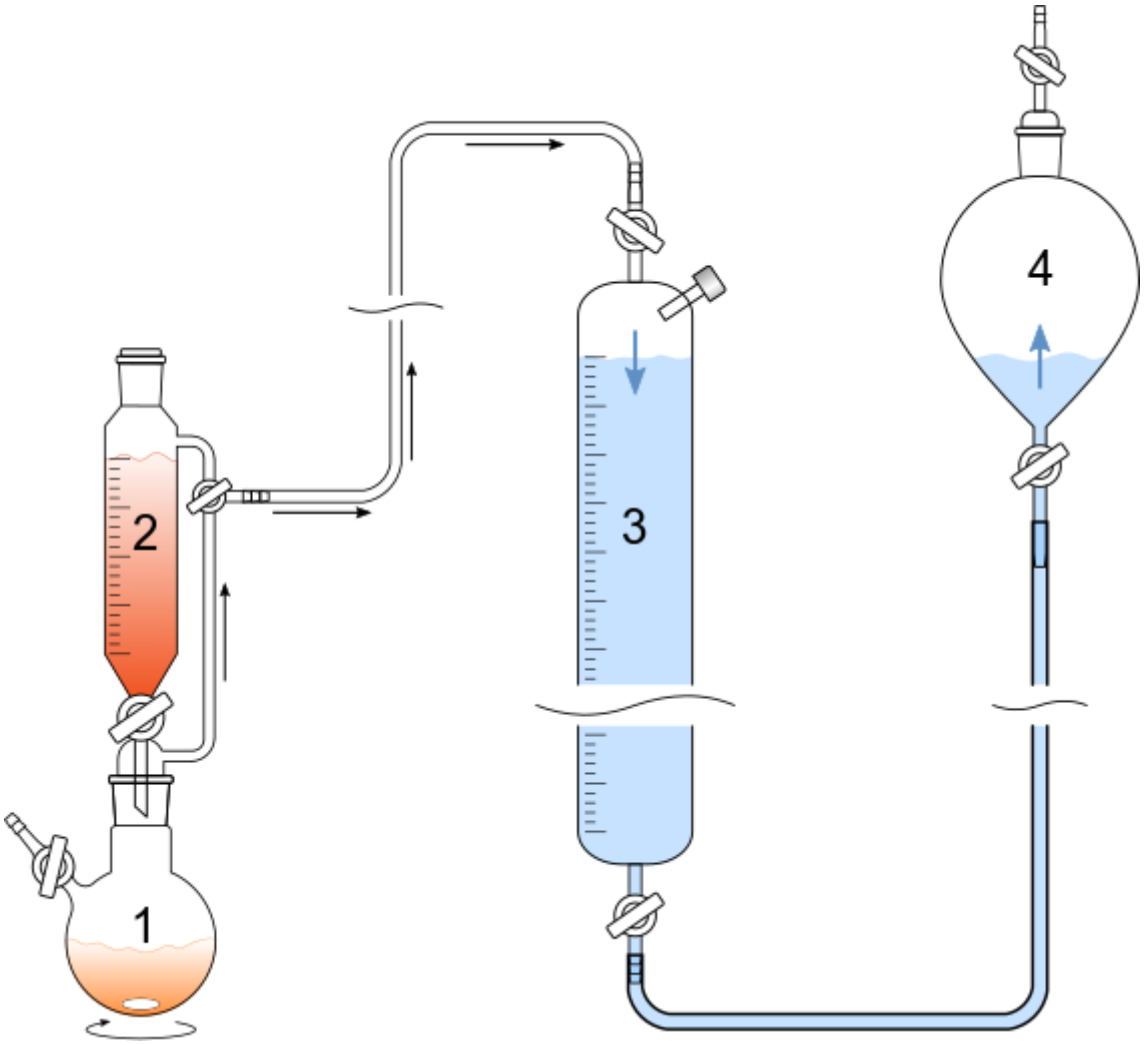

Figure 18: Gas titration apparatus.
(1**) Schlenk flask; (2) Dropping funnel; (3) Collecting tube; (4) Equalizing tank.**
Black arrows indicate gas flow; Blue arrows indicate barrier liquid level movement.

5.2.3 Procedure

The following considerations were made to determine the outlines of the experiments:

As per definition by the *German Industry Standard* for the determination of the MC of solid wood by oven drying (Deutsches Institut für Normung DIN EN 13183-1:2002-07), wood is absolutely dry after oven drying at 103 °C when a constant weight is reached. For wood species containing volatile compounds, vacuum drying at a maximum temperature of 50 °C is recommended. The temperature of 103 °C was chosen as the “high” drying temperature. As the temperature control was restricted to heating only, a temperature above ambient, in this case 30 °C, was chosen as the “low” drying temperature value. The measured gas development after “low” temperature drying would be associated to the reaction of $AlMe_3$ with the wood substrate, free and bound water, as well as remaining wood extractives. On the other hand, the gas development after “high” temperature drying would be associated to the wood substrate and remaining extractives only. Drying was performed for 120 min in all cases. According to the actual factor equation determined in the previous section (Chapter 4) for high vacuum and pine wood, these conditions would lead to respective MCs of 2.40 and 0.08 %, i.e. 6.66 and 0.22 mmol.

All titrations were performed at an ambient temperature or 30 °C for 35 min until gas development reached a plateau. In chosen experiments, a temperature increase to 60 °C was performed and gas development was logged for another 35 min, again until a plateau was reached. This was done to investigate if a temperature increase after the initial gas development had come to a halt would lead to further reaction. This is important if in a polymerization process, the $AlMe_3$ treatment temperature and polymerization temperature are chosen differently. If no further reaction is detected, the amount of $AlMe_3$ does not need to be adjusted accordingly. If in fact a temperature increase leads to further gas development, a polymerization temperature change would need to be accommodated by adjusted $AlMe_3$ addition. Blank titrations without $AlMe_3$ or MAO were performed, in order to account for gas expansion and evaporation. The blank values were subtracted from the actual measurements.

The gas titration experimental setup resultant from the previous considerations comprised of three main steps. Table 5 lists the three steps with the corresponding control and independent variables.

Table 5: Workings steps and settings of gas titration experiments.

Steps	Variables	Values	
Drying	Wood amount:	5 g	Const.
	Vacuum:	High*	Const.
	Time:	120 min	Const.
	Temp.:	30 and 103 °C	Categorical, ordinal
Al addition	Procedure:	1- or 5-step	Categorical, nominal
	Substance:	AlMe3 or MAO	Categorical, nominal
	Amount:	Excess or zero	Numeric, discrete
	Temp.:	30 °C	Const.
Gas development	Intervals:	5 min	Const.
	Time:	70 min	Const.
	Temp.:	30 to 60 °C	Numeric, discrete

* Rotary vane pump achieved pressure between 1.2 and 0.2 mbar

The **drying step** was performed within the same flasks which were later used for the titration. The flask was connected to a vacuum-gas-manifold (Schlenk line) for the direct application of vacuum and nitrogen. The MC of the C100 stock was determined before each experiment using an IR-moisture analyzer scale (MLS-D, Kern & Sohn GmbH, DE). The weighted portion of each experiment was corrected for moisture and represents dry weight. 5 g of C100 were placed into a flask and vacuum dried for 120 min. The vacuum was kept as constant as possible and ranged from 1.2 mbar at the beginning to 0.2 mbar at the end of the drying cycle. In the first series the drying temperature was not actively controlled but the ambient temperature was logged. In the following series the two drying temperatures, 30 and 103 C, were investigated. After drying three purge-and-refill cycles were applied using nitrogen.

Thereafter, 100 ml of dried toluene was added to the WF containing flasks and 50 ml of Al/toluene solution was filled into the funnel of the titration apparatus. The wood-toluene containing flask was then attached to the funnel. All these steps were carried out under a nitrogen countercurrent.

The **aluminum addition** was carried out at an ambient temperature of 30 °C. The effect of the rate at which the Al-solution was added, was investigated by comparing a 1-step to a 5-step process. Analogous titration experiments were carried out with $AlMe_3$ and MAO, which were added in excess, in order to allow for maximum gas development. The Al-concentrations investigated ranged from 20 to 260 mmol/l, which corresponds to an Al to wood ratio between 0.6 to 7.8 mmol/g. Blank measurements of analogous gas titration experiments were carried out without any aluminum source, in order to account for gas generation or expansion caused by other factors.

The **gas development** was measured every 5 min for 70 min; after 35 min the temperature of the oil bath was raised from 30 to 60 °C. The oil bath temperature as well as the ambient temperature were logged and the chemical amount of the produced methane was calculated according to the general gas equation. Gas volume, ambient temperature and standard atmospheric pressure were measured and used as input values.

The gas titration experiments were divided into four series, which are displayed in Table 6 and will be described in more detail below.

Table 6: Gas titration experiments investigated independent variables.

Series	Drying temp. [°C]	Al substance	Al Amount [mmol]	Procedure
1	Ambient	AlMe3	3	1- and 5-step
2	30, 103	AlMe3	10	1-step
3	30, 103	MAO	20	1-step
4	30, 103	-	-	-

In the **first series**, the mode of addition was investigated, in order to assess the influence it may have on the hydrolysis reaction. The amount of aluminum solution was chosen in consideration of the average amount of reaction recorded in pilot experiments, in which an excess of aluminum was used. 50 ml $AlMe_3$/toluene solution was added in a 1-step and a 5-step process. In the 5-step process each addition was 5 min apart. The gas development was logged for 35 min and compared to titrations where the $AlMe_3$/toluene solution was added in one step only. If the gas development at the beginning of the experiment exceeded an equivalent of one reaction per $AlMe_3$ molecule, it would be clear that either the moisture or the $AlMe_3$ molecules were mobile and could migrate or diffuse. If then the final gas development was comparable to that of the analogous one step process, chemical rearrangement must be possible, moving towards an equilibrium. The latter would mean that the final state of the reaction between wood and $AlMe_3$ is somewhat independent of the rate at which they are brought together. If the final gas development were to differ significantly, the process at which the $AlMe_3$ is added would influence the final state of the product from the reaction. The 1-step process was the first series to be conducted and was measured nine times, in order to assess the reproducibility. Four measurements were conducted in the 5-step process.

In the **second series**, 50 ml $AlMe_3$/toluene solution was added in 1-step. A surplus of $AlMe_3$ was used to investigate the maximum gas development and its deviation. Experiments with WF dried at 30 and at 103 °C were conducted. The gas development at 30 °C was logged for 35 min, after which the temperature was raised to 60 °C and the gas development was logged for another 35 min. Four experiments per WF drying temperature were conducted.

In the **third series**, 50 ml MAO/toluene solution was added in 1-step. This was done, in order to investigate the potential differences when compared to $AlMe_3$. To account for the larger and possible less mobile molecules compared to $AlMe_3$, a higher amount of MAO was used. As a general prediction, they should generate very similar values and trends. However, slight variations may be caused by the fact that the WF used here was from another batch. Experiments with WF dried at 30 and at 103 °C were conducted. The gas development at 30 °C was logged for 35 min; then the temperature was raised

to 60 °C and the gas development was again logged for a further 35 min. Two experiments per WF drying temperature were conducted.

In the **fourth series**, 50 ml of neat dried toluene was added in one step. This series was performed to attain blank values, in order to account for gas expansion and evaporation caused by the varying temperatures during the experiment. These gas titration experiments were conducted analogous to the second and third series. Two experiments per WF drying temperature were conducted.

5.3 Results

Figure 19 displays the gas development caused by the 1-step addition of $AlMe_3$-toluene solution to WF dispersed in toluene at ambient temperature. The black line chart represents the hypothetical gas development corresponding to the sum of one reaction per molecule over the total amount of available $AlMe_3$. It is shifted slightly to the right to visualize that the aluminum solution was added after the first measurement at 0 min was taken. The colored dots represent measurements taken from nine repeated runs with WF vacuum dried at ambient temperature.

After 5 min the gas development is lower than one reaction per added $AlMe_3$ molecule. After 10 min gas development starts to equal and, as time goes on, surpasses one reaction per $AlMe_3$ molecule. After 35 min the gas development deviates around one reaction per $AlMe_3$ molecule with a range of 0.39 … 0.59 … 0.74 mmol/g. The standard deviation is at 0.12 mmol/g. All nine experiments were conducted within one month and ambient lab temperatures ranged from 22 to 29 °C. However, low and high gas development occurred independent of the ambient temperature. The variability also occurred between two measurements conducted on one single day, where the ambient temperature was constant. The raw data from the first series 1-step gas titration experiments can be found in the Annex (Table 28).

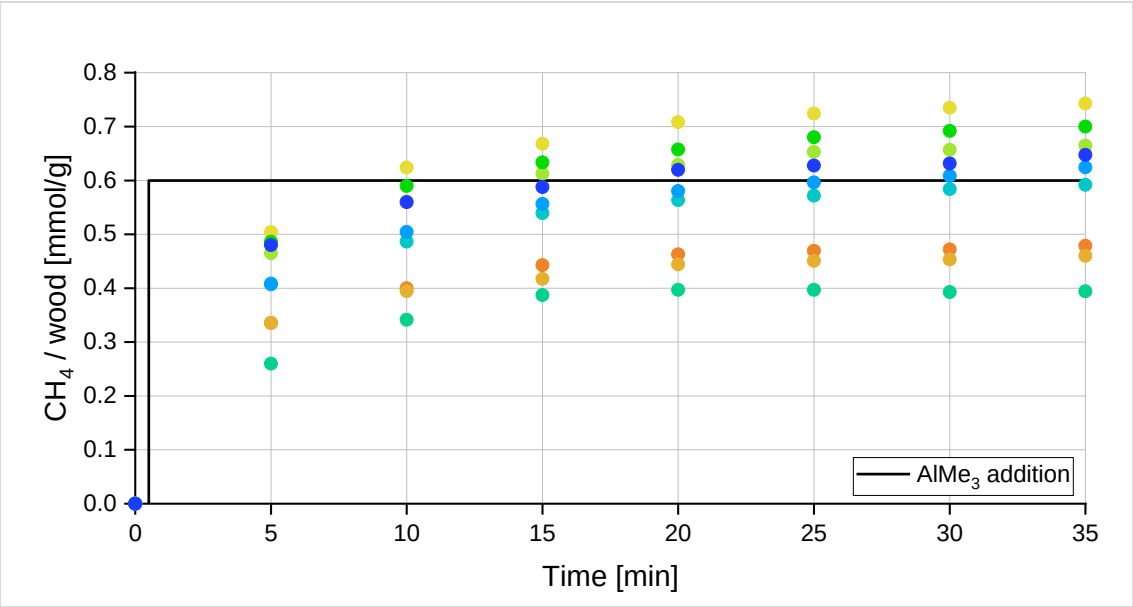

Figure 19: Results from 1-step procedure experiments as in methane developments per wood mass as function of time after one single additions of $AlMe_3$.

Figure 20 displays the gas development caused by the 5-step addition of $AlMe_3$/toluene solution to 5 g of WF dispersed in toluene at 30 °C. The measurements of gas volume, oil bath temperature and ambient temperature were taken just before the $AlMe_3$ additions. Again, the black vertical step chart represents the hypothetical gas development corresponding to the sum of one reaction per molecule over the total amount of available $AlMe_3$. It is shifted slightly to the right to visualize that the aluminum solution was added after the consecutive measurements were taken. The colored dots represent measurements taken from four repeated runs with WF vacuum dried at ambient temperature. 10 ml of aluminum solution was added at 0 min, containing a total of 0.6 mmol $AlMe_3$. Four further additions were performed 5 min apart each, reaching the final amount of 3.0 mmol at 20 min. The comparison of the black line vertical step chart to the colored dots elucidates if more, less or equal than one reaction per $AlMe_3$ molecule occurred.

The gas development after 5, 10 and 15 min surpasses one reaction per $AlMe_3$ molecule and at 20 min the gas development equals one reaction per molecule. At 25, 30 and 35 min the gas development is slightly lower than one reaction per single Al-molecule. The final gas development range is 0.45 … 0.48 … 0.52 mmol/g, given as minimum, mean and maximum value. The standard deviation is at 0.03 mmol/g. All four experiments were conducted on two successive days and ambient lab temperatures were fairly constant at 26 °C. The range of the measured gas development is much smaller than in the 1-step process. However, the results are well within the range of the 1-step results, which suggests similarity. The raw data from the first series 5-step gas titration experiments can be found in the Annex (Table 29).

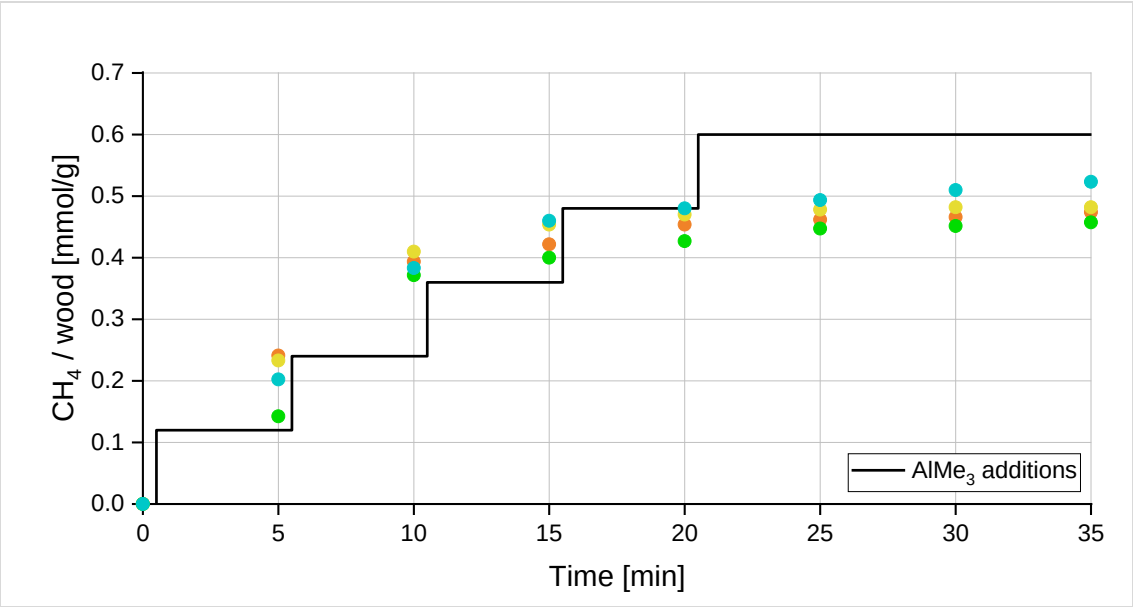

Figure 20: Results from 5-step procedure experiments as in methane development over wood mass as function of time after five successive additions of $AlMe_3$.

Figure 21 aggregates the results from the second, third and fourth series gas titration experiments. The gas development at an oil bath temperature of 30 °C was logged for 35 min, after which the temperature was raised to 60 °C and the gas development was logged for a further 35 min. The results of $AlMe_3$ and MAO in combination with WF dried at 30 and at 103 °C are displayed. All sets of measurements were corrected by subtracting the blank measurement values gathered in series four.

In the case of vacuum drying at 30 °C, the gas development reached a plateau after around 30 min. This may not be obvious when considering the progression of the graph displayed, however, the logged raw gas volume changes after around 30 min were at the limit of what was technically distinguishable with the utilized equipment. After the temperature increase, the gas development again reaches a plateau after around 30 min.

In the case of vacuum drying at 103 °C, the gas development in the first 35 min was very low and at the limit of what was technically measurable with the utilized equipment. In the second 35 min the gas development increased slightly.

All blank measurements from the fourth series showed comparatively steep increases in gas development between 40 and 60 min. After blank-correcting the gas developments, a dip in gas development at 55 min could be observed in the light blue, green and yellow line. The same effect was present in the case of the orange line, but was less pronounced. The steep increase of the blank values seemed to follow the increasing oil bath temperature by approximately 5 min.

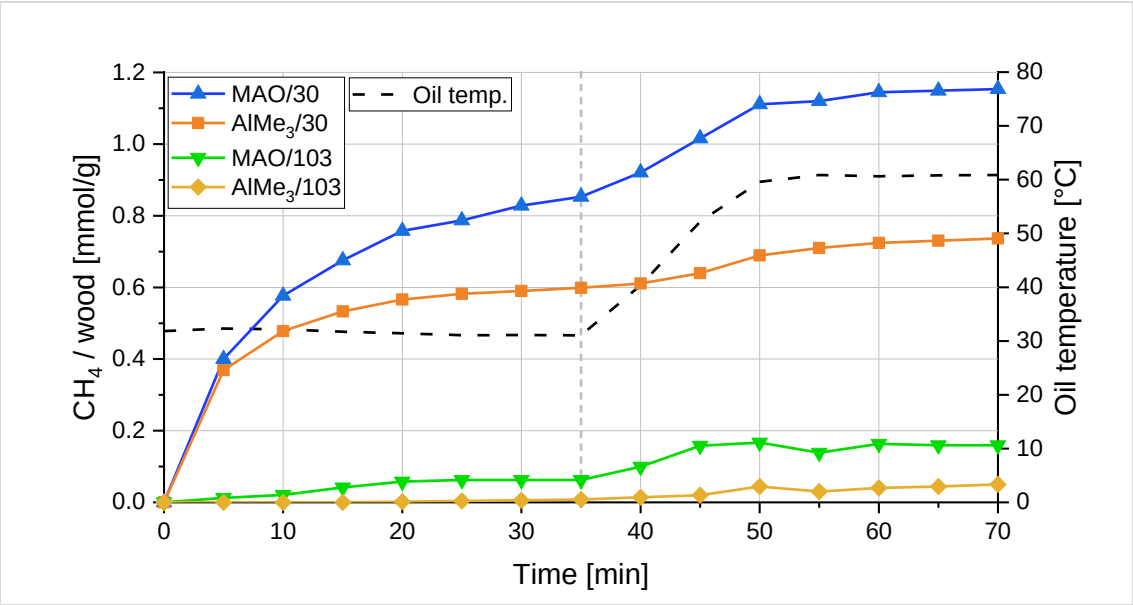

Figure 21: Summarized results from gas titration experiments – Methane development per wood mass as function of time and temperature-change after one single $AlMe_3$ addition. Vertical dashed line marks the moment of temperature setting change.

Table 7 displays the mean average gas development, the standard deviation and the coefficient of variation after 35 and 70 min of reaction time. The mean and SD of $AlMe_3$/30 °C after 35 min closely match the values from the first series, where the mean and SD were at 0.59 and 0.12 mmol/g respectively. In spite of the high statistical deviation observed, the repeatability appears to be valid. This suggests that the high statistical deviation is somewhat inherent to the applied method. The statistical deviation is not the same in all experiments. However, only two experiments with MAO per drying temperature were conducted. These could be conducted on the same day, increasing control over environmental factors and potentially reducing deviation. The four $AlMe_3$ experiments per drying temperature had to be stretched over several days, which made controlling all external factors more difficult, potentially increasing deviation. Owing to the fact that the measured values in the case 103 °C vacuum drying were at the limit of what was technically measurable, the relevance of the corresponding statistical deviation should not be overestimated.

Even though the overall behavior is similar, it is evident that the gas generated by MAO is elevated in comparison with $AlMe_3$. The average gas developments per gram of wood dried at 30 °C after 35 and 70 min are a respective 41.67 % and 64.35 % higher. The average gas developments per gram of wood dried at 103 °C after 35 and 70 min are a respective 6x and 3.2x higher.

Table 7: Aggregated corrected gas development data from the second and third series.

Al-source and drying temp.	Gas dev. after 35 min and 30 °C [mmol/g]			Gas dev. after 70 min and 60 °C [mmol/g]		
	Mean	SD	CV	Mean	SD*	CV**
$AlMe_3$/30 °C	0.60	0.11	0.18	0.74	0.13	0.14
MAO/30 °C	0.85	0.07	0.08	1.15	0.10	0.07
$AlMe_3$/103 °C	0.01	0.02	0.82	0.05	0.02	0.10
MAO/103 °C	0.06	0.00	0.01	0.16	0.00	0.01

* Standard deviation; ** Coefficient of variation

WF dried at 103 °C did not appear to offer large quantities of accessible and reactive hydroxyl groups for $AlMe_3$ or MAO to react with. This is again surprising, as wood should offer an abundance of hydroxyls for reaction. Under the assumption of absolute dryness, the measured values would directly correspond to reactions with wood.

Furthermore, the temperature increase from 30 to 60 °C after 35 min lead to a distinct increase in gas development in all experiments. In the case of $AlMe_3$ and MAO, the average gas developments per gram of wood dried at 30 °C increased by a respective 23.33 % and 35.29 %. The average gas developments per gram of wood dried at 103 °C increased a respective 5x and 2.6x.

5.4 Discussion

Considering the actual factor equation for pine wood determined in Chapter 4, the MCs of the WF dried at 30 °C would be 2.40 %. Per 1 g this corresponds to 23 mg or 1.30 mmol of water. As $AlMe_3$ was provided in excess, it is thought unlikely that an available and mobile water molecule would only undergo one reaction. Each water molecule can participate in two hydrolysis reactions, doubling the methane generation potential to 2.60 mmol. The MC of WF dried at 103 °C would be 0.90 %. Per 1 g this corresponds to 9 mg or 0.49 mmol of water. The methane generation potential of that amount of water is 0.98 mmol. Table 8 compares these values to the determined methane development.

Table 8: Comparison of amount of water according to cKFT and amount of methane development from gas titration.

	Drying temp.	30 °C		103 °C	
	Reaction time	35 min	70 min	35 min	70 min
cKFT	**H_2O [mmol] (1x/2x)**	1.30 / 2.60		0.49 / 0.98	
$AlMe_3$	**CH_4 [mmol]**	0.60	0.74	0.01	0.05
MAO	**CH_4 [mmol]**	0.85	1.15	0.06	0.16

It is evident that in all experiments less methane was generated than the theoretic amount of water and far less than the calculated potential, which is more pronounced in

the case of very low MCs. These results coincide favorably with findings of earlier studies, where, the lower the MC of native starch was, the smaller the portion of that water seemed to be available for reaction with $AlMe_3$ (Mende 1981; Mädler 1987) This is supported by observations were dry starch did not react at all with $AlMe_3$. Findings of trapped or hard to remove water in cellulosic materials substantiate this further (Hergt and Christensen 1965; Hill et al. 2015).

The confinement in the cKFT experimental setup was not equal but tighter than in the gas titration experiments, leading to somewhere in between molecular or transitional flow behavior. In the gas titration experiments, the flow behavior in the tighter parts of the apparatus were in between transitional and viscous. The different flow behaviors could possibly lead to lower residual moisture in the gas titration experiments than in cKFT. Three nitrogen purge-and-refill cycles were applied after every drying cycle, in order to equalize these potential differences.

The occurrence of $AlMe_3$ as dimer may cause one associated molecule to be immobilized by the other, leading to less mobile Al-molecules available to react with immobile reaction sites. The 5-step experiment showed that $AlMe_3$ is able to react more than once per molecule. Also, the rate of addition did not seem to affect the overall gas development. Furthermore, $AlMe_3$ was provided in excess in the third series. There was no evidence that the amount of $AlMe_3$ affected the methane development in the range investigated. The dimerized form of $AlMe_3$ does not seem to prevent single molecule mobility and is therefore unlikely to be responsible for the low methane development.

The reaction between MAO and wood also generates less methane than the theoretically available amount of water, but it generates considerably more methane than the $AlMe_3$. There are two possible explanations. Under the assumption that bound water mobility and accessibility is the same for both Al-reagents, it is likely that a large proportion of the higher gas development is due to reactions between wood hydroxyls and MAO. On the other hand, under the assumption that some water molecules may be adsorbed on the wood particle surface more closely than others, the ability of $AlMe_3$ and MAO to wrench off closely bonded molecules may be different and thereby lead to different methane generation. In both cases, the presence of oxygen in the Al-component may lead to higher intermolecular interaction with adsorbed water and hydroxyls alike. Another possible explanation for the higher gas generation by MAO could be the fact that the WF used in series three was from another batch. The composition of that second batch may be of a slightly different composition and thereby have caused the variation.

The methane development of MAO after a treatment time and temperature of 70 min and 60 °C in combination with WF dried at 103 °C amounted to 0.16 mmol/g. This coincides with results gathered by Spottog (pending). She used WF that was vacuum dried for two hours at 85 °C. She observed no active ethylene polymerization when 0.2 mmol/g of MAO were used. The next higher MAO amount of 0.4 mmol/g led to active polymerization. This substantiates that thoroughly dried WF seems to adsorb or react with only small amounts of MAO.

In earlier studies, $AlMe_3$ and MAO did not appear to react with or adhere to starch or wood dried at high temperature (Spottog pending; Mende 1981; Dutschke 1985; Mädler

1987). This is in agreement with the results of this study, where almost no gas development was detected with wood dried at a high temperature. However, in these earlier studies, $AlMe_3$ did adhere to moist biofillers and de-mixing of the received composite material was observed. This is where the phenomena of hornification and surface inactivation introduces the possibility of a more complex combination of dependencies. The reactivity of wood hydroxyls is reduced by intensive drying. This means it remains possible that $AlMe_3$ and MAO react with hydroxyl groups at higher MCs but much less at lower MCs. Adding to this complexity, the reactivity of thin molecular layers of water is known to be considerably lower than that of bulk water (Fumagalli et al. 2018). This means that at higher MCs, thicker layers of sterically available surface bound water might react more readily with $AlMe_3$ and MAO than thinner layers at lower MCs. Intensive drying would lower the reactivity of both the remaining bound water and the hydroxyl groups. The observed rapid decrease of the amount of reaction following intensive drying may therefore be caused by a combination of these two phenomena.

In the case of moist wood, water forms molecular layers that potentially shield wood hydroxyls from the non-polar solvent, retaining their mobility. This phenomenon is supported by separate experiments, where moist WF formed a discrete phase from toluene whereas dry WF was readily wetted by and dispersed in toluene. A grouping of wood-hydroxyl and hydrogen bonded water molecules could be more responsive to $AlMe_3$. A hydrolysis reaction with the water molecule would result in an $AlMe_2OH$ product. Hydrogen bonds could be formed between the Al-hydroxyl and the wood hydroxyl, which are in close proximity to one another. The enhanced compatibility and reduced distance could also facilitate actual reaction with the wood hydroxyl. On the other hand, dry wood hydroxyls may undergo passivation in toluene. They may be overall less reactive but especially unreceptive for $AlMe_3$ absent of any oxygen.

The temperature rise during titration led, in all cases, to increased methane development, i.e. more hydrolysis reaction. This could be due to the temperature induced emission of water previously bound within the bulk material. In Chapter 4, samples vacuum dried at 103 °C emitted additional moisture at ambient pressure and 103 °C. However, the assumption that wood dried in high vacuum at 103 °C emits additional water upon a temperature increase from 30 to 60 °C under ambient pressure conditions, appears somewhat odd. Again, this could also be due to changes in accessibility, mobility and reactivity of residual moistured and hydroxyl groups. Another possible explanation could be the faster reaction rate at higher temperatures. This could lead to the observed increase in reaction reaching a level that would take more time to reach at lower temperatures.

The results of the gas titrations were subject to high variations. These variations did not seem to follow a particular pattern and no external variable could be identified as cause. High variations were also reported by other earlier studies. Gas titration is known to be a delicate method, biomaterials are generally inhomogeneous and the MC recorded in Chapter 4 also displayed variability. A combination of these effects could be the cause of the exhibited statistical deviation. Nevertheless, the matching average gas development of temporary, separately conducted analogous test series indicate high repeatabil-

ity. This means, in combination with the findings of the results of cKFT, it appears possible to exercise a certain amount of control over MC and amount of hydrolysis reaction by vacuum drying.

5.5 Conclusion

Gas titration experiments were successful in showing that by adjusting MC of WF by altering vacuum drying conditions the amount of hydrolysis reaction between WF and aluminum alkyls, such as $AlMe_3$ and MAO, can be controlled. This verifies the possibility of using wood as carrier of moisture for subsequent chemical reactions. The gathered data on gas development, i.e. amount of hydrolysis reaction, in relation to the applied drying conditions should serve well as starting point for the investigation of *in situ* MAO synthesis. If higher polymerization temperatures are desired, the amount of $AlMe_3$ should be adjusted accordingly. Successful ethylene polymerization would be seen as proof of an active MAO species. If preconditioning processes are altered or other biomaterials are intended to be used, respective gas titrations to gather specific data are recommendable.

The overall amount of reaction was shown to be lower than one would expect considering MC and ubiquity of hydroxyls. The occurrence of presumed water release at conditions that are considerably less severe than the prior drying conditions remains an odd phenomenon paying tribute to still unresolved basic research questions. Hence, without further research, knowledge of MC is not sufficient to make predictions on the amount of hydrolysis reaction. To what degree the developed gas originates from reaction with water or hydroxyls remains unknown. Whether Al-alkyls undergo chemical reaction with wood hydroxyls at all or are merely attracted by physisorption remains an open question. However, at this stage only low amounts of chemical reaction seem likely.

In general, gas titration is well suited to quantify hydrolysis reactions between aluminum alkyls, such as $AlMe_3$ and MAO, and designated bio-carrier materials containing protonic groups. Its usefulness comes from the fact that it can be executed with standard lab equipment and that it requires little prior training. However, this can lead to the underestimation of the high precision and control over external factors that is required to keep the otherwise inherent statistical deviation low. The inhomogeneous and ambiguous behavior of wood makes handling far more challenging than more standardized alternatives. Special care should be taken when handling such hygroscopic bio-materials with regards to their treatment history as well as the surrounding lab environmental, as they can influence the outcome of such experiments in an uncontrolled manner.

Future investigation could include WF particle surface area as an influencing factor. Correlating surface area, MC and amount of reaction could provide further insights on the reaction between Al-alkyls and moist wood.

6 Wood Bound Water as Catalytically Active Part in the Synthesis of Wood Polyethylene Composites by Polymerization Filling Technique

6.1 Introduction

The application of the polymerization filling technique (PFT) in conjunction with MAO and lignocellulosic materials entails tradeoffs. The biomaterial needs to be absolutely dry, otherwise the performance of prefabricated MAO will suffer from reaction with any residual water (Mädler 1981; Eberhardt et al. 2001). On the other hand, intensive drying requires high amounts of energy and adds cost. Previous studies have also indicated that $AlMe_3$ and MAO do not adhere reliably onto thoroughly dried lignocellulosic (Spottog pending) and carbohydrate (Mende 1981; Dutschke 1985) materials. In order to perform true PFT, where all of the catalyst is anchored to solid surfaces, it appears that biomaterials need to contain some amount of residual water or must not have undergone any form of intensive drying. The *in situ* synthesis of MAO by partial hydrolysis of $AlMe_3$ with wood bound water (w-H_2O) seems promising in regards to addressing these issues. $AlMe_3$ is more affordable than MAO and the need for bio-filler drying would be moderate or even unnecessary, saving overall costs. Furthermore, this approach promises to provide enhanced catalyst immobilization while retaining high polymerization activity.

The approach of synthesizing MAO *in situ*, by partially hydrolyzing $AlMe_3$ with traces of water within the subsequent polymerization reaction chamber, dates back to the discovery of MAO and is described in detail in Chapter 3.5. It has been well documented that metallocenes are quickly deactivated by $AlMe_3$. This combination is thereby unsuitable for catalyzing meaningful olefin polymerization. Metallocenes only show long lasting high catalytic activity in combination with MAO. The widely recognized basic MAO building block of $[\text{-AlR-O-}]_n$ represents an Al to H_2O ratio of 1:1. However, it was established that polymerization activity profits from a surplus of $AlMe_3$. Andresen et al. (1976) recorded maximum activities at ratios between 2:1 and 5:1. Scheel (2014) investigated $AlMe_3$ as an alternative to MAO in the *in situ* polymerization (ISP) of ultra-high-molecular-weight polyethylene / halloysite nanotube composites. These nanotubes incorporate water in their crystalline structure. The $AlMe_3$ can be partially hydrolyzed by that water to form MAO. Varying $AlMe_3$ concentrations and nanotube amounts were investigated. It was observed that the activity is dependent on the $AlMe_3$ to nanotube ratio and that not all water was available for the hydrolysis reaction. In the master thesis of Schoeneberger (2016), technical toluene containing small amounts of water was added to the $AlMe_3$ toluene solution within the reaction chamber. The homogeneous polymerization was initiated by the subsequent addition of a bis(imino phenyl)pyridin catalyst. Water amounts of 0.00 – 0.33 mmol/l were investigated in combination with 1.0 mmol/l $AlMe_3$. Results were compared to 1.26 mmol/l MAO. Logged ethylene consumption showed that the higher the added water amount the earlier peak polymerization activity was reached. Highest activities were recorded at a water concentration of 0.23 mmol/l, which approx. corresponds to an Al to H_2O ratio of 4:1. At this ratio, the avg. activity of the $AlMe_3$ / H_2O cocatalyst even exceeded that of prefabricated MAO.

Biomaterials as catalyst supports and fillers have also been investigated before, which is described in Chapter 3.6. In a number of studies the synthesis of MAO, by partially hydrolyzing $AlMe_3$ with moisture contained in the biomass has been reported. Mende (1981) investigated the combination of Cp_2ZrMe_2 / $AlMe_3$ with undried and thoroughly dried starch. 15 mmol of $AlMe_3$ per 5 g of starch were used. No active polymerization was observed in the case of starch, which was vacuum dried at 90 °C for 12 h. Successful ethylene polymerization was reported in the case of undried starch. However, the MCs of the starch were not recorded or investigated specifically. Mädler (1981) investigated the combination of Cp_2ZrMe_2 / $AlMe_3$ and starch as well as MCC. Moist starch exhibited much lower activities than moist cellulose. No polymerization was observed in the case of thoroughly dried starch or MCC. Again, the MCs of the materials were not recorded or investigated specifically. In his dissertation, (Mädler 1987) comprehensively investigated, whether the synthesis of the MAO cocatalyst could be simplified by utilizing the moisture of starch, cellulose or other carbohydrates to partially hydrolyze $AlMe_3$. Again, Cp_2ZrMe_2 was used as catalyst. The highest polymerization activity was recorded in the case of potato starch with a MC of 9 % and an $AlMe_3$ to H_2O ratio of 0.8:1. Activities came to a halt at ratios of 2:1 (insufficient moisture) and 0.5:1 (degree of hydrolysis to high). Comparative experiments between different grades of starch and MCC led Mädler to conclude that it was not the overall amount of water, but rather its availability that was governing the *in situ* MAO formation. Furthermore, the rate of reaction between the bound water and $AlMe_3$ also appeared to play a role. It is postulated that, in the case of amorphous and native starch, the high rates of reaction between bound water and $AlMe_3$ produced MAO-species that led to higher polymerization rates and resultant polymer molecular weights. However, this seems not to be universally applicable to other carbohydrates, as MCC showed by far the fastest reaction rate between bound water and $AlMe_3$, but the resultant polymerization activities were low. All studies that utilized carbohydrates as a carrier of moisture for the *in situ* synthesis of MAO reported lower polymerization activities compared to prefabricated MAO.

Chapter 4 describes how the residual MC of WF can be controlled in vacuum drying by choice of drying temperature, time and pressure. In Chapter 5 the hydrolysis reaction of the aluminum alkyls $AlMe_3$ and MAO with WF was investigated. It showed that not all w-H_2O is available for reaction. By governing the drying conditions, the degree of hydrolysis of $AlMe_3$ can be controlled to a certain extent. A rise in temperature during the aluminum alkyl treatment increases the amount of reaction further. High drying temperatures lead to very low amounts of reaction.

The primary objective of this chapter is to investigate, whether the ***in situ* formation of MAO** by partial hydrolysis of $AlMe_3$ with residual wood moisture, can lead to an active cocatalyst species. By combining the indications given by the other authors mentioned above with the results gathered in the prior chapters of this study, a variety of slurry polymerization experiments were conducted. High olefin polymerization rates would be seen as proof for the presence of an active MAO-species.

The type of reaction between carbohydrate hydroxyl groups and $AlMe_3$ or MAO as well as the mechanism of **catalyst immobilization** on such supports has been discussed in

Chapter 5. It was reported that $AlMe_3$ and MAO do not appear to react with hydroxyls of thoroughly dried starch, nor do they adhere to them. Successful immobilization was reported in the case of wet biomaterials. Furthermore, segregation of wood and polymer fraction was observed, where thoroughly dried WF was used. The gas titration experiments conducted in this study support these observations of low amounts of hydrolysis reaction in the case of thoroughly dried WF. One possible explanation for the low immobilization was brought forward by Mende (1981). Small $AlMe_3$ can enter the cavities and fibrous networks of a bio-filler structure. When it reacts with water the newly forming aluminoxane-structure grows in size and locks itself into place. Free solvated aluminum-structures might adhere to the mechanically anchored ones and would thereby also be immobilized. This would only occur if water is available for reaction. In order to review these observations, in this chapter, polymerizates will be examined for segregation. Furthermore, the encapsulation of WF particles will be investigated by SEM.

Although no grafting of olefins to the catalyst support occurs (Mende 1981; Mädler 1981; Kaminsky 1983; Spiehl 1984), improved **interfacial adhesion** is stated as one major incentive for ISP and PFT (Kaminsky 1983; Kaminsky et al. 2008; see also Chapter 3.6). In order to gain indications on the interface between wood filler and PE matrix cryo-microfractography on injection molded specimens was performed. In the case of ductile materials, such as many polymers, plastic deformation may occur before fracture, rendering the interpretation of the fracture surface cumbersome. The lowering of the material's temperature to below its glass transition, leads to brittle fractures (Gul et al. 2003; Michler 2008; Spiegelberg et al. 2016). The fracture surfaces were examined for predominant failure in the matrix or in interfaces. Surfaces cut via microtome from injection molded specimens were also investigated for the separation between wood filler and matrix polymer.

In metallocene olefin polymerization, the **molecular weight** (MW) of the resultant polymer is not only governed by the type of catalyst (D'Agnillo et al. 1998) but also by the polymerization temperature and the metallocene to monomer ratio (Kaminsky et al. 1983; Kaminsky and Sinn 2013). Metallocenes produce high MWs at lower temperatures and will produce mainly short-chained alpha-olefins at temperatures above 100 °C (Kaminsky 1981). Lower catalyst concentrations lead to higher MWs (Kaminsky et al. 1983). Monomer pressure, on the other hand, is reported not to affect the MW of a PE produced by a Zr-type catalyst (D'Agnillo et al. 1998). Homogeneous catalysts produce considerably narrower molecular weight distributions (MWD) than heterogeneous catalysts (Brintzinger et al. 1995; McDaniel 2010). Metallocene-catalysts immobilized on solid supports exhibit lower activity and produce higher MWs and higher MWD. This is presumably caused by the bonding between catalyst and support, which alters the catalyst ever so slightly, changing the properties of the active center and thereby the polymer (Kaminsky 1996). The MW in the polymerizations of PE in the presence of bio-fillers was only slightly increased when prefabricated MAO was used. However, in the case where $AlMe_3$ and moist bio-fillers were used, MWs and MWDs increased considerably. The differences between prefabricated MAO and *in situ*-formed MAO decreased with increas-

ing metallocene concentration (Spiehl 1984; Mädler 1987). In order to assess the influence of wood fillers and the *in situ*-formed MAO species on MW and MWD, the MWs of received PEs were determined.

The **crystallinity** (X_c) distinctly influences polymer properties (Ohlberg et al. 1959) and the X_c of thermoplastic semi-crystalline polymers may range between 30 and 70 % (Menges et al. 2011). The branching of a polymer sharply influences its ability to form crystals, i.e. the lower the branching of a PE, the higher its X_c. To a certain extent, the X_c of a polymer can be governed by the rate by which a polymer is cooled from the molten state. Slower cooling gives polymer molecules more time to rearrange into crystalline structures, leading to higher X_c. On the contrary, faster cooling leads to larger amorphous shares (Franck et al. 2011). Fillers also influence the crystalline structure of a polymer material, as they may function not only as nucleation agents but also spatially hinder crystal growth.

The effect of wood fillers on melting temperatures (T_m), onset crystallization temperatures (T_o), peak crystallization temperatures (T_c) and degree of crystallinity (X_c) of polyolefins has been investigated via Differential Scanning Calorimetry (DSC) before.

The T_m of HDPEs is reported to lie between 130 and 146 °C (Franck et al. 2011). In the reviewed literature, the influence of fillers on T_m is seen as negligible (Nuñez et al. 2002; Xie et al. 2002; Hristov and Vasileva 2003). Controversially, Cui et al. (2010) report increasing T_M with increasing wood filler contents. However, they investigated recycled HDPE where other factors may come into play.

It is generally agreed that wood fillers are classified as nucleation agents (Lampke 2001; Xie et al. 2002; Hristov and Vasileva 2003). According to literature, the addition of wood filler leads to an increase of the T_o and the T_c of PE/WF- (Guo et al. 2007; Bouafif et al. 2009) and PP/WF-composites (Lampke 2001; Nuñez et al. 2002; Xie et al. 2002; Hristov and Vasileva 2003; Radovanovic 2007). Cui et al. (2010) reported differing results again, where recycled HDPE showed decreasing T_o and T_c with increasing wood filler contents.

In addition to the wood filler, aluminum microparticles or agglomerates of aluminum nanoparticles have been found to act as nucleation agents, facilitating crystallization. On the other hand, well dispersed nanoparticles hindered the crystallization process (Huang et al. 2007). Aluminum particles originating from $AlMe_3$, free of or attached to wood surfaces, may also influence the crystallization behavior.

The described nucleating function of wood fillers may be the cause of observations made elsewhere, where X_c increases sharply by an initial addition of filler, but then decreases again with increasing contents, as in the case of PE/WF- (Guo et al. 2007) and PP/WF-composites (Xie et al. 2002; Hristov and Vasileva 2003). This decrease is thought to be caused by fillers hindering crystal growth, leading to smaller crystals and larger amorphous shares (Lampke 2001; Xie et al. 2002). The conclusion that X_c of the overall composite decreases linearly with increasing wood content, and may therefore be used as measure for actual filler content, is proposed by other authors for PP/WF-composites (Lampke 2001; Radovanovic 2007). In the case of *in situ* PP-composites containing carbon nanotubes, this phenomenon is also reported, but at much lower filler contents overall (Bonduel et al. 2005; Rosehr 2019).

6.2 Experimental

6.2.1 Materials

6.2.1.1 Catalysts

The catalysts that were used in this study, are depicted in Figure 22.

Bis(n-butylcyclopentadienyl)zirconium(IV)dichloride ((*n*-BuCp)$_2$ZrCl$_2$) was used as catalyst in a 0.5 mmol/l toluene solution. The catalyst was retrieved from university stock.

According to a producer of that catalyst (Merck KGaA) DE), it is capable of performing ethylene polymerization and copolymerization of ethylene-alpha-olefins. It has been successfully used in a number of studies (Spottog pending; Goretzki et al. 1999; Santos et al. 1999; Alexandre et al. 2000; van Grieken et al. 2007; Johannsen 2011; Casas et al. 2012; Scheel 2014; Bashir et al. 2016; Käselau et al. 2018; Käselau 2019).

Furthermore **Bis(cyclopentadienyl)titanium(IV)dichloride** (Cp_2TiCl_2) and **(Cyclopentadienyl)titanium trichloride** ($CpTiCl_3$) were also used as catalysts in a 0.5 mmol/l toluene solution. The catalysts were retrieved from university stock.

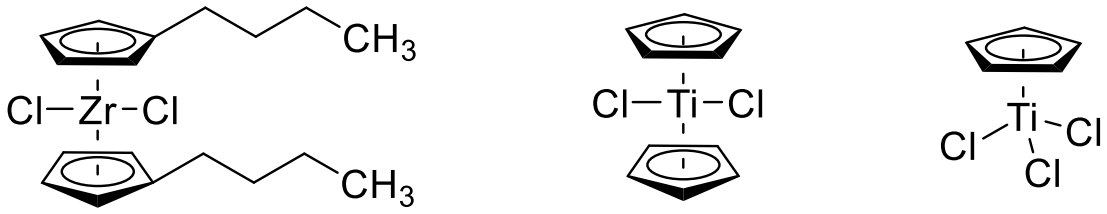

Figure 22: Sandwich and half-sandwich catalysts (*n*-BuCp)$_2$ZrCl$_2$, Cp$_2$ZrCl$_2$ and CpTiCl$_3$.

6.2.1.2 Cellulosic Materials

The same extracted **wood flour** “Arbocel C100” (J. Rettenmaier & Söhne GmbH & Co. KG, DE) that was used in gas titration experiments (Chapter 5) was also used in polymerization experiments.

The length of the tracheid fiber cells of the named softwoods may range from 1.3 - 4.8 mm (Wagenführ 2006). In correspondence with the mentioned particle sizes of 70 – 150 µm of C100, it is evident that the largest proportion of particles are cell wall fragments with open cell lumen. As a consequence of this, almost their entire surface area should be readily accessible for reagents.

6.2.1.3 Chemicals

Acetone 99 %, denatured **ethanol** 96 %, **isopropyl alcohol** 99 % (all from BCD Chemie GmbH, DE) and an isomeric mixture of **xylene** ≥97 % (Carl Roth GmbH und Co. KG, DE) were used for cleaning, quenching and extraction purposes. Reagent grade **1,2,4-trichlorobenzene** ≥ 99 % (Honeywell International Inc., US) was used for solvation experiments.

Toluene 99 % (BCD Chemie GmbH, DE) was purified by distillation and passing through columns filled with a 4 Å molecular sieve as well as the PuriStar R3-11G catalyst (BASF SE, DE).

6.2.1.4 Cocatalysts

Trimethylaluminum was purchased as a 2 mol/l toluene solution (Prod. no. 198048, Sigma-Aldrich, subsidiary of Merck KGaA, DE).

Methylaluminoxane in toluene solution (AXION CA 1310, formerly Chemtura Organometallics GmbH; at the time of writing a subsidiary of Lanxess AG, DE). From the data provided by the product data sheet (5.1 wt-% Al cont.), the overall concentration of aluminum and the concentration of aluminum associated with the basic MAO structure were calculated. The overall aluminum concentration was approx. 1.7 mol/l. The concentration of aluminum associated with the structural unit $[\text{-Al}(CH_3)\text{-O-}]_n$ was approx. 1.1 mol/l.

6.2.1.5 Gases

Grade 3.0 **Ethylene** 99.8 % (GHC Gerling, Holz & Co. Handels GmbH, DE) was used as monomer for polymerizations. The ethylene was purified by passing through columns filled with 4 Å molecular sieve as well as the PuriStar R3-11G catalyst (BASF SE, DE).

Grade 5.0 **Nitrogen** 99.999 % (Linde GmbH, DE) was used as inert gas.

6.2.2 Methods

6.2.2.1 1l-Autoclave

All slurry polymerizations were conducted in the 1l-autoclaves described in Chapter 4.2.2.1. The input of monomer gas was regulated via a mass flow controller (MFC 5850TR Series, Brooks Instrument GmbH, DE) calibrated for propene. Ethylene flow was calculated via conversion factors provided by the manufacturer. Temperature, pressure and monomer inflow were monitored in real-time. Anchor design stirrers were used for mixing.

6.2.2.2 Injection Molding

Specimens of the dimension 80 x 10 x 4 for cryo-microfractography were injection molded with a “HAAKE MiniJet Piston Injection Molding System” (Thermo Fisher Scientific Inc., US). As the amount of polymerizate available per variation was very low, it was only possible to produce a few specimens each. Hence, further characterization for mechanical properties and the like was not possible.

The injection molding settings that were used for specimen production are presented in the following Table 9. Because of the high melt viscosity, which led to inferior consolidation, variations of the temperature settings were tried, following the guideline that composites with higher wood contents, generally demand a higher cast temperature.

Table 9: Injection molding settings for the production of neat PE and WPC dumbbell-shaped specimens.

Cylinder temperature:	180 – 210 °C
Mold temperature neat PE:	40 – 60 °C
Cast temperature neat PE:	70 °C
Cast temperature WPC:	100 – 110 °C
Switchover pressure:	600 bar
Post-injection pressure:	500 bar
Post-injection pressure time:	10 s

6.2.3 Procedure

All polymerizations within this chapter were carried out in water heated 1l-autoclaves.

In comparative **pilot experiments**, three different catalysts were tried. These polymerizations were conducted in close correspondence to procedures used by Spottog (pending). The catalysts $CpTiCl_3$, Cp_2TiCl_2 and $(n\text{-}BuCp)_2ZrCl_2$ were used. All three catalysts were tested in homogeneous polymerizations and in ISPs in combination with MAO as well as $AlMe_3$. The WF in the ISPs with MAO was dried thoroughly to exclude moisture. The WF in the ISPs with $AlMe_3$ was dried gently according to the drying conditions in the gas titration experiments (Chapter 5), in order to preserve a certain amount of moisture. The pilot experimental procedure is summarized in Table 10.

Table 10: Pilot homogeneous and *in situ* polymerization procedures comparing the cocatalysts MAO and $AlMe_3$ in combination with either one of the catalysts $CpTiCl_3$, Cp_2TiCl_2 and $(n\text{-BuCp})_2ZrCl_2$.

Step	Variables	Values Homogeneous polymerization		Values *in situ* polymerization	
		MAO	$AlMe_3$	MAO	$AlMe_3$
Drying	Wood flour:	-		5 g	
	Vacuum:	Fine*		Fine*	
	Temperature:	85 °C		85 °C	30 °C
	Time:	120 min		120 min	90 min
Solvent addition	Solvent:	Toluene		Toluene	
	Volume:	300 ml		300 ml	
	Stirring:	260 rpm		260 rpm	
Aluminum addition	Amount:	1.4 mmol	1.0 mmol	27.6 mmol	4.0 mmol
	Temperature:	30 °C		30 °C	
	Duration:	120 min		120 min	
Catalyst addition	Amount:	0.5 µmol		0.5 µmol	
	Temperature:	30 °C		30 °C	
	Duration:	60 min		60 min	
Ethylene addition	Pressure:	2.7 bar		2.7 bar	
	Temperature:	30 °C		30 °C	
Polymerization	Duration:	90 min		90 min	

* Between 1.0 and 0.1 mbar

A **Reference** ISP series with MAO and $(n\text{-BuCp})_2ZrCl_2$ was conducted. The procedure utilized was again in close correspondence to Spottog (pending). It comprised of six steps which are listed in Table 11.

In the **drying step**, 5 g of C100 WF was placed into the reactor and vacuum dried for 120 min at 85 °C. The vacuum was kept as constant as possible and ranged from just below 1.0 mbar at the start to just above 0.1 mbar at the end of the drying cycle. After the drying time had elapsed, three purge-and-refill cycles were applied using nitrogen. The temperature was lowered to the subsequent polymerization temperature of either 30 or 60 °C. In the step **solvent addition**, 300 ml dried toluene was dosed to the WF containing reactor. The rotational speed of the anchor stirrer was set to approx. 260 rpm. The **aluminum addition** was carried out using a syringe under nitrogen countercurrent. 6.1 mmol of MAO was dosed in one step. This approximates to the 1.2 mmol/g of WF suggested by Spottog. The temperature at the moment of addition was either 30 or 60 °C. The impregnation time was 120 min. The **ethylene addition** was performed at 2.7 bar partial pressure until saturation was reached. The polymerization was started by the **catalyst addition**. The amount of $(n\text{-BuCp})_2ZrCl_2$ of 0.5 µmol was kept constant throughout all polymerizations. The temperature was either 30 or 60 °C. The polymerization was stopped after 90 min by quenching.

Table 11: Reference *in situ* polymerization procedures with (*n*-BuCp)$_2$ZrCl$_2$ / MAO.

Step	Variables	Values
Drying	Wood flour: Vacuum: Temperature: Time:	5 g 1.0 – 0.1 mbar 85 °C 120 min
Solvent addition	Solvent: Volume: Stirring:	Toluene 300 ml 260 rpm
Aluminum addition	Amount: Temperature: Time:	6.1 mmol 30 or 60 °C 120 min
Ethylene addition	Pressure: Temperature:	2.7 bar 30 or 60 °C
Catalyst addition	Amount: Temperature:	0.5 µmol 30 or 60 °C
Polymerization	Time:	90 min

In the second experimental part, two ISP series with $AlMe_3$ were conducted (Table 12). In Series 1, the influence of a varied drying time and temperature on the polymerization was investigated. In Series 2, the amount of $AlMe_3$ in relation to WF mass was investigated. Repetitions were made where either the catalyst was added before the ethylene or the other way around.

In **Series 1**, the process from the reference polymerizations was adopted but the drying conditions were varied. 5 g of WF were used. The drying temperatures 30, 55 and 80 °C were tested in combination with the drying times 30, 90 and 195 min for a total of nine experiments. After the drying step, the temperature was, if necessary, adjusted to subsequent polymerization temperature of 30 °C. The maximum aluminum consumption during gas titration experiments (Chapter 5) after drying at 30 °C for 120 min was 0.75 mmol/g. In order to provide $AlMe_3$ in slight excess, this value was rounded up, leading to 0.80 mmol/g or a total addition of 4.0 mmol. In these experiments, the zirconocene catalyst was added before the ethylene, all other settings being applied as before.

Table 12: *in situ* polymerization procedures with (*n*-BuCp)$_2$ZrCl$_2$ / AlMe$_3$.

Step	Variables	Values Series 1	Values Series 2
Drying	Wood flour:	5 g	5 g
	Vacuum:	1.0 – 0.1 mbar	1.0 – 0.1 mbar
	Temperature:	30, 55, 80 °C	30 °C
	Time:	30, 90, 195 min	120 min
Solvent addition	Solvent:	Toluene	Toluene
	Volume:	300 ml	300 ml
	Stirring:	260 rpm	260 rpm
Aluminum addition	Amount:	4.0 mmol	3.0 to 11.2 mmol
	Temperature:	30 °C	30 and 60 °C
	Time:	120 min	120 min
Catalyst addition	Amount:	0.5 µmol	0.5 µmol
	Temperature:	30 °C	30 and 60 °C
Ethylene addition	Pressure:	2.7 bar	2.7 bar
	Temperature:	30 °C	30 and 60 °C
Polymerization	Time:	90 min	90 min

In **Series 2**, the process from the reference polymerizations was adopted but polymerization temperature and AlMe$_3$ amount were varied. To retain sufficient moisture, in order to form MAO, moderate drying conditions of 120 min and 30 °C were deemed feasible. To be able to investigate polymerizations at higher temperatures, the temperature was raised from 30 to 60 °C during the AlMe$_3$ impregnation. In addition to the polymerization temperature, the amount of AlMe$_3$ added was varied. The amounts of AlMe$_3$ added were chosen in accordance with the avg. results gathered by gas titration experiments at 30 and 60 °C, corresponding to 0.60 and 0.74 mmol/g respectively. The total amounts were calculated in reference to the exact weighted mass of WF. The resultant AlMe$_3$ addition ranged from 3.0 to 11.2 mmol, which corresponded to Al to methane development ratios of approx. 1:1, 2:1 and 3:1. This was done to investigate the effect of such a ratio on the polymerization process. Three repetitions were conducted per setting combination. In the third repetition, the zirconocene catalyst was added before the ethylene or vice versa. All other settings were used as before.

All received materials were visually checked for segregated WF. Finding isolated WF would mean that not all wood particles were vested with sufficient catalytically active sites for encapsulation. This would hint at a low degree of catalyst immobilization. To investigate this further, the received materials were observed via SEM. Finding large amounts of bare wood particles would substantiate low degree of catalyst anchoring.

The interfacial adhesion was evaluated by assessing cryo-microfracture surfaces from injection molding specimens using SEM. The observation of bare wood surfaces could be interpreted in the following ways: Signs of low adhesion between wood and PE would be large amounts of visible bare wood surfaces, pulled out fibers and gaps between filler and matrix. In the case of high adhesion, failures would be expected to occur either within

the matrix or the filler material. High filler mechanical properties and high interfacial adhesion would lead to failure within the matrix polymer. A fracture surface showing large amounts of matrix polymer and low amounts of bare filler surfaces, pulled out fibers and interfacial gaps would indicate this. On the other hand, high matrix mechanical properties and high interfacial adhesion could lead to fracturing of filler particles. This would show itself by large amounts of bare wood surfaces. X-ray elemental analysis was performed to highlight and differentiate wood from polymer fraction. Microtome cut surfaces were investigated for gaps between polymer matrix and wood filler. Predominant occurrence of gaps between matrix and filler would indicate low level of adhesion.

The relative MWs and MWDs of the PEs received from the Pilot_1, Pilot_2 and Series 2 were determined with high-temperature gel permeation chromatography. The recorded MW values correspond to a polystyrene standard and are not directly comparable to other literature values.

The crystallinity, crystallization and melting points of the synthesized polymers were determined by thermal analysis using DSC. The crystalline structure was investigated by polarized light microscopy.

6.2.4 Material Characterization

6.2.4.1 Field-Emission Scanning Electron Microscopy

The morphology of the received materials was investigated via field emission scanning electron microscopy (SEM) (Gemini 1525, LEO Electron Microscopy Inc., US) and energy-dispersive X-ray spectroscopy (EDX) (Octane plus Silicone Drift Detector, EDAX, Ametek Inc., US). Samples were steam-coated with carbon, generating a carbon-coating of approx. 40 nm. FESEM images were captured with an in-lens and a SE2 detector at an electron acceleration voltage of 5 kV. EDX was captured at an electron acceleration voltage of 20 kV. The software used for the elementary analysis was “TEAM Version 4.1” (EDAX, Ametek Inc., US). The signals for carbon, oxygen and aluminum are 0.277 keV (Kα), 0.525 keV (Kα) and 1.486 keV (Kα) correspondingly.

The polymerizates were investigated as is. Cryo-microfractography was performed on injection molded specimens, which were then submerged in liquid nitrogen and fractured thereafter. Samples with no or low amounts of WF were notched because of their high impact strength. Solid wood sample surfaces were cut via a sledge microtome equipped with a stainless steel knife, in order to attain the required smoothness.

6.2.4.2 High-Temperature Gel Permeation Chromatography

The MWDs of the synthesized polyethylenes were measured with high temperature gel permeation chromatography (HT-GPC). A “PL-GPC 220” (Agilent Technologies Inc., US) in combination with the “Chromatographica V1.0.25” software (hs GmbH, DE) was used. Approx. 8 mg of sample material was solvated in 4 ml of 1,2,4-trichlorobenzene. Measurements were conducted at 135 °C at a flow rate of 0.5 ml/min. Signals were recorded with a refraction index detector.

The number avg. molecular weight (M_n), the weight avg. molecular weight (M_w) and the the dispersity (Đ) were calculated. The resultant values are correspondent to a polystyrene standard.

$$M_n = \frac{\sum M_i N_i}{\sum N_i} \qquad M_w = \frac{\sum M_i^2 N_i}{\sum M_i N_i} \qquad Đ = \frac{M_w}{M_n}$$

6.2.4.3 Differential Scanning Calorimetry

The melting and crystallization of the materials were determined with differential scanning calorimetry. A “DSC1” in combination with the “STAR^e” software (Mettler-Toledo International Inc., US) was used. Nitrogen was used as furnace purge gas. Calibrations for temperature and heat flow were done with indium (T_m = 156.6 °C) and zinc (T_m = 419.5 °C). 40 µl crucibles with punctured lids were used; with a constant puncture size of 0.4 mm the crucibles are considered to be “open”, circumventing the buildup of a discrete atmosphere. Sample powders were placed into the crucibles and pressed flat with a rubber stamp. One DSC measurement of each received polymerizate was performed.

Non-isothermal crystallization experiments (Figure 23) were conducted with two heating cycles. The first cycle was started by heating the samples from 25 – 200 °C at a rate of 20 K/min. Within this first heating cycle, the evaporation of moisture and the melting of nascent polymer crystals occurs. The temperature was kept isothermal at 200 °C for 5 min, in order to equalize the thermal history of all samples. They were then cooled to 25 °C at a rate of 20 K/min. The crystallization recorded in the first cooling cycle was used to analyze the onset and peak of crystallization. The temperature was kept isothermal at 25 °C for 5 min before the second heating cycle was started, the temperature being raised again to 200 °C at a rate of 20 K/min. From the second heating cycle, the melting points and the degree of crystallinities were determined.

The T_g of the CW constituents is discussed in Chapter 3.1. The T_g of cellulose in wood with 230 °C is well above the investigated temperatures. The T_g of lignin in dry wood is reported to be around 100 °C. Hence, these two values should not interfere with the measurements, as the melting and crystallization mainly occur in the range between 120 and 140 °C. However, the T_g of hemicelluloses in dry wood is reported to be at around 120 °C. It may therefore interfere with the measurements slightly.

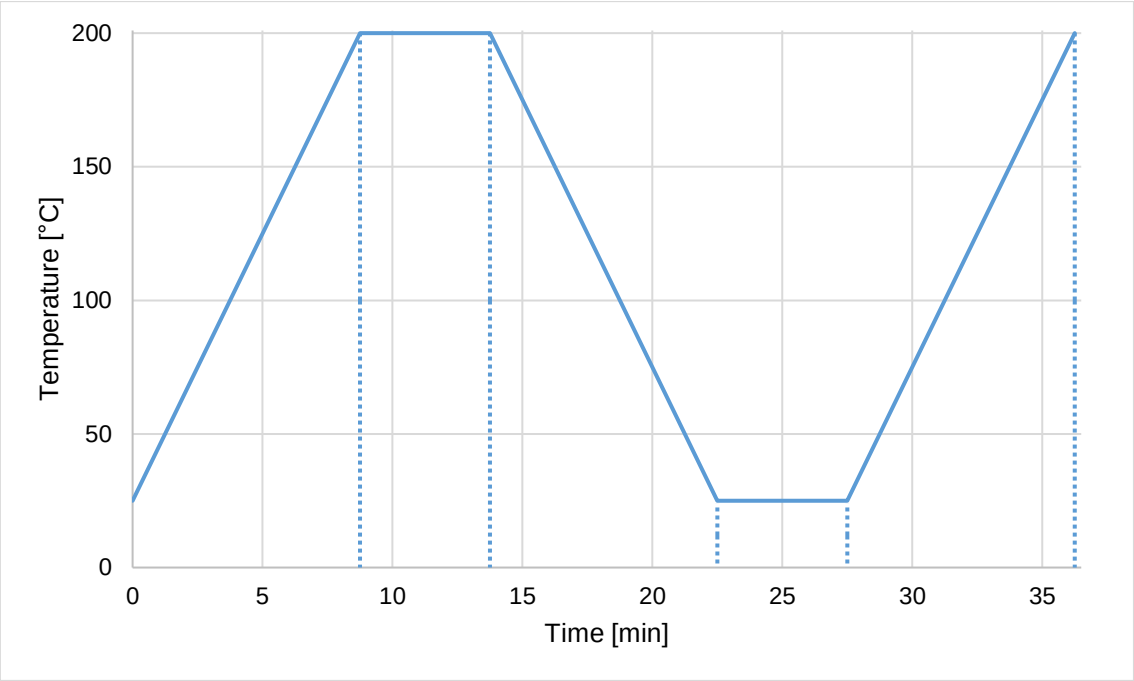

Figure 23: Heating- and cooling cycles of the non-isothermal DSC measurements of neat and composite PE.

The integral of a fusion peak corresponds to the enthalpy of fusion of the composites PE fraction. It is proportional to the amount of crystallites within a PE fraction. The degree of crystallinity is determined by comparing the measured enthalpy of fusion with the theoretical enthalpy of fusion of 100 % crystalline PE of ΔH_m = 293 J/g (Poltimäe et al. 2011). According to the ASTM D4020-05 the theoretical enthalpy of fusion of 100 % crystalline PE of ΔH_m = 289.3 J/g (Kurtz 2016). In this study the latter was used.

6.3 Results

6.3.1 Polymerization

Table 13 displays the results of the comparative **pilot experiments**.

$CpTiCl_3$ showed almost no ethylene polymerization activity visible under the applied conditions. In homogeneous polymerization with MAO, only a few filaments formed in the slurry. In combination with $AlMe_3$ no activity was observed. Polymerizations in the presence of WF were inactive.

Cp_2TiCl_2 showed distinct but very low homogeneous polymerization activity in combination with MAO, producing approx. 1.8 g of PE. The polymerizate, still soaked with toluene appeared smudgy. In the polymerization with $AlMe_3$, the solution turned turbid after a few seconds of starting the reaction and a few small flakes formed. After this event, no further activity was observed. These observations are typical for metallocenes in combination with alkylaluminums, showing only short-lived active olefin polymerization which generally comes to a halt very quickly (Patat and Sinn 1958; Long 1959; Henrici-Olivé and

Olivé 1967). The ISP with MAO produced higher output of approx. 4.2 g while the ISP with $AlMe_3$ showed very low activity.

(*n*-BuCp)$_2$ZrCl$_2$ achieved very high activities under the applied conditions and was therefore chosen for all further experiments. In the following text this homogeneous polymerization and this ISP will be referred to as Pilot_1 and Pilot_2 respectively.

Table 13: Results of pilot homogeneous and *in situ* polymerizations comparing the cocatalysts MAO and $AlMe_3$ as well as the catalysts $CpTiCl_3$, Cp_2TiCl_2 and (*n*-BuCp)$_2$ZrCl$_2$.

Catalyst	Yield [g]			
	Homogeneous polymerization		*in situ* polymerization	
	MAO	$AlMe_3$	MAO	$AlMe_3$
$CpTiCl_3$	< 1	-	-	-
Cp_2TiCl_2	1.8	< 1	4.2	< 1
(*n*-BuCp)$_2$ZrCl$_2$	60.0*	-	75.4**	15.1

* Pilot_1; ** Pilot_2

The **Reference** polymerizations with MAO were conducted in close relation to the results from gas titration experiments as well as in consideration of preliminary work by Spottog (pending). Table 14 displays a selection of process parameters and the PE yield. In these two runs the polymerization temperatures 30 and 60 °C were compared. All other parameters were kept constant. It is evident that higher temperatures lead to increased yields.

Table 14: Reference *in situ* polymerizations with (*n*-BuCp)$_2$ZrCl$_2$ / MAO.

Run	Cocatalyst		Drying		Polymerization		Result
	Type	Amount [mmol]	Temp. [°C]	Time [min]	Temp. [°C]	Pressure [bar]	Yield* [g]
Ref_1	MAO	6.1	85	120	30	2.7	5.8
Ref_2	MAO	6.1	85	120	60	2.7	21.6

* Excluding wood flour

In **Series 1**, polymerizations with $AlMe_3$ were conducted. Table 15 displays a selection of process parameters, resultant MCs – calculated from actual factor equations determined in Chapter 4 with drying conditions as input parameters – and PE yield. In these nine runs, the drying temperatures of 30, 55 and 80 °C as well as the drying times of 30, 90 and 195 min were compared. Polymerizations were all conducted at 30 °C. All other parameters were kept constant. It is evident that the drying temperature has a pronounced influence on the MC and yield.

Table 15: Series 1 *in situ* polymerizations with (*n*-BuCp)$_2$ZrCl$_2$ / AlMe$_3$.

Run	Cocatalyst		Drying		MC	Polymerization		Result
	Type	Amount	Temp.	Time	Calc.*	Temp.	Pressure	Yield**
		[mmol]	[°C]	[min]	[%]	[°C]	[bar]	[g]
S1_1	AlMe$_3$	4.0	30	30	2.52	30	2.7	10.1
S1_2	AlMe$_3$	4.0	30	90	2.44	30	2.7	15.4
S1_3	AlMe$_3$	4.0	30	195	2.31	30	2.7	12.2
S1_4	AlMe$_3$	4.0	55	30	2.00	30	2.7	6.5
S1_5	AlMe$_3$	4.0	55	90	1.92	30	2.7	4.2
S1_6	AlMe$_3$	4.0	55	195	1.79	30	2.7	1.5
S1_7	AlMe$_3$	4.0	80	30	1.49	30	2.7	1.4
S1_8	AlMe$_3$	4.0	80	90	1.41	30	2.7	0.9
S1_9	AlMe$_3$	4.0	80	195	1.27	30	2.7	0.0

* Calculated from actual factor equations for pine wood determined in Chapter 4; ** Excluding wood flour

Figure 24 displays the yield as function of calculated MCs. The MC shows a strong effect on the polymerization yield. An increase in drying temperature from 30 to 55 °C leads to a diminishment in yield of around 67 %. An increase from 55 to 80 °C shows another attenuation of around 80 %, leading to almost no polymerization activity. On the contrary, the influence of the drying time is inconclusive. At 55 and 80 °C shorter drying times lead to slightly higher yields. However, at 30 °C the order is reversed. At 30 °C the overall highest and second highest yield are achieved at 90 and 195 min of drying time. These two come closest to the drying conditions during gas titration experiments, from which the addition of AlMe$_3$ was calculated.

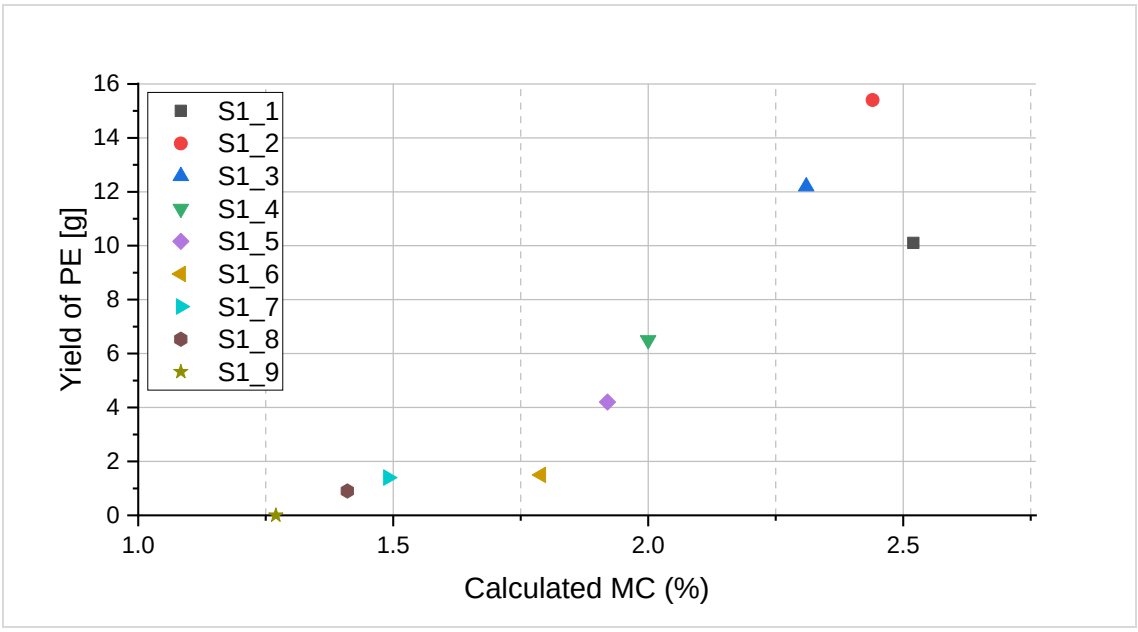

Figure 24: Series 1 – Yield of PE as function of calculated MC with drying temperature and time as input factors.

In **Series 2**, polymerizations with $AlMe_3$ were conducted. Table 16 displays a selection of process parameters and PE yield. In these eighteen runs, the polymerization temperatures of 30 and 60 °C were investigated. The amount of $AlMe_3$ was varied from one, two and three parts aluminum per measured reaction in the gas titrations. The total amount of added aluminum varied slightly, corresponding to the actual weighted portion of dry weight WF utilized. Furthermore, the order of catalyst and ethylene addition were compared. All other parameters were kept constant. The influence of the polymerization temperature is most pronounced, which coincides with observations made in the Reference polymerizations.

Table 16: Series 2 *in situ* polymerization with (n-BuCp)$_2ZrCl_2$ / $AlMe_3$.

Run	Cocatalyst		Drying		Polymerization		Result
	Type	Amount [mmol]	Temp. [°C]	Time [min]	Temp. [°C]	Pressure [bar]	Yield* [g]
S2_1	$AlMe_3$	3,2	30	120	30	2.7	4.4
S2_2	$AlMe_3$	3.0	30	120	30	2.7	6.9
S2_3**	$AlMe_3$	3.0	30	120	30	2.7	3.7
S2_4	$AlMe_3$	6.0	30	120	30	2.7	5.9
S2_5	$AlMe_3$	6.0	30	120	30	2.7	5.8
S2_6**	$AlMe_3$	6.2	30	120	30	2.7	6.2
S2_7	$AlMe_3$	9.0	30	120	30	2.7	5.0
S2_8	$AlMe_3$	9.0	30	120	30	2.7	5.5
S2_9**	$AlMe_3$	9.0	30	120	30	2.7	7.0
S2_10	$AlMe_3$	3.8	30	120	60	2.7	14.2
S2_11	$AlMe_3$	3.8	30	120	60	2.7	11.3
S2_12**	$AlMe_3$	3.8	30	120	60	2.7	11.4
S2_13	$AlMe_3$	7.4	30	120	60	2.7	12.0
S2_14	$AlMe_3$	7.4	30	120	60	2.7	10.9
S2_15**	$AlMe_3$	7.4	30	120	60	2.7	9.3
S2_16	$AlMe_3$	11.2	30	120	60	2.7	10.2
S2_17	$AlMe_3$	11.2	30	120	60	2.7	7.8
S2_18**	$AlMe_3$	11.2	30	120	60	2.7	14.1

* Excluding wood flour; ** Ethylene was applied prior to catalyst addition

Figure 25 displays the yield as a function of aluminum addition per methane development, i.e. the Al to CH_4 ratio, and polymerization temperature. The CH_4 of that ratio is the total amount of methane gas measured in the gas titration experiments, where analogous WF pre-treatment and drying was applied. The amount of methane developed is considered to be a number of the total reactions having taken place. Experiments with three different ratios of $AlMe_3$ to the amount of reactions where conducted. The influence of that ratio is inconclusive. A surplus of $AlMe_3$ does not seem to lead to higher polymerization activity.

An increase of the temperature during the $AlMe_3$ impregnation from 30 to 60 °C led to overall higher yields.

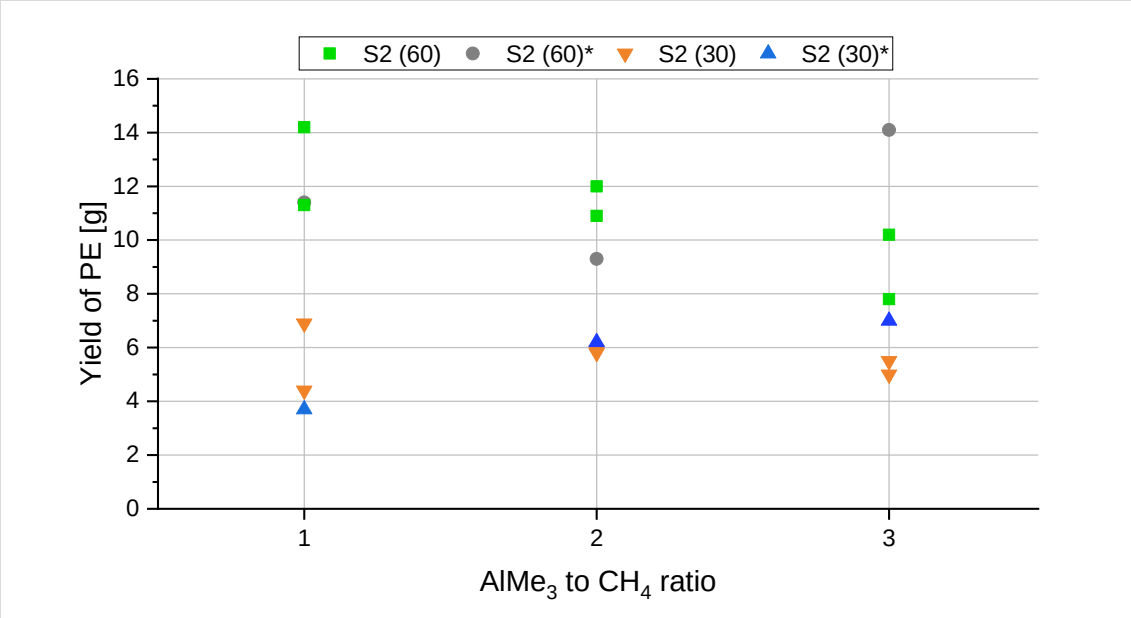

Figure 25: Series 2 – Yield of PE as function of Al to CH_4 ratio.
*** Ethylene was applied prior to catalyst addition.**

A general observation was made in the majority of all polymerizations using $AlMe_3$ in combination with moist wood. Shortly after initializing the polymerization, the WF would start to agglomerate and cling to the stirrer. A variety of processing parameters were tried to remedy this; they, however, were only slightly successful as agglomerations persisted to occur to a varying degree. A similar phenomenon is described elsewhere (Chanzy and Revol 1973) and may be caused by the formation of hot spots by overheating of catalytic centers during the initial stages of the polymerization process (Böhm 2003).

6.3.2 Material Characterization

Catalyst immobilization

The composite materials received from processes using MAO and dried WF exhibited segregation. After joggling the material in a transparent bag, low amounts of WF were deposited at the bottom of the bag, appearing bare of attachment. A phenomenon that was not observed in any of the materials received from processes where WF that had not been intensively dried was used.

The micrograph in Figure 26 originates from a polymerization utilizing MAO and dry wood. In spite of PE making up approx. 94 % of the polymerizate, bare wood particles are visible. They do not appear to be covered by polymer. In fact, their surfaces appear to be in their original state. Analogous observations were made in all investigated polymerizates originating from processes using MAO and dry wood.

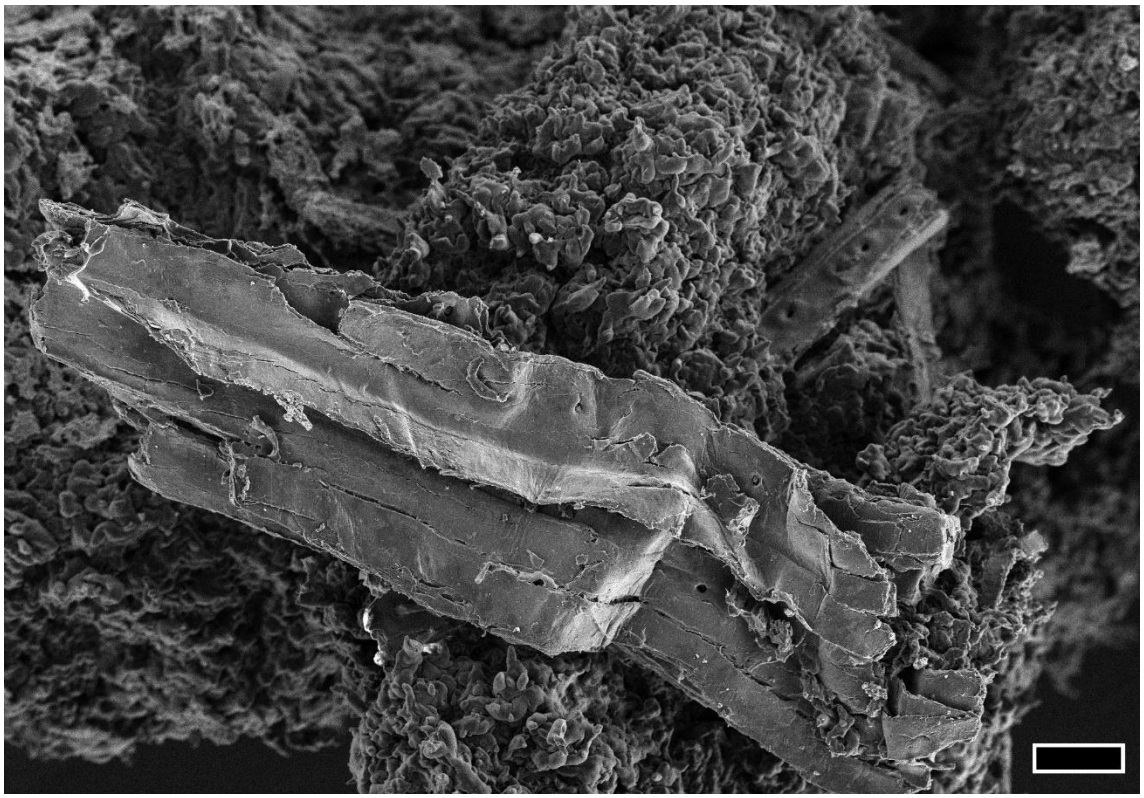

Figure 26: Polymerizate from (*n*-BuCp)$_2$ZrCl$_2$ / MAO *in situ* polymerization from pilot experiments containing ~94 % PE showing exposed fiber without visibly attached polymer. Scale bar 40 µm.

The micrograph in Figure 27 originated from a polymerization utilizing $AlMe_3$ and moist WF. It appears to show a wood fiber encapsulated by PE with the polymer coating varying in thickness. Larger aggregates of PE, measuring tenths of micrometers across, are attached to the fiber. Other areas are free of large aggregates. These areas are covered by a thinner layer showing brittle cracks, which also appears to consist of polymer. However, it is also possible that this layer consists of catalyst residues. In most cases where $AlMe_3$ and moist wood were used, wood particles were incorporated beyond visibility. If fibers were visible, they were clearly still partially incorporated or had polymer attached to them.

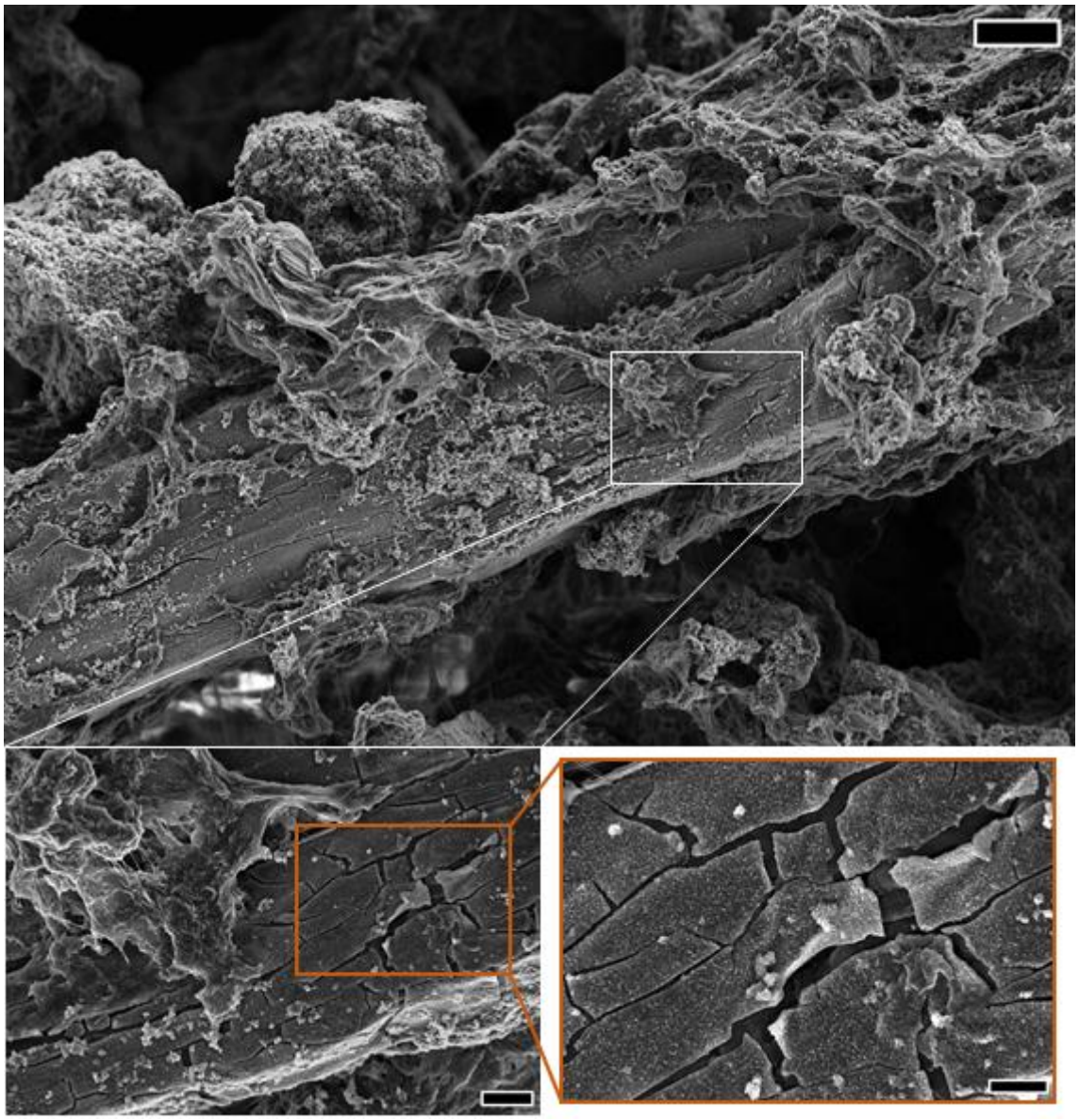

Figure 27: Micrographs of polymerizate from (*n*-BuCp)$_2$ZrCl$_2$ / AlMe$_3$ and moist wood *in situ* polymerization containing ~40 % PE.
Scale bar above 20 µm; Scale bar lower left 4 µm; Scale bar lower right 2 µm.

Interfacial adhesion

The micrograph in Figure 28 shows a microfracture surface of an injection molded specimen produced from Ref_2, i.e. (*n*-BuCp)$_2$ZrCl$_2$ / MAO with dry WF. The PE share was approx. 81 %. Wood fiber surfaces are readily visible and seem to be free of polymer attachment. This indicates that fractures appeared mainly in the interface between polymer and filler or within the wood particles. Analogous observations were made in all fracture surfaces investigated.

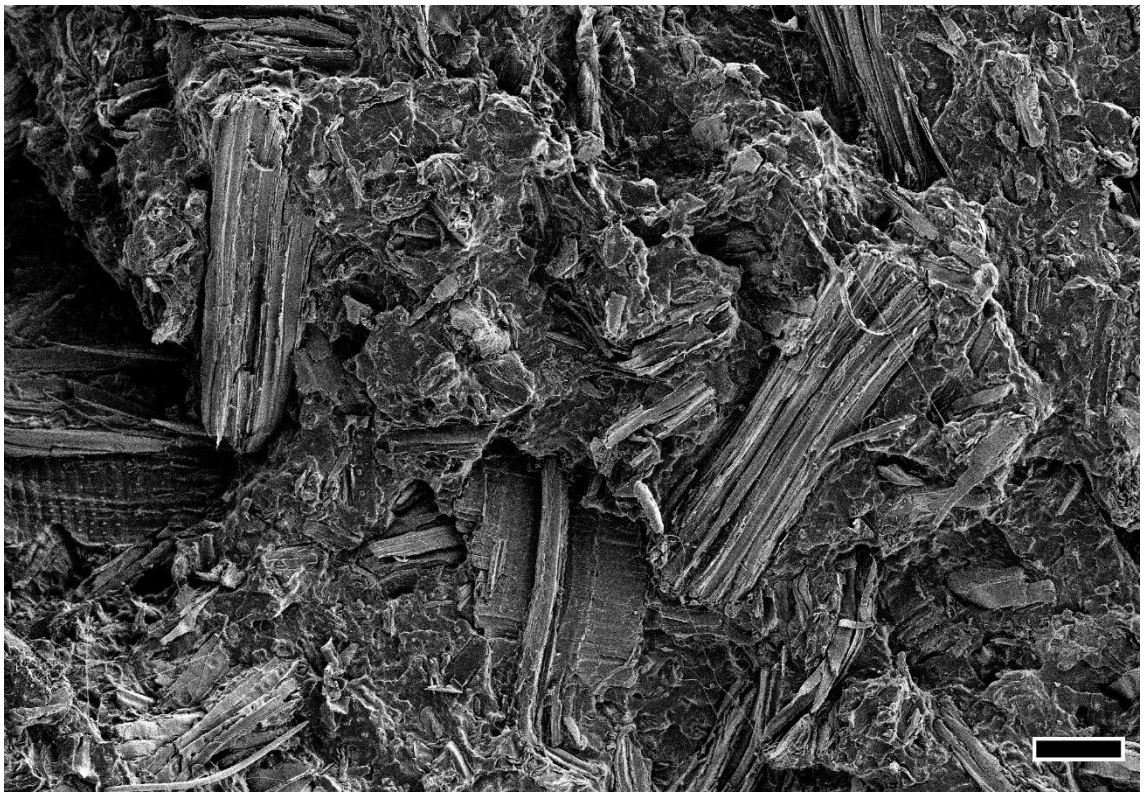

Figure 28: Microfracture surface from injection molded specimen from Ref_2 containing ~81 % PE showing bare fiber fragments.
Scale bar 100 µm.

The micrograph in Figure 29 shows the X-ray elemental analysis of a microfracture surface of an injection molded specimens produced from S2_1, i.e. (*n*-BuCp)$_2$ZrCl$_2$ / AlMe$_3$ with moist WF. The corresponding spectrum (see Figure 60 in Annex) shows clear oxygen and carbon signals. The PE share was approx. 47 %. The elements oxygen and carbon are coded for by green and magenta respectively. Wood contains oxygen as well as carbon whereas PE only contains carbon. Wood is depicted by a share of green and magenta dots. PE surfaces are depicted by a higher density of magenta dots. The two composite constituents are thereby highlighted and clearly distinguishable. Again, wood surfaces appear relatively bare of polymer. A large amount of failure seems to have occurred within the interface or within the wood substrate.

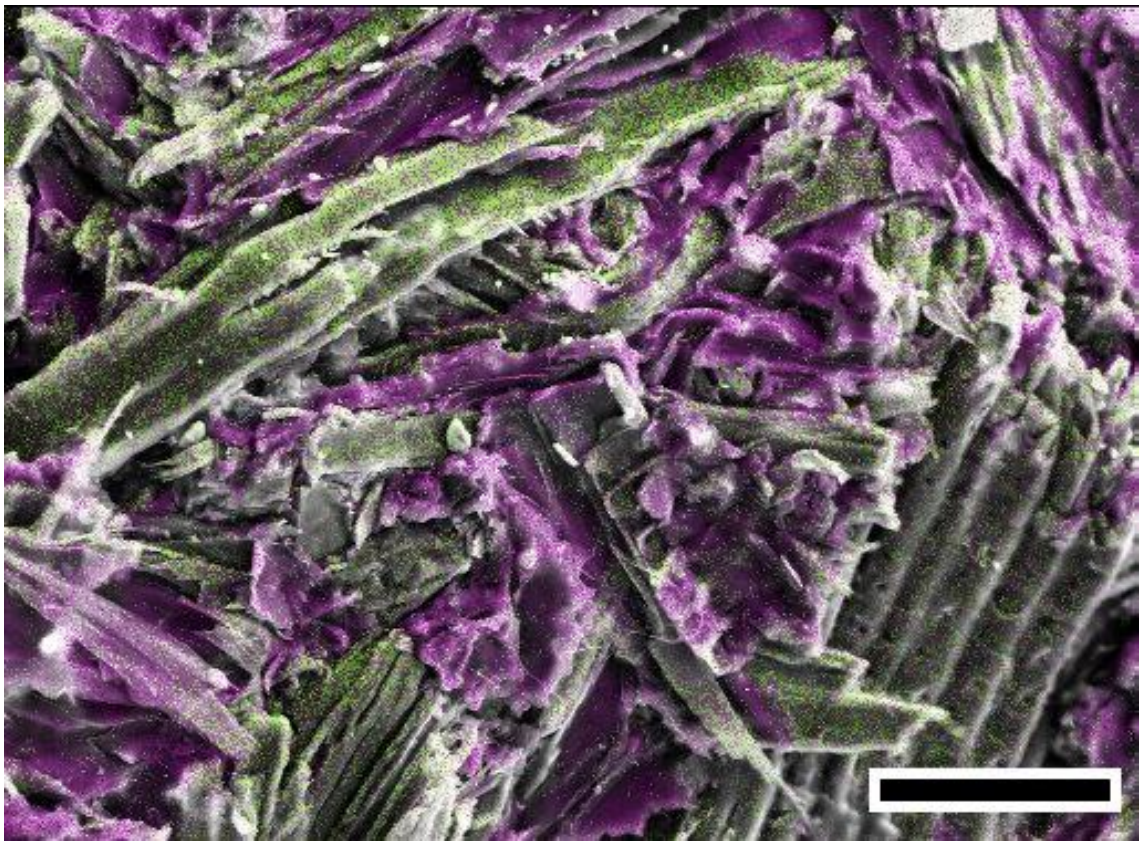

Figure 29: SEM-EDX analysis on microfracture surface of injection molded specimen from S2_1 containing ~47 % PE illustrating wood filler and polymer matrix distribution. Green: Oxygen; Magenta: Carbon; Scale bar 100 µm.

The micrograph in Figure 30 originates from an injection molded sample produced from Ref_2 polymerization utilizing MAO and dry wood. The sample contained approx. 94 % PE and was cut by microtome to attain a smooth surface. Observations shown in this micrograph are representative across multiple investigated areas. Gaps are clearly visible between what appears to be the polymer matrix and the filler. The gaps show no apparent orientation, i.e. they are not broader in one direction compared to another and appear to surround most particles relatively uniformly. A considerable amount of rather regular filaments are visible crossing the gaps. Their avg. diameter was determined with ImageJ software and was 45 nm.

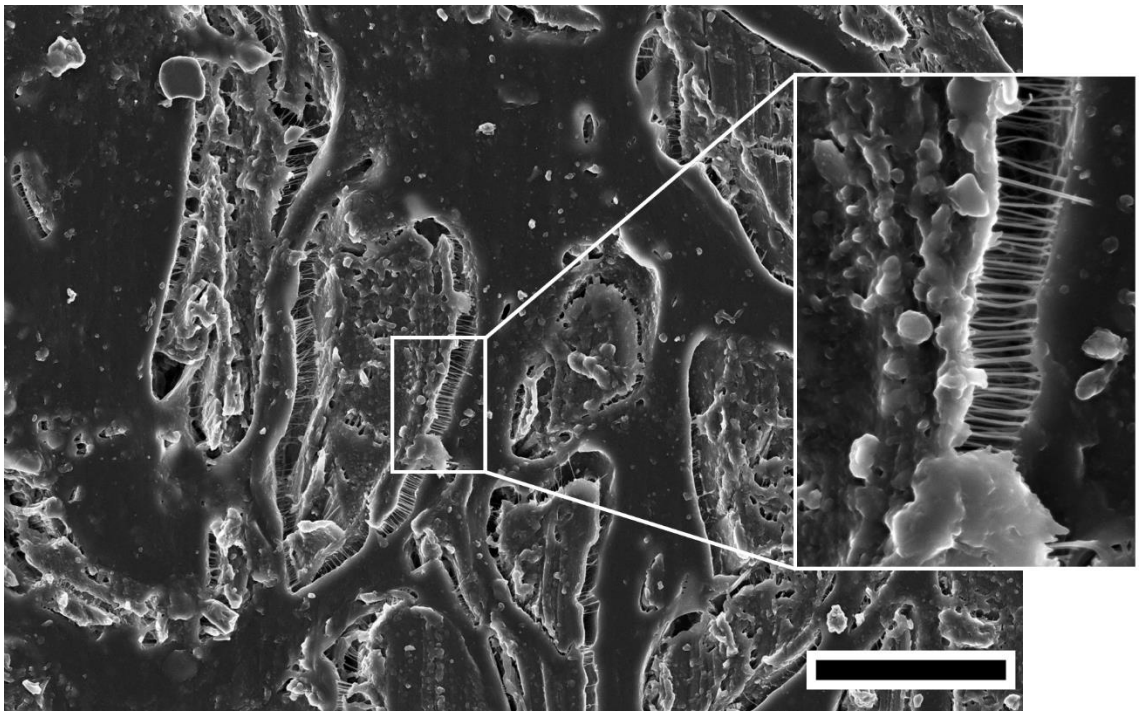

Figure 30: Microtome cutting surface from injection molding specimen from (*n*-BuCp)$_2$ZrCl$_2$ / MAO pilot experiments containing ~94 % PE showing interfacial voids between fiber and matrix.
Scale bar 10 µm.

Molecular weight and molecular weight distribution

Table 17 displays the results of HT-GPC. The results of four specimens were discarded due to apparent measurement error. All but two exceptions showed monomodal distributions. S2_5 and S2_13 show bimodal distributions.

Prefabricated MAO produces PE with overall lower MWs than *in situ* fabricated MAO at 60 °C polymerization temperature. Lower polymerization temperature leads to overall higher MWs.

The avg. Đ is approx. 2.2 and shows no distinct differences between the two MAO types or the polymerization temperature.

The succession of catalyst and monomer addition, where either the zirconocene was added before the ethylene or the other way around, shows no conclusive differences.

Table 17: HT-GPC results from ethylene polymerization in the presence of wood flour with (*n*-BuCp)$_2$ZrCl$_2$ / AlMe$_3$ / w-H$_2$O in comparison to MAO; Results relative to styrene standard.

Run	Polymerization	Molecular weight		
	Temp.	M_n	M_w	Đ
	[°C]	[g/mol]	[g/mol]	[M_w/M_n]]
Pilot_1 homo*	60	213,343	476,874	2.2
Pilot_2 *in situ*	60	211,183	451,851	2,1
S2_1	30	814,676	2,176,370	2.7
S2_2	30	741,737	1,614,310	2.2
S2_3**	30	-	-	-
S2_4	30	776,613	1,459,080	1.9
S2_5	30	810,023	1,803,510	2.2
S2_6**	30	1,035,690	1,655,070	1.6
S2_7	30	786,815	1,499,870	1.9
S2_8	30	806,643	1,509,740	1.9
S2_9**	30	-	-	-
S2_10	60	432,487	765,655	1.8
S2_11	60	-	-	-
S2_12**	60	-	-	-
S2_13	60	383,338	946,108	2.5
S2_14	60	367,128	819,835	2.2
S2_15**	60	312,100	793,027	2.5
S2_16	60	426,240	918,531	2.2
S2_17	60	370,476	897,292	2.4
S2_18**	60	376,026	843,438	2.2

* Homogeneous; ** Ethylene was applied prior to catalyst addition

The avg. MW values and the Đ (Table 17) of the PEs derived from homogeneous and *in situ* polymerizations using prefabricated MAO are very similar. Figure 31 displays the MWD of the PEs from the pilot experiments. Despite the presence of WF, the distributions resemble each other.

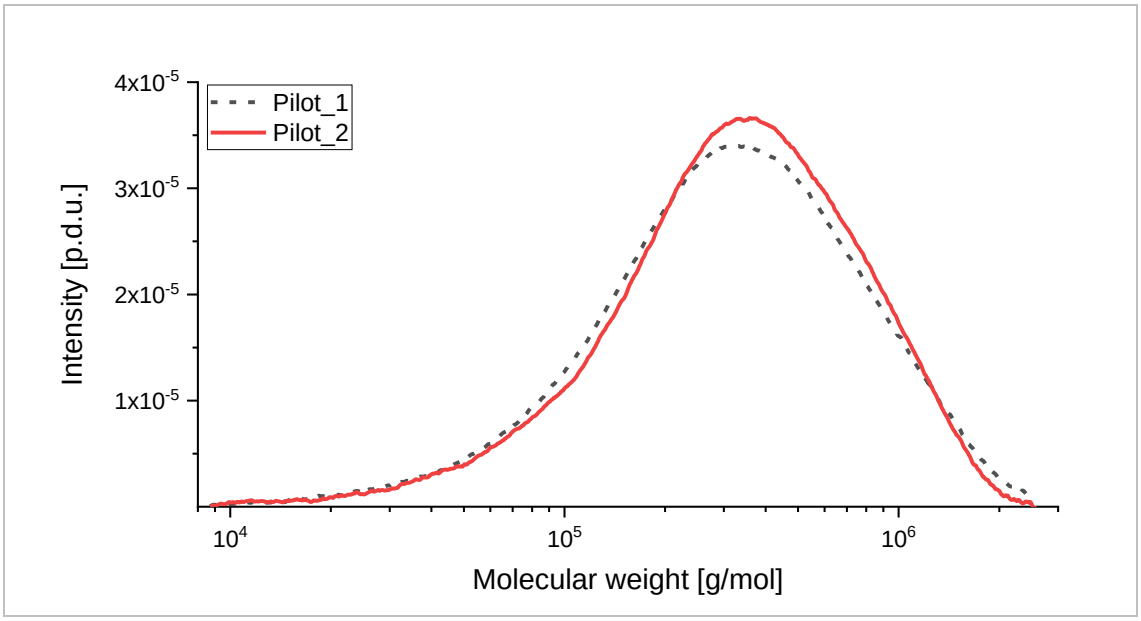

Figure 31: Molecular weight distribution of PE polymerized in homogeneous and *in situ* processes utilizing prefabricated MAO (procedure defined unit).

Figure 32 compares the MWDs of prefabricated MAO to *in situ* fabricated MAO as well as the MWDs of the polymerization temperatures 30 and 60 °C. The prefabricated MAO and the *in situ* fabricated MAO produced different MWDs at identical polymerization temperatures of 60 °C. Lowering the polymerization temperature from 60 to 30 °C clearly shifts the MWD towards higher MWs.

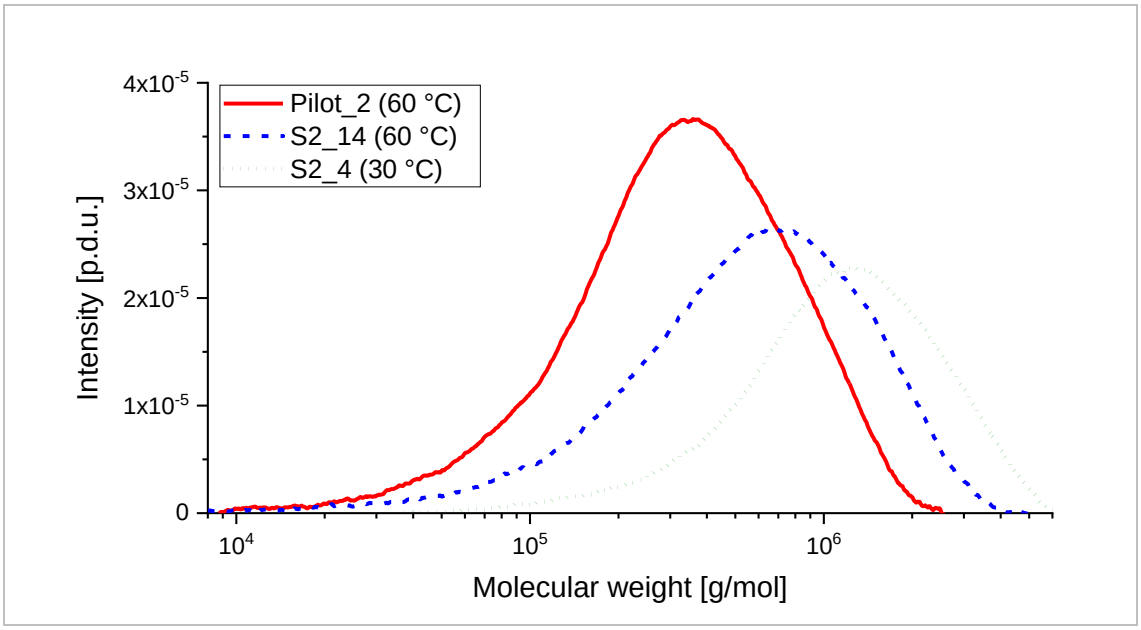

Figure 32: Molecular weight distribution of PE originating from *in situ* polymerizations, comparing the effect of different cocatalysts and polymerization temperatures (procedure defined unit).

Thermal analysis and crystalline structure

Table 18: Summarized DSC results from PEs received from Pilot, Reference, Series 1 and Series 2 experiments.

Run	Matrix & filler shares		Crystallization		Melting point	Crystallinity	
	PE	Wood	Onset	Peak	Peak	PE + W	PE
	[%]	[%]	[°C]	[°C]	[°C]	[%]	[%]
Pilot_1	100.0	-	117.0	108.7	139.6	-	65.2
Pilot_2	93.9	6.1	116.0	110.6	138.9	51.2	54.5
Ref_1	53.3	46.7	116.7	111.9	137.8	27.6	51.8
Ref_2	83.5	16.5	116.7	107.7	143.6	53.6	64.2
S1_1	66.9	33.1	115.0	108.0	141.4	36.3	54.2
S1_2	56.4	43.6	116.4	112.2	137.6	26.9	47.7
S1_3	21.3	78.7	117.2	114.5	134.0	8.9	42.0
S1_4	75.4	24.6	116.4	105.9	144.0	51.2	67.9
S1_5	45.7	54.3	116.9	113.4	136.4	22.3	48.9
S1_6	14.8	85.2	117.0	114.1	133.6	6.4	42.9
S1_7	70.9	29.1	115.6	107.9	141.5	38.6	54.4
S1_8	23.1	76.9	117.4	114.5	134.2	8.8	38.0
S1_9	0.0	100.0	-	-	-	-	-
S2_1	46.4	53.6	117.8	114.6	135.9	24.8	53.5
S2_2	58.1	41.9	117.3	112.5	138.5	30.2	52.0
S2_3*	42.7	57.3	117.8	113.4	137.9	25.2	59.1
S2_4	54.1	45.9	117.2	113.2	138.5	26.2	48.5
S2_5	53.7	46.3	116.8	112.5	138.6	25.1	46.7
S2_6*	55.2	44.8	117.7	113.0	136.4	27.0	48.9
S2_7	50.1	49.9	117.6	114.2	136.9	25.2	50.4
S2_8	52.5	47.5	117.2	112.2	138.8	25.1	47.8
S2_9*	58.3	41.7	118.0	114.7	136.8	30.2	51.8
S2_10	73.9	26.1	117.7	111.7	140.0	48.7	65.9
S2_11	69.3	30.7	117.8	112.6	139.1	44.2	63.8
S2_12*	69.5	30.5	118.5	112.7	139.3	41.9	60.4
S2_13	70.6	29.4	119.5	113.4	138.3	44.2	62.6
S2_14	68.6	31.4	119.1	113.1	138.6	43.9	64.0
S2_15*	65.0	35.0	119.4	113.6	138.4	39.1	60.1
S2_16	67.2	32.8	120.5	112.4	140.1	41.5	61.8
S2_17	61.0	39.0	120.1	115.4	137.6	36.6	60.0
S2_18*	73.8	26.2	119.3	113.1	138.2	47.7	64.7

* Ethylene was applied prior to catalyst addition

The results of thermal analysis by DSC measurements are collectively displayed in the prior Table 18. The polymer to filler ratio is displayed as one possible influencing factor. The crystallization is characterized by the onset ($\mathbf{T_o}$) and peak ($\mathbf{T_p}$) temperatures. The melting process is characterized by the peak melting point ($\mathbf{T_m}$) temperature. Values of crystallinity ($\mathbf{X_c}$) are given relative to the combined mass of the composite as well as to the mass of the PE fraction.

Possible influences on T_o are surveyed in Figure 33. The results of the different experimental series are color coded.

In the upper left figure it is visible that the wood content does not exhibit a clear influence. T_o values of neat PE from Pilot_1 (60), polymerized at 60 °C, are almost equal to composites with wood contents of around 80 %. Composites with wood contents between 30 to 40 % feature T_o between 115 and just above 120 °C. The results of S1 (30), polymerized at 30 °C, show relatively high deviation in wood content and in T_o. The results of S2 (30), polymerized at 30 °C, show low deviation in wood content and T_o, whereas S2 (60), polymerized at 60 °C, show high deviation in T_o.

In the upper right figure it is visible that the polymerization temperature may affect T_o. In spite of high deviation, higher polymerization temperatures seem to facilitate crystallization, which is indicated by the black arrow. However, this is only reflected by the experiments where $AlMe_3$ and moist WF were used as cocatalysts. In all cases where prefabricated MAO was used, i.e. Pilot and Reference experiments, T_o are almost equal independent of polymerization temperature.

In the lower left figure, the influence of the M_n on T_o is assessed. The MW was not determined for all materials received from the different polymerization experiments. S2 (3) composites exhibit considerably higher M_n than the Pilot_1 (60) neat PE. In spite of this, they exhibit almost equal T_o. The S2 (60) composites exhibit intermediate M_n but – apart from one exception – higher T_o.

In the lower right figure, the influence of the amount of $AlMe_3$ added is assessed, to futher investigate the higher T_o values exhibited by S2 (60). All T_o of S2 (30) are relatively equal. However, the T_o of S2 (60) clearly shows a positive trend with the increasing $AlMe_3$ amount. In this case, higher amounts of the cocatalyst appear to facilitate crystallization.

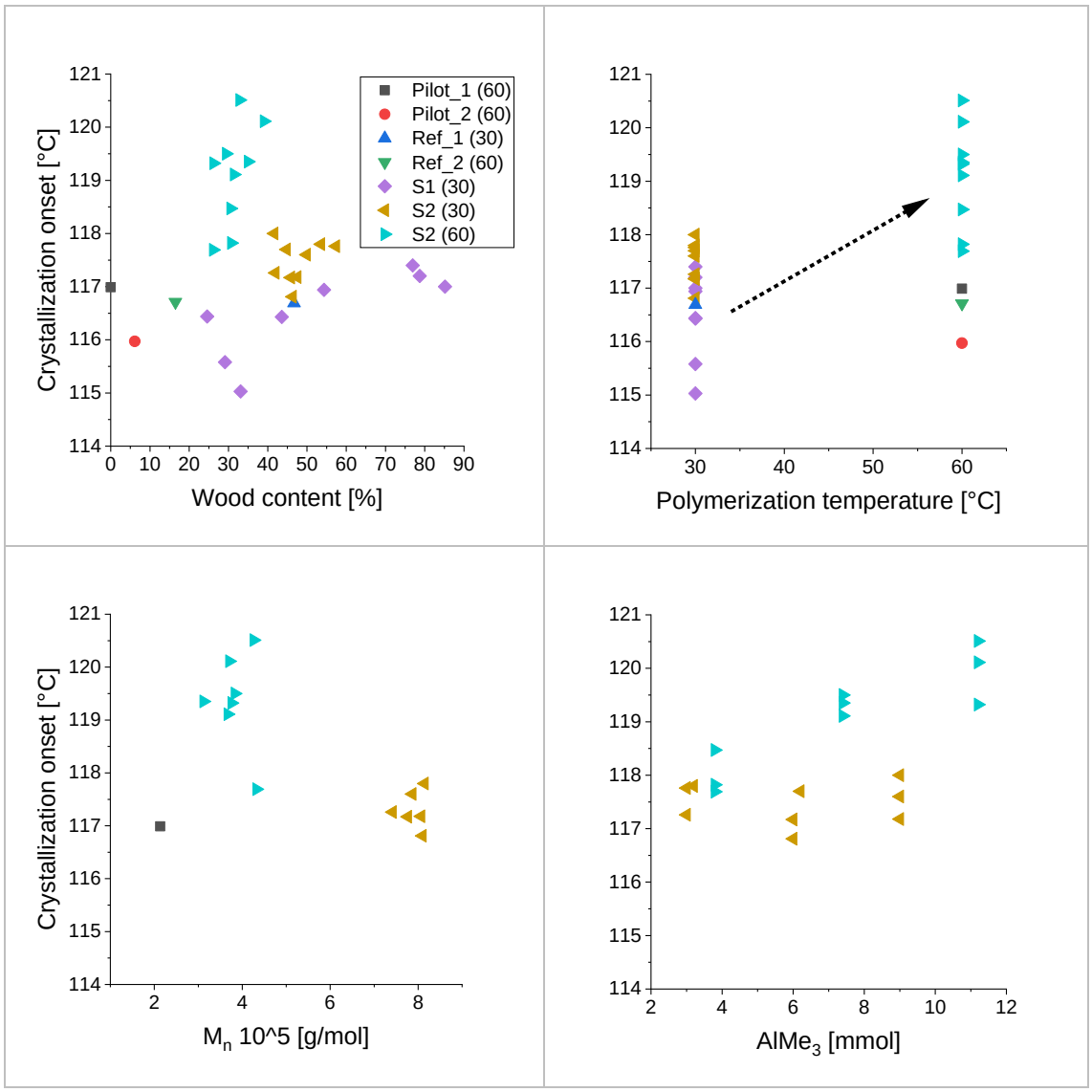

Figure 33: Crystallization onset temperature as function of wood content (upper-left), polymerization temperature (upper-right), number avg. molecular weight (lower-left) and amount of added $AlMe_3$ (lower-right).

The range of T_o values exhibited by S1 (30) and S2 (60) is equally broad. In S1 (30) the effect of different drying conditions, i.e. MCs, on the polymerization process was investigated. It has to be noted that the addition of $AlMe_3$ was kept constant in S1 (30). With the actual factor equations determined in Chapter 4 in combination with the vacuum drying conditions applied in S1 (30), presumed resultant MCs were calculated. Figure 34 puts these calculated MCs in relation to the determined T_o values. In S1 (30) the calculated MCs appear to influence T_o, with higher MCs prolonging crystallization.

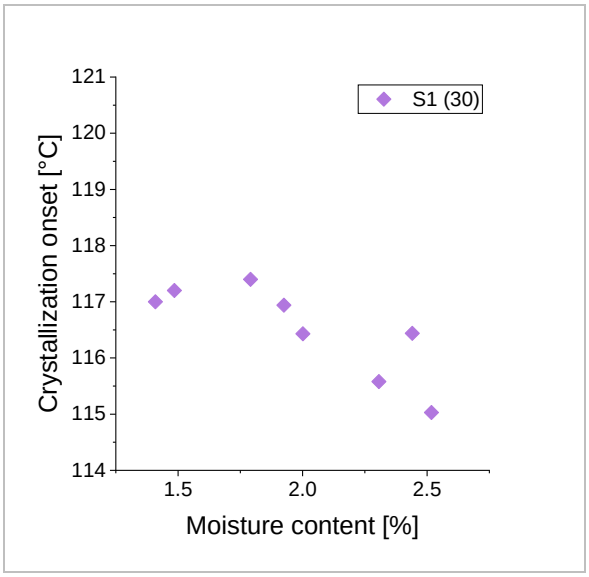

Figure 34: Crystallization onset temperature as function of presumed MCs, calculated with the actual factor equation for pine wood and high vacuum and the input of drying conditions applied in S1.

The T_p as function of wood content is displayed in the left Figure 35. T_p of neat PE was detected at just above 108.7 °C. Four samples that were polymerized at 30 °C – three from S1 and Ref_2 – with wood contents in the region of approx. 15 to 35 %, exhibited lower T_p. However, the main share of the samples containing above 25 % WF exhibited T_p above 111 °C. In between this group, the wood content does not appear to influence the T_p.

The T_m as function of wood content is displayed in the right figure and exhibits a clear downward trend with increasing shares of wood. The two Pilot experiments, where relatively high amounts of MAO were used, appear a bit apart from the rest. Other factors such as polymerization temperature, MW or amount of added cocatalyst did not considerably affect T_m considerably in the experiments conducted here.

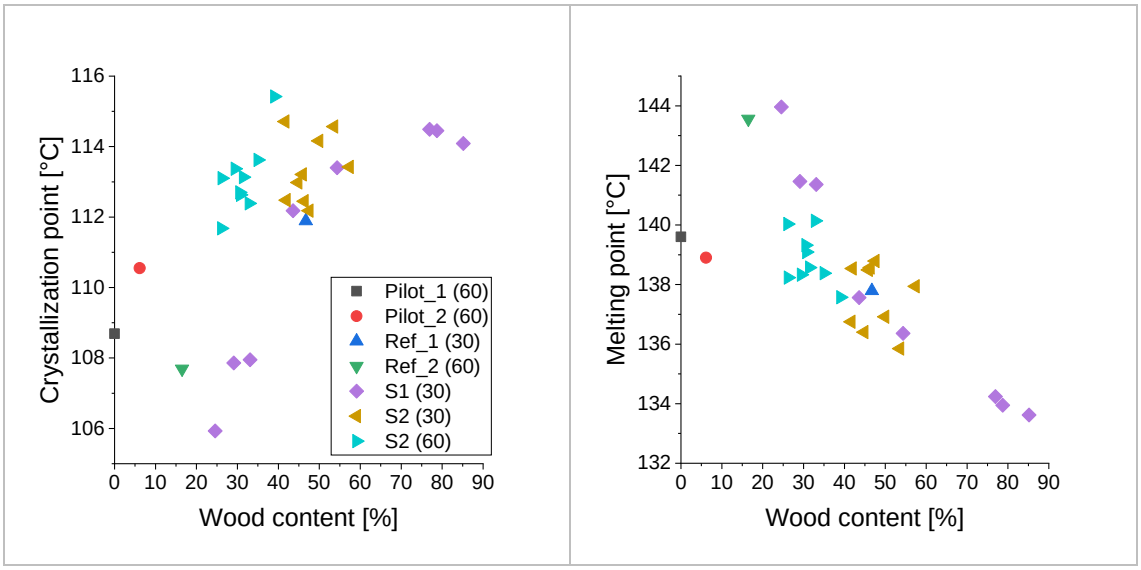

Figure 35: Peak crystallization point (left) and peak melting point (right) as function of wood content.

The influence of the wood content on the X_c of the received polymerizates and of the PE fraction of same polymerizates is displayed in Figure 36.

In the left figure, the X_c of a composite as a whole exhibits a negative linear dependency, i.e. higher contents lead to lower X_c. Here, the neat PE of Pilot_1 (60) exhibits the highest X_c of approx. 65 %. Sample S1_6 (30) with the highest wood content 85.2 % exhibits the lowest X_c of 6.4 %.

In the right figure, this dependency appears weaker when only the PE fraction of these composites is considered. A number of PE fractions, from samples with wood contents in the range of 20 to 30 %, exhibit relatively high X_c with values around 65 %, equaling that of neat PE from Pilot_1 (60). On the other hand, the PE fraction of the Pilot_2 (60) polymerizate exhibits low X_c of approx. 54 %, in spite of its wood content being just over 6 %. If the Pilot experiments, where high amounts of aluminum cocatalyst were used, were disregarded, the dependency would appear stronger. The composites received from the Reference, Series 1 and Series 2 polymerizations, where less aluminum cocatalyst was used, show similar properties.

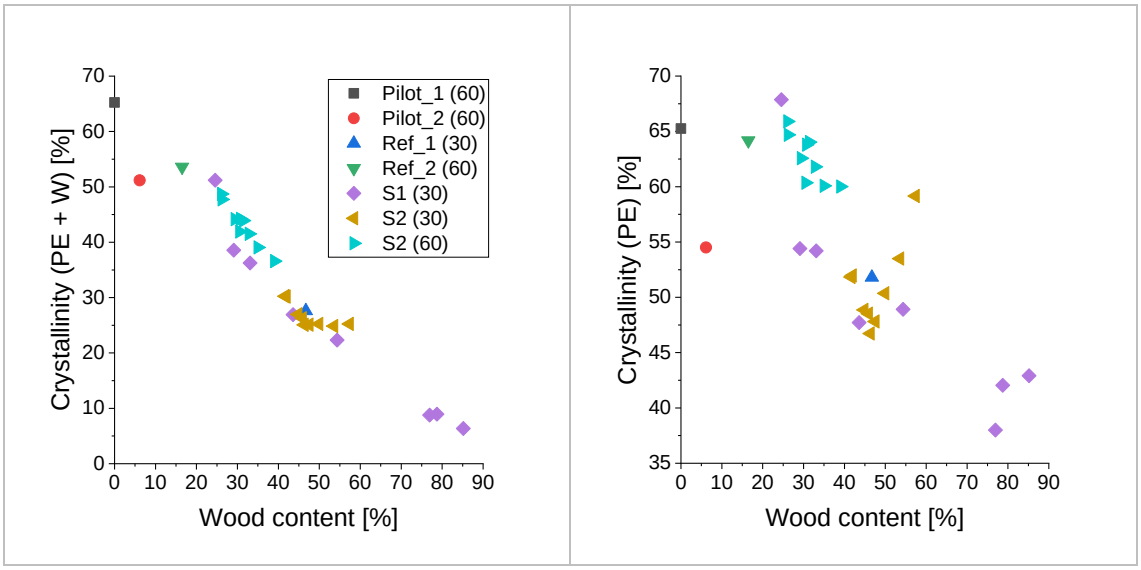

Figure 36: Crystallinity of received compound (left) and its neat PE fraction (right) as function of wood content.

The following images were produced via polarized light microscopy, in order to illustrate the crystalline structure of the received materials. ImageJ was used to take size measurements on these micrographs.

The above micrograph (Figure 37) represents neat PE polymerized with MAO from Pilot_1 (60). The areas of the spherulites of neat PE range from 60 µm² to 240 µm², with the avg. lying above 200 µm². These measurements are likely to be skewed towards the larger spherulites, because the smaller they are, the less perceptible they become.

The middle micrograph (Figure 38) represents the WPC with 17 % wood content polymerized with MAO from Ref_2 (60). The centered wood fiber has a length of 130 µm and an avg. thickness of 16 µm. The lighter trans-crystalline region around this fiber appears to have an avg. thickness of 9.4 µm. Spherulites within the PE matrix between the fibers are hardly perceptible and appear to be much smaller than in neat PE.

The below micrograph (Figure 39) represents the WPC received from S2_1 (30) with approx. 54 % wood content, polymerized with $AlMe_3$. The cross section of a large wood particle is visible in the center of the frame; it has an avg. diameter of 109 µm, which corresponds to an area above 9000 µm². Overall, the frame is dominated by visible wood parts, with the matrix polymer no longer being distinguishable.

Figure 37: Polarized light micrograph of neat PE. Scale bar 50 µm.

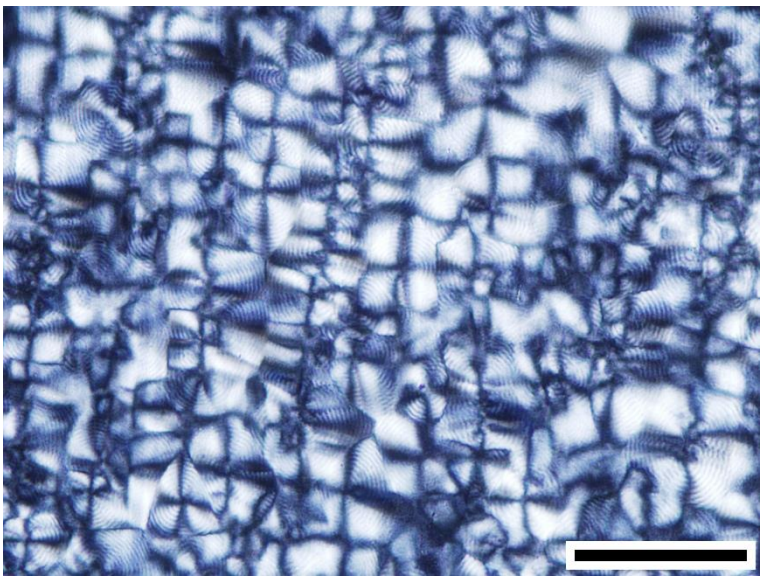

Figure 38: Polarized light micrograph of WPC with a wood content of 17 %. Scale bar 50 µm.

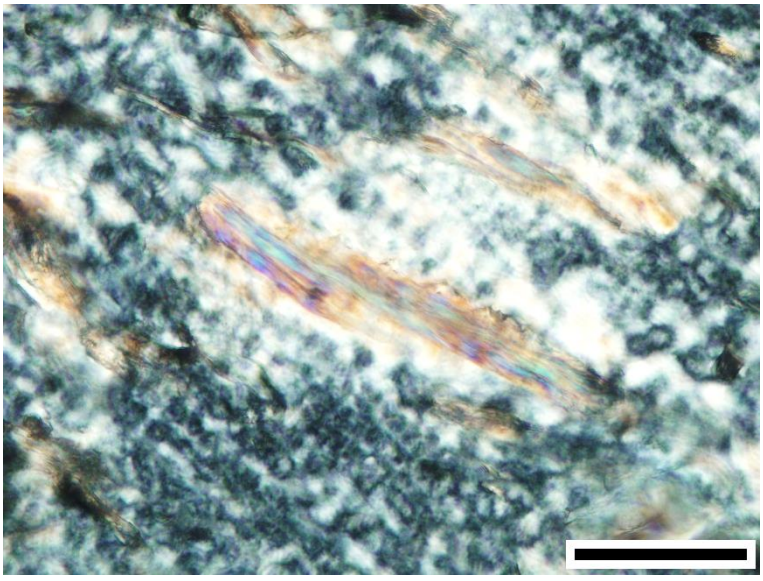

Figure 39: Polarized light micrograph of WPC with a wood content of 54 %. Scale bar 50 µm.

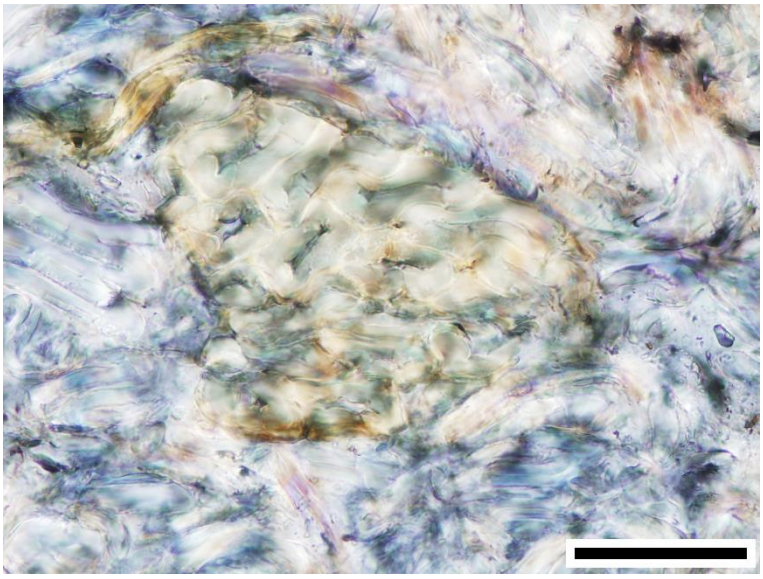

6.4 Discussion

6.4.1 Polymerization

The results of the comparative **pilot experiments** have clearly revealed that metallocenes do not form active olefin polymerization catalysts in combination with $AlMe_3$ (Chapter 3.5) Hence, if active polymerization is observed in the case of ISPs employing residual moisture and $AlMe_3$, a MAO-like species must have formed.

The total inactivity of **$CpTiCl_3$** has a variety of possible reasons. Monocyclopentacienyl titanium complexes were used by Park and Choi (2009) to perform ISP of multi-walled carbon nanotubes / ultrahigh-molecular-weight polyethylene composites. However, they immobilized the catalyst directly onto the carbon nanotubes by pysisorption between the carbon nanotube and the cyclopentadienyl ligand, possibly altering its active site. Chien and Rausch (1999) state that monocyclopentacienyl titanium complexes show poor ethylene polymerization activities. They further state that their activities may be improved by coordinative substituents on the CP ligand.

Cp_2TiCl_2 showed no activity in homogeneous polymerizations in combination with $AlMe_3$, which is a known phenomenon and likely due to fast deactivation of the titanocene by the aluminum alkyl. It is also reported that MAO-activated Cp_2TiCl_2 is rapidly deactivated at temperatures above 0 °C, most likely due to reduction of the titanium (Cam et al. 1994; cited in Brintzinger et al. 1995; cited publication does not contain the provided information), which would explain the low yield of the homogeneous polymerization in combination with MAO. However, the catalyst appeared to profit from higher MAO addition in the ISP.

(*n*-BuCp)$_2$$ZrCl_2$ achieved the highest activities under the mentioned conditions. In combination with MAO, it performed at least tenfold higher than with Cp_2TiCl_2. Activities were also high in the ISPs with MAO. In the homogeneous polymerization with $AlMe_3$ the solution only turned turbid, indicating short-lived active polymerization followed by quick deactivation. However, in the ISP with WF and $AlMe_3$, high activity was achieved. Therefore, for the purpose of this work this zirconocene catalyst was deemed most suitable and was used for all further investigations.

These pilot experiments confirmed that the partial hydrolysis of $AlMe_3$ with w-H_2O can lead to a MAO-species that is able to cocatalyze ethylene polymerization.

The **Reference** polymerizations with (*n*-BuCp)$_2$$ZrCl_2$ / MAO served to produce orientation values. The polymerization temperatures 30 and 60 °C were compared. The higher polymerization temperature led to 3.7x the yield. That the polymerization activity of metallocenes increases with increasing temperatures, is generally well established.

These results are somewhat contradictory in view of the gas titration results (Chapter 5), where the degree of hydrolysis of MAO by wood was approx. 2.7x higher at 60 than at 30 °C. Prior studies by other authors have shown that the higher the ratio of pre-fabricated MAO to bio-filler, the higher the polymerization activity. This indicates that the efficacy to act as cocatalyst of pre-fabricated MAO is statistically degraded by the amount of bio-filler interaction. By that reasoning, higher temperatures during the treatment of

WF with MAO should cause more intense MAO-wood filler interaction, lower its efficacy to cocatalyze and thus lead to a lower yield.

A likely explanation for this is the surplus of MAO provided. The amount of hydrolysis measured in gas titration experiments only amounted to a fraction of the added MAO. This could mean that the effect of the differences in the hydrolysis reaction is overshadowed by the temperature induced increase of catalyst activity.

Another explanation may be the ambiguous sorption behavior of wood. In Chapter 4, the complex dependencies between wood MC and its treatment history are illustrated. The phenomenon of varying amounts of water retention and the release thereof are described. In gas titration experiments, the temperature was raised during treatment and resulted in an increase of gas development. Strictly speaking, only the effect of temperature increase was investigated. In other words, the procedural steps of cooling and subsequent heating may in fact be the cause of the observed increase in reaction, not the temperature itself. It is not evident if the higher treatment temperature in general would lead to higher gas development. If the temperature were to be lowered from a high drying temperature to the treatment temperature of 60 °C straightaway, skipping the heating step from 30 – 60 °C, the effect of higher treatment temperatures may be less pronounced. This could be easily investigated in further gas titration experiments.

In **Series 1**, the influence of the drying temperature and duration on the polymerization yield, i.e. the influence of the MC on the formation of an active MAO cocatalyst species, was investigated. Higher drying temperatures clearly lead to lower yield. Longer drying times – with one exception – also lead to lower yields. In the case where WF was dried at 30 °C for 30 min, the yield is lower than when longer drying times were applied.

Higher drying temperature and longer drying times both lead to lower MCs. With the exclusion of the mentioned exception, it is evident that higher MCs lead to higher yield.

The observed exception may be caused by excessive hydrolysis of the $AlMe_3$. It was shown by Mädler (1987) that the $AlMe_3$ to H_2O ratio runs through a minimum, an optimum and a maximum in terms of resultant polymerization activity. In all experiments of Series 1, the same amount of $AlMe_3$ of 0.8 mmol/g was provided. This corresponds to the rounded up maximum amount of hydrolysis reaction observed in gas titration experiments after drying at 30 °C for 120 min. When drying for a mere 30 min, the resultant MC was higher. The $AlMe_3$ to H_2O ratio may have gone past its peak, leading to higher than optimum hydrolysis and thereby decreasing the yield. However, it is also important to note that the sample size was only one. The statistical deviation in MC (Chapter 4) and gas titration experiments (Chapter 5) was high so that the observed exception may too be due to variations.

In **Series 2**, three $AlMe_3$ to WF ratios were investigated. More specifically, the amount of $AlMe_3$ added was chosen in accordance with the results gathered by gas titration experiments at 30 and 60 °C and multiples thereof. Polymerizations were conducted at 30 and 60 °C, in order to investigate the influence of temperature. The temperature was raised during the treatment of the wood filler with $AlMe_3$.

Earlier studies have reported that polymerization activity benefits from a surplus of $AlMe_3$. This was not replicated in the experiments conducted in this study, however, the statistical deviation was high and may obscure trends.

It is generally reported that the polymerization activity of metallocene catalysts increases with increasing temperature. This is confirmed by the results of this study, where all polymerizations conducted at 60 °C produced higher yields than those at 30 °C. This may also have partially been caused by an increased amount of reaction between $AlMe_3$ and wood-moisture, due to the temperature increase, i.e. an increased amount of MAO.

The active MAO-species, formed by the reaction between wood residual moisture and $AlMe_3$, performs surprisingly well compared to pre-fabricated MAO. At a polymerization temperature of 30 °C the yields achieved in the References with MAO and in Series 2 with *in situ* formed MAO are equal, with 5.8 g and an avg. of 5.6 g respectively. This however changes when looking at a polymerization temperature of 60 °C, where pre-fabricated MAO produces 21.6 g and *in situ* formed MAO produces an avg. of 11.2 g.

The similar yields of pre-fabricated and *in situ* formed MAO at 30 °C polymerization temperature suggest resembling chemical amounts and structure. The amount of pre-fabricates MAO added in the Reference experiments was kept constant. Hence, the increase in yield at a polymerization temperature of 60 °C must be due to temperature induced higher catalytic activity. The increase in temperature in Series 2 should – by increasing hydrolysis in the presence of abundant $AlMe_3$ – increase the amount of available *in situ* MAO and, thus, the yield. The lower increase in yield in the case of *in situ* formed MAO in Series 2 indicates that there are other factors at play.

Prior studies have suggested that the structure and degree of oligomerization of MAO influences its efficacy as a cocatalyst (Chapter 3.5). Furthermore, not only the amount of water held by a bio-filler but also the availability and mobility of that water influences the formation of MAO structures (Chapter 6.1). Taking this into account could mean that the *in situ* MAO is of a slightly different morphology than its pre-fabricated counterpart. These differences may be more pronounced at high catalytic activities, i.e. at high polymerization temperatures. Furthermore, *in situ* MAO may be mechanically anchored to the WF particles and less mobile than prefabricated MAO. The higher mobility of the prefabricated MAO may facilitate faster catalysis.

The agglomeration of WF at the beginning of the polymerization process occurred to a varying degree in all polymerizations. Similar observations were made in polymerizations with catalytically activated starch grains in earlier studies (Chapter 3.6). This was attributed to the tackiness of the first layers of PE covering the starch grains. Catalysts are more or less encapsulated by these agglomerations. In order for the polymerization to continue, ethylene monomer needs to migrate into these agglomerations, which could slow down the process. The agglomerations were not uniform in either the single experiments nor between them. These irregular agglomerations may have added to the high statistical deviation found in the polymerization experiments of this study.

In polyolefin based WPC, the general appeal is to increase the wood proportion as far as possible, mainly because the price of wood filler is lower than that of the polyolefin but also because this is seen as a way to make WPC more environmentally friendly

(Chapter 3.3). In polyethylene-based WPC, the proportions of WF are regularly are as high as 70 % or more. In order to reach this, only 2 g of PE need to be polymerized in the presence of 5 g of WF. In all examples where (*n*-BuCp)$_2$ZrCl$_2$ / AlMe$_3$ was used in conjunction with moist wood, more PE was produced. The performed polymerization experiments show that MAO-species, formed by the reaction between wood residual moisture and AlMe$_3$, perform sufficiently well to substitute pre-fabricated MAO in the production of macro bio-filler composites. They would in fact be preferable owing to their lower price and sufficient performance at low amounts.

6.4.2 Material properties

Catalyst immobilization

The observation of segregated WF particles suggest a low degree of catalyst anchoring in cases where thoroughly dried WF was used. This is likely because prefabricated MAO does not adhere reliably to dry WF. This was similarly reported in a number of previous studies, where this seems to extend to AlMe$_3$ as well as other polymeric carbohydrates. The adherence of AlMe$_3$ to dry wood was not investigated separately in this study, as it did not catalyze active ethylene polymerization. However, in gas titration experiments with AlMe$_3$ and dry wood (Chapter 5), almost no methane development was recorded. Hence, there is no reason to expect AlMe$_3$ to adhere to dry wood more than MAO. This would mean that in the corresponding process no true PFT is possible when using polymeric carbohydrate based support materials that were intensively dried beforehand. Procedures utilizing such supports would fall into the category of ISP, where largely homogeneous polymerization occurs in close proximity to filler particles, these being thereby encapsulated by chance.

In all successful polymerizations achieved with the combination of AlMe$_3$ and moist wood, no segregation was observed and almost no bare wood was visible in the SEM micrographs. The absence of segregated particles implies complete encapsulation, which would suggest that all particle surfaces were catalytically active. This coincides well with findings of earlier studies, where similar phenomena were reported for either cocatalyst, AlMe$_3$ and MAO, when used in conjunction with moist carbohydrates. Prefabricated MAO was not separately investigated. However, in gas titration experiments with MAO and moist wood, high amounts of methane development was recorded. It is therefore considered likely that AlMe$_3$ and MAO adhere to moist wood similarly. This would mean that true PFT is possible when using carbohydrate based supports containing residual moisture.

Cocatalysts and catalysts may be anchored to filler surfaces by mechanical interlocking, by physisorption or through the formation of a covalent bond. Overall it seems clear that aluminum alkyls only adhere well to or react with carbohydrate and lignocellulosic microscale sized materials that have not been intensively dried or contain residual amounts of water. There are a number of possible reasons for this.

The theory of mechanical interlocking proposes that AlMe$_3$ enters the cavities and fibrous network structures of a filler containing moisture. By reacting with that moisture, polymeric aluminoxane-structures are formed. These grow in size and thereby interlock

themselves. Free and dissolved aluminum-structures may adhere to the newly formed, interlocked ones. That way, the majority of aluminum-structures may become immobilized. It is conceivable that larger prefabricated MAO cannot access surface pores and fibrous regions as well as the smaller $AlMe_3$; less interlocking would therefore be expected.

This mechanism would be independent of filler-surface chemistry. The absence of water, not the changes induced by intensive drying – such as the described hornification and surface inactivation – would be responsible for lacking catalyst immobilization. If this is true, rewetting the bio-fillers should restore their ability to immobilize $AlMe_3$ and MAO.

The theory of covalent bond forming proposes that MAO or $AlMe_3$ undergo hydrolysis reaction with filler-hydroxyl groups. The theory of physisorption proposes that MAO or $AlMe_3$ are attracted by filler-hydroxyls without undergoing chemical reaction. As MAO and $AlMe_3$ adhere similarly to moist but not to dry bio-fillers, neither mechanism can be the sole cause of the observed phenomena. The filler-surface chemistry and changes thereof must be the determining factor. Hydroxyls of polymeric carbohydrate and lignocellulosic materials have been reported to be more reactive in a never-dried state. Furthermore, a water monolayer on the wood surface could shield it from the non-polar solvent, preserving their mobility and reactivity. This would make either – physisorption and chemical reactions – more likely when using moist material. None of the two mechanisms can be ruled out at this stage. If either mechanism dominates over the other, cannot conclusively be stated. However, in view of the gas developments recorded in Chapter 6, where less reaction was recorded than water was presumably available, high amounts of chemical reaction are seen as unlikely at this point.

Interfacial adhesion

All cryo-microfracture surfaces revealed predominate bare wood surfaces. This is an indication of failure in the interfaces and poor interfacial adhesion but may also be caused by failure in the wood substrate of the filler particles. Microtome cut surfaces revealed ubiquitous gabs between polymer matrix and wood filler. The lack of orientation of the gaps indicate that they are not primarily caused by microtome cutting. Their uniformity indicates that they have been caused by shrinkage of the polymer matrix during cooling down, due to crystallization. These gaps substantiate the assumption of low interfacial adhesion. In combination with reports from earlier studies, easy separation of polymer and filler by extraction indicate no improvement of interfacial adhesion.

Analyzing samples via EDX revealed that it is possible to distinguish wood from PE by mapping for carbon and oxygen. This was surprising, as the samples were carbon coated. In addition, wood and PE both contain large amounts of carbon. The canceling out of the carbon coating is attributed to the penetration depth of the electron beam and excitation volume from which the detected X-rays originate. The different carbon densities of wood and PE are sufficiently high to be clearly detectable. The additional mapping for oxygen clearly highlights the wood fraction.

Elemental mappings were performed on fracture surfaces. Visible wood fragments appeared mostly free of polymer. The color coding visibly separated wood from polymer. Owing to the mentioned penetration depth and excitation volume, it is possible that this

differentiation would not show thin layers of polymer still attached to the wood surfaces. Hence, this method is seen as inadequate in evaluating fracture surfaces for interfacial adhesion conclusively on its own.

Molecular weight

Metallocenes indirectly immobilized by MAO coated supports are reported to preserve their single-site character and thus produce a very similar polymer when compared to that of a homogeneous process. In the case of bio-fillers, slightly higher avg. MWs as well as broader MWDs were reported. In this study, the MW and MWD of the PEs produced in homogeneous and ISPs, where very high amounts of prefabricated MAO were used, were alike. In addition, in this and in earlier studies it was observed that the amount of interaction between MAO and thoroughly dried bio-fillers is very low. If this is the case, a large part of the added MAO would not have been immobilized on the WF but rather in solution. Hence, mostly homogeneous polymerization in the presence of wood particles occurred, leading to similar results as seen in the absence of a filler.

In cases where less MAO is added, such as the Reference polymerizations of this study, a relatively larger share of that MAO would be in contact with the filler's surface. In that case, the effect of such an interaction described by other authors could come into effect, i.e. lead to higher MWs and MWDs.

MAO-like species, formed by utilizing moisture contained in bio-fillers, are reported to produce considerably higher MWs than prefabricated MAO. This is reflected by the results of this study, where the avg. MWs are in fact distinctly higher. Lower catalyst concentrations have been reported to lead to higher MWs. Shares of zirconocene may have been deactivated by wood functional groups or polar wood extractives, leading to these lower catalyst concentrations. Although this is certainly possible, in view of the use of extracted WF and the provided surplus of $AlMe_3$, it is seen as unlikely.

The MWDs, in contrast to the MWs, are all relatively uniform. MAO-like species, formed by utilizing moisture contained in bio-fillers, are reported to produce considerably higher MWDs than prefabricated MAO. In this study, the MWDs appear mostly unaffected. The avg. Đ is approx. 2.2, which is regarded as evidence that only one single catalytically active site is present (Brintzinger et al. 1995; McDaniel 2010). This indicates that the state of the zirconocene is not significantly altered by interactions with bio-filler surfaces or extractives.

It is well documented that a higher polymerization temperature leads to higher catalytic activity, accompanied by lower MWs. This is reflected by the experiments of Series 2, where PE polymerized at 30 °C showed distinctly higher MWs compared to PE polymerized at 60 °C.

Monomodal distributions were observed in all but two exceptions: S2_5 and S2_13 show bimodal distributions. Bimodal distributions are generally explained by the existence of two or more catalyst species. The immobilization of catalysts onto solid supports is well reported in the literature (Chapter 3.6). The nature of a metallocene's active center is changed when directly immobilized onto a support. If MAO does not completely occupy the surface of thoroughly dried carbohydrate supports, it would be left accessible for the

metallocene catalyst to interact with. The recorded multi-modal distributions could indicate direct filler-catalyst interaction.

Crystallinity

It is generally agreed upon that wood fillers act as nucleation agents. The addition of wood fillers to polyolefin polymers was reported to lead to an increase in onset and peak crystallization temperatures.

In this study, the larger share showed very similar T_o, independent of wood content. Only one set of experiments showed higher T_o, i.e. the experiments of Series 2, where the temperature at which the WF was treated with $AlMe_3$, was raised from 30 to 60 °C during treatment.

The polymerization temperature appears to exert a positive influence on T_o. However, under close examination, only that same set of experiments is contributing to the observed higher T_o values. The other composites show very similar T_o, independent of the polymerization temperature.

Higher polymerization temperatures led to lower molecular weights, which leads to the assumption of the molecular weight influencing T_o. It has to be noted that the molecular weights were only determined for a few of the produced composite materials. Therefore, only an incomplete picture can be considered here. Within Series 2, composites polymerized at 60 °C show lower M_n and higher T_o than those polymerized at 30 °C. However, neat PE of Pilot_1 polymerized at 60 °C and featuring even lower M_n does not follow that relationship. The Reference composites were polymerized at 30 and 60 °C and should therefore feature different molecular weights. However, they do exhibit equal T_o. Considering all this, the influence of the molecular weight on T_o is inconclusive.

It has been reported in earlier studies that Al-particles are also able to act as nucleation agents. The influence of the differing amounts of $AlMe_3$ additions within Series 2 was also considered. The drying conditions were equal in all experiments, therefore the amount of water should have been equal. In the case of composites received from polymerizations performed at 60 °C, higher $AlMe_3$ additions clearly led to higher T_o. However, the T_o of composites received from polymerizations performed at 30 °C was not influenced by the amount of $AlMe_3$ added. Furthermore, the high amounts of cocatalyst used in the Pilot experiments did not facilitate crystallization. Hence, high amounts of cocatalyst do not appear to cause higher T_o on their own.

In experiments where the MCs were varied but the $AlMe_3$ addition was kept constant, higher MC prolonged crystallization.

It seems that the T_o is governed by a complex phenomenon, possibly involving an interplay between MC, moisture availability, $AlMe_3$ amount and wood surfaces. This interplay could lead to morphologically different aluminoxane-structures and grain sizes, which in turn either do or do not affect crystallization. There is no clear indication that the wood itself facilitates crystallization.

The peak crystallization point T_p is increased considerably by wood contents of around 30 % and above. The T_p is lifted from values around 108 °C to temperatures around

114 °C. However, a wood content at which this shift occurs was not precisely identifiable. It appears that an initial WF addition does affect the T_p heavily and that in a certain WF range a shift to a higher temperature occurs. After that shift additional WF does not increase T_p further. This could be because the increasing T_p is approaching the T_o.

The melting point T_m exhibits a strong dependence on the wood content. The addition of WF clearly lowers the melting point. The two pilot experiments where large quantities of prefabricated MAO were used, exhibited low melting points compared to their low wood contents. Excluding the two pilot experiments and only considering those experiments, where aluminum compound was added in amounts adjusted to the amount of wood filler, the observed dependency would be even more apparent.

The results of X_c determined in this study coincide well with results of earlier studies. Higher wood contents lead to overall lower X_c. The X_c of the composite is a negative linear function of wood content. The X_c of the PE fraction of a composite also shows a linear negative function of the wood content. However, the gradient is much smaller and the deviation higher.

Micrographs of neat PE and WPCs with 17 and 53 % wood content visualized the effect of microscale wood fillers on the crystallinity of the PE matrix. The presence of only 17 % WF led to distinctly smaller crystallites. The addition of 53 % WF led to micrographs dominated by wood fragments. This clearly shows that wood filler acted as a spatial confinement for growing crystallites and thereby lead to overall smaller crystallites.

The later results coincide well with each other. The confinement of the growing crystals by wood filler particles lead to smaller crystals, larger amorphous shares and lower melting points.

6.5 Conclusion

Using w-H_2O as an active part in the catalytic ethylene polymerization of PE based WPC has been proven highly successful. Yields well beyond the practical necessity of highly filled commodity products – with 60 % or higher wood filler contents – were reached. Yields were in part on par with those produced using prefabricated MAO. In addition, catalyst immobilization was improved by the utilization of moist wood compared to thoroughly dried wood, leading to enhanced encapsulation and reduced adjacent homogeneous polymerization from solvated catalyst, indicating that the applied method predominantly leads to true polymerization filling.

$AlMe_3$ / w-H_2O demonstrated the exceptional potential of saving energy during polymerization while preserving high polymer properties. Considerably higher MWs were received from $AlMe_3$ / w-H_2O compared to prefabricated MAO, enabling the production of analogous PEs at lower temperatures. The dispersity of all received PEs remained similarly low at an avg. of 2.2, indicating low degree of direct filler-catalysts interaction and the preservation of the single-site character of the zirconocene catalyst. The crystalline structure of the received composite materials was shown to predominantly be a function of wood content, again indicating very similar morphology of the received polymers. Raising the polymerization temperature leads to distinctly increased yields and reduced avg.

MWs, offering the possibility of tailoring resultant composite properties to the requirements of the anticipated application.

Moisture management has been shown to hold the potential of reaching even higher polymerization yields. Vacuum drying conditions, i.e. moisture contents, directly influence the catalytic activity and the polymerization yield. The application of mild drying conditions in combination with constant $AlMe_3$ addition – within limits – led to higher yields. This indicates that even greater polymerization activities and yields are possible when combining higher MCs with higher additions of $AlMe_3$. Raising the $AlMe_3$ addition while keeping the drying conditions constant, i.e. raising the $AlMe_3$ to w-H_2O ratio, revealed no clear influence on the yield.

These results offer good reason to believe that the use of $AlMe_3$ / w-H_2O is applicable in combination with most – if not all – catalysts that are known to function well with prefabricated MAO. This in turn opens up the possibility of polymerizing and copolymerizing a vast array of monomer types with such systems, potentially leading to new hybrid materials offering unique property profiles.

Now that the feasibility of utilizing moist wood as catalyst support has been proven, future work should focus on investigating novel value-added material concepts that may be received by such processes.

Some evidence of improved adhesion between wood filler and matrix PE was observed in this work. Only a small amount of research on the mechanical properties of composites produced by catalysts immobilized on bio-filler has been published and no true comparisons with conventional composites were made. Future work should focus on substantiating possible improvements regarding interfacial adhesion, filler dispersion and mechanical properties.

In composites where only low shares of polymer are desired, such as WPC, a reduced amount of catalyst may potentially suffice. Using less catalyst would make for a more economical process. However, whether low amounts of catalysts in relation to wood filler lead to irregular encapsulation and less stable processes, needs to be investigated.

ISP or PFT may hold potential in producing fiber reinforced composites. In traditional processing high shear and pressure lead to better composite properties. However, long fibers are degraded and shortened by intensive processing and therefore cannot reach their full reinforcing potential. ISP or PFT may lead to pre-composites that require less processing to form high quality composite materials, preserving the high aspect ratio of fiber fillers.

ISP or PFT may hold particularly high potential in forming UHMWPE fiber composites. UHMWPE generally features higher impact resistance but lower moduli than HDPE. Due to its inherent high melt viscosity, it is generally formed by techniques such as compression molding rather than processes that utilize a lot of shear and torque. Laminates of LDPE coated paper have been shown to feature high mechanical properties (Michell et al. 1976). By encapsulating long bio-fibers with UHMWPE and forming products thereof by compression molding, the production of materials with impact properties superior to common WPCs and moduli superior to neat UHMWPE may be possible.

Special attention should be given to nanocellulose as a catalyst support. Encapsulating single nanofibers with a polymer would yield a free flowing polymerizate and prevent agglomeration. In nanocomposites, high effects can be achieved from very low filler contents, which could make use of the high polymerization activities of modern catalysts. Modern methods of derivatization have led to nanocellulose that disperses well in non-polar organic solvents as well as polyolefins (Navarro and Edlund 2017). The individual encapsulation of such derivatized nanocellulose would lead to even dispersion, good interfacial interaction and potentially very high material properties.

7 Macro-Confined Catalytic Polymerization of Ethylene in Wood Cell Lumen

7.1 Introduction

Lumen modification, in contrast to other wood preservation measures (Chapter 3.2), refers to processes where cell lumen are filled or inner cell wall surfaces are coated by a desirable agent, generally without penetrating and swelling the cell walls (Ibach and Ellis 2005). Lumen modification is generally used to improve properties such as surface hardness, toughness and abrasion resistance as well as to reduce the rate of water sorption and the resistance to biodegradation (Ibach and Ellis 2005; Scholz et al. 2012). More specialized functionalization, such as fire retardance (Merk et al. 2015), magnetization (Merk et al. 2014) or transparency (Fink 1992; Zhu et al. 2016; Li et al. 2018) may also be achieved by lumen modification.

The effectiveness of any lumen modification method is highly influenced by its macrodistribution, i.e. the extent of penetration and distribution within the pore volume of wood. The degree of cell loading with filler agent generally has a positive effect on mechanical property improvements (Ibach and Ellis 2005). Deep penetration is important, as shallow surface treatments rarely provide long-term protection, because degrading organisms can attack the interior of the wood (Sell 1977; Richardson 2001).

It is evident that sufficient **wood permeability** is highly important, in order to permit the required penetration and retention of a treatment agent (Richardson 2001). The favored path for the movement of fluids through the interconnected capillary system of wood depends on the type of wood, the type of fluid as well as the driving force (Rowell 1984; Walker 2006). Pit configuration, subject to wood species and drying conditions, is one major governing factor. In aspirated pits, the torus adheres to the pit border like a plug, effectively preventing the flow of fluids (Comstock and Côté 1968; Siau 1984). In general, the sapwood of many softwoods are quite accessible. Pine sapwood is a prominent example, as it is highly treatable (Buro and Buro 1959; Rijckaert et al. 2001; Lebow 2010), finds broad use in contemporary research (Scholz et al. 2010b; Scholz et al. 2010a; Ghosh et al. 2013; Reinprecht et al. 2013; van Opdenbosch et al. 2013) and may in fact be considered as a standard material in wood modification research. It was therefore deemed suitable for the purpose of this study.

The **Impregnation of wood with liquid** treatment agents may be performed by mere soaking or steeping, but the application of pressure or vacuum generally leads to deeper penetration and higher retention (Lebow 2010). In the case of organic liquids, increasing viscosity led to the diminishment of impregnation (Bauch and Liese 1966).

The advantages of **penetration with gaseous systems** are: better diffusion due to the greater mobility of treatment agent, the avoidance of blocked pores, permeation is achieved by lower pressure differences and the recycling of the treatment agent is facilitated. Best results were achieved by oscillating pressure treatments (Barnes et al. 1969). Longitudinal diffusion of gases is reported to be rapid, with complete diffusion through 25.5 mm pine sapwood occurring after 10 to 60 min (Scheffrahn et al. 1992). Gas-wood

interaction such as sorption showed the tendency to counteract penetration (Ren et al. 1997).

The effectiveness of a treatment is also highly influenced by the **retention** of the treatment agent within wood. Fixation may occur either through chemical interaction between the treatment agent and the cell wall substrate, between the agent components themselves or by physical deposition as result of solvent loss or solidification (Rowell 1984). Attachment of the treatment agent to the cell wall generally has a positive influence on the desired modification (Ibach and Ellis 2005). Low levels of fixation may lead to leaching, also referred to as bleeding or oozing out, of the active reagent. Leaching of the treatment agent over time generally diminishes the long-term effect, however may also pose health and environmental risks (Lebow 2010).

The treatment of wood with waxes, in order to make it more water repellent has been well documented since ancient times, and today, these products are readily commercialized (Richardson 2001; Scholz et al. 2010c). Even very low degrees of wax loading can have a considerable effect on capillary water uptake and on contact angle measurements (Sell 1977). The impregnation with waxes have also been shown to positively influence the mechanical properties of wood, with high hardness and high molecular weight waxes having the most pronounced effect (Ibach and Ellis 2005; Scholz et al. 2010b).

In the case of wax-impregnation, the phenomenon of leaching upon heating, e.g. when exposed to direct sunlight, is a well reported issue and is closely linked to the waxes' low melting temperatures. In the case of hydrocarbon waxes, higher melting temperatures are generally accompanied by higher melt viscosities (Wolfmeier et al. 2011), which antagonizes deep impregnation (Burmester 1970).

The ISP procedure holds the potential to bypass the relation between high melting point and high viscosity. By introducing catalysts and monomer solvated in low viscosity solvents or as gas, deep penetration and relatively uniform distribution should be possible. The affinity of $AlMe_3$ and MAO towards hydroxyl groups should make the immobilization of catalysts on the inner cell wall surfaces within cell lumen possible. Subsequent polymerization from these catalytically activated surfaces should lead to the coating of the cell walls with polymer. Deep penetration, uniform distribution and the coating of the CWs promise a considerably effect at relatively low loading. Furthermore, utilizing the appropriate catalysts would yield PEs with melting points higher than 120 °C, i.e. well above the practical application temperatures of wood. This should all but prevent leaching.

In order to investigate the most efficient pathways for impregnating bulk wood lumen with catalytic compounds, tests were conducted. Wood was treated with pure liquid $AlMe_3$ as well as with gaseous $AlMe_3$.

Polymerization experiments, in close reference to the slurry polymerizations conducted in Chapter 6, were performed. In these experiments samples were impregnated with a cocatalyst and catalyst in toluene solution. Samples were either left soaked or were submerged in toluene. Monomer gas was applied. This means that polymerization would occur in the macro-confinement within the toluene filled wood lumen.

Gas-phase polymerizations utilizing a novel Flow-Reactor design were performed, in order to investigate enhanced monomer delivery to catalytic sites confined within the porous wood structure. Successful gas-phase polymerization using (*n*-BuCp)$_2$ZrCl$_2$ (Ihmels 2004) and other metallocenes (Tajima et al. 2000) is reported. In gas-phase polymerizations, samples were impregnated with cocatalyst and catalyst solutions, but were dried before the monomer was applied. This means that polymerization would occur in the macro-confinement within the wood, in a gaseous atmosphere containing varying proportions of inert gas and monomer.

7.2 Experimental

7.2.1 Materials

7.2.1.1 Catalysts

The same **(*n*-BuCp)$_2$ZrCl$_2$** catalyst that was used previously in the Slurry-Polymerization experiments, was again used here in the form of a 0.5 mmol/l toluene solution. For more information refer to Chapter 6.2.1.1.

7.2.1.2 Cellulosic Materials

Solid pine sapwood samples – as displayed in Figure 40 – were used for polymerization within solid wood. Samples were cut from commercially kiln-dried pine sapwood to the dimensions of 25 x 25 x 10 mm (rad x tan x long) in accordance with the *German Industry Standard* Deutsches Institut für Normung DIN 52184:1979-05, for the determination of swelling and shrinking of solid wood. The average bulk density was 0.59 g/cm³. With an assumed true density of the cell wall of 1.5 g/cm³, the porosity of the wood samples was at approximately 60.6 %, which coincides well with literature values (Sixta 2006). If not stated otherwise, wood samples were stored at 20 °C and 35 % RH. The transfer of samples from the climate chamber to the laboratory was done in sealed containers.

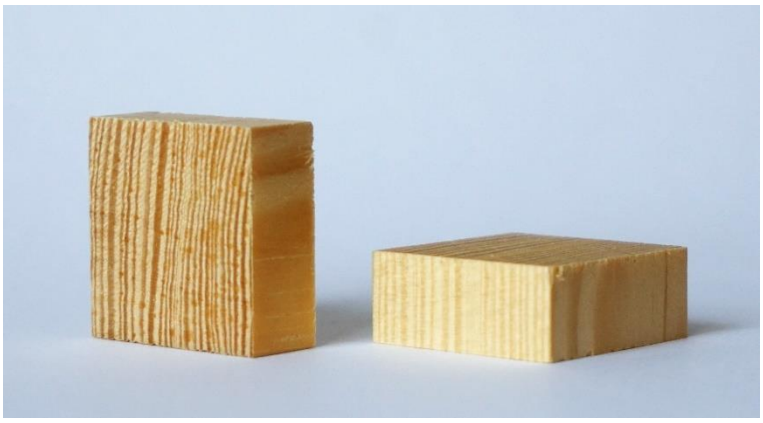

Figure 40: Solid pine sapwood samples.

7.2.1.3 Chemicals

Acetone 99 %, denatured **ethanol** 96 % and **isopropyl alcohol** 99 % (all from BCD Chemie GmbH, DE) were used for cleaning and quenching.

Toluene 99 % (BCD Chemie GmbH, DE) was purified by distillation and passing through columns with 4 Å molecular sieve as well as BASF catalyst PuriStar R3-11G.

7.2.1.4 Cocatalysts

Methylaluminoxane in toluene solution (AXION CA 1310, formerly Chemtura Organometallics GmbH; at the time of writing a subsidiary of Lanxess AG, DE). From the data provided by the product data sheet (5.1 wt-% Al cont.) the concentrations of total aluminum and of aluminum associated with the basic MAO structure where calculated. The total aluminum concentration was at approx. 1.7 mol/l. The concentration of aluminum associated with the structural unit $[\text{-Al}(CH_3)\text{-O-}]_n$ was at approx. 1.1 mol/l.

Trimethylaluminum was used in two forms, pure (Prod. No. 257222-100G, Sigma-Aldrich, subsidiary of Merck KGaA, DE) and as a 2 mol/l toluene solution (Prod. no. 198048, Sigma-Aldrich, subsidiary of Merck KGaA, DE).

Despite its name and its basic formula, trimethlyaluminum is actually arranged as the dimer Al_2Me_6, where both molecules are connected by two 3-center-2-electron bonds.

7.2.1.5 Gases

Grade 3.0 **Ethylene** 99.8 % (GHC Gerling, Holz & Co. Handels GmbH, DE) was used as monomer for polymerizations. The ethylene was purified by passing through columns filled with 4 Å molecular sieve as well as the PuriStar R3-11G catalyst (BASF SE, DE).

Grade 5.0 **Nitrogen** 99.999 % (Linde GmbH, DE) was used as inert gas.

7.2.2 Methods

7.2.2.1 1l-Autoclave

All solid wood slurry polymerizations were conducted in the 1l-autoclaves described in Chapter 4.2.2.1 and 6.2.2.1.

Custom holders were manufactured and attached to the stirrer shaft instead of the standard anchor design stirrer. The schematics of the custom holders are displayed in Figure 41. The holder consisted of a metal block with two recess slots, enabling it to accommodate wood samples on opposite sides. The holders were equipped with a clamp on either side, in order to lock samples in place.

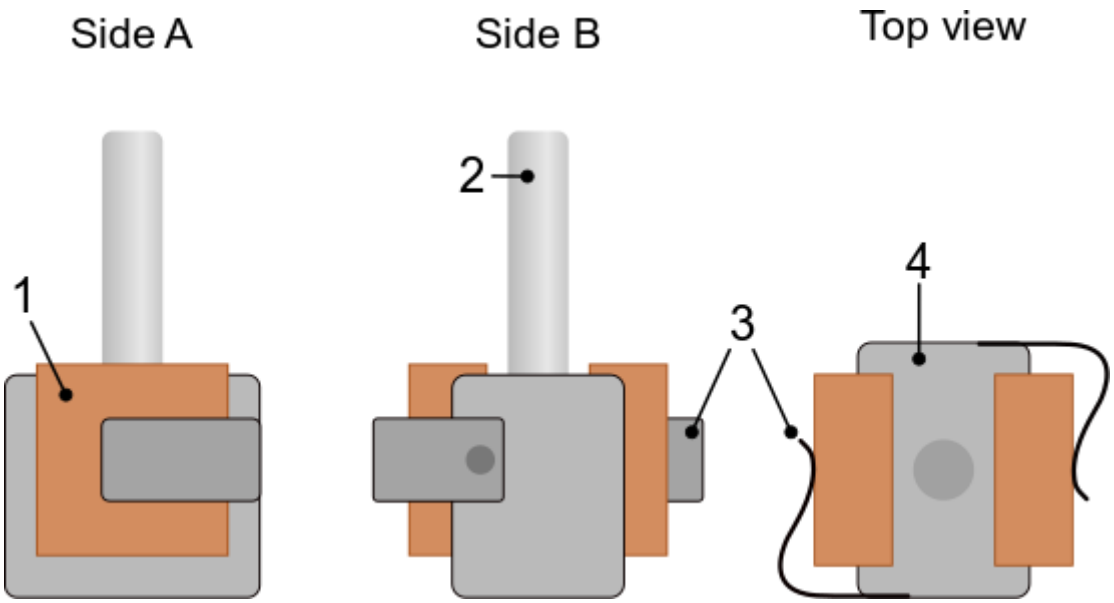

Figure 41: Schematics of custom holder for wood samples.
(1) Sample; (2) Shaft; (3) Clamp; (4) Metal block with slot.

7.2.2.2 Flow-Reactor

A novel reactor was designed to change the mechanism by which reagents are transported into bulk wood samples from slow diffusion to faster viscous flow. The reactor design allowed for the passage of fluids through a 25 x 25 x 10 mm wood sample (Figure 42). The design comprised of a stainless steel flange with a recessed slot to accommodate the wood sample. The flange was fastened with six screws and sealed by an O-ring. Tubes were connected to either side of the flange. Each was equipped with two smaller in- and outlet tubes. 3-way cocks were connected to the in- and outlet tubes.

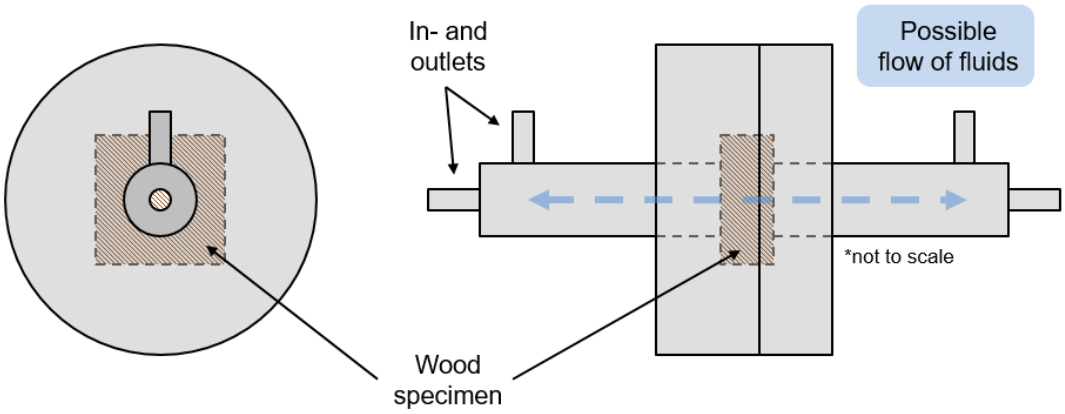

Figure 42: Novel Flow-Reactor design to accommodate passage of fluids trough a porous sample such as wood.

With this reactor design, working exclusively with gaseous reagents can be achieved in both the vertical and horizontal orientation. A vertical orientation of the reactor is preferred when working with liquid reagents. In such an orientation, it is possible to insert liquid reagents through the upper in-line inlet under a nitrogen countercurrent applied through the upper perpendicular inlet. The lower in-line outlet can be used to discharge liquid and the lower perpendicular outlet can be used to apply a vacuum to facilitate drainage. In order to prevent drainage from entering the perpendicular outlet, a slightly tilted orientation of the reactor with the outlet pointing up is favorable.

7.2.3 Procedures

7.2.3.1 Catalyst Impregnation Pathways

$AlMe_3$ is well suitable for analyzing the impregnation of wood with a reagent that is prone to reacting with the substrate. Untreated dry wood only contains 1 – 10 mg/kg of aluminum (Faix 2008). Hence, any significant amount detected is likely to correspond with the treatment. In addition, aluminum generates a strong signal in energy dispersive X-ray analysis, i.e. it is easily detectable.

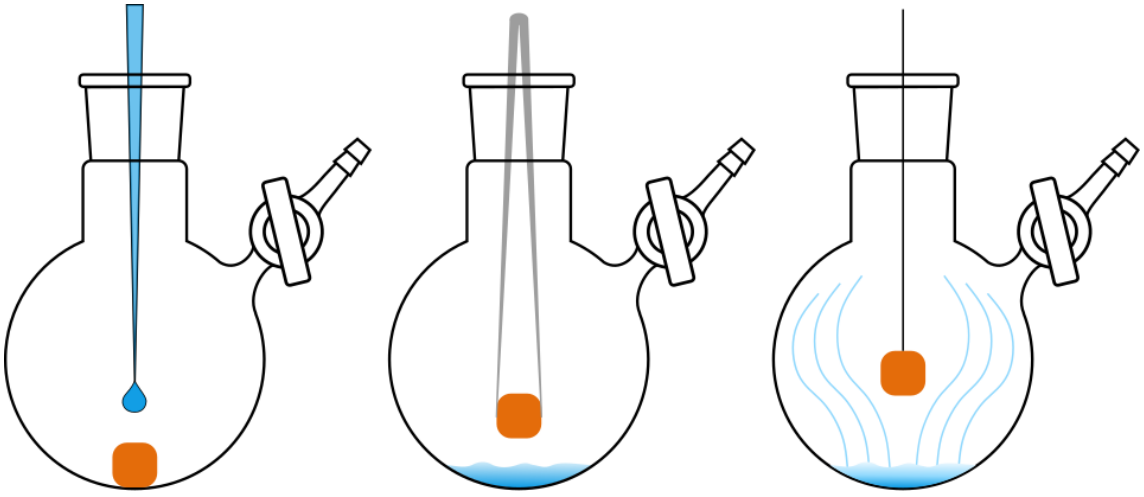

Figure 43: Investigated catalyst impregnation pathways.
Left: Catalyst applied directly onto wood; Middle: Wood placed directly into pool of catalyst; Right: Wood exposed to catalyst vapor phase.

In order to account for the small aperture of the flasks used, the solid pine sapwood samples of the dimensions of 25 x 25 x 10 mm were roughly divided into four smaller, same sized rectangular pieces.

In Impregnation Pathway 1a (**IP1a**) – displayed in Figure 43 on the left – a sample was vacuum dried for 12 h at ambient temperature in a Schlenk-flask. Pure, liquid $AlMe_3$ was directly applied onto the cross section of the dry wood under a nitrogen countercurrent. The flask's top joint was fitted and shut by a stopcock. After the wood had absorbed the liquid, the sample was removed from the flask and rinsed off with toluene. In another similar approach (**IP1b**), liquid $AlMe_3$ was directly applied to undried wood.

In Impregnation Pathway 2 (**IP2**) – displayed in the middle – a sample was vacuum dried for 12 h at ambient temperature in a Schlenk-flask. Liquid $AlMe_3$ was added to the bottom of another flask. The wood sample was transferred to the other flask under a nitrogen countercurrent and placed – with its cross section facing down – directly into the liquid $AlMe_3$. The flask's top joint was fitted and shut by a stopcock. The wood was only immersed by about one third in a longitudinal direction. After the wood appeared to have soaked up the liquid and seemed entirely wetted by it, it was removed from the flask and rinsed off with toluene. This experiment was conducted twice.

In Impregnation Pathway 3 (**IP3**) – displayed on the right – a sample was strapped to a polytetrafluoroethylene-thread and fixated in the middle of a Schlenk-flask. It was vacuum dried for 12 h at ambient temperature. $AlMe_3$ was added to the bottom of the flask under a nitrogen countercurrent. The flask's top joint was fitted and shut by a stopcock. The sample was left exposed to the $AlMe_3$ vapor phase for 20 h; thereafter it was removed from the flask and rinsed off with toluene. This experiment was conducted once.

The aluminum distribution within the samples was subsequently investigated via scanning energy-dispersive X-ray spectroscopy. For that purpose, samples were split perpendicular to the fiber orientation, roughly in the middle of the samples. The cross sections were cut with a sledge microtome, in order to attain smooth surfaces.

7.2.3.2 Macro-Confined Slurry Polymerization

All slurry polymerization experiments were carried out in the water heated 1l-autoclaves equipped with the custom holders, both described in Chapter 7.2.2.

In **Series 1**, samples were vacuum dried at a relatively high temperature, in order to minimize their MC. Diffusion as means of catalyst impregnation was investigated.

Three experiments with two samples each were carried out (Table 19). Two pine sapwood samples were clamped onto a custom holder with their radial faces in a horizontal orientation. In the **drying step**, they were vacuum dried for 120 min at 80 °C. After the drying time had elapsed, three purge-and-refill cycles were applied using nitrogen. The temperature was lowered to the subsequent polymerization temperature of 30 °C. In the step **solvent addition**, 300 ml dried toluene was dosed to the reactor, covering the wood samples entirely. The rotational speed of the anchor stirrer was set to approx. 260 rpm. For the **aluminum addition**, the total amount of 12 mmol of $AlMe_3$ was added under a nitrogen countercurrent. The aluminum was added in the form of a 2 mol/l solution and the impregnation time was 120 min. The **catalyst addition** was carried out with a syringe under a nitrogen countercurrent. The amount of $(n\text{-BuCp})_2ZrCl_2$ of 0.5 µmol was kept constant and the impregnation time was 120 min. The polymerization was started by the **ethylene addition.** The partial monomer pressure was set to 2.7 bar. The polymerization was stopped after 120 min by quenching.

Table 19: Series 1 *in situ* solid wood slurry-polymerization procedure with (n-BuCp)$_2$ZrCl$_2$ / AlMe$_3$.

Step	Variables	Values Series 1
Drying	Wood: Vacuum: Temperature: Time:	Pine sapwood 1.0 – 0.1 mbar 80 °C 120 min
Solvent addition	Solvent: Volume: Stirring:	Toluene 300 ml 260 rpm
Aluminum addition	Amount: Temperature: Time:	12.0 mmol 30 °C 120 min
Catalyst addition	Amount: Temperature: Time:	0.5 µmol 30 °C 120 min
Ethylene addition	Pressure: Temperature:	2.7 bar 30 °C
Polymerization	Time:	120 min

In **Series 2**, the process from the prior polymerizations was adopted but a lower drying temperature was used, in order to retain higher MCs. The succession and method of aluminum and toluene addition were investigated. Furthermore, the ethylene was applied before the catalyst was added.

Two experiments with two samples each were carried out (Table 20). Two pine sapwood samples were clamped onto a custom holder. They were vacuum dried for 120 min at 30 °C. After the drying time had elapsed, three purge-and-refill cycles were applied using nitrogen. In **2a**, the autoclave was filled with 300 ml of toluene before the total amount of 12 mmol of AlMe$_3$ was added. The impregnation time was 30 min. In **2b**, the AlMe$_3$-toluene solution was dosed to the bottom of the autoclave before it was filled with the toluene. The impregnation time was 30 min. The ethylene was applied at 2.7 bar partial pressures until saturation was reached. The polymerization was started by the catalyst addition, which was carried out under a nitrogen countercurrent. The amount of (n-BuCp)$_2$ZrCl$_2$ of 0.5 µmol was kept constant. The polymerization was stopped after 60 min by quenching.

Table 20: Series 2 *in situ* solid wood slurry-polymerization procedures with (n-BuCp)$_2$ZrCl$_2$ / AlMe$_3$.

Step	Variables	Values	
		Series 2a	Series 2b
Drying	Wood:	Pine sapwood	
	Vacuum:	1.0 – 0.1 mbar	
	Temperature:	30 °C	
	Time:	120 min	
Solvent addition	Solvent:	Toluene	-
	Volume:	300 ml	
	Stirring:	260 rpm	
Aluminum addition	Amount:	12.0 mmol	12.0 mmol
	Temperature:	30 °C	30 °C
	Time:	30 min	-
Solvent addition	Solvent:	-	Toluene
	Volume:		300 ml
	Stirring:		260 rpm
	Time:		30 min
Ethylene addition	Pressure:	2.7 bar	
	Temperature:	30 °C	
	Time:	30 min	
Catalyst addition	Amount:	0.5 µmol	
	Temperature:	30 °C	
Polymerization	Time:	60 min	

In **Series 3**, the process from the prior polymerizations was adopted but the autoclave was not filled with solvent. The AlMe$_3$ was applied directly onto the samples; additionally, the drying times and impregnation times were shortened while the polymerization time was extended.

Four experiments with two samples each were carried out (Table 21). Two pine sapwood samples were clamped onto a custom holder and vacuum dried for 20 min at 30 °C. After the drying time had elapsed, three purge-and-refill cycles were applied using nitrogen. 3 ml of AlMe$_3$-toluene solution was dosed straight onto each wood sample using a long syringe, resulting in an AlMe$_3$ addition of 6 mmol per sample. The impregnation time was 20 min. 0.5 ml of (n-BuCp)$_2$ZrCl$_2$-toluene solution was dosed straight onto each of the two wood samples using a long syringe, resulting in a total addition of 1.0 µmol. The impregnation time was 20 min. The polymerization was started by the addition of ethylene. The partial monomer pressure was set to 2.7 bar. The polymerization was stopped after 360 min by releasing the monomer pressure, purging with nitrogen and exposing the samples to ambient air.

Table 21: Series 3 *in situ* solid wood slurry-polymerization procedures with (n-BuCp)$_2$ZrCl$_2$ / AlMe$_3$.

Step	Variables	Values Series 3
Drying	Wood: Vacuum: Temperature: Time:	Pine sapwood 1.0 – 0.1 mbar 30 °C 20 min
Aluminum addition	Amount: Temperature: Time:	12.0 mmol 30 °C 20 min
Solvent addition	Solvent: Volume: Stirring:	-
Catalyst addition	Amount: Temperature: Time:	1.0 µmol 30 °C 20 min
Ethylene addition	Pressure: Temperature:	2.7 bar 30 °C
Polymerization	Time:	360 min

Samples were weighted after the polymerization process in order record weight gains. A selection of microscopic and spectroscopic methods were utilized to characterize the received materials.

Scanning electron microscopy (SEM) was used to investigate the general state and topology of the received materials. SEM energy-dispersive X-ray spectroscopy (SEM-EDX) was performed to assess distribution and possible agglomeration of catalyst elements. It was revealed in Chapter 6 that X-ray analysis is able differentiate between wood and PE in WPC by mapping for carbon and oxygen. By mapping for carbon, oxygen and aluminum, the three materials: wood, aluminum oxide and PE, can be differentiated by method of elimination. Wood should produce a strong oxygen and carbon signal. Aluminum oxide should produce a strong aluminum and oxygen signal. PE should produce a strong carbon signal and, if at all, weak oxygen and aluminum signals. By that differentiation first indications on successful polymerization are given.

Evaluating the morphology of bulk materials via SEM has its limits. The internal microscopic morphology can remain hidden and very fine surface features may be overcast by conductive coating. Transmission electron microscopy (TEM) was used to investigate the morphology of the received materials in more detail. TEM-EDX was used to differentiate between wood, aluminum oxide and PE.

Electron microscopy and X-ray analysis only elucidate morphology and elemental composition but present no information on molecular structure. In order to proof successful

polymerization within wood cells, Raman microscopy was performed. With Raman spectroscopy, it is possible to record and differentiate between the spectra that are specific to wood and PE.

Polarized light microscopy (PLM), with its lower magnification, was performed on radial sections, in order to receive a broader overview as regards the distribution of reagents and polymerizate within the wood samples. Polarization was used to identify crystalline fillings.

7.2.3.3 Macro-Confined Gas Phase Polymerization

All gas phase polymerization experiments were carried out in the Flow-Reactor described in Chapter 7.2.2.2. The reactor was mounted in a slightly tilted vertical orientation. The upper and lower perpendicular inlets were connected to a vacuum-gas-manifold.

In **Series 4**, samples were pre-dried, in order to minimize their MC. Prefabricated MAO was used as cocatalyst.

Two experiments, each with a single sample, were carried out (Table 22). The wood samples were pre-dried in a desiccator over phosphorus pentoxide. A pine sapwood sample was placed into the recessed slot of the Flow-Reactor. In the **drying step**, the sample was vacuum dried for 120 min at ambient temperature. After the drying time had elapsed, three purge-and-refill cycles were applied using nitrogen. The **aluminum addition** was carried out with a syringe through the upper in-line inlet under a nitrogen countercurrent. 3 ml of MAO-toluene solution was dosed straight onto the cross section of a wood sample. This corresponds to a total aluminum addition of approx. 5.1 mmol or an addition of 3.3 mmol of MAO-associated aluminum. By applying low nitrogen pressure and low vacuum through the upper and lower perpendicular inlets respectively, a pressure gradient was created to force the aluminum solution through the wood sample. The **catalyst addition** was carried out with a syringe through the upper in-line inlet under a nitrogen countercurrent. 0.5 µmol of $(n\text{-BuCp})_2ZrCl_2$ were added and forced through the wood sample by applying a pressure gradient. The polymerization was started by the **ethylene addition.** The partial monomer pressure was set to 2.7 bar. In the first experiment (4a), the monomer pressure was maintained for 120 min. In the second experiment (4b), the monomer pressure was maintained for 18 h. The polymerization was stopped by releasing the monomer pressure and slowly introducing ambient air.

Table 22: Series 4 *in situ* solid wood gas phase polymerization procedure with (n-BuCp)$_2$ZrCl$_2$ / MAO.

Step	Variables	Values	
		Series 4a	Series 4b
Drying	Wood:	Pine sapwood	
	Vacuum:	1.0 – 0.1 mbar	
	Temperature:	Ambient	
	Time:	120 min	
Aluminum addition	Amount:	5.1 mmol	
	Temperature:	Ambient	
	Time:	30 min	
Catalyst addition	Amount:	0.5 µmol	
	Temperature:	Ambient	
Ethylene addition	Pressure:	2.7 bar	
	Temperature:	Ambient	
	Time:	30 min	
Polymerization	Time:	120 min	18 h

In **Series 5**, another approach was tested. Wood samples that were stored at 20 °C and 35 % RH were treated with catalyst solutions in large diameter test tubes, before being transferred to the Flow-Reactor. AlMe$_3$ was used as cocatalyst.

Two experiments, each with a single sample, were carried out (Table 23). The wood samples – preconditioned at 20 °C and 35 % RH – were each placed into large diameter Schlenk-test tube each. The test tubes were connected to a vacuum-gas-manifold and placed into an actively heated oil bath. In the **drying step**, they were vacuum dried for 120 min at 30 °C. After the drying time had elapsed, three purge-and-refill cycles were applied using nitrogen. The **aluminum addition** was carried out with a syringe under a nitrogen countercurrent. In order to immerse the sample entirely, 25 ml of AlMe$_3$-toluene solution was added to the flask. The aluminum was added in the form of a 0.8 mol/l solution, resulting in an AlMe$_3$ addition of 20 mmol per sample. To facilitate uniform impregnation, alternating nitrogen pressure and vacuum were applied. In the first experiment (5a), the impregnation time was 120 min. In the second experiment (5b), the impregnation time was 24 h. After impregnation the excess aluminum solution was removed using a syringe and the wood samples were dried by vacuum. The **catalyst addition** was carried out with a syringe under a nitrogen countercurrent. 0.5 ml of catalyst-toluene solution, i.e. 0.5 µmol of (n-BuCp)$_2$ZrCl$_2$, was dosed directly onto the middle of the samples cross sections. 12 ml of toluene was added, in order to immerse the samples. To facilitate uniform impregnation, alternating nitrogen pressure and vacuum were applied. The impregnation time was 120 min. After impregnation the excess solvent was removed using a syringe and the wood samples were dried by vacuum.

After the treatment with catalysts, the dried samples were transferred from the test tube to the Flow-Reactor within a glove box. Thereafter the reactor was returned to the lab, mounted in a slightly tilted vertical orientation and refitted with all necessary supplies.

The polymerization was started by the **ethylene addition.** The partial monomer pressure was set to 2.7 bar. In the first experiment (5a), the monomer pressure was maintained for 300 min. In the second experiment (5b), the monomer pressure was maintained for 48 h. The polymerization was stopped by releasing the monomer pressure and slowly introducing ambient air.

Table 23: Series 5 *in situ* solid wood gas phase polymerization procedure with (*n*-BuCp)$_2$ZrCl$_2$ / AlMe$_3$.

Step	Variables	Values	
		Series 5a	Series 5b
Drying	Wood:	Pine sapwood	
	Vacuum:	1.0 – 0.1 mbar	
	Temperature:	30 °C	
	Time:	120 min	
Aluminum addition	Amount:	20 mmol	
	Temperature:	30 °C	
	Time:	120 min	24 h
Catalyst addition	Amount:	0.5 µmol	
	Temperature:	30 °C	
	Time:	120 min	
Ethylene addition	Pressure:	2.7 bar	
	Temperature:	Ambient	
	Time:	30 min	
Polymerization	Time:	300 min	48 h

Samples were weighed after the polymerization process in order record weight gains.

SEM was used to investigate the general state and topology of the received materials. SEM energy-dispersive X-ray spectroscopy (SEM/EDX) was performed, in order to locate aluminum and PE.

7.2.4 Material Characterization

7.2.4.1 Field-Emission Scanning Electron Microscopy

The morphology of the received materials was investigated via field emission scanning electron microscopy (Gemini 1525, LEO Electron Microscopy Inc., US) and energy-dispersive X-ray spectroscopy (Octane plus Silicone Drift Detector, EDAX, Ametek Inc., US). Samples were steam-coated with carbon, generating a carbon coating of approx. 40 nm. FESEM images were captured with an in-lens and a SE2 detector at an electron acceleration voltage of 5 kV. EDX was captured at an electron acceleration voltage of 20 kV. The software used for the elementary analysis was “TEAM Version 4.1” (EDAX, Ametek Inc., US). The signals for carbon, oxygen and aluminum are 0.277 keV (Kα), 0.525 keV (Kα) and 1.486 keV (Kα) correspondingly.

7.2.4.2 Polarized Light Microscopy

Polarized light microscopy was utilized to compare the crystalline structures of PE in WPC to neat PE. Thin-sections of injection molded samples were prepared via sledge-microtome equipped with a stainless steel knife. A “BX51” microscope equipped with a “DP70” camera system (Olympus Europa SE & Co. KG, DE) was used. The software “cellSens Standard 1.16” (Olympus Europa SE & Co. KG, DE) was used for image taking.

7.2.4.3 Transmission Electron Microscopy

Transmission electron microscopy was used to evaluate the polymerization of ethylene within wood. In the course of this study, three different TEMs were utilized. Initial explorative micrographs were taken with an “EM 902” (Carl Zeiss AG, DE) equipped with a 2K-Wide-angle slow-scan CCD-Camera Type 7899. Further micrographs were taken with a “JEM-1011 LaB6” (JEOL Ltd., JP). For EDX analysis a Cs-corrected “JEM-2200 FS” (JEOL Ltd., JP) equiped with a “SDD X-Max 100 LTE” detector (Oxford Instruments plc, GB) was used.

Wood samples were embedded in Spurr-resin (Spurr 1969). 50 nm thin sections were cut with a ultra-microtome equiped with a diamond knife. A cryo-ultra-microtome equiped with a diamond knife was used to produce thin sections of neat PE. Filmed copper 100 mesh grids and unfilmed folding copper 100 mesh grids were used as specimen holder.

7.2.4.4 Raman Microscopy

Raman microscopy has been described as a simple and powerful technique for mapping polymer distribution within plant cells (Berglund and Burgert 2018). The methodology used in this study is based on the comprehensive descriptions of Raman microscopy of plant cell walls by Gierlinger et al. (2012).

15 and 50 µm thick cross-sections were prepared with a solid knife sledge microtome. The first unimpaired sections, received from the region just below the surface of the wood cubes, were chosen for analysis. Sections were placed on a microscope slide, after which they were immersed in water and covered by a coverslip, before being sealed with nail polish in order to prevent drying.

Spectra were acquired with the confocal Raman microscope (alpha300 R, WITec GmbH, DE) equipped with an oil immersion 100× objective (N-Achroplan, NA = 1.25, WD = 0.29 mm, 0.17 mm glass-coverslip correction, from Carl Zeiss, DE), a 532 nm laser, a spectrometer (NIR UHTS400, WITec GmbH, DE) with a spectral resolution of 3.75 cm^{-1} and a back illuminated CCD sensor cooled to 60 °C by a Peltier-element. Raman images were taken by acquiring spectra at a lateral resolution of 0.3 µm. An integration time of 10 ms and laser power of 10 mW were chosen. Measurements were conducted utilizing manual topography correction.

Data treatment and analysis was performed using the “Project 5.1” software (WITec GmbH, DE). To visualize the distribution of specific components within the scanned region, specific bands were integrated. Based on that integration, false-color images were

built. Extracted spectra were cut, background corrected (Sub BG) and cosmic rays were removed as necessary. True component analysis and K-means cluster analyses was performed.

7.3 Results

7.3.1 Catalyst Impregnation

Upon the application of pure, liquid $AlMe_3$ onto wood samples (IP1a), white smoke developed. The smoke development was noticeably pronounced in the case of undried wood (IP1b). In the case where a wood block was soaked in pure liquid $AlMe_3$ (IP2), small bubbles arose from the sample. No smoke development was noticeable in the experiment where a wood sample was hung in midair in an atmosphere containing gaseous $AlMe_3$ (IP3).

In all cases, when retrieving the wood blocks from the flasks and upon ambient air contact, the samples self-ignited. The sample suspended in the $AlMe_3$ vapor phase also self-ignited, but less violently. Rinsing off samples with fresh toluene before retrieving them led to less violent self-ignition.

Two general observations were made when analyzing the samples by way of scanning energy-dispersive X-ray spectroscopy. The bulk of the cell walls returned diffuse aluminum signals (1.486 keV Kα) at an intensity not separable from the background noise. Empty voids of the cell lumen returned no signals.

The aluminum distribution of **IP1a**, where pure liquid $AlMe_3$ was directly applied onto dried wood, is displayed in Figure 44. The corresponding spectrum (see Figure 61 in Annex) shows a clear aluminum signal. The micrograph displays one representative region of interest (ROI). The distribution of the aluminum is not uniform. Single cells or groups of cells show distinct signal intensities at the interfaces between cell wall and cell lumen. In other areas, the aluminum signal of the cell wall is weak and diffuse. The wood ray in the middle of the micrograph shows the strongest signal. Other ROIs of that same sample showed similar trends with higher signal intensities along rays and next to the resin canals.

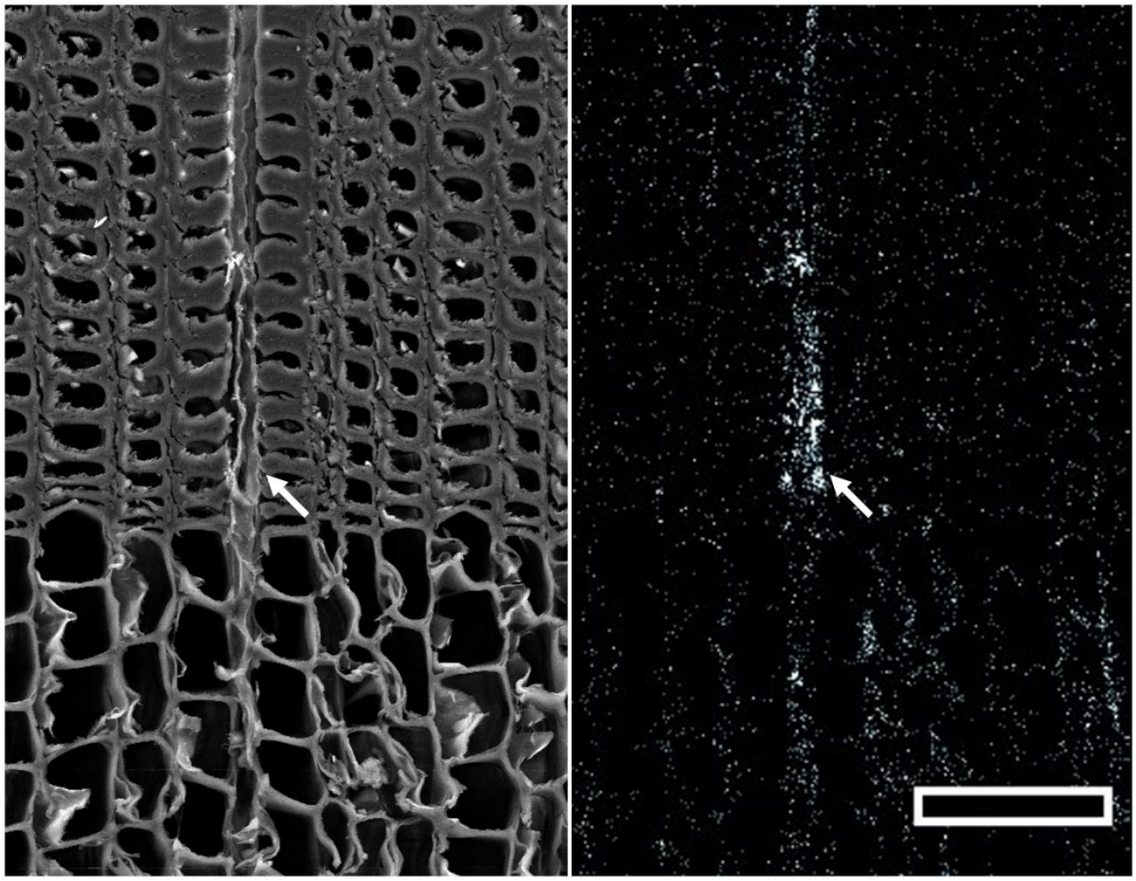

Figure 44: SEM-EDX analysis showing the aluminum distribution in a cross section originating from the center region of IP1a.
Scale bar 100 µm.

The elemental analysis of **IP1b**, where pure liquid $AlMe_3$ was directly applied onto wet wood, did not show a signal peak corresponding to aluminum.

The aluminum distribution of **IP2**, where dried wood was soaked in pure liquid $AlMe_3$, is displayed in Figure 45. The corresponding spectrum (see Figure 62 in Annex) shows a clear aluminum signal. The micrograph displays one representative ROI. Other ROIs of that same sample showed similar trends. In spite of some clusters of higher signal intensity, the distribution of the aluminum was more uniform than in IP1a. The majority of cells exhibited strong signals along the interface between the cell wall and the cell lumen.

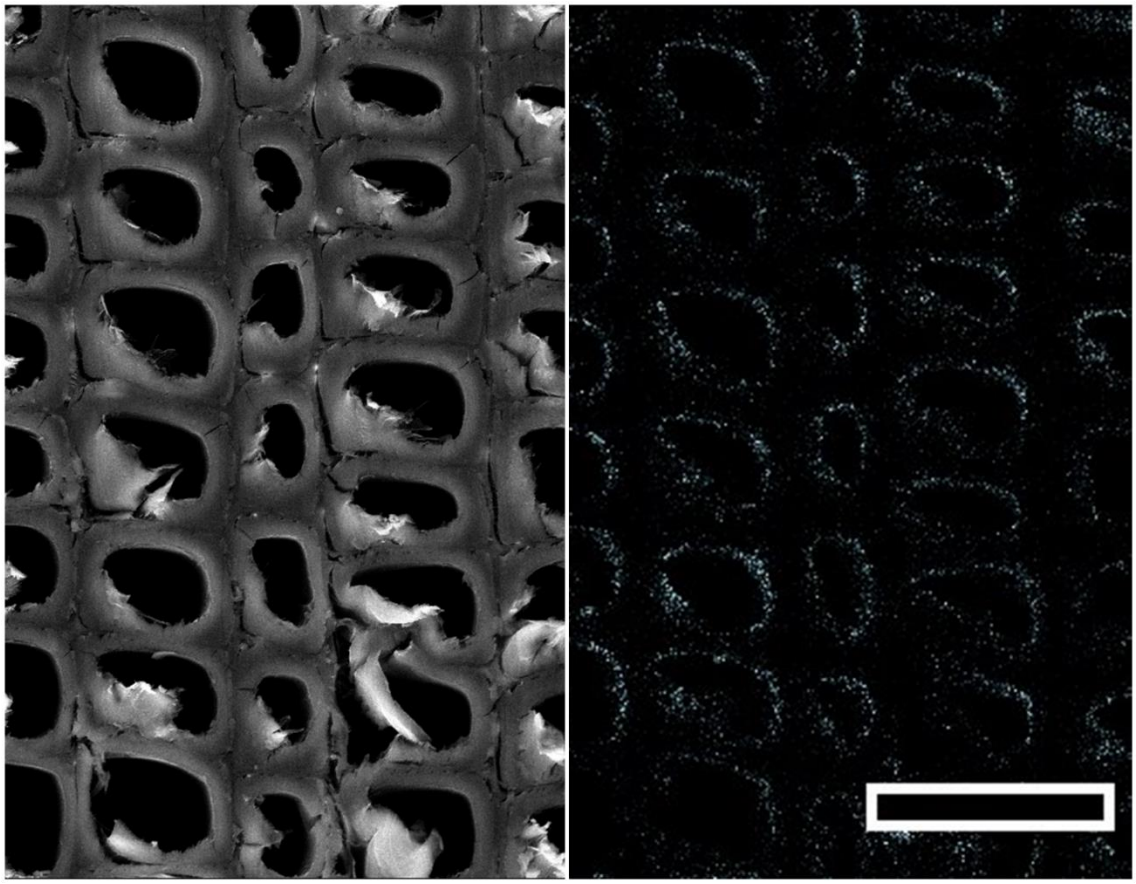

Figure 45: SEM-EDX analysis showing the aluminum distribution in a cross section originating from the center region of IP2.
Scale bar 50 µm.

The aluminum distribution of **IP3**, following vapor phase $AlMe_3$ impregnation, led to an uneven distribution and a low amount of detectable aluminum. In a few cases the inside cell walls returned a distinct aluminum signal. However, the overall occurrence of such cells was lower than in IP1 and IP2. In contrast to IP1 and IP2, small granular agglomerates were found in IP3, marked by white arrows in Figure 46. The corresponding spectrum (see Figure 63 in Annex) shows a clear aluminum signal. Similar granular agglomerates adjoining inner cell walls were found in other ROIs of that same sample.

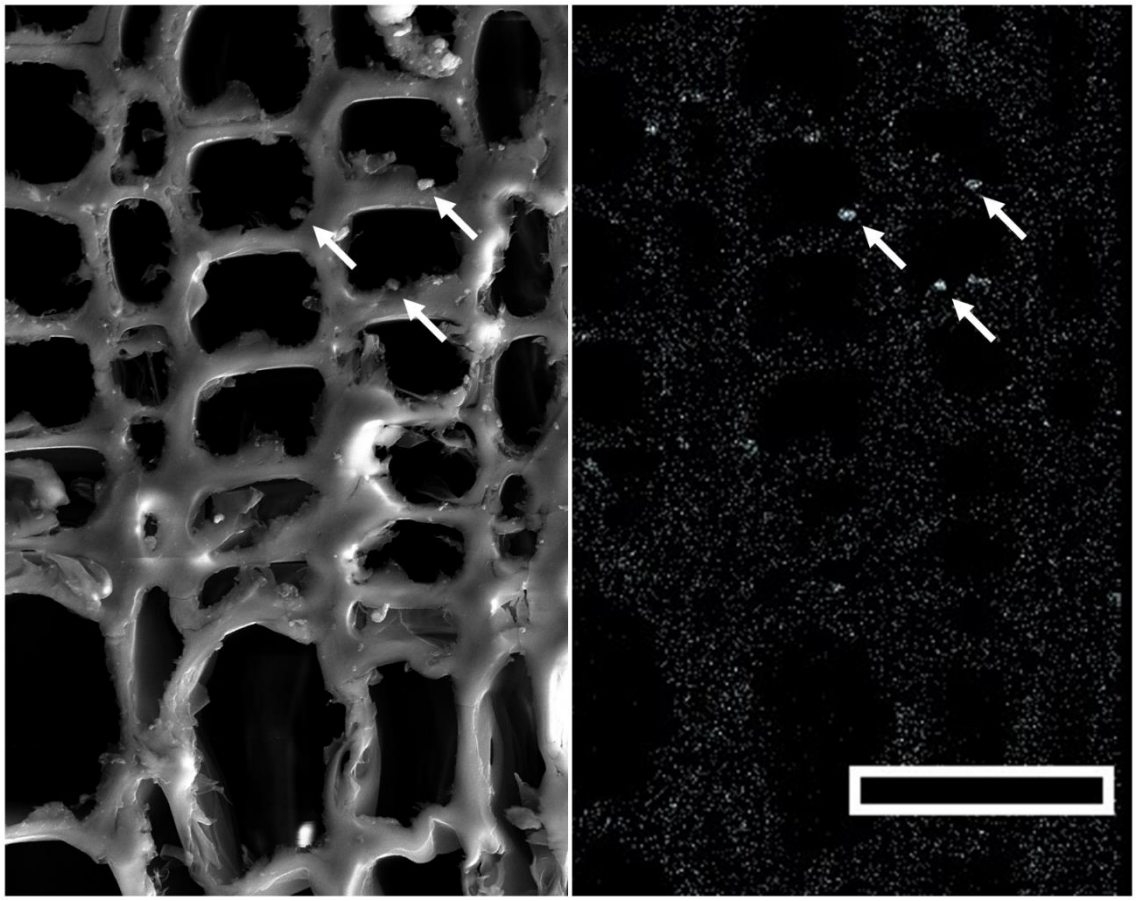

Figure 46: SEM-EDX analysis showing the aluminum distribution in a cross section originating from the center region of IP3.
Scale bar 50 µm.

7.3.2 Macro-Confined Slurry Polymerization

Some general observations were made to varying degree in all slurry polymerizations.

In all cases where $AlMe_3$ was applied onto the samples directly, white smoke developed. The application of aluminum solution left samples with a white coating (Figure 47, compare to Figure 40 in Chapter 7.2.1.2). In cases were toluene was added before $AlMe_3$ only minor smoke development was detectable.

Figure 47: Solid pine sapwood samples showing white coating after the application of $AlMe_3$-toluene solution.

In experiments where the toluene was added before the $AlMe_3$, the solvent turned turbid during polymerization. In some cases, visible polymerization occurred within the solvent detached from the wood sample. In experiments where the cocatalyst was successfully applied directly onto the samples, the solvent remained mostly clear of turbidity and no particles formed.

All polymerizations exhibited low to very low monomer infeed at around 5 ml/min and below. If visible polymerization occurred, it occurred within the slurry and on sample surfaces. The slurry filtrates each amounted to a fraction of a gram.

The weight gains of all samples were below the weight of the added aluminum, i.e. approx. 0.45 g. In Series 1 the avg. weight gain was below 0.01 g. That means that weight gains were basically zero in experiments where aluminum was not directly applied onto the wood samples and where wood samples were intensively dried. In Series 2 the avg. weight gain was 0.28 g, showing very similar results for 2a and 2b. That suggests that higher weight gains were achieved by drying less intensively. In Series 3 the avg. weight gain was 0.35 g. That means that slightly higher weight gains were achieved by applying aluminum directly onto wood samples.

The coating on samples varied in thickness and was hard to remove (Figure 48). Removing it by shaving held the risk of either removing too little or too much material.

Figure 48: Solid pine sapwood samples showing thick white coating after slurry polymerization.

To evaluate the success of ethylene polymerization within wood cells, microscopic and spectroscopic methods were applied to locate and identify alien materials within the cell lumen. Table 24 summarizes the experiments, the analytical methods applied and the general observations made.

Table 24: Summarized slurry *in situ* polymerization within wood experiments, analytical methods applied and general results.

Series	Experiment	Samples	Analytical method	Observations*
S1	1	1, 2	SEM	G, S
	2	1, 2	SEM	G, S
	3	1, 2	SEM	G, S
S2	4	1, 2	SEM	G, S, W
	5	1, 2	SEM	G, S, W
S3	6	1, 2	SEM	G, S, W
			SEM-EDX	S w/ strong Al- and O-signal
			Raman	Conclusive PE spectrum
	7	1, 2	SEM	S, W
			SEM-EDX	S w/ Al- and O-signal, W w/ C-signal
	8	1, 2		
	9	1, 2	PLM	G, polarizing, varying luminosity
			TEM	Granules
			TEM-EDX	Granules w/ Al- and O-signal
			Raman	Conclusive PE spectrum

* Observed alien material morphologies: Grainy (G), shard-like (S), wax like (W)

Some general observations were made regarding the morphology of the alien materials found in cell lumen utilizing SEM. Fillings of grainy, shard-like and waxy appearance were repeatedly observed.

Figure 49 shows the radial face of the inside of a pine sapwood sample treated with $AlMe_3$- and zirconocene-toluene solutions. The inside of the cell wall shows attachments of a granular structure that are not present in the pristine wood (compare Figure 2 in Chapter 3.1). These granules have the tendency to exist in the form of agglomerations. The avg. single grain diameter of 210 nm was determined using ImageJ software. However, the visible agglomerations of these grains clearly reach dimensions in the micrometer range that would potentially be able to block the openings of the margo, with the avg. determined diameters of 0.8 µm. The observation of granular attachments on the inner cell walls was made in all investigated samples that were exclusively treated with catalyst solutions, either with only an aluminum solution or with both aluminum and zirconocene solutions.

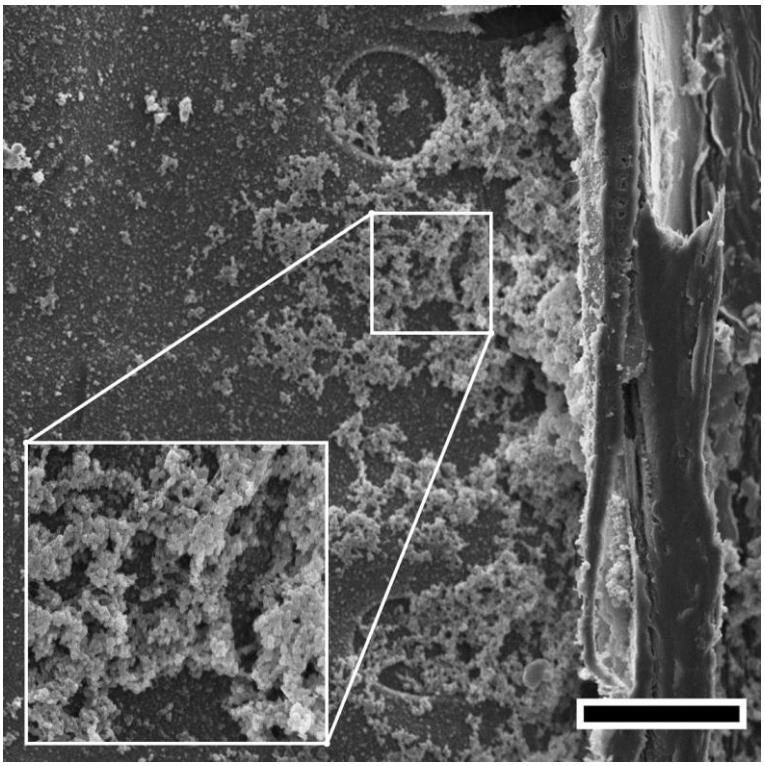

Figure 49: SEM micrograph showing grainy alien material covering the inner cell wall of a pine sapwood tracheid after treatment with $AlMe_3$ and zirconocene-toluene solution. Scale bar 10 µm.

Alien materials of a shard-like and waxy appearance were sporadically found in samples used in the polymerization experiments. As an example of successful slurry polymerization, Sample 7_1 of Series 3 is displayed in Figure 50. The visible area originates from the outer layers of the sample. To attain a smooth surface, samples were cut using a sledge microtome. Cell walls and the materials within the cell lumen all seem distorted in an upward direction, presumably in the direction of the microtome cutting. Cutting faces are not clean but rather show tearing and fringing.

Examples of shard-like fragments are marked by white arrows and were found in many samples. It has been observed that this material type often occurred as the inner coating of the cell wall. Also, it appears that this brittle material is easily detached from the inner surface by e.g. microtome cutting, leading to individual shards. Their appearance suggests a brittle material.

The second alien material recognizable in the micrograph appears relatively smooth and uniform. It is more or less smeared in the microtome cutting direction, showing a waxy ductile behavior. This type of waxy material was recognized in all Series 2 and 3 specimens that were investigated with SEM.

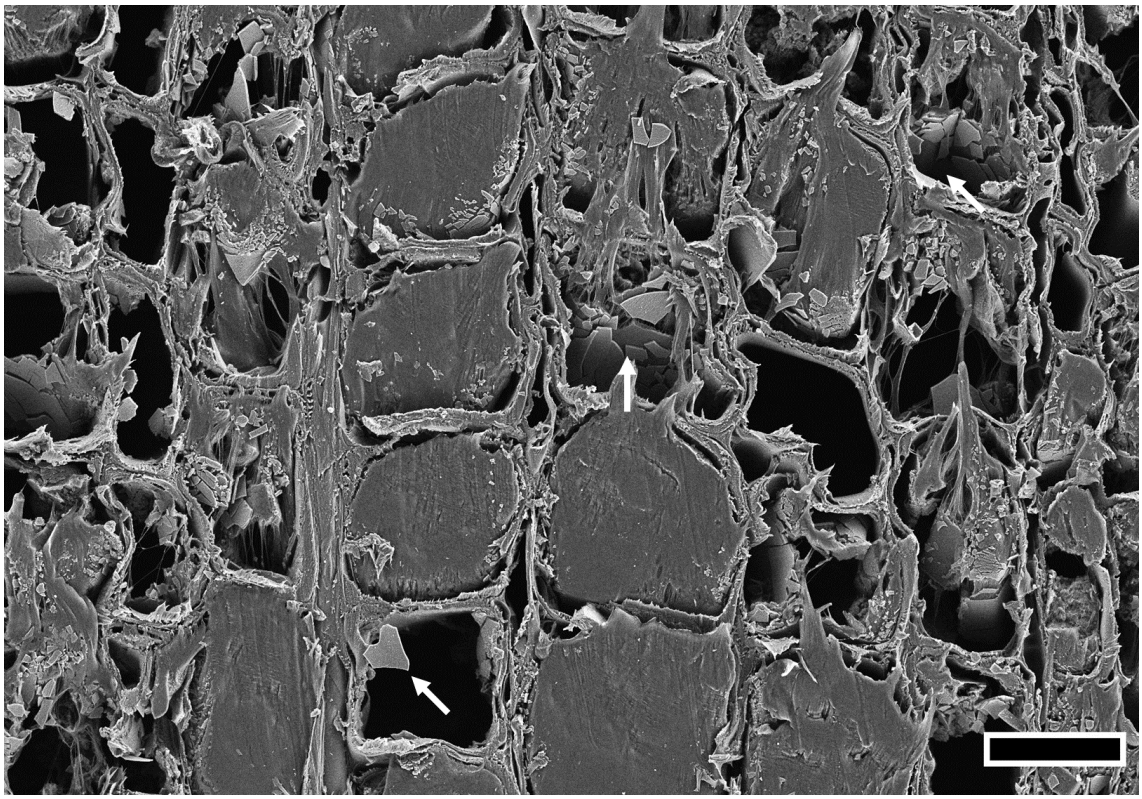

Figure 50: SEM micrograph of a cross section originating from the outer layers of Sample 7_1 of Series 3 showing different cell lumen filling materials.
Scale bar 20 µm.

Figure 51 displays another section of Sample 7_1 of Series 3. However, this time the surface displayed originates approx. from the middle of the sample. All cells appear empty. X-ray analysis of that same section revealed no aluminum, zirconium or chlorine peaks.

The cell wall depicted in the micrograph shows clear signs of disintegration. The damage seems to be concentrated within the middle of the cell wall, i.e. where middle lamella and primary wall are situated, impairing the bonding between individual cells. Similar signs of disintegration were found in many investigates samples. Very similar cell wall disinte-

gration is described elsewhere (Williams 2005) as the result of UV-exposure and is associated with the destruction of the middle lamella, which, along with the primary wall contains a large share of lignin (Fengel and Wegener 1989; Gandini and Naceur Belgacem 2008). A number of possible reasons may have caused the disintegration of these layers. Chemical reaction with one of the used reagents is seen as an unlikely cause, as in most cases these observations did not correlate with the presence of aluminum, zirconium or chlorine. In some investigated samples fungi hyphae were identified. Sequential white-rot fungi mainly break down lignin (Schmidt 2006) and may thereby have disintegrated and weakened these layers. Additionally, the samples were exposed to harsh pressure alterations during vacuum drying and impregnation, which may have induced high amounts of stress. A combination of these factors may have led to the observations regarding disintegration.

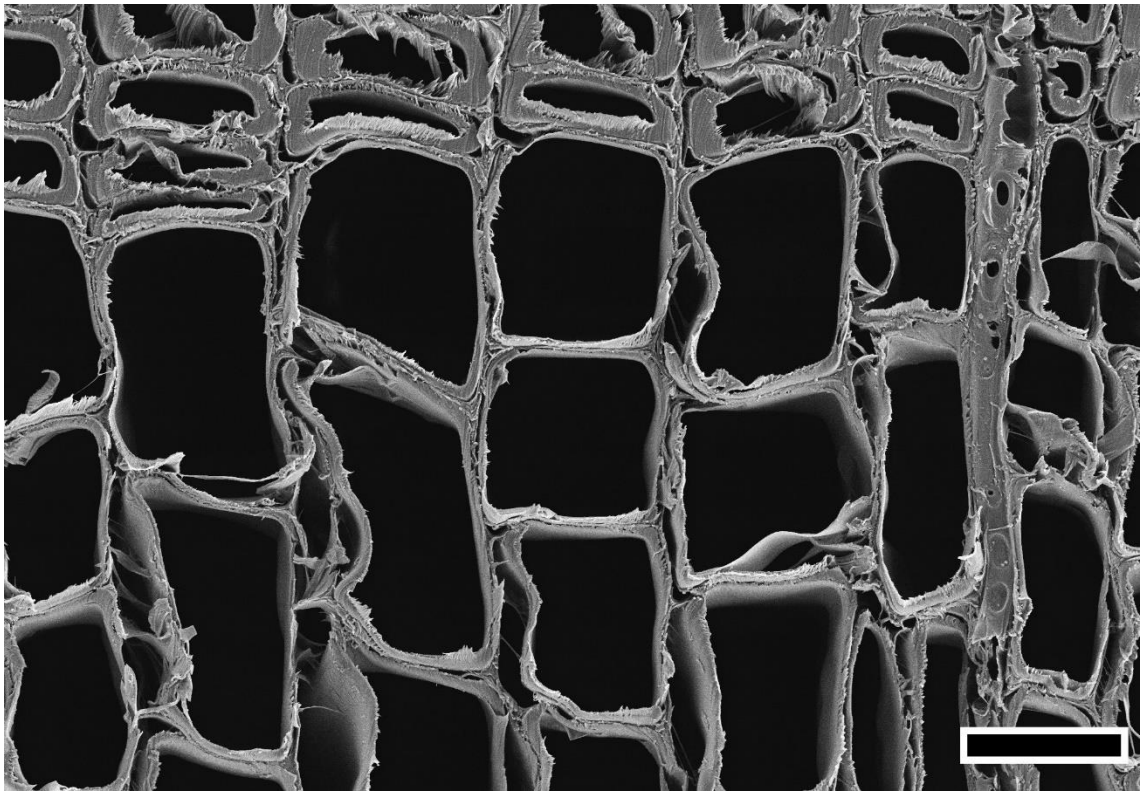

Figure 51: SEM micrograph of a cross section originating from the center region of Sample 7_1 of Series 3 showing empty cell lumen and disintegrated cell walls.
Scale bar 20 µm.

Figure 52 displays an X-ray analysis of another section of Sample 7_1 of Series 3. The corresponding spectrum (see Figure 64 in Annex) shows clear carbon, oxygen and aluminum signals. The cutting direction of the microtome went from the lower part of the image upwards. The purple, green and blue dots represent carbon, oxygen and aluminum respectively.

In the first image from the left, three wood cells are displayed. The middle and upper cells are entirely filled with a uniform mass of waxy and ductile appearance. Some signs

of smearing are visible in upward direction. The lower cell contains shard-like fragments, which also appear to be sheared upwards.

The second image from the left displays the carbon distribution. The waxy fillings of the middle and upper cells return strong carbon signals. The cell walls return distinct but weaker carbon signals. The shard-like fragments of the lower cell do not return any corresponding carbon signal.

The third image from the left displays the oxygen distribution. The cell wall returns a strong oxygen signal. The shard-like fragments of the lower cell return an oxygen signal of similar intensity. Conversely, the fillings of the middle and upper cells do not return an oxygen signal.

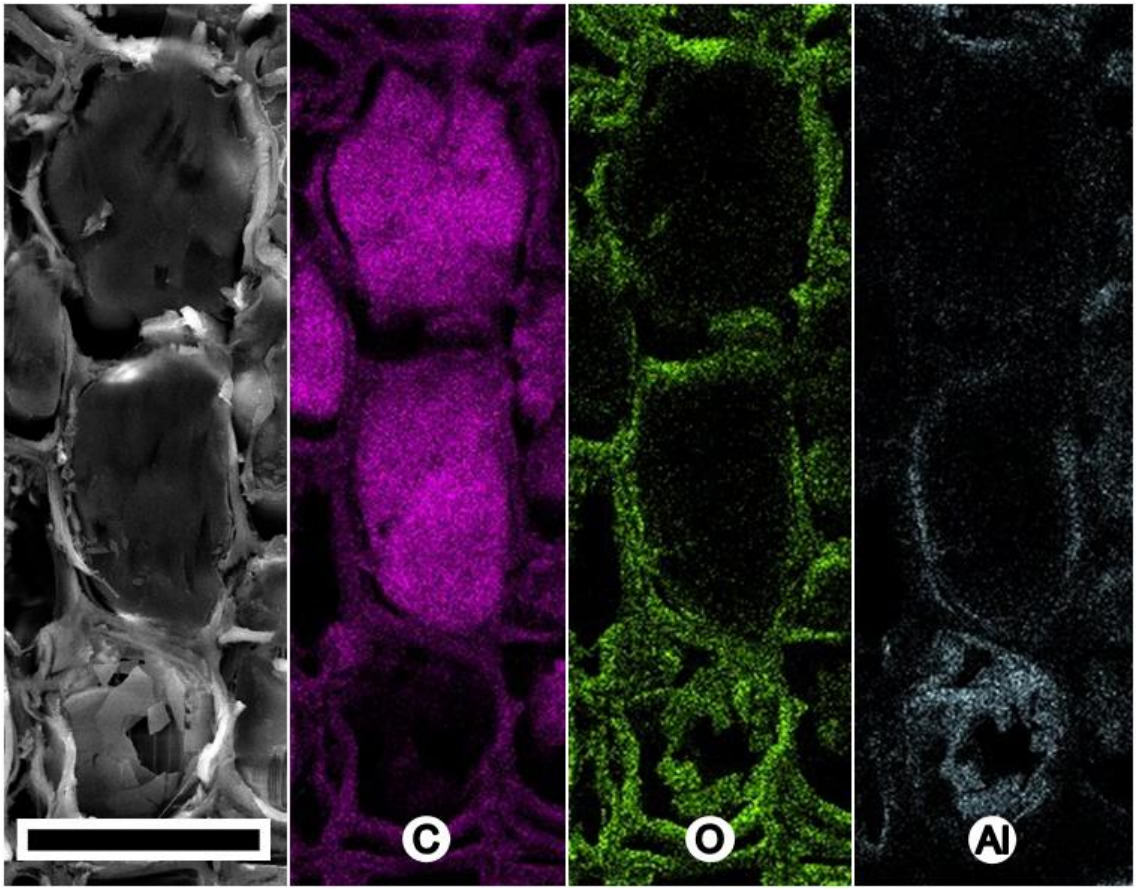

Figure 52: SEM-EDX analysis of a cross section originating from the outer layers of Sample 7_1 of Series 3 showing shard fragments in the lower cell lumen and waxy filling in the middle and upper cell lumen.
(C) Carbon; (O) Oxygen; (Al) Aluminum; Scale bar 50 µm.

The fourth image from the left (Figure 52) displays the aluminum distribution. The fillings of the middle and upper cells do not return an aluminum signal, neither does the bulk of the cell walls. However, the middle cell wall returns a distinct circumferential aluminum signal, situated on what appears to be the inner cell wall surface. The most pronounced signal is returned by the shard-like fragments in the lower cell.

In summary, the cell walls return distinct carbon and oxygen signals, the upper two fillings only return strong carbon signals and the shards in the lower cell return oxygen and aluminum signals. The occurrence of aluminum coating the inner cell wall surface is also visible.

TEM and TEM-EDX was used to investigate the observed structures in more detail. Figure 53 displays two TEM micrographs of Sample 9_2 of Series 3.

The left micrograph was taken with the Carl Zeiss EM 902 and displays a partial cell segment. The cell wall is visibly bulged in one orientation. The cell is filled with granules, which are on avg. 550 nm long and 180 nm across. In the largest share the granules are all uniformly oriented in parallel with the bulged cell wall. The darker area in the center of the cell appears to represent an agglomeration of granule material, possibly originating from the sectioning process. The lighter grey value in the center of the cell represents the film of the utilized filmed mesh grids. The darker grey layer between cell wall and granules represents another filling, which likely correspond with the embedding resin but may also represent PE.

The right image displays a close-up of a cell intersection of the same sample, taken with the JOEL JEM-1011 LaB6. The returned grey value appear darker overall. The cell wall appears bulged again. This time granules are covering the inside of the cell wall of the upper cell. The cell lumen are uniformly filled, which again likely corresponds with the embedding resin but may also represent PE. The light grey between the grains and cell wall represents the film of the utilized filmed mesh grids.

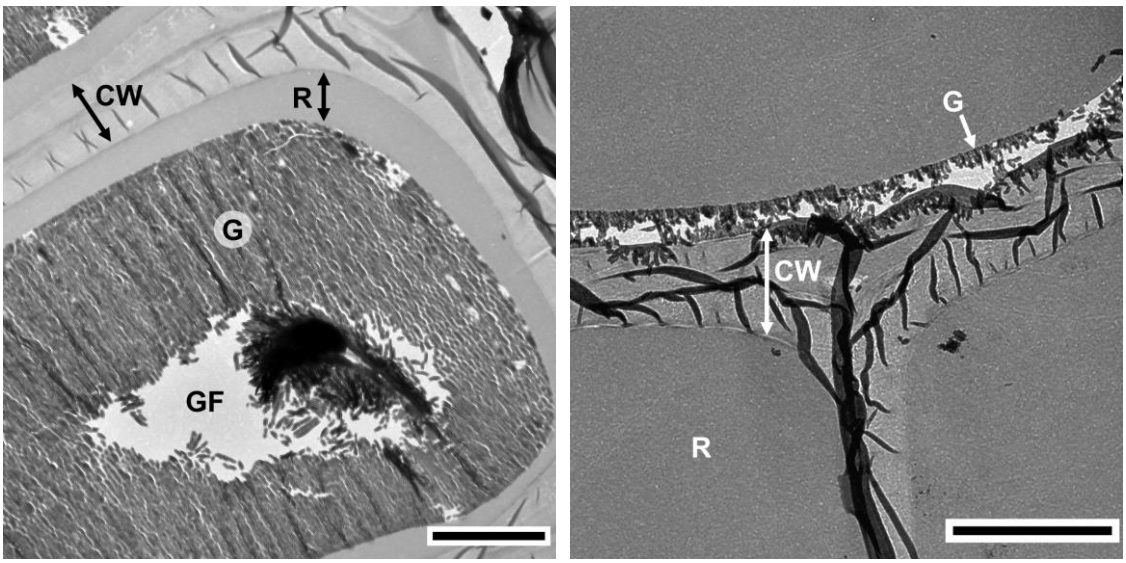

Figure 53: TEM micrographs of microtome sections originating from the outer layers of Sample 9_2 of Series 3 showing details of different cell lumen filling materials.
(CW) Cell walls; (G) Granular structures; (GF) Grid film grey value (R) Embedding resin grey value; Both scale bars 5 µm.

In order to gain more knowledge about the observed structures in Sample 9_2 of Series 3, TEM X-ray analysis was performed utilizing a JOEL JEM-2200 FS. Figure 54 displays a close up of a cell wall, a part of dark grey filling and the granules in between the two. The green, cyan and red colors represent carbon, oxygen and aluminum respectively. The corresponding spectrum (see Figure 65 in Annex) shows clear carbon, oxygen and aluminum signals. Mapping for carbon returned similar high values for the cell wall and the grey filling. The carbon corresponding signal is less pronounced in the granule-layer. However, the granule-layer returns a strong oxygen signal, whereas the cell wall and the grey filling similarly return considerably weaker signals. The granule layer additionally returns a strong aluminum signal, while the cell wall and the grey filling exhibit very weak aluminum signals.

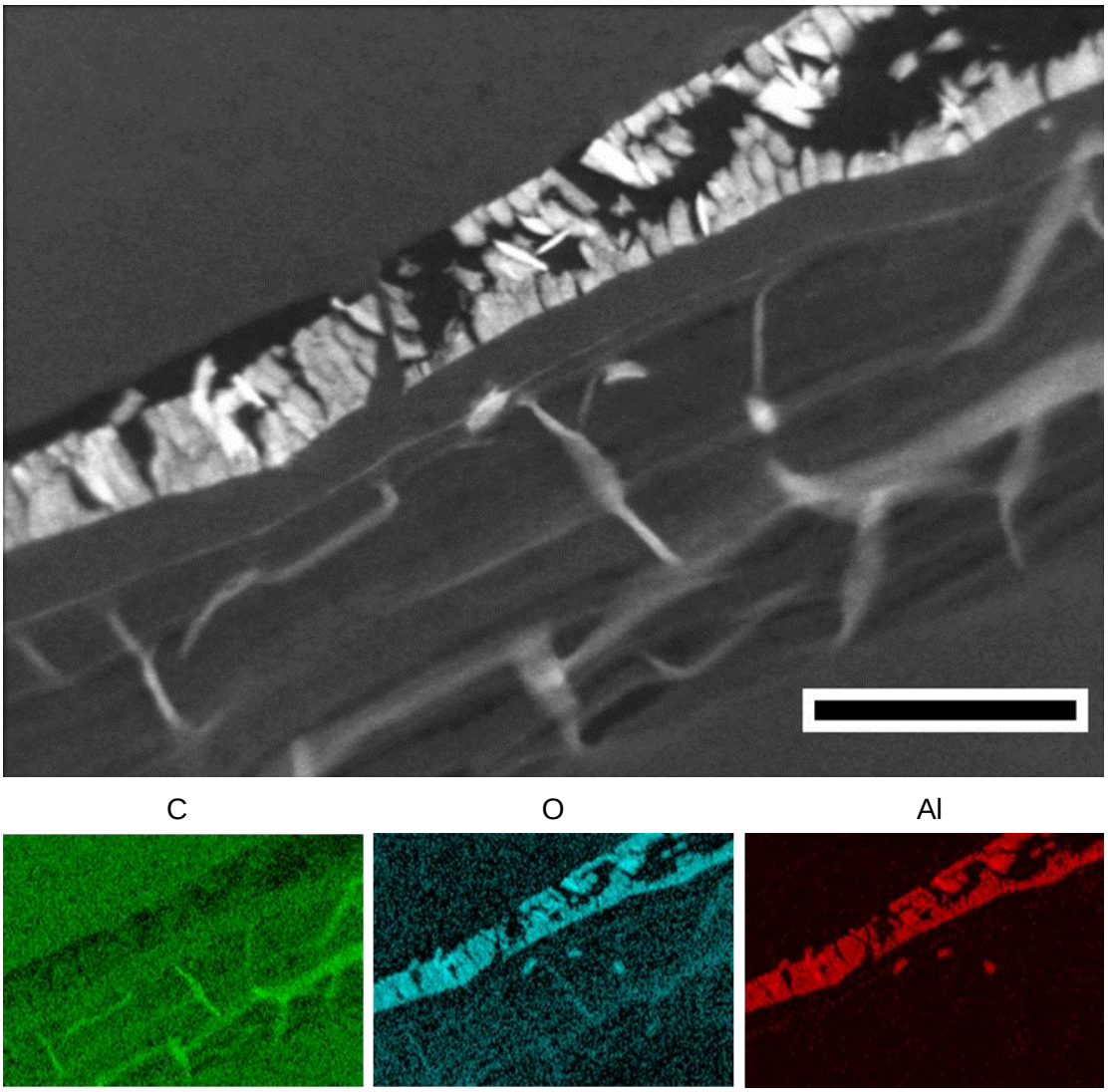

Figure 54: TEM-EDX analysis of cross section originating from the outer layers of Sample 9_2 of Series 3 investigating observed granular structures filling cell lumen or covering a cell walls.
(C) Carbon; (O) Oxygen; (Al) Aluminum; Scale bar 2 µm.

To attain conclusive evidence of successful ethylene polymerization within cell lumen, chemical analysis was necessary. Raman microscopy was performed not only to identify but also to localize PE.

Figure 55 displays a Raman heat map and corresponding spectrum of a thin section of compression molded neat PE, originating from the pilot homogeneous polymerization with (*n*-BuCp)$_2$ZrCl$_2$ / MAO performed in Chapter 6. The recorded Raman bands between 1000 and 1500 cm^{-1} as well as between 2800 and 2900 cm^{-1} correspond well with PE spectra reported elsewhere (Sato et al. 2002; Larkin 2011). The recorded spectra were of varying intensity.

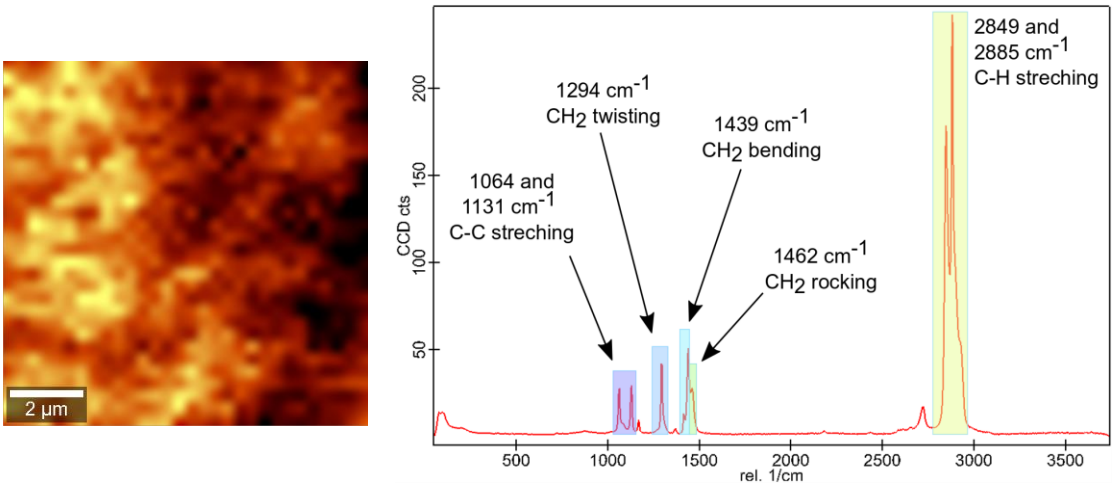

Figure 55: Raman analysis of a thin section of compression molded neat PE. Left: False color heat map; Right: Characteristic PE spectrum.

Figure 56 displays a Raman-mapping of Sample 9_2 of Series 3. The image on the left, taken with a polarizer, shows the original region of interest, in which five cells are visible. The lumen of the two cells on the left show strong illumination. The lumen of the upper and lower cell on the right show slightly less intense illumination, while the lumen of the middle cell on the right shows no illumination at all. Raman-mapping was performed within the marked area, comprising parts of all five cell lumen. The illuminated cell lumen of the left cells returned characteristic PE spectra, similar to those recorded from neat PE. The false color heat map displays the regions where PE-associated spectra of varying intensity were recorded. A false color binary image differentiates more clearly between areas where PE-associated spectra were detected and where no such spectra were detected. From these mappings it is evident that the illuminated regions correspond to said spectra. Cell walls and dark cell lumen did not return such spectra.

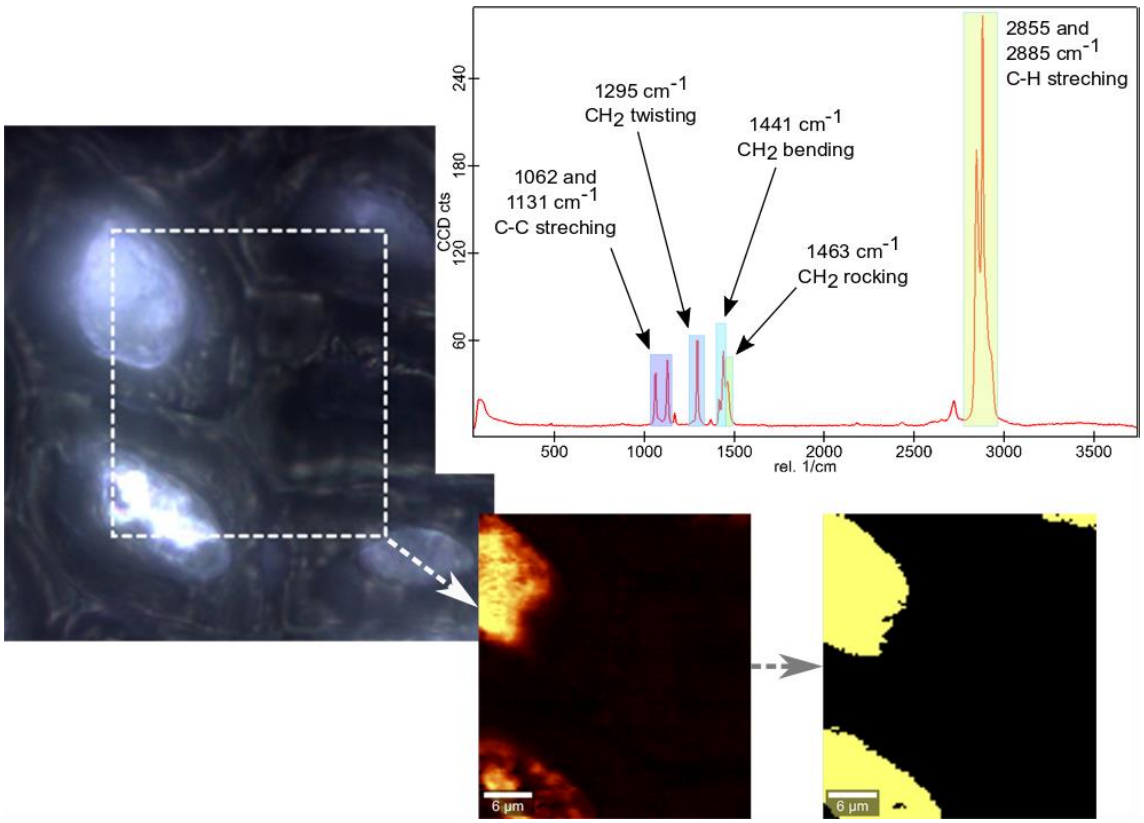

Figure 56: Raman analysis of a cross section originating from the outer layers of Sample 9_2 of Series 3 investigating the chemical nature of observed fillings in cell lumen.
Left: Polarized light micrograph of original region of interest; Above-right: Characteristic PE spectrum; Below-middle: False color heat map of areas corresponding to PE spectrum; Below-right: False color binary map of areas corresponding to PE spectrum.

Light microscopy, offering lower magnification than electron microscopy, was performed on radial sections, in order to receive a broader overview over the distribution of reagents and polymerizate within the wood samples. It was shown in previous work that polarized light microscopy is useful for locating paraffin in wax-impregnated wood lumen (Buro and Buro 1959). Polarization was therefore used to identify crystalline regions. Figure 57 displays two images of a section of Sample 9_2 of Series 3 reaching approx. 0.5 mm from the surface into the material. The first image was taken without and the second image with polarization.

In the image on the left, the vertical tracheid cells are visibly separated by their cell walls. Pits, represented by a round dark spots surrounded by a lager circle, are visible within the most left tracheid. Tracheids and pits of the same sample stock are described in Chapter 3.1. At the lower end of the sample, representing the original surface of the sample cut by circular saw, the cell walls are deformed and bent towards the right. A grainy brownish substrate covers the samples surface and a similar looking grainy substrate fills a large portion of visible cells. The brightness of these fillings varies between relatively light, brown and very dark, the latter being opaque. Three tracheids appear mostly empty of any deposited alien materials.

The image on the right shows the same section utilizing a polarized light source. The cell walls are very dark and the pits return weak Maltese-cross polarization. The bent cell walls on the samples original surface show strong luminescence. The grainy lamination on the samples surface turned dark beyond recognition and areas of darker grainy fillings turned even darker, showing no distinct luminescence. The centered area of lighter grainy filling shows strong luminescence. The first, third and the lower part of the fourth cell from the right show weak but distinct luminescence that is uniform in appearance.

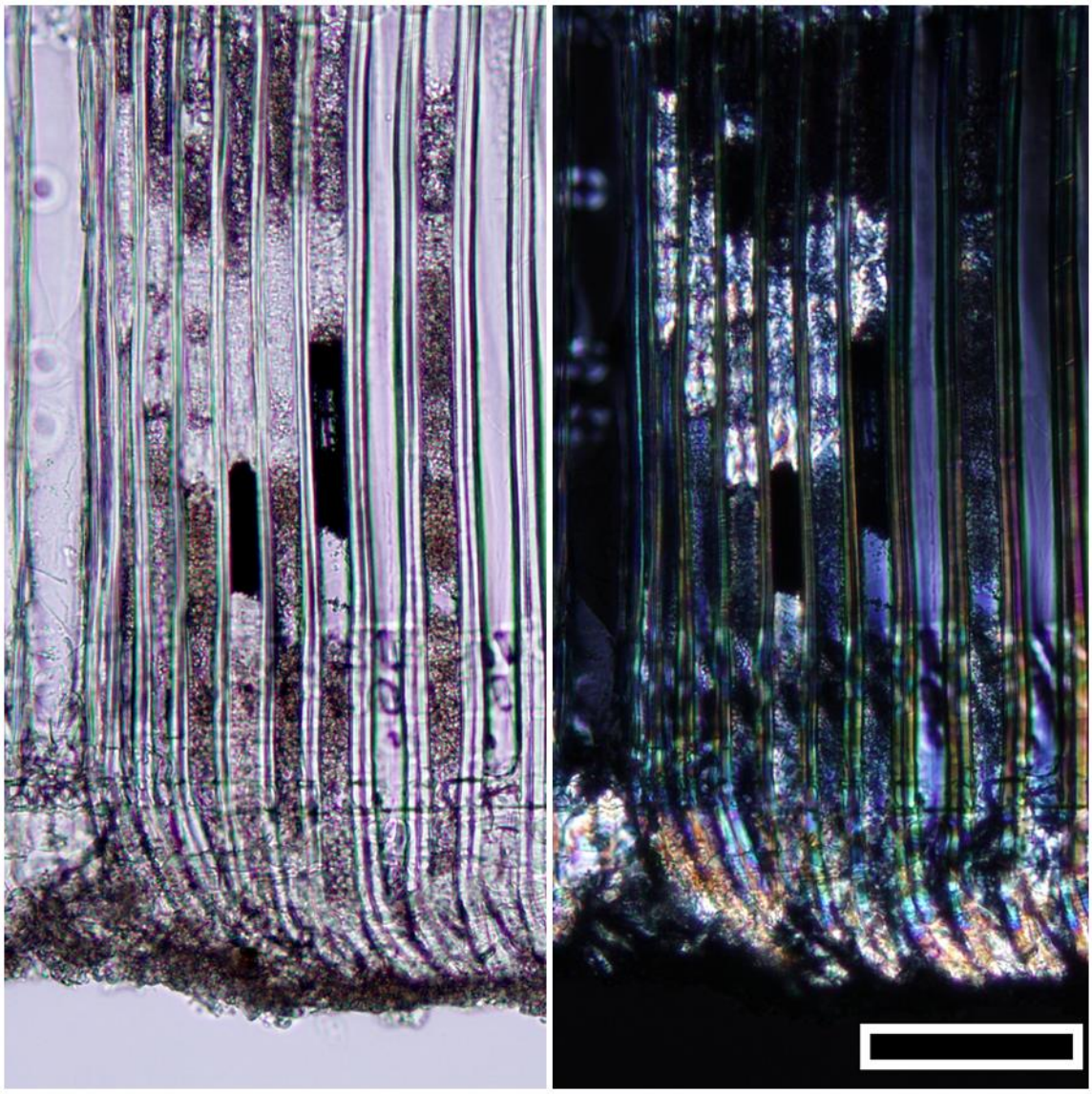

Figure 57: Light microscopic image taken of a radial section from the outer edge of Sample 9_2 of Series 3 showing granular fillings within cell lumen.
Left: No polarization; Right: With polarization; Scale bar 100 µm.

7.3.3 Macro-Confined Gas Phase Polymerization

A general observation that occurred during all gas phase polymerizations was that the ethylene monomer infeed descended quickly. In Series 4 it remained just above zero, whereas in Series 5 it dropped to zero rapidly.

In Series 5, where samples were impregnated with cocatalyst- and catalyst-toluene solutions, little bubbles arose from the samples during vacuum application. This was observed in all recurring vacuum applications and again towards the end of the impregnation process.

To evaluate the success of ethylene polymerization within wood cells, weight gains were recorded. SEM and SEM-EDX were applied to locate and identify alien materials within the cell lumen. Table 25 summarizes the experiments, weight gains and analytical results.

Before calculating the weight gains, the PE attached to the samples was removed. Weight gains were calculated by subtracting the dry weight pre-, from the dry weight post-polymerization. The measured weight gains were between 0.12 and 0.28 g or 3.5 and 8.5 %. There are no clear trends separating the two series. In both series, the experiment with the considerably longer polymerization time show lower weight gains.

Table 25: Summarized *in situ* gas phase polymerization within wood experiments, analytical methods applied and general results.

Series	Experiment	Sample	Weight gain	Analytical method	Observations
S4	1	1	0.20 g / 5.8 %		
	2	1	0.12 g / 3.5 %	SEM SEM-EDX	CW disintegration Weak Al signal
S5	3	1	0.28 g / 8.5 %	SEM SEM-EDX	CW disintegration Weak Al signal
	4	1	0.14 g / 4.1 %	SEM SEM-EDX	CW disintegration Distinct Al signal

In Series 4, where MAO toluene solution was applied directly onto the samples, PE formed on top of the sample. In the case of Sample 1_1 of Series 4, a small round plate of PE, resembling the size and form of the upper tube from the Flow-Reactor, was loosely sitting on top of the sample (Figure 58). In the case of Sample 2_1 of Series 4, small PE particles were loosely sitting on top of the sample. These particles were placed into a beaker containing hydrochloric acid, where aluminum oxide would dissolve but PE would not. The particles did not dissolve.

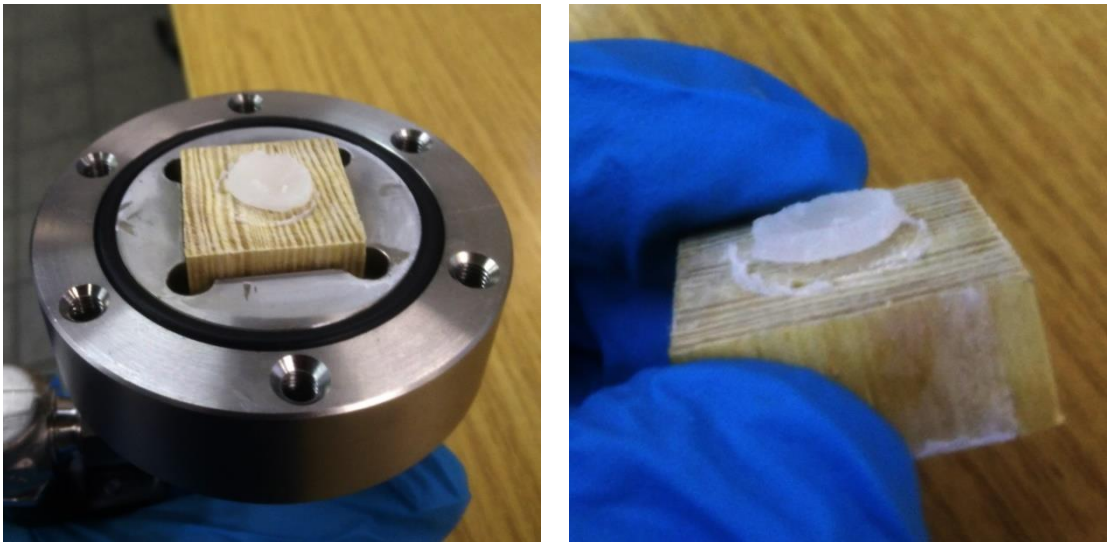

Figure 58: Small round PE plate on top of Sample 1_1 of Series 4 after polymerization.

Investigations with SEM gave very similar results for all samples. Analogous to samples from slurry polymerization, all samples from gas phase polymerization showed cell wall disintegration to a varying degree (compare Figure 51). However, no shard-like, grainy or waxy fillings, resembling the observations made in slurry polymerizations were identified.

SEM-EDX analysis also gave very similar results for all samples. In all spectra aluminum peaks in the outer as well as in the inner regions of the samples were observed. Aluminum was detected in considerably lower quantities in the middle compared to the outer layer of the samples. The overall aluminum signal was weakest in Sample 2_1 of Series 4 and considerably higher in Sample 3_1 and 4_1 of Series 5. No zirconium or chlorine were detected. No strong evidence for the presence of PE was found.

Figure 59 shows a SEM micrograph and SEM-EDX analysis of Sample 4_1 of Series 5. The corresponding spectrum (see Figure 66 in Annex) shows clear carbon, oxygen and aluminum signals. In the left image, three cells are visible. Their cell walls appear disintegrated and the middle cell is partly filled. The analysis for carbon returns equally strong signals for the cell walls and the filling in the middle cell. The cell walls return strong oxygen signals, whereas the filling shows weaker signals. The inner surfaces of all three cells return distinct aluminum signals. The filling only returns a weak aluminum signal.

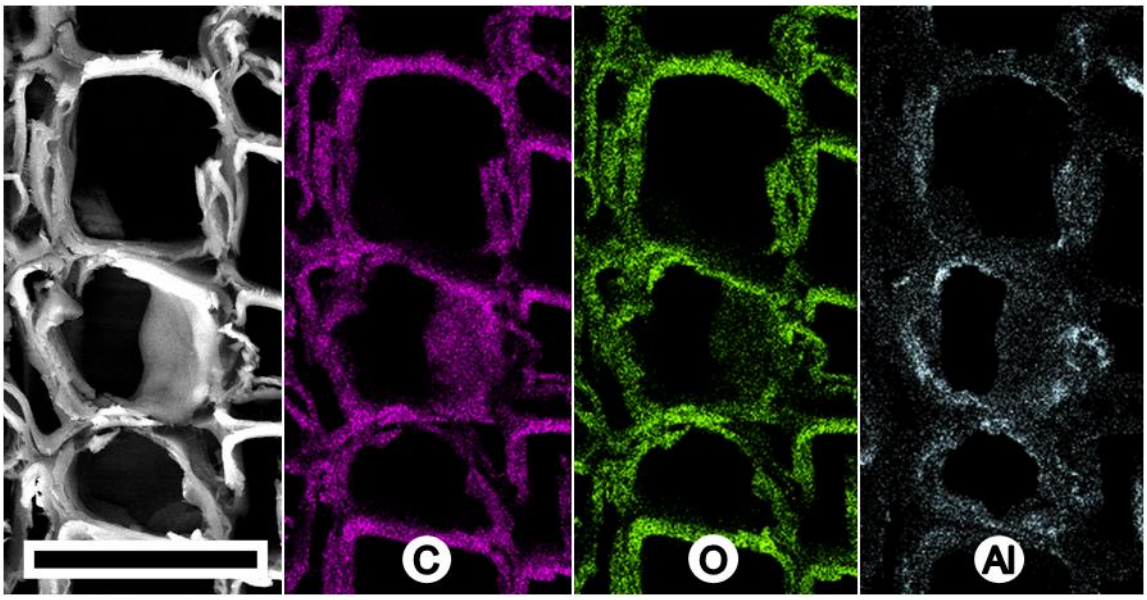

Figure 59: SEM-EDX analysis of a cross section originating from the outer layers of Sample 4_1 of Series 5 (Rneo gas phase polymerization) showing mostly empty cells.
(C) Carbon; (O) Oxygen; (Al) Aluminum; Scale bar 50 µm.

7.4 Discussion

Catalyst impregnation pathways

X-ray analysis suggests that it is possible to introduce pure $AlMe_3$ into wood by applying it directly, via soaking as well as in the form of a gas.

The non-uniform distribution of aluminum detected in wood, differing from cell to cell, was a reoccurring phenomenon. The higher amount of aluminum detected in wood ray and ray-surrounding structures was also reoccurring. The relatively high accessibility of wood rays has been described before (Rijckaert et al. 2001). The non-uniform distribution suggests variations in the openness of the pits connecting individual cells to one another. Soaking appears to lead to the most uniform and thorough distribution.

In the case of undried wood with high MC, no aluminum was found inside of the wood sample. The higher MC appears to hinder aluminum penetration into the deeper regions of the wood. This could be caused by intense interaction between moist wood substrate and $AlMe_3$. A strong interaction between wood and treatment agent has been shown to counteract penetration before (Ren et al. 1997).

A presented SEM image (Figure 49) of grainy aluminum compounds covering the inside of cell walls showed that agglomerations thereof readily reach sizes large enough to block small diameter openings such as pits. A presented light microscopic image (Figure 57) also shows granular alien materials filling the entire cross section of cells. These fillings may in part be composed of aluminum oxide. In the case that moisture and $AlMe_3$ are present in sufficient quantities, it is considered possible that the reaction of the two could create enough aluminum oxide to fill and block the diameter of entire cell lumen.

Slurry Polymerization

The morphologies of alien materials found within cell lumen in SEM images were classified into grainy, shard-like and wax like. Applying X-ray analysis, the bulk cell walls generally returned distinct carbon and oxygen signals but no aluminum signal. The grainy and shard-like materials generally returned aluminum and oxygen signals but no carbon signal. These grainy and shard-like materials likely represent two forms of aluminum oxide, as in its pure form it would only contain aluminum and oxygen. The observed waxy materials generally returned strong carbon signals but no oxygen and no aluminum signal. This material likely represents polyethylene, which in its pure form only contains carbon and hydrogen. By the method of elimination and in this case specifically, X-ray analysis is seen as a valid tool, able to produce strong evidence for successful polymerization of ethylene within wood lumen.

In all slurry polymerization attempts where gently dried wood and $AlMe_3$ were used, cells filled with waxy polymer were found. Raman-microscopy provided conclusive proof of successful ethylene polymerization. Fillings that showed illumination in polarized light microscopy returned clear Raman-spectra characteristic to polyethylene.

In polymerization attempts where thoroughly dried wood was used in combination with $AlMe_3$ no cells filled with waxy polymer were found. What was true in Polymerization Filling Experiments (Chapter 6) appears similarly valid for bulk wood, i.e. that intensively dried wood contains insufficient moisture to partially hydrolyze $AlMe_3$ and form an active cocatalyst species.

No polymer was found in the center regions of the specimens, indicating only shallow impregnation. The low degree of impregnation may be due to the application method as well as the amount of catalyst solution applied. The prior catalyst impregnation experiments showed that pure $AlMe_3$ was in principle able to penetrate into small, dry wood blocks. However, the amount of aluminum found in the middle of the sample was relatively low, considering an undiluted reagent was used. In the polymerization experiments, diluted $AlMe_3$ was used. The overall lower amount applied could mean that all of the reagent is absorbed onto wood substrate in the outer layers, with none being left to impregnate further. Furthermore, prior catalyst impregnation experiments also showed that soaking led to better impregnation.

The porosity of the pine sapwood specimens was calculated to be around 60 % (Chapter 7.2.1.2). The volume of a sample amounts to approx. 6.25 cm^3, resulting in a pore volume of 3.75 cm^3. If this pore volume were to be filled with HDPE with an avg. density of 0.95 g/cm^3, the weight of the wood sample would be raised by 3.56 g, i.e. the weight of the samples would approx. double. Wax impregnation was reported to reach approx. 80 % of the potential maximum weight gain (Scholz et al. 2010d), which would translate to an approx. weight gain of 3.0 g of PE in this study.

The results of the conducted Polymerization Filling Experiments (Chapter 6) clearly show that the applied procedure and utilized amount of catalysts is in principle capable of producing more than enough PE to fill the entire pore volume within the wood samples. However, the overall amount of polymerization occurring within the lumen was low. Judging the success of polymerization within wood cells by monomer infeed was not practical.

The weight gain of the wood samples was very low and therefore also not practical as measure of polymerization success. The low monomer infeed in combination with the low weight gains and the attachment layers on the sample surfaces mean that the margin of error was potentially high.

Gas Phase Polymerization

The occurrence of PE plate and particles on top Samples 1_1 and 2_1 of Series 4 shows that (*n*-BuCp)$_2$ZrCl$_2$ / MAO situated in close proximity on top of wood surfaces is able to perform ethylene polymerization. The catalyst solutions were only drained through the wood samples and no additional drying step was performed before ethylene addition. Whether the catalysts were absolutely dry or still in solution with residual toluene remains unclear.

In the case of the Samples 3_1 and 4_1, no PE was found sitting on top of the samples. In fact, the samples did not show any obvious difference from pre- to post-ethylene addition. The ethylene infeed dropped to zero quickly, indicating no active polymerization.

Evaluating the success of polymerization by weight gain was not practical, as weight gains were low. No trends in the different experiments of Series 4 and 5 were found and there was no apparent difference between the prefabricated MAO and the *in situ* formed MAO. Hence, the type of cocatalyst was not the governing factor here. Prolonged polymerization also did not lead to higher weight gains. This further indicates that polymerization within the porous wood structure was very low or entirely inactive.

Active draining and alternating pressure impregnation clearly led to better and deeper impregnation of catalysts when compared to slurry polymerizations. All samples of Series 4 and 5 showed aluminum deposition in their centers; however, this did not lead to improved polymerization activities over the slurry polymerizations.

In Series 4, low polymerization activity within the porous wood structure might have been caused by the following factors: Draining the MAO solution through the wood may have led to an increased deposition of MAO in the uppermost layers of the wood sample, blocking many pits and cell lumen. By adhering to MAO, the zirconocene may also mainly have been deposited in the top layers of the sample. Polymerization will be most active in these MAO- and zirconocene-rich areas, possibly consuming a large part of available monomer before it reaches the deeper layers. This would also clog up the samples pores, further hindering monomer flow into the deeper areas.

In Series 5, the undiscernible polymerization activity might have been caused by the following factors: The $AlMe_3$ to H_2O ratio may have been too high or too low, leading to insufficient or excessive hydrolysis. Unbound liquid $AlMe_3$ may have evaporated during vacuum drying. It has been reported that metallocenes are relatively resistant to dry carbohydrates (Dutschke 1985). In spite of this, the zirconocene may still have been poisoned by protonic groups of the wood substrate during alternating-pressure impregnation, which would have promoted intense wood-catalyst interactions.

Overall, it is true for slurry and gas phase polymerizations alike that in order for the polymerization to work, all participating reactants need to be present in every single cell lumen in the correct amounts. If the ratio between $AlMe_3$ and H_2O is too high or too low

no active cocatalyst species will be formed. The permeability of wood differs from cell to cell, which hinders uniform impregnation with $AlMe_3$. The distribution of moisture within wood is not necessarily uniform. This means that the degree of $AlMe_3$-hydrolyzis will vary accordingly. Aluminum oxides, reported to feature effective barrier properties (George 2010), may clog pits and alter the permeability of the continuous pore system, which in turn influences the catalyst impregnation. This means that not all lumen that were accessible for $AlMe_3$ would similarly be accessible for the catalyst solution. Commencing polymerization upon ethylene addition may actually swiftly close up catalytically activated pits quickly. This could reduce the permeability of awood sample to effectively zero. A combination of the described effects may be the cause of the low weight gains recorded.

7.5 Conclusion

For the first time, successful slurry PE synthesis within the macro-confinement of the porous wood structure was achieved by utilizing (*n*-BuCp)$_2$ZrCl$_2$ / $AlMe_3$ / w-H_2O as a catalyst. This proves the macro-confined formation of an active cocatalyst species by partial hydrolysis of $AlMe_3$ with w-H_2O within a cellular solid such as wood. Furthermore, the observation of PE filled lumen proves that it is possible to impregnate individual wood cells with all three catalyst components in the necessary amounts for active catalysis. PE containing cells were shown to be filled almost entirely with polymer, showing that high polymerization activities were reached.

Gas phase polymerization with catalysts immobilized on wood surfaces was successfully demonstrated. However, no lumen-filling was observed. Improving on catalyst impregnation would likely enable gas phase polymerization within the lumen and is seen as a promising path for reaching homogeneous distribution and loading with polymer. Further experiments to deliver verification and proof of concept should be performed.

The affinity of the utilized catalytic system towards the wood substrate was originally seen as an advantage in the quest to coat the inner cell walls of wood with polymer, by anchoring polymerization catalysts onto said surfaces. However, the results of this study imply that the tendency of the catalysts to adhere to the wood substrate may cause non homogeneous distribution of catalyst and – consequently – of polymer.

In the case of strong wood-catalyst interaction, the catalyst may be deposited on the outer layers of the wood sample, i.e. it may be filtered out, reducing the available catalyst to penetrate into deeper regions of the sample. Furthermore, pits may be blocked by the catalytic agent adsorbed onto the pit membranes and margo. Pits may additionally be blocked by polymerizate during the polymerization process. Catalysts that do not interact or adhere to the cell wall constituents are thought to prevent filtering and pit blocking. Choosing a catalytic system or process that minimizes wood-catalyst interaction is now thought beneficial for deep and homogeneous impregnation.

Low level wood-catalyst interaction may be achieved even with metallocene / MAO catalysts, by altering the process conditions. It was observed in this and earlier studies that $AlMe_3$ and MAO do not adhere well to thoroughly dried starch or wood. Metallocenes were shown to not adhere well when treatment is performed at high temperatures

(Spottog pending; Mende 1981; Dutschke 1985). Hence, thorough drying of wood samples and an elevated temperature during treatment should lead to better impregnation of these catalysts. By lowering the temperature once impregnation is complete, anchoring of the catalyst onto the inner cell wall could be regained.

The attempt to use a three component catalytic system presumably reduces the likelihood of all components being present in adequate quantities within the confinement of the individual wood cells. The use of one-component catalysts is seen as means of simplifying and thereby improving the likelihood of success. Pre-activation of metallocenes with MAO would effectively yield a one component system. The impregnation of thoroughly dried wood with a pre-activated metallocene / MAO system potentially leads to an enhanced distribution of active sites within the lumen.

Other classes of one-component catalysts pose promising alternatives, offering a large degree of flexibility in solvents and resultant polymers. Nickel-Ylide catalysts do not require activation by a cocatalyst but feature high tolerance towards polar groups, high ethylene polymerization activities as well as the possibility of tuning molecular weights from oligomers up to UHMWPE (Younkin et al. 2000; Starzewski 2006). It has been reported that some late-transition metal catalysts are able to polymerize ethylene in polar solvents and even water (Starzewski and Josef 1982; Mecking and Claverie 2006). Such catalysts would likely combine deep impregnation, uniform distribution and high weight gains, all the while being easier to handle and allowing for the use of solvents that pose less health and environmental concerns. A vast variety of polymers may be catalytically synthesized within the wood, possibly adding new functionalities.

Atomic Layer Deposition (ALD) or Chemical Vapor Deposition (CVD) represent further unexploited procedures that could offer uniform application of atomic or molecular layers of catalytic compounds on wood surfaces. Uniform deposition of thin layers measuring only nanometers in thickness (George 2010) would circumvent the clogging of pits. ALD & CVD have already been performed on cotton fabrics (Li et al. 2007), carbonized pulp fibers (Luo et al. 2017), cellulose aerogels (Kettunen et al. 2011; Korhonen et al. 2011) as well as bulk wood surfaces (Lu and Hu 2016; Yang et al. 2020). Gregory et al. (2020) performed ALD on bulk wood samples using $TiCl_4$. Atomic layers of $TiCl_4$ deposited on internal wood surfaces could be used to perform subsequent Ziegler-Natta polymerization therefrom.

In addition to large volume bulk wood modification other areas of small scale applications may offer even higher potential. Wood, with its unique hierarchical structure and properties, has been identified as an attractive bio-scaffold for functionalization. With its aligned continuous pore system, it is particularly promising for the fabrication of advanced functional materials (Burgert et al. 2015; Berglund and Burgert 2018). In these applications where only small cross sections need to be treated, the limited impregnation of catalysts that adhere to the wood substrate are less of an issue. In fact, the immobilization of catalysts may be required, in order to reach the desired effects.

8 General Conclusion and Outlook

The applicability of catalytic olefin polymerization in wood technology has proven highly promising. Proof of concept of the macro-confined metallocene catalyzed polymerization of ethylene has been demonstrated successfully. Using w-H_2O as an active part in metallocene catalysis in the production of PE based WPC has been proven highly successful and recommendable. Moisture management has been shown to be paramount. Not all w-H_2O is available for reaction but the amount of reaction can be fine-tuned by moisture management, which is possible via vacuum drying.

Future research should focus on the following:

- Vacuum drying of particulate wood, i.e. drying under the exclusion of moisture transport through the macro-porous wood structure, is insufficiently researched. Basic research should give special attention to the influence of relative humidity vs. absolute pressure on drying dynamics under vacuum conditions.
- Advantages drawn from processes such as ISP and PFT in the production of wood or cellulose filled or reinforced composites need to be established, showing production pathways or products that exhibit properties superior when compared to conventional processing or products. Special attention should be given to investigating material concepts that are difficult or impossible to manufacture by conventional means.
- Macro-confined polymerization, in order to uniformly fill wood cell lumen with polymer or other desirable products, likely profits from catalysts that show low levels of interaction with the cell wall. Respective catalytic systems should be investigated for their ability to impregnate deeply and uniformly into wood. In addition, low activity catalysts may lead to higher overall loadings by preventing the rapid reduction in wood permeability. Once such a process has been identified, attention should be given to the properties of resultant materials.
- Vapor deposition processes promise a new effective pathway for uniformly coating the inner cell walls of wood with layers measuring only atoms or molecules in thickness; thereby potentially preventing the blocking of pits. Experiments, proving the possibility of coating the inner surfaces of wood with catalysts by such processes should be performed.

9 Annex

9.1 Additional Data

Table 26: DoE raw data from vacuum drying experiments.

Run	Variable 1 Temp. [°C]	Variable 2 Duration [min]	Variable 3 Pressure* [mbar]	Variable 4 Material	Response MC [%]
1	103.0	10	Medium	Beech	8.73
2	103.0	10	High	MCC	0.73
3	30.0	900	High	Beech	0.15
4	77.5	1440	Medium	MCC	3.86
5	103.0	1440	Medium	Beech	2.45
6	30.0	10	High	Pine	3.29
7	55.2	1440	High	Beech	0.05
8	42.8	10	Medium	Pine	13.29
9	30	10	High	Beech	3.00
10	55.2	1440	High	Beech	0.05
11	74.5	900	High	MCC	0.03
12	30.0	10	High	MCC	1.77
13	103.0	900	Medium	Pine	5.12
14	30.0	1440	Medium	Pine	10.84
15	103.0	10	High	Pine	0.80
16	30.0	1440	High	Pine	0.14
17	30.0	360	Medium	MCC	7.68
18	30.0	10	Medium	Beech	12.70
19	101.5	900	Medium	MCC	2.82
20	30.0	1440	Medium	Pine	9.01
21	66.5	900	Medium	Beech	8.20
22	103.0	10	Medium	MCC	4.71
23	30.0	1440	High	MCC	0.13
24	103.0	360	High	Beech	0.03
25	59.2	900	High	Pine	0.06
26	30.0	360	Medium	MCC	7.22
27	103.0	360	High	Beech	0.04
28	42.8	10	Medium	Pine	13.16
29	68.7	360	Medium	MCC	4.86
30	103.0	1440	High	Pine	0.02
31	30.0	1440	Medium	Beech	10.66
32	103.0	900	Medium	Pine	5.73
33	103.0	1440	High	MCC	0.03
34	103.0	1440	Medium	Beech	0.29

* Medium vacuum 150 mbar; high vacuum between 1.0 and 0.1 mbar

Table 27: ANOVA for reduced 2FI model from vacuum drying experiments.

Source	Sum of squares	df	Mean of squares	F-values	p-values	
Model	621.60	11	56.51	51.27	< 0.0001	significant
A-Temp.	78.73	1	78.73	71.44	< 0.0001	
B-Duration	50.00	1	50.00	45.37	< 0.0001	
C-Pressure	379.49	1	379.49	344.34	< 0.0001	
D-Material	31.33	2	15.66	14.21	0.0001	
AC	30.59	1	30.59	27.76	< 0.0001	
AD	7.31	2	3.65	3.31	0.0552	
BC	7.47	1	7.47	6.78	0.0162	
CD	24.09	2	12.05	10.93	0.0005	
Residual	24.25	22	1.10			
Lack of Fit	19.94	15	1.33	2.16	0.1535	not significant
Pure Error	4.31	7	0.6150			
Cor. Total	645.85	33				

Table 28: Comprised results from Series 1 1-step gas titration experiments using $AlMe_3$.

	Time	[min]	0	5	10	15	20	25	30	35
	$T_{ambient}$	[°C]	28	28	29	29	29	29	29	29
1/1_1	Vol.	[ml]	0	50	61	68	71	72	73	74
	n_{CH4}/g_H	[mmol/g]	0.00	0.34	0.41	0.45	0.47	0.48	0.49	0.49
	$T_{ambient}$	[°C]	29	29	29	29	29	29	29	29
1/1_2	Vol.	[ml]	0	50	60	64	68	69	70	71
	n_{CH4}/g_H	[mmol/g]	0.00	0.34	0.40	0.43	0.46	0.46	0.47	0.48
	$T_{ambient}$	[°C]	26	26	26	26	26	26	26.5	26.5
1/1_3	Vol.	[ml]	0	63	79	85	90	92	94	95
	n_{CH4}/g_H	[mmol/g]	0.00	0.50	0.63	0.68	0.72	0.74	0.75	0.76
	$T_{ambient}$	[°C]	28	28	28	28	28	28	28	28
1/1_4	Vol.	[ml]	0	58	71	78	80	83	84	85
	n_{CH4}/g_H	[mmol/g]	0.00	0.46	0.57	0.63	0.64	0.67	0.67	0.68
	$T_{ambient}$	[°C]	29	29	29	29	29	29.5	29.5	29.5
1/1_5	Vol.	[ml]	0	61	75	81	84	87	89	90
	n_{CH4}/g_H	[mmol/g]	0.00	0.49	0.60	0.65	0.67	0.69	0.71	0.72
	$T_{ambient}$	[°C]	25	25	25	24	23	23	23	22
1/1_6	Vol.	[ml]	0	32	43	49	50	50	50	50
	n_{CH4}/g_H	[mmol/g]	0.00	0.26	0.35	0.40	0.41	0.41	0.41	0.41
	$T_{ambient}$	[°C]	24	24	25	25	25	25	25	25
1/1_7	Vol.	[ml]	0	50	61	68	71	72	74	75
	n_{CH4}/g_H	[mmol/g]	0.00	0.41	0.49	0.55	0.58	0.58	0.60	0.61
	$T_{ambient}$	[°C]	26	27	27	27	27	27	27	27
1/1_8	Vol.	[ml]	0	51	64	71	74	76	78	80
	n_{CH4}/g_H	[mmol/g]	0.00	0.41	0.51	0.57	0.59	0.61	0.62	0.64
	$T_{ambient}$	[°C]	28	28	28	28	28	28	28	28
1/1_9	Vol.	[ml]	0	60	71	75	79	80	81	83
	n_{CH4}/g_H	[mmol/g]	0.00	0.48	0.57	0.60	0.63	0.64	0.65	0.66

Table 29: Comprised results from Series 1 5-step gas titration experiments using $AlMe_3$.

	Time	[min]	0	5	10	15	20	25	30	35
	$T_{ambient}$	[°C]	26	26	26	62	26	26	26	26
1/5_1	Vol.	[ml]	0	30	50	54	58	59	60	61
	n_{CH4}/g_H	[mmol/g]	0.00	0.24	0.40	0.43	0.47	0.47	0.48	0.49
	$T_{ambient}$	[°C]	26	26	26	26	26	26	26	26
1/5_2	Vol.	[ml]	0	29	52	58	60	61	62	62
	n_{CH4}/g_H	[mmol/g]	0.00	0.23	0.42	0.47	0.48	0.49	0.50	0.50
	$T_{ambient}$	[°C]	26	26	26	27	27	27	26	26.5
1/5_3	Vol.	[ml]	0	21	56	61	65	68	69	70
	n_{CH4}/g_H	[mmol/g]	0.00	0.14	0.38	0.41	0.44	0.46	0.47	0.47
	$T_{ambient}$	[°C]	27	26	26	26	26	26	26	26
1/5_4	Vol.	[ml]	0	30	58	70	73	75	78	80
	n_{CH4}/g_H	[mmol/g]	0.00	0.20	0.39	0.47	0.49	0.51	0.53	0.54

Table 30: Comprised results from Series 2 gas titration experiments after drying at 30 °C using $AlMe_3$.

	Time	[min]	0	5	10	15	20	25	30	35
2/30_1	$T_{heating}$	[°C]	31.5	31.2	31.0	30.8	30.6	30.8	30.5	30.8
	$T_{ambient}$	[°C]	25	25	25	25	25	25	25	25
	Vol.	[ml]	0	60	70	73	77	79	80	80
	n_{CH4}/g_H	[mmol/g]	0.00	0.49	0.57	0.60	0.63	0.65	0.66	0.66
2/30_2	$T_{heating}$	[°C]	32.8	32.4	31.8	31.2	31.2	30.9	30.8	31.2
	$T_{ambient}$	[°C]	25	25	25	26	25	26	26	25.5
	Vol.	[ml]	0	51	72	82	86	89	91	92
	n_{CH4}/g_H	[mmol/g]	0.00	0.42	0.59	0.67	0.71	0.73	0.74	0.75
2/30_3	$T_{heating}$	[°C]	35.2	34.5	33.7	32.8	32.1	31.5	30.8	31.0
	$T_{ambient}$	[°C]	25	25	25	25	25	25	25	25
	Vol.	[ml]	0	30	45	53	58	60	62	64
	n_{CH4}/g_H	[mmol/g]	0.00	0.25	0.37	0.43	0.47	0.49	0.51	0.52
2/30_4	$T_{heating}$	[°C]	31.5	31.6	31.2	30.8	31.0	31.0	31.0	30.8
	$T_{ambient}$	[°C]	25	25	25	25	25	25	25	25
	Vol.	[ml]	0	39	50	58	61	62	63	64
	n_{CH4}/g_H	[mmol/g]	0.00	0.32	0.41	0.48	0.50	0.51	0.52	0.53
	Time	**[min]**	**40**	**45**	**50**	**55**	**60**	**65**	**70**	
2/30_1	$T_{heating}$	[°C]	40.3	51.1	58.2	62.4	60.5	61.7	62.0	
	$T_{ambient}$	[°C]	25	25	25	25	25	25	25	
	Vol.	[ml]	84	92	103	111	114	115	118	
	n_{CH4}/g_H	[mmol/g]	0.69	0.76	0.85	0.91	0.94	0.94	0.97	
2/30_2	$T_{heating}$	[°C]	40.1	53.7	59.9	60.5	60.7	60.5	61.1	
	$T_{ambient}$	[°C]	26	26	26	26	26	26	26	
	Vol.	[ml]	94	102	112	120	124	127	128	
	n_{CH4}/g_H	[mmol/g]	0.77	0.83	0.92	0.98	1.01	1.04	1.05	
2/30_3	$T_{heating}$	[°C]	41.2	53.0	59.6	60.5	60.0	60.6	60.7	
	$T_{ambient}$	[°C]	25	25	25	25	25	25	25	
	Vol.	[ml]	68	77	88	95	98	100	100	
	n_{CH4}/g_H	[mmol/g]	0.56	0.63	0.72	0.78	0.80	0.82	0.82	
2/30_4	$T_{heating}$	[°C]	38.0	49.8	58.8	60.9	60.0	60.6	60.5	
	$T_{ambient}$	[°C]	25	25	25	25	25	25	25	
	Vol.	[ml]	66	73	81	90	93	94	95	
	n_{CH4}/g_H	[mmol/g]	0.54	0.60	0.67	0.74	0,76	0.77	0.78	

Table 31: Comprised results from Series 2 gas titration experiments after drying at 103 °C using $AlMe_3$.

	Time	[min]	0	5	10	15	20	25	30	35
2/103_1	$T_{heating}$	[°C]	30.8	32.8	33.2	32.8	32.1	31.5	31.2	30.8
	$T_{ambient}$	[°C]	25	25	26	26	25	25	25	25
	Vol.	[ml]	0	2	3	4	4	4	4	4
	n_{CH4}/g_H	[mmol/g]	0.00	0.02	0.03	0.03	0.03	0.03	0.03	0.03
2/103_2	$T_{heating}$	[°C]	33.3	32.6	31.9	31.2	31.2	31.0	31.0	31.0
	$T_{ambient}$	[°C]	25	25	25	25	25	25	25	25
	Vol.	[ml]	0	0	0	0	0	0	0	0
	n_{CH4}/g_H	[mmol/g]	0.00	0.00	0.00	0.00	0.00	0.00	0.00	0.00
2/103_3	$T_{heating}$	[°C]	31.5	31.0	30.8	31.0	31.0	30.8	31.2	30.8
	$T_{ambient}$	[°C]	25	25	25	25	25	25	25	25
	Vol.	[ml]	0	0	0	1	2	3	3	3
	n_{CH4}/g_H	[mmol/g]	0.00	0.00	0.00	0.01	0.02	0.02	0.02	0.02
2/103_4	$T_{heating}$	[°C]	30.6	30.8	31.2	30.8	30.8	31.0	31.0	31.2
	$T_{ambient}$	[°C]	25	25	25	25	25	26	26	26
	Vol.	[ml]	0	1	3	4	5	5	6	7
	n_{CH4}/g_H	[mmol/g]	0.00	0.01	0.02	0.03	0.04	0.04	0.05	0.06
	Time	[min]	40	45	50	55	60	65	70	
2/103_1	$T_{heating}$	[°C]	40.0	50.7	58.8	60.9	60.0	61.3	59.9	
	$T_{ambient}$	[°C]	25	25	25	25	25	25	25	
	Vol.	[ml]	6	11	19	22	25	26	27	
	n_{CH4}/g_H	[mmol/g]	0.05	0.09	0.16	0.18	0.21	0.22	0.23	
2/103_2	$T_{heating}$	[°C]	42.0	53.9	60.4	60.9	60.6	60.5	61.1	
	$T_{ambient}$	[°C]	25	25	25	25	25	25	26	
	Vol.	[ml]	4	9	18	21	22	23	24	
	n_{CH4}/g_H	[mmol/g]	0.03	0.07	0.15	0.17	0.18	0.19	0.20	
2/103_3	$T_{heating}$	[°C]	42.4	55.0	60.4	60.2	61.5	60.2	61.1	
	$T_{ambient}$	[°C]	25	25	25	25	25	25	25	
	Vol.	[ml]	5	10	19	22	25	26	27	
	n_{CH4}/g_H	[mmol/g]	0.04	0.08	0.15	0.18	0.20	0.21	0.22	
2/103_4	$T_{heating}$	[°C]	42.4	55.0	60.4	60.5	61.1	60.6	60.7	
	$T_{ambient}$	[°C]	26	26	26	26	26	26	26	
	Vol.	[ml]	8	14	22	28	30	31	31	
	n_{CH4}/g_H	[mmol/g]	0.06	0.11	0.18	0.22	0.24	0.25	0.25	

Table 32: Comprised results from Series 3 gas titration experiments after drying at 30 or 103 °C using MAO.

	Time	[min]	0	5	10	15	20	25	30	35
3/30_1	$T_{heating}$	[°C]	34	33	33	32	32	31	30	30
	$T_{ambient}$	[°C]	23	22	23	23	23	23	23	23
	Vol.	[ml]	0	49	75	90	100	102	110	112
	n_{CH4}/g_H	[mmol/g]	0.00	0.40	0.61	0.74	0.82	0.84	0.90	0.92
3/30_2	$T_{heating}$	[°C]	30	30	30	30	30	30	30	30
	$T_{ambient}$	[°C]	21	21	21	21	21	21	21	21
	Vol.	[ml]	0	48	67	77	87	92	95	99
	n_{CH4}/g_H	[mmol/g]	0.00	0.40	0.56	0.64	0.72	0.76	0.79	0.82
3/103_1	$T_{heating}$	[°C]	31	31	30	30	30	30	30	30
	$T_{ambient}$	[°C]	20	20	20	20	20	20	20	20
	Vol.	[ml]	0	3	5	7	9	10	10	10
	n_{CH4}/g_H	[mmol/g]	0.00	0.02	0.04	0.06	0.07	0.08	0.08	0.08
3/103_2	$T_{heating}$	[°C]	30	30	30	30	30	30	30	30
	$T_{ambient}$	[°C]	19	19	19	19	19	19	19	19
	Vol.	[ml]	0	3	5	8	10	10	10	10
	n_{CH4}/g_H	[mmol/g]	0.00	0.02	0.04	0.07	0.08	0.08	0.08	0.08
	Time	[min]	40	45	50	55	60	65	70	
3/30_1	$T_{heating}$	[°C]	49	65	65	62	60	60	60	
	$T_{ambient}$	[°C]	23	23	23	23	23	23	23	
	Vol.	[ml]	120	137	160	166	170	170	170	
	n_{CH4}/g_H	[mmol/g]	0.98	1.12	1.31	1.36	1.39	1.39	1.39	
3/30_2	$T_{heating}$	[°C]	55	60	60	60	60	60	60	
	$T_{ambient}$	[°C]	20	20	20	20	20	20	20	
	Vol.	[ml]	110	125	133	140	145	148	150	
	n_{CH4}/g_H	[mmol/g]	0.91	1.04	1.11	1.16	1.21	1.23	1.25	
3/103_1	$T_{heating}$	[°C]	51	60	60	60	60	60	60	
	$T_{ambient}$	[°C]	20	20	20	20	20	20	20	
	Vol.	[ml]	15	28	33	35	40	40	40	
	n_{CH4}/g_H	[mmol/g]	0.12	0.23	0.27	0.29	0.33	0.33	0.33	
3/103_2	$T_{heating}$	[°C]	52	59	60	60	60	60	60	
	$T_{ambient}$	[°C]	19	19	19	19	19	19	19	
	Vol.	[ml]	17	27	35	37	40	40	40	
	n_{CH4}/g_H	[mmol/g]	0.14	0.22	0.29	0.30	0.33	0.33	0.33	

Table 33: Comprised results from Series 4 blank gas titration experiments after drying at 30 or 103 °C using no reagent.

	Time	[min]	0	5	10	15	20	25	30	35
4/30_1	$T_{heating}$	[°C]	30.6	30.4	30.4	30.2	30.2	30.3	32.5	32.6
	$T_{ambient}$	[°C]	26	26	26	26	26	26	26	26
	Vol.	[ml]	0	0	1	1	1	1	2	2
	n_{CH4}/g_H	[mmol/g]	0.00	0.00	0.01	0.01	0.01	0.01	0.02	0.02
24/30_2	$T_{heating}$	[°C]	31.9	32.7	32.6	31.9	31.5	30.8	30.3	29.8
	$T_{ambient}$	[°C]	26	26	26	26	26	26	26	26
	Vol.	[ml]	0	0	1	2	2	2	2	2
	n_{CH4}/g_H	[mmol/g]	0.00	0.00	0.01	0.02	0.02	0.02	0.02	0.02
4/103_1	$T_{heating}$	[°C]	30.6	33.7	33.9	33.4	32.7	31.9	31.2	30.8
	$T_{ambient}$	[°C]	26	26	26	26	26	26	25	26
	Vol.	[ml]	0	1	3	3	3	3	3	3
	n_{CH4}/g_H	[mmol/g]	0.00	0.01	0.02	0.02	0.02	0.02	0.02	0.02
4/103_2	$T_{heating}$	[°C]	33.0	33.3	33.0	32.6	32.1	31.5	31.2	31.5
	$T_{ambient}$	[°C]	26	26	26	25	25	25	25	25
	Vol.	[ml]	0	2	2	2	2	2	2	2
	n_{CH4}/g_H	[mmol/g]	0.00	0.02	0.02	0.02	0.02	0.02	0.02	0.02
	Time	**[min]**	**40**	**45**	**50**	**55**	**60**	**65**	**70**	
4/30_1	$T_{heating}$	[°C]	41.5	54.1	61.7	60.2	61.3	60.2	61.3	
	$T_{ambient}$	[°C]	26	26	26	26	26	26	26	
	Vol.	[ml]	4	8	13	18	20	21	21	
	n_{CH4}/g_H	[mmol/g]	0.03	0.06	0.11	0.15	0.16	0.17	0.17	
4/30_2	$T_{heating}$	[°C]	37.9	49.0	58.1	61.5	60.4	61.6	60.2	
	$T_{ambient}$	[°C]	26	26	26	26	26	26	26	
	Vol.	[ml]	3	8	11	17	18	19	20	
	n_{CH4}/g_H	[mmol/g]	0.02	0.07	0.09	0.14	0.15	0.16	0.16	
4/103_1	$T_{heating}$	[°C]	39.9	51.9	59.2	61.1	60.2	61.0	61.3	
	$T_{ambient}$	[°C]	26	26	26	26	26	26	26	
	Vol.	[ml]	4	8	13	20	21	21	21	
	n_{CH4}/g_H	[mmol/g]	0.03	0.07	0.11	0.16	0.17	0.17	0.17	
4/103_2	$T_{heating}$	[°C]	40.5	51.5	59.4	60.6	60.9	60.6	60.6	
	$T_{ambient}$	[°C]	26	26	26	26	26	26	26	
	Vol.	[ml]	4	9	15	19	20	21	21	
	n_{CH4}/g_H	[mmol/g]	0.03	0.07	0.12	0.15	0.16	0.17	0.17	

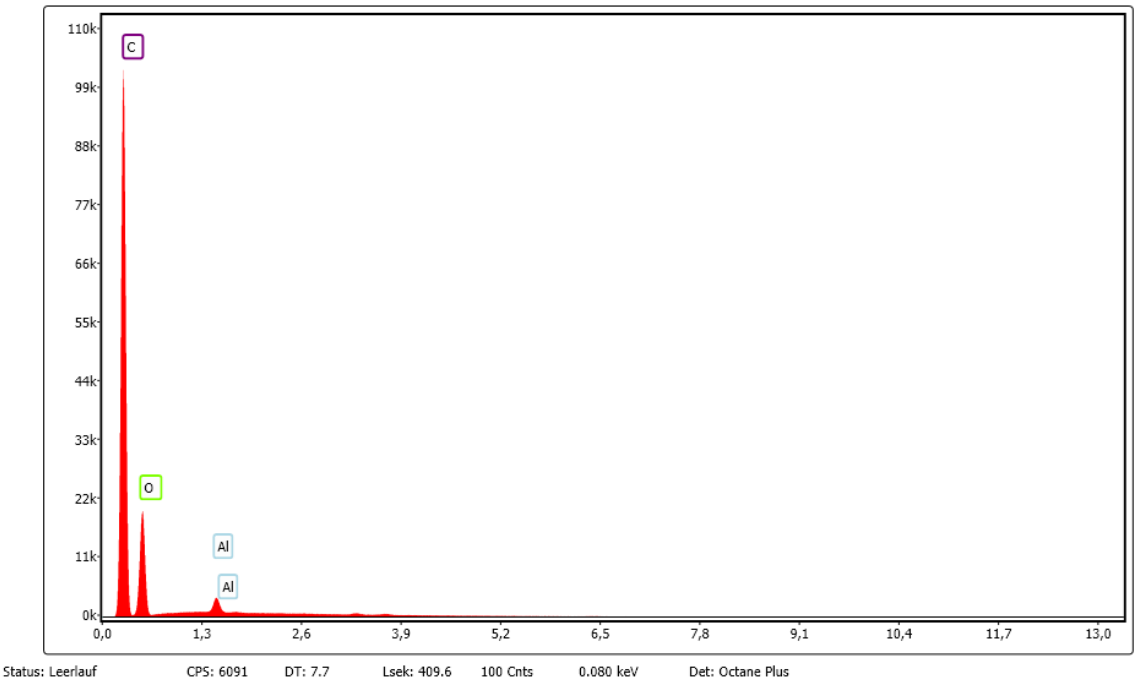

Figure 60: EDX spectrum from SEM micrograph of a microfracture surface of an injection molded WPC specimen S2_1 containing ~47 % PE.
Corresponding to Figure 29 in Chapter 6.3.2 *in situ* WPC.

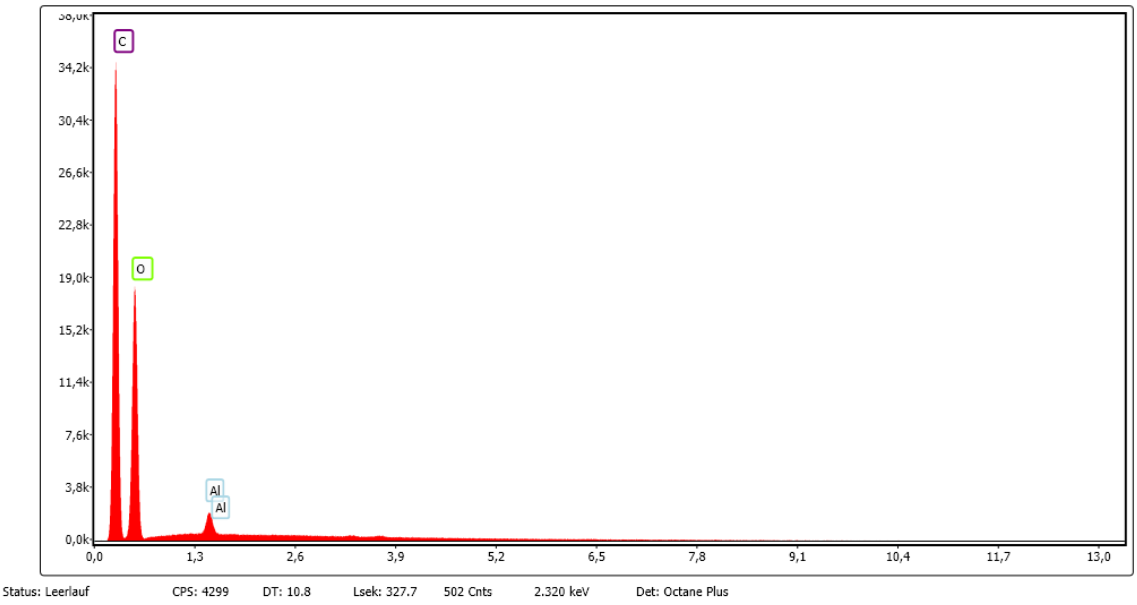

Figure 61: EDX spectrum from SEM micrograph showing the aluminum distribution in a cross section originating from the center region of IP1a.
Corresponding to Figure 44 in Chapter 7.3.1 *in situ* Wood.

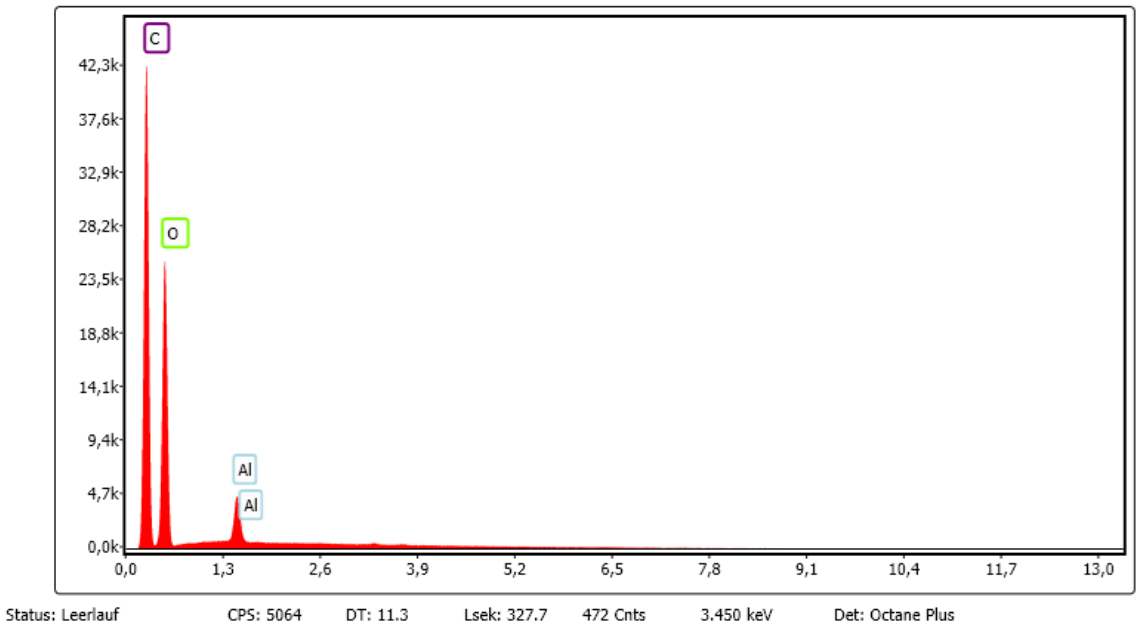

Figure 62: EDX spectrum from SEM micrograph showing the aluminum distribution in a cross section originating from the center region of IP2.
Corresponding to Figure 45 in Chapter 7.3.1 *in situ* Wood.

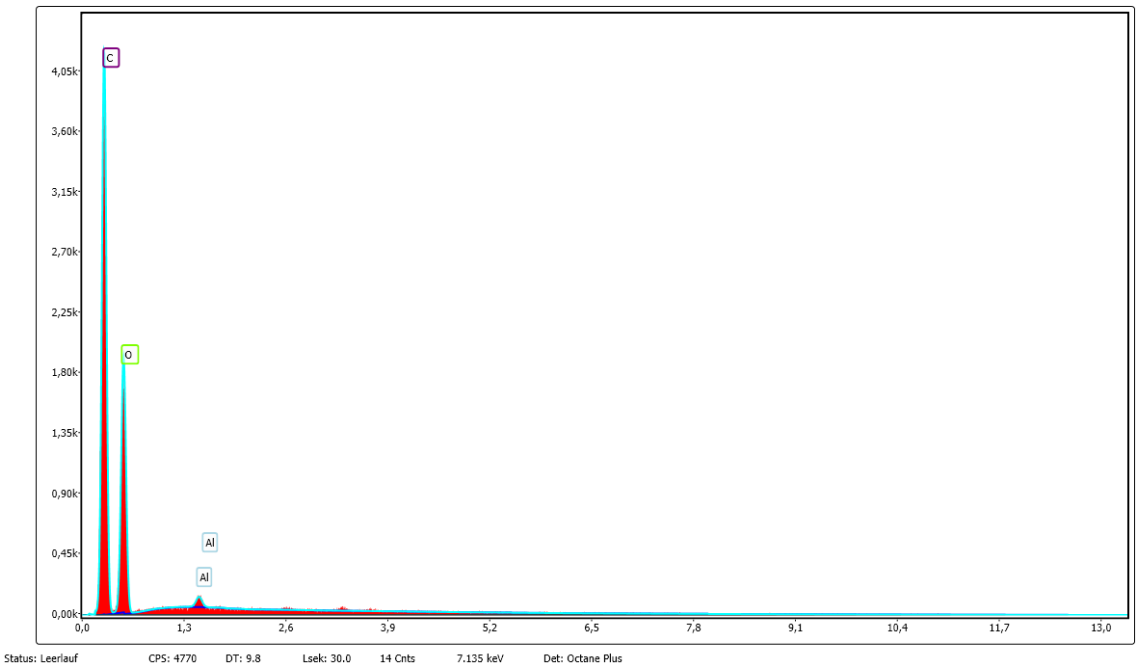

Figure 63: EDX spectrum from SEM micrograph showing the aluminum distribution in a cross section originating from the center region of IP3.
Corresponding to Figure 46 in Chapter 7.3.1 *in situ* Wood.

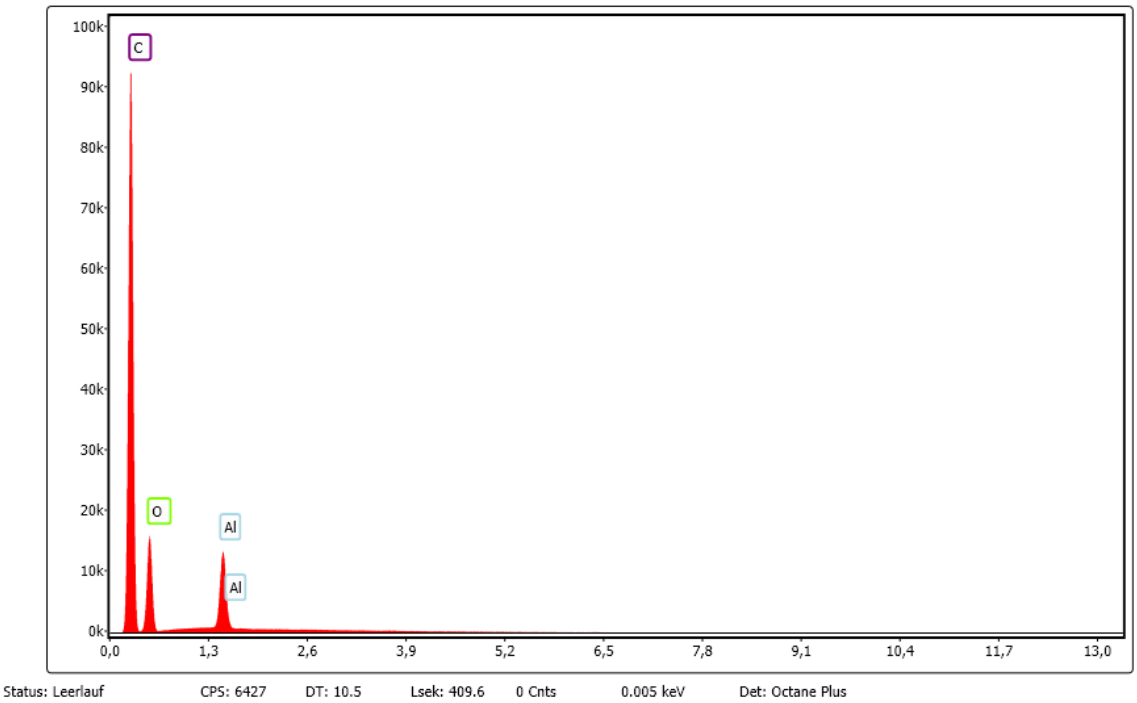

Figure 64: EDX spectrum from SEM micrograph showing the cross section originating from the outer layers of Sample 7_1 of Series 3.

Corresponding to Figure 52 in Chapter 7.3.2 *in situ* Wood.

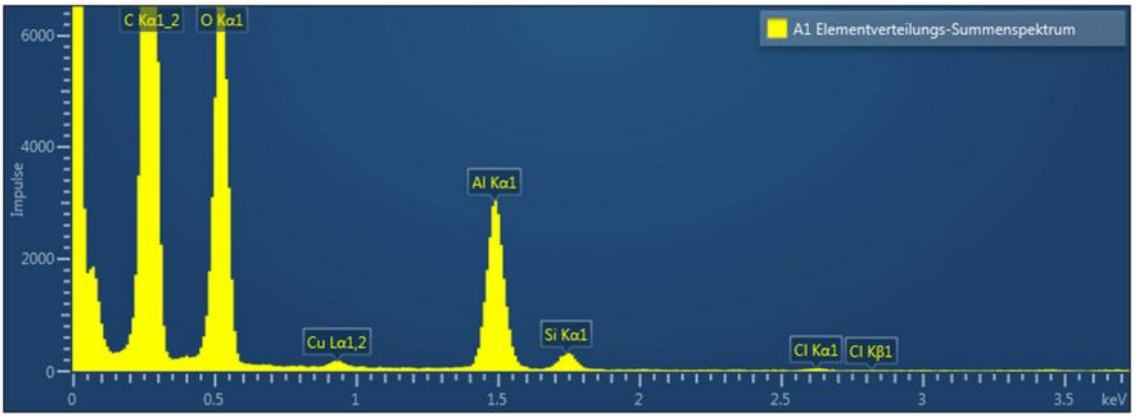

Figure 65: EDX spectrum from TEM micrograph investigating observed granular structures within cell lumen of Sample 9_2 of Series 3.

Corresponding to Figure 53 in Chapter 7.3.2 *in situ* Wood.

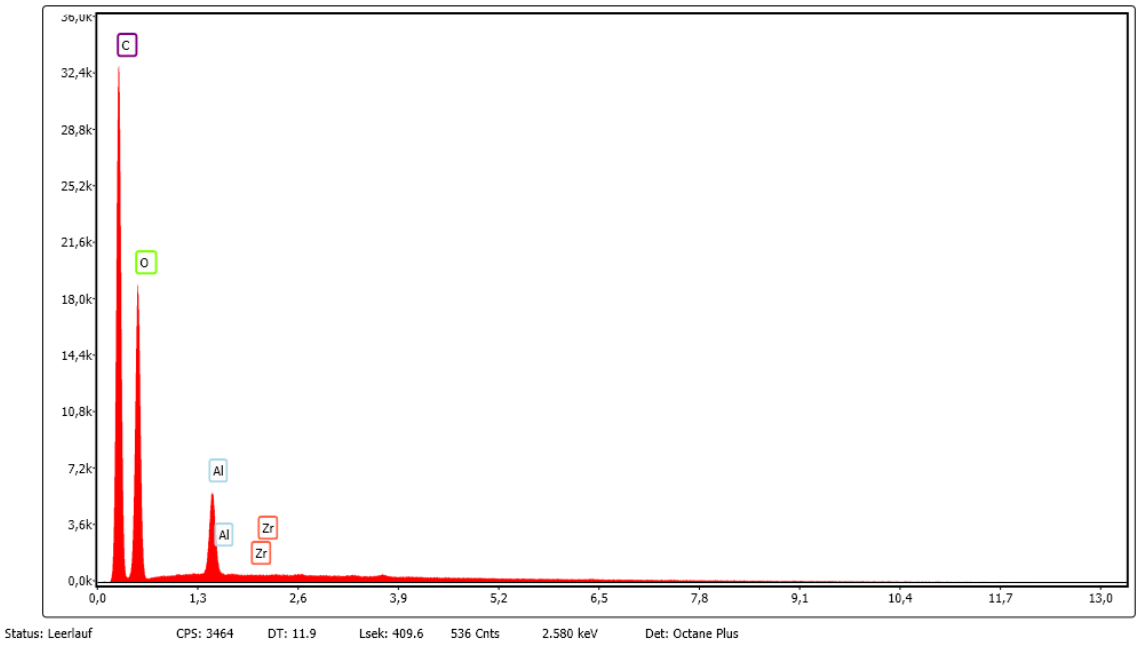

Figure 66: EDX spectrum from SEM micrograph showing the cross section of Sample 4_1 of Series 5 solid wood Gas-Phase Polymerizations.
Corresponding to Figure 59 in Chapter 7.3.3 gas phase Wood.

9.2 Safety and Disposal

All used chemicals and hazardous substances were disposed in accordance with the requirements of the German Chemicals Act (ChemG) and the Ordinance on Hazardous Substances (GefStoffV). Halogen-free and halogen-containing solvents were disposed separately into designated containers. Solvents containing metal alkyls were diluted with toluene and quenched by cautious hydrolysis with isopropyl alcohol, ethanol and water. After acidifying the solution with diluted hydrochloric acid the aqueous and organic phases were separately disposed in the aforementioned containers. Contaminated solids were dried and disposed in the appropriate containers.

Table 34: Classification and labelling of utilized chemicals in accordance with GHS*.

Hazardous Substances	GHS pictograms	H-Statements	P-Statements
Acetone		225-319-336-EUH066	210-240-305/351/338-403/233
Ethanol		225-319	210-240-305/351/338-403/233
Ethylene		220-280-336	210-260-304/340-315-377-381-405-403
Hydranal Coulomat AG-Oven		373-370-360D-318-301-311-331-225	260-280-284
Isopropyl alcohol		225-319-336	210-233-240-305/351/338-403/235
Methylaluminoxane** (10 % in Toluene)		225-260-304-314-318-336-361d-373-412-EUH014	210-231/232-260-280-301/330/331-303/361/353-304/340/310-305/351/338/310-370/378-422-501
Hydrochloric acid (7 %)		290-314-335	260-280-303/361/353-304/340/310-305/351/338
Toluene		225-304-315-336-361d-373	210-240-301/310/330-302/352-314-403/233
1,2,4-Trichlorobenzene		302-315-410	273-302/352
Trimethylaluminum		250-260-314-EUH014	210-231/232-280-305/351/338-370/378-422
Wood dust, respirable		German TRGS905	
Xylene		226-304-312/332-315-H319-335-373	210-260-280-301/310-305/351/338-370/378
Zirconium(IV) chloride		302-314-EUH014	280-301/330/331-305/351/338-309/310

* Source: GESTIS; ** According to producer LANXESS

10 References

Akelah, A.; Sherrington, D. C. (1982): Preparation and synthetic application of cellulose-supported phase transfer catalysts. In *Eur. Polym. J.* 18 (4), pp. 301–305. DOI: 10.1016/0014-3057(82)90159-8.

Alexandre, Michaël; Martin, Eric; Dubois, Philippe; Garcia-Marti, Miguel; Jérôme, Robert (2000): Use of metallocenes in the polymerization-filling technique with production of polyolefin-based composites. In *Macromol. Rapid Commun.* 21 (13), pp. 931–936.

Alt, H. G.; Köppl, A. (2000): Effect of the Nature of Metallocene Complexes of Group IV Metals on Their Performance in Catalytic Ethylene and Propylene Polymerization. In *Chem. Rev.* 100 (4), pp. 1205–1222. DOI: 10.1021/cr9804700.

Andresen, Arne; Cordes, Hans-Günther; Herwig, Jens; Kaminsky, Walter; Merck, Alexander; Mottweiler, Renke et al. (1976): Halogen-Free Soluble Ziegler Catalysts for the Polymerization of Ethylene. Control of Molecular Weight by Choice of Temperature. In *Angew. Chem. Int. Ed.* 15 (10), pp. 630–632. DOI: 10.1002/anie.197606301.

Argyropoulos, D. S.; Menachem, S. B. (1998): Chapter 12. Lignin. In David L. Kaplan (Ed.): Biopolymers from Renewable Resources. Berlin Heidelberg: Springer (Macromolecular Systems - Materials Approach, 1), pp. 292–322.

Arlman, E. J. (1964): Ziegler-Natta Catalysis II. Surface Structure of Layer-Lattice Transition Metal Chlorides. In *J. Catal.* 3 (1), pp. 89–98. DOI: 10.1016/0021-9517(64)90096-X.

Arlman, E. J.; Cossee, P. (1964): Ziegler-Natta catalysis III. Stereospecific Polymerization of Propene with the Catalyst System $TiCl_3$-$AlEt_3$. In *J. Catal.* 3 (1), pp. 99–104. DOI: 10.1016/0021-9517(64)90097-1.

Babushkin, Dmitrii E.; Naundorf, Corinna; Brintzinger, Hans H. (2006): Distinct methylalumoxane(MAO)-derived Me-MAO^- anions in contact with a zirconocenium cation–a ^{13}C-NMR study. In *Dalton Trans.* (38), pp. 4539–4544. DOI: 10.1039/b611028m.

Barnes, David K. A.; Galgani, Francois; Thompson, Richard C.; Barlaz, Morton (2009): Accumulation and fragmentation of plastic debris in global environments. In *Philos. Trans. R. Soc. B* 364 (1526), pp. 1985–1998. DOI: 10.1098/rstb.2008.0205.

Barnes, H. M.; Choong, E. T.; McIlhenny, R. C. (1969): Several vapor phase chemical treatments for dimensional stabilization of wood. In *Forest Prod. J.* 19 (3).

Bashir, Muhammad Ahsan; Vancompernolle, Tom; Gauvin, Régis M.; Delevoye, Laurent; Merle, Nicolas; Monteil, Vincent et al. (2016): Silica/MAO/(n-BuCp)$_2$$ZrCl_2$ catalyst: effect of support dehydroxylation temperature on the grafting of MAO and ethylene polymerization. In *Catal. Sci. Technol.* 6 (9), pp. 2962–2974. DOI: 10.1039/C5CY01285F.

Bauch, Josef; Liese, Walter (1966): Über die axiale Wegsamkeit von saftfrischem Tannen- und Fichten-Splintholz für organische Lösungsmittel. In *Holzforschung* 20 (6).

Belelli, P. G.; Eberhardt, A.; Ferreira, M. L.; Vaya, V. C.; Santos, J. H. Z. dos; Damiani, D. E. (2000): An experimental study of metallocene heterogeneization on inorganic and

biopolimeric supports for olefin polymerization. In *Curr. Trends Polym. Sci.* 5, pp. 79–90.

Berglund, Lars A.; Burgert, Ingo (2018): Bioinspired Wood Nanotechnology for Functional Materials. In *Adv. Mater.* 30 (19), pp. 1–15.

Böhm, Ludwig L. (2003): Die Ethylenpolymerisation mit Ziegler-Katalysatoren 50 Jahre nach der Entdeckung. In *Angew. Chem.* 115 (41), pp. 5162–5183. DOI: 10.1002/ange.200300580.

Bonduel, Daniel; Mainil, Michaël; Alexandre, Michaël; Monteverde, Fabien; Dubois, Philippe (2005): Supported coordination polymerization: a unique way to potent polyolefin carbon nanotube nanocomposites. In *ChemComm* (6), pp. 781–783. DOI: 10.1039/b414164d.

Bouafif, Hassine; Koubaa, Ahmed; Perré, Patrick; Cloutier, Alain; Riedl, Bernard (2009): Wood Particle/High-Density Polyethylene Composites: Thermal Sensitivity and Nucleating Ability of Wood Particles. In *J. Appl. Polym. Sci.* 113 (1), pp. 593–600. DOI: 10.1002/app.30129.

BP p.l.c. (2019): BP Statistical Review of World Energy 2019. 68th ed. London, United Kingdom (BP Statistical Review of World Energy). Available online at https://www.bp.com/content/dam/bp/business-sites/en/global/corporate/pdfs/energy-economics/statistical-review/bp-stats-review-2019-full-report.pdf, checked on 6/24/2019.

Breslow, David S.; Newburg, Norman R. (1959): Bis-(cyclopentadienyl)-titanium Dichloride-Alkylaluminum Complexes as Soluble Catalysts for the Polymerization of Ethylene. In *J. Am. Chem. Soc.* 81 (1), pp. 81–86. DOI: 10.1021/ja01510a018.

Brintzinger, Hans H.; Fischer, David; Mülhaupt, Rolf; Rieger, Bernhard; Waymouth, Robert M. (1995): Stereospecific Olefin Polymerization with Chiral Metallocene Catalysts. In *Angew. Chem. Int. Ed.* 34 (11), pp. 1143–1170. DOI: 10.1002/anie.199511431.

Brookhart, Maurice; Green, Malcolm L. H.; Parkin, Gerard (2007): Agostic interactions in transition metal compounds. In *Proc. Natl. Acad. Sci. USA* 104 (17), pp. 6908–6914. DOI: 10.1073/pnas.0610747104.

Brookhart, Maurice; Green, Malcolm L.H. (1983): Carbon-hydrogen-transition metal bonds. In *J. Organomet. Chem.* 250 (1), pp. 395–408. DOI: 10.1016/0022-328X(83)85065-7.

Brunner, Reinhard (1987): Brunner-Hildebrand. Die Schnittholztrocknung. 5. Auflage. 5th ed. Hannover: Hildebrand Holztechnik GmbH und Brunner Trockentechnik GmbH.

Burgert, Ingo; Cabane, Etienne; Zollfrank, C.; Berglund, Lars A. (2015): Bio-inspired functional wood-based materials – hybrids and replicates. In *Int. Mater. Rev.* 60 (8), pp. 431–450. DOI: 10.1179/1743280415Y.0000000009.

Burmester, Arno (1970): Formbeständigkeit von Holz gegenüber Feuchtigkeit. Grundlagen und Vergütungsverfahren. Berlin: Bundesanstalt für Materialprüfung (BAM-Bericht, Nr. 4).

Buro, Andreas; Buro, Eva-Anne (1959): Beitrag zur Kenntnis der Eindringwege für Flüssigkeiten in Kiefernholz. In *Holzforschung* 13 (3).

Cabane, Etienne; Keplinger, Tobias; Merk, Vivian; Hass, Philipp; Burgert, Ingo (2014): Renewable and Functional Wood Materials by Grafting Polymerization Within Cell Walls. In *ChemSusChem* 7 (4), pp. 1020–1025. DOI: 10.1002/cssc.201301107.

Callister, William D., Jr. (2007): Material Science and Engineering. An Introduction. With assistance of David G. Rethwisch. 7th ed. New York, NY: John Wiley & Sons.

Cam, Darinn; Giannini, Umberto (1992): Concerning the reaction of zirconocene dichloride and methylalumoxane: homogeneous Ziegler-Natta catalytic system for olefin polymerization. In *Macromol. Chem. Phys.* 193 (5), pp. 1049–1055. DOI: 10.1002/macp.1992.021930502.

Cam, Darinn; Sartori, Franco; Maldotti, Andrea (1994): Reduction of bis(η^5-cyclopentadienyl)zirconium dichloride in the presence of methylalumoxane. In *Macromol. Chem. Phys.* 195 (8), pp. 2817–2826. DOI: 10.1002/macp.1994.021950813.

Carraher, Charles E. (Ed.) (2003): Seymour/Carraher's Polymer Chemistry. 6th ed., rev. and expanded. New York: M. Dekker (Undergraduate chemistry, 16).

Carus, Michael; Eder, Asta; Dammer, Lara; Korte, Hans; Scholz, Lena; Essel, Roland et al. (2015a): WPC/NFC Market Study 2014-10 (Update 2015-06). Wood-Plastic Composites (WPC) and Natural Fibre Composites (NFC): European and Global Markets 2012 and Future Trends in Automotive and Construction (short version). Edited by nova-Institut für politische und ökologische Innovation GmbH. Available online at https://compositesuk.co.uk/system/files/documents/WPC-NFC-Market-Study-Short-Verson%202015.pdf, checked on 10/8/2019.

Carus, Michael; Eder, Asta; Scholz, Lena (2015b): Bioverbundwerkstoffe. Naturfaserverstärkte Kunststoffe (NFK) und Holz-Polymer-Werkstoffe (WPC). Edited by Fachagentur Nachwachsende Rohstoffe e. V. (FNR) (227). Available online at http://www.fnr.de/fileadmin/allgemein/pdf/broschueren/Broschuere_Bioverbundwerkstoffe-web-V01.pdf, checked on 10/8/2019.

Carus, Michael; Partanen, Asta (2018): Natural fibre-reinforced plastics: establishmentand growth in niche markets. Edited by nova-Institut für politische und ökologische Innovation GmbH. Available online at https://edepot.wur.nl/494568, checked on 10/8/2019.

Casas, E.; van Grieken, R.; Escola, J. M. (2012): Polymerization of ethylene with $(nBuCp)_2ZrCl_2$ supported over mesoporous SBA-15 functionalized with sulfonic acid groups. In *Appl. Catal. A Gen.* 437-438, pp. 44–52. DOI: 10.1016/j.apcata.2012.06.015.

Cathcart, Brian (2004): Sir Michael Willcox Perrin. (1905–1988). Edited by Oxford University Press pages. Oxford Dictionary of National Biography. Available online at https://www.oxforddnb.com/view/10.1093/ref:odnb/9780198614128.001.0001/odnb-9780198614128-e-70394, updated on 5/24/2008, checked on 4/19/2020.

Ceresana ek (2014a): Market Study: Ethylene. Konstanz, Germany. Available online at https://www.ceresana.com/upload/Marktstudien/brochueren/Ceresana_Brochure_Market-Study_Ethylene_2nd_ed.pdf, checked on 3/3/2020.

Ceresana ek (2014b): Market Study: Propylene. Konstanz, Germany. Available online at https://www.ceresana.com/upload/Marktstudien/brochueren/Ceresana_Brochure_Market-Study_Propylene_2.pdf, checked on 3/3/2020.

Chanzy, H.; Day, A.; Marchessault, R. H. (1967): Polymerization on Glass-supported Vanadium Trichloride: Morphology of Nascent Polyethylene. In *Polymer* 8, pp. 567–588. DOI: 10.1016/0032-3861(67)90068-7.

Chanzy, H. D.; Bonjour, E.; Marchessault, R. H. (1974): Nascent structures during the polymerization of ethylene. II. Calorimetric study. In *Kolloid-Zeitschrift & Zeitschrift für Polymere* 252 (1), pp. 8–14. DOI: 10.1007/BF01381688.

Chanzy, H. D.; Côté, W. A.; Marchessault, R. H. (1968): Encapsulation of Pulp Fibers by Vanadium Trichloride-Catalyzed Polymerization of Ethylene. In *Text. Res. J.* 38 (6), pp. 583–591. DOI: 10.1177/004051756803800604.

Chanzy, H. D.; Revol, J. F. (1973): Potato Starch Encapsulation with Polyethylene. I. Catalysis and Polymerization. In *Starch* 25 (4), pp. 131–136. DOI: 10.1002/star.19730250406.

Chanzy, H. D.; Revol, J. F. (1974): Potato Starch Encapsulation with Polyethylene. II. Morphology of the Encapsulated Granules. In *Starch* 26 (6), pp. 197–200. DOI: 10.1002/star.19740260606.

Chanzy, H. D.; Revol, J. F.; Guiroy, G.; Quéré, J. (1975): Polyethylene encapsulation of groundwood pulp and applied to paper. Presented at the Fourth Canadian Wood Chemistry Symposium, Quebec, July 4-6, 1973. In *Svensk Papperstidning* (7), 258-260.

Chanzy, H. D.; Revol, J. F.; Marchessault, R. H.; Lamandé, A. (1973): Nascent structures during the polymerization of ethylene. I. Morphology and model of growth. In *Kolloid-Zeitschrift & Zeitschrift für Polymere* 251 (8), pp. 563–576. DOI: 10.1007/BF01498579.

Chen, Eugene You-Xian; Marks, Tobin J. (2000): Cocatalysts for Metal-Catalyzed Olefin Polymerization. Activators, Activation Processes, and Structure−Activity Relationships. In *Chem. Rev.* 100 (4), pp. 1391–1434. DOI: 10.1021/cr980462j.

Chen, Zhangjing (1997): Primary Driving Force in Wood Vacuum Drying. Dissertation. Virginia Polytechnic Institute and State University, Blacksburg, Virginia, USA. Available online at https://vtechworks.lib.vt.edu/handle/10919/26255.

Chen, Zhangjing; Lamb, Fred M. (2002): Theoretical equilibrium moisture content of wood under vacuum. In *Wood Fiber Sci.* 34 (4), pp. 553–559.

Chien, James C. W.; Rausch, Marvin D. (1999): Monocyclopentadienyl Titanium Catalyst. In Walter Kaminsky (Ed.): Metalorganic Catalysts for Synthesis and Polymerization. Recent Results by Ziegler-Natta and Metallocene Investigations. Berlin Heidelberg: Springer, pp. 446–464.

Christensen, G. N.; Hergt, H. F. A. (1969): Effect of Previous History on Kinetics of Sorption by Wood Cell Walls. In *J. Polym. Sci. A Polym. Chem.* 7 (8), pp. 2427–2430. DOI: 10.1002/pol.1969.150070839.

Christensen, G. N.; Kelsey, K. E. (1959): Die Sorption von Wasserdampf durch die chemischen Bestandteile des Holzes. In *Eur. J. Wood Wood Prod.* 17 (5), pp. 189–203. DOI: 10.1007/BF02608811.

Christiansen, Alfred W. (1990): How Overdrying Wood Reduces Its Bonding to Phenol-Formaldehyde Adhesives: A Critical Review of the Literature. Part I. Physical Responses. In *Wood Fiber Sci.* 22 (4), pp. 441–459.

Christiansen, Alfred W. (1991): How Overdrying Wood Reduces Its Bonding to Phenol-Formaldehyde Adhesives: A Critical Review of the Literature. Part II. Chemical Reactions. In *Wood Fiber Sci.* 23 (1), pp. 69–84.

Cihlář, Jaroslav; Mejzlík, Jiří; Hamřík, Oldřich (1978): Influence of Water on Ethylene Polymerization Catalyzed by Titanocene Systems. In *Macromol. Chem. Phys.* 179 (10), pp. 2553–2558. DOI: 10.1002/macp.1978.021791021.

Clemons, Craig (2002): Wood-Plastic Composites in the United States. The Interfacing of Two Industries. In *Forest Prod. J.* 52 (6), pp. 11–18.

Collins, Scott; Kelly, W. Mark; Holden, David A. (1992): Polymerization of Propylene Using Supported, Chiral, ansa-Metallocene Catalysts: Production of Polypropylene with Narrow Molecular Weight Distributions. In *Macromolecules* 25 (6), pp. 1780–1785. DOI: 10.1021/ma00032a025.

Comstock, G. L.; Côté, W. A. (1968): Factors affecting permeability and pit aspiration in coniferous sapwood. In *Wood Sci. Technol.* 2 (4), pp. 279–291. DOI: 10.1007/BF00350274.

Cornelius, Frauke; Scholtyssek, Julia; Thole, Volker (2014): Verfahren zur Herstellung von biomaterial-verstärkten Kompositen und modifizierten Biomaterialien sowie entsprechend hergestellte Komposite und Biomaterialien. Applied for by Fraunhofer-Gesellschaft zur Förderung der Angewandten Forschung e.V. on 6/10/2014. Patent no. WO 2014/198692 A1.

Cossee, P. (1964): Ziegler-Natta Catalysis I. Mechanism of Polymerization of $_{\alpha}$-Olefins with Ziegler-Natta catalysts. In *J. Catal.* 3 (1), pp. 80–88. DOI: 10.1016/0021-9517(64)90095-8.

Cossee, P. (1966): On the mechanism of cis-ligand insertion. In *Recl. Trav. Chim. Pays-Bas* 85 (11), pp. 1151–1160. DOI: 10.1002/recl.19660851109.

Cui, Y. H.; Tao, J.; Noruziaan, B.; Cheung, M.; Lee, S. (2010): DSC Analysis and Mechanical Properties of Wood—Plastic Composites. In *J. Reinf. Plast. Compos.* 29 (2), pp. 278–289. DOI: 10.1177/0731684408097766.

D'Agnillo, Luigi; Soares, Joao B. P.; Penlidis, Alexander (1998): Controlling molecular weight distributions of polyethylene by combining soluble metallocene/MAO catalysts. In *J. Polym. Sci. A Polym. Chem.* 36 (5), pp. 831–840. DOI: 10.1002/(SICI)1099-0518(19980415)36:5<831::AID-POLA16>3.0.CO;2-H.

Dankovics, A.; Erdélyi, J.; Koltai, M. (1969): Kinetic Studies on the Cellulose–Propylene System in Presence of Ziegler-Natta Catalysts. In *J. Appl. Polym. Sci.* 13 (9), pp. 1809–1824. DOI: 10.1002/app.1969.070130901.

Diestel, Sylvia; Krause, Andreas (2018): Wood-based composites with thermoplastic polyurethane as matrix polymer. In *J. Appl. Polym. Sci.* 135 (25), p. 46344.

Domininghaus, Hans; Elsner, Peter; Eyerer, Peter; Hirth, Thomas (Eds.) (2012): Kunststoffe. Eigenschaften und Anwendungen. 8.th ed. Berlin, Heidelberg: Springer-Verlag.

Dubois, Philippe (2020): Publications regarding Rémy Francq's master thesis. e-mail to Julius Gurr, 3/1/2020.

Dubois, Philippe; Alexandre, Michaël; Hindryckx, F.; Jérôme, Robert (1998): Polyolefin-Based Composites by Polymerization-Filling Technique. In *Polym. Rev.* 38 (3), pp. 511–565. DOI: 10.1080/15583729808546031.

Dutschke, Joachim (1985): Polymerisationen von Ethylen auch in Gegenwart von Füllstoffen in Blassäulen- und Wirbelschichtreaktoren mit löslichen Zieglerkatalysatoren. Dissertation. Universität Hamburg, Hamburg. Technische und Makromolekulare Chemie.

Dyachkovskii, F. S. (1988): Distinctive Features of Olefin Polymerization on the Surface of Supports. In Walter Kaminsky, Hansjörg Sinn (Eds.): Transition Metals and Organometallics as Catalysts for Olefin Polymerization. Berlin, Heidelberg: Springer Berlin Heidelberg, pp. 67–78.

Eberhardt, A. M.; Ferreira, M. L.; Damiani, D. E. (2001): Heterogeneization of Polymerization Catalysts on Natural Substances. In *Polym. Eng. Sci.* 41 (6), pp. 946–954. DOI: 10.1002/pen.10794.

Ehrenstein, Gottfried W. (2006): Faserverbund-Kunststoffe. Werkstoffe - Verarbeitung - Eigenschaften. 2. völlig überarbeitete Auflage. München: Hanser.

Engelund, Emil Tang; Thygesen, Lisbeth Garbrecht; Svensson, Staffan; Hill, Callum A. S. (2013): A critical discussion of the physics of wood–water interactions. In *Wood Sci. Technol.* 47 (1), pp. 141–161. DOI: 10.1007/s00226-012-0514-7.

Ermeydan, Mahmut A.; Cabane, Etienne; Gierlinger, Notburga; Koetz, Joachim; Burgert, Ingo (2014a): Improvement of wood material properties *via in situ* polymerization of styrene into tosylated cell walls. In *RSC Adv.* 4 (25), pp. 12981–12988. DOI: 10.1039/c4ra00741g.

Ermeydan, Mahmut A.; Cabane, Etienne; Hass, Philipp; Koetz, Joachim; Burgert, Ingo (2014b): Fully biodegradable modification of wood for improvement of dimensional stability and water absorption properties by poly(ε-caprolactone) grafting into the cell walls. In *Green Chem.* 16 (6), pp. 3313–3321. DOI: 10.1039/c4gc00194j.

Ermeydan, Mahmut A.; Cabane, Etienne; Masic, Admir; Koetz, Joachim; Burgert, Ingo (2012): Flavonoid Insertion into Cell Walls Improves Wood Properties. In *ACS Appl. Mater. Interfaces* 4 (11), pp. 5782–5789. DOI: 10.1021/am301266k.

Espinoza, Omar; Bond, Brian (2016): Vacuum Drying of Wood—State of the Art. In *Curr. For. Rep.* 2 (4), pp. 223–235. DOI: 10.1007/s40725-016-0045-9.

Faix, Oskar (2004): Grundlagen der Holzchemie Teil 1. Die Gerüstsubstanzen, fachübergreifende und historische Zusammenhänge, Holz als Chemierohstoff, Umweltchemie, relevante Verfahren und Produkte der chemischen Holztechnologie, Entwicklungstendenzen. Vorlesungsmanuskript. Universität Hamburg, Hamburg. Zentrum Holzwirtschaft.

Faix, Oskar (2008): Chemie des Holzes. In André Wagenführ, Frieder Scholz (Eds.): Tschenbuch der Holztechnik. München: Carl Hanser Verlag, pp. 47–74.

FAO (2016): Global Forest Resources Assessment 2015. How are the world's forests changing? 2nd ed. Rome. Available online at http://www.fao.org/forest-resources-assessment/en/, checked on 6/26/2019.

Fengel, Dietrich; Wegener, Gerd (1989): Wood. Chemistry, Ultrastructure, Reactions. Berlin: Walter de Gruyter & Co.

Fernandes Diniz, J. M. B.; Gil, M. H.; Castro, J. A. A. M. (2004): Hornification–its origin and interpretation in wood pulps. In *Wood Sci. Technol.* 37 (6), pp. 489–494. DOI: 10.1007/s00226-003-0216-2.

Deutsches Institut für Normung DIN EN 13183-1:2002-07;: Feuchtegehalt eines Stückes Schnittholz - Teil 1: Bestimmung durch Darrverfahren.

Fink, Gerhard; Steinmetz, Bernd; Zechlin, Joachim; Przybyla, Christian; Tesche, Bernd (2000): Propene Polymerization with Silica-Supported Metallocene/MAO Catalysts. In *Chem. Rev.* 100 (4), pp. 1377–1390.

Fink, Siegfried (1992): Transparent Wood - A New Approach in the Functional Study of Wood Structure. In *Holzforschung* 46 (5), pp. 403–408.

Fisa, B.; Marchessault, R. H. (1974): Preparation of a Microporous Composite: Encapsulation of Paper by Polyethylene. In *J. Appl. Polym. Sci.* 18 (7), pp. 2025–2037. DOI: 10.1002/app.1974.070180711.

Fohr, J-P.; Chakir, A.; Arnaud, G.; Du Peuty, M. A. (1995): Vacuum Drying of Oak Wood. In *Dry. Technol.* 13 (8-9), pp. 1675–1693. DOI: 10.1080/07373939508917046.

Fox, S. Carter; Li, Bin; Xu, Daiqiang; Edgar, Kevin J. (2011): Regioselective Esterification and Etherification of Cellulose: A Review. In *Biomacromolecules* 12 (6), pp. 1956–1972. DOI: 10.1021/bm200260d.

Franck, Adolf; Herr, Bernd; Ruse, Hans; Schulz, Gerhard (2011): Kunststoff-Kompendium. 7.th ed. Würzburg: Vogel Buchverlag.

Francq, Rémy (2002): Synthèse et caractérisation physico-mécanique de nouveaux composites HDPE - cellulose par catalyse métallocène supportée. Master thesis. Université de Mons-Hainaut, Mons, Belgium. Faculté des sciences.

Frihart, Charles R.; Hunt, Christopher G. (2010): Chapter 10. Adhesives with Wood Materials. Bond Formation and Performance. In Robert J. Ross (Ed.): Wood Handbook. Wood as an Engineering Material. Madison, Wisconsin: U.S. Department of Agriculture, Forest Service, Forest Products Laboratory.

Fumagalli, L.; Esfandiar, A.; Fabregas, R.; Hu, S.; Ares, P.; Janardanan, A. et al. (2018): Anomalously low dielectric constant of confined water. In *Science* 360 (6395), pp. 1339–1342. DOI: 10.1126/science.aat4191.

Gandini, Alessandro; Naceur Belgacem, Mohamed (2008): -1-. The State of the Art. In Mohamed Naceur Belgacem, Alessandro Gandini (Eds.): Monomers, Polymers and Composites from Renewable Resources. Oxford, Boston: Elsevier, 1-16.

Gellerstedt, Göran; Henriksson, Gunnar (2008): -9-. Lignins: Major Sources, Structure and Properties. In Mohamed Naceur Belgacem, Alessandro Gandini (Eds.): Monomers, Polymers and Composites from Renewable Resources. Oxford, Boston: Elsevier, pp. 201–224.

George, Steven M. (2010): Atomic Layer Deposition: An Overview. In *Chem. Rev.* 110 (1), pp. 111–131.

Geyer, Roland; Jambeck, Jenna R.; Law, Kara Lavender (2017): Production, use, and fate of all plastics ever made. In *Sci. Adv.* 3 (7). DOI: 10.1126/sciadv.1700782.

Ghosh, Shyamal C.; Militz, Holger; Mai, Carsten (2013): Modification of Pinus sylvestris L. wood with quat- and amino-silicones of different chain lengths. In *Holzforschung* 67 (4), pp. 421–427. DOI: 10.1515/hf-2012-0103.

Gibson, Lorna J.; Ashby, Michael F. (1999): Cellular solids. Structure and properties. Second edition. 2nd ed.: Cambridge University Press.

Gibson, Lorna J.; Ashby, Michael F.; Harley, Brendan A. (2010): Cellular Materials. in Nature and Medicine: Cambridge University Press.

Gierlinger, Notburga; Keplinger, Tobias; Harrington, Michael (2012): Imaging of plant cell walls by confocal Raman microscopy. In *Nat. Protoc.* 7 (9), pp. 1694–1708.

Gilbert, R. D.; Kadla, J. F. (1998): Chapter 3. Polysaccharides - Cellulose. In David L. Kaplan (Ed.): Biopolymers from Renewable Resources. Berlin Heidelberg: Springer (Macromolecular Systems - Materials Approach, 1), pp. 47–95.

Goretzki, Ralf; Fink, Gerhard; Tesche, Bernd; Rieger, Rainer; Uzick, Wolfram (1999): Unusual Ethylene Polymerization Results with Metallocene Catalysts Supported on Silica. In *J. Polym. Sci. A Polym. Chem.* 37 (5), pp. 677–682.

Gregory, Shawn A.; McGettigan, Connor P.; McGuinness, Emily K.; Rodin, David Misha; Yee, Shannon K.; Losego, Mark D. (2020): Single-Cycle Atomic Layer Deposition on Bulk Wood Lumber for Managing Moisture Content, Mold Growth, and Thermal Conductivity. In *Langmuir* 36 (7), pp. 1633–1641. DOI: 10.1021/acs.langmuir.9b03273.

Grigull, Ulrich (Ed.) (1988): NBS/NRC Wasserdampftafeln. Thermodynamische und Transportgrößen mit Computerprogrammen für Dampf und Wasser in SI-Einheiten. Berlin, Heidelberg: Springer Berlin Heidelberg.

Grosse, Charlotte; Thevenon, Marie-France; Noel, Marion; Gerardin, Philippe (2016): Optimising wood chemical modification with lactic acid oligomers by screening of processing conditions and chemical additives. Section 4 Processes and properties. In *IRG/WP 16-30701* (47th).

Grosser, Dietger (1977): Die Hölzer Mitteleuropas. Ein mikrophotographischer Lehratlas. Mit 87 Abbildungen in 344 Teilfiguren und drei Falttafeln. Berlin Heidelberg: Springer-Verlag.

Grubbs, Robert H.; Coates, Geoffrey W. (1996): α-Agostic Interactions and Olefin Insertion in Metallocene Polymerization Catalysts. In *Acc. Chem. Res.* 29 (2), pp. 85–93. DOI: 10.1021/ar9501683.

Gruber, Erich (2006): IV. Analytical Characterization of Pulps. In Herbert Sixta (Ed.): Handbook of Pulp. 1st ed. Weinheim: Wiley-VCH, 1211-1289.

Gul, Rizwan M.; McGarry, Frederick J.; Bragdon, Charles R.; Muratoglu, Orhun K.; Harris, William H. (2003): Effect of consolidation on adhesive and abrasive wear of ultra high molecular weight polyethylene. In *Biomaterials* 24, pp. 3193–3199.

Guo, G.; Wang, K. H.; Park, C. B.; Kim, Y. S.; Li, G. (2007): Effects of Nanoparticles on the Density Reduction and Cell Morphology of Extruded Metallocene Polyethylene/Wood Fiber Nanocomposites. In *J. Appl. Polym. Sci.* 104 (2), pp. 1058–1063. DOI: 10.1002/app.25778.

Habibi, Youssef (2014): Key advances in the chemical modification of nanocelluloses. In *Chem. Soc. Rev.* 43 (5), pp. 1519–1542. DOI: 10.1039/c3cs60204d.

Hatakeyama, H. (1992): 4.8 Thermal Analysis. In Stephen Y. Lin, Carlton W. Dence (Eds.): Methods in Lignin Chemistry. Berlin, Heidelberg: Springer-Verlag (Springer Series in Wood Science), pp. 200–214.

Hebeish, Ali; Guthrie, James Thomas (1981): The Chemistry and Technology of Cellulosic Copolymers. Berlin, Heidelberg: Springer (Polymers, Properties and Applications, 4).

Hees, Timo; Zhong, Fan; Rudolph, Tobias; Walther, Andreas; Mülhaupt, Rolf (2017): Nanocellulose Aerogels for Supporting Iron Catalysts and In Situ Formation of Polyethylene Nanocomposites. In *Adv. Funct. Mater.* 27 (11), pp. 1–8. DOI: 10.1002/adfm.201605586.

Hendren, Keith D.; Baughman, Travis W.; Deck, Paul A.; Foster, E. Johan (2020): *In situ* dispersion and polymerization of polyethylene cellulose nanocrystal-based nanocomposites. In *J. Appl. Polym. Sci.* 137 (13), p. 48500. DOI: 10.1002/app.48500.

Henrici-Olivé, G.; Olivé, S. (1967): Die aktive Spezies in homogenen Ziegler-Natta-Katalysatoren für die Äthylenpolymerisation. In *Angew. Chem.* 79 (17-18), pp. 764–773. DOI: 10.1002/ange.19670791705.

Heräjärvi, Henrik; Kunttu, Janni; Hurmekoski, Elias; Hujala, Teppo (2020): Outlook for modified wood use and regulations in circular economy. In *Holzforschung* 74 (4), pp. 334–343. DOI: 10.1515/hf-2019-0053.

Hergt, H. F. A.; Christensen, G. N. (1965): Variable Retention of Water by Dry Wood. In *J. Appl. Polym. Sci.* 9 (7), pp. 2345–2361. DOI: 10.1002/app.1965.070090703.

Herman, D. F.; Dunlap, I. R. (1965): Polyethylene Encapsulated Cellulose– A New Papermaking Fiber. In *TAPPI J.* 48 (7).

Herman, D. F.; Kruse, U.; Brancato, J. J. (1965): Polyethylene-Encapsulated Cellulose. In *J. Polym. Sci. C Polym. Symp.* 11 (1), pp. 75–95. DOI: 10.1002/polc.5070110107.

Herwig, Jens (1976): Molekulargewichts-Regelung bei der Äthylenpolymerisation mit halogenen Ziegler-Katalysatoren. Diploma. Universität Hamburg, Hamburg. Institut für Anorganische und Angewandte Chemie.

Herwig, Jens; Kaminsky, Walter (1983): Halogen-Free Soluble Ziegler Catalysts with Methylalumoxan as Catalyst. In *Polym. Bull.* 9-9 (8-9). DOI: 10.1007/BF00265329.

Hill, Callum A. S. (2006): Wood Modification. Chemical, Thermal and Other Processes. Chichester, England: John Wiley & Sons (Wiley Series In Renewable Resource Series).

Hill, Callum A. S. (2011): Wood Modification: An update. In *Bioresources* 6 (2), pp. 918–919.

Hill, Callum A. S.; Ramsay, J.; Gardiner, B. (2015): Variability in water vapour sorption isotherm in Japanese Larch (Larix kaempferi Lamb.) – earlywood and latewood influences. In *Int. Wood Prod. J.* 6 (2), pp. 53–59. DOI: 10.1179/2042645314Y.0000000090.

Hoffmann, Per (2003): Naturwissenschaftler zur Kogge. I. Die Konservierung der Bremer Kogge. In Gabriele Hoffmann, Uwe Schnall (Eds.): Die Kogge. Sternstunde der deutschen Schiffsarchäologie. 60 volumes. Hamburg: Convent Verlag, pp. 78–105.

Hoffmeyer, Preben; Engelund, Emil Tang; Thygesen, Lisbeth G. (2011): Equilibrium moisture content (EMC) in Norway spruce during the first and second desorptions. In *Holzforschung* 65 (6), pp. 875–882. DOI: 10.1515/HF.2011.112.

Hogan, John Paul; Banks, Robert L. (1956): Polymers and production thereof on 3/26/1956. App. no. 573,877. Patent no. 2,825,721.

Holik, Herbert (Ed.) (2006): Handbook of paper and board. 1st ed. Weinheim: Wiley-VCH.

Hristov, Velichko; Vasileva, Stefanka (2003): Dynamic Mechanical and Thermal Properties of Modified Poly(propylene) Wood Fiber Composites. In *Macromol. Mater. Eng.* 288 (10), pp. 798–806.

Huang, Xingyi; Ke, Qingquan; Kim, Chonung; Zhong, Hanfang; Wei, Ping; Wang, Genlin et al. (2007): Nonisothermal Crystallization Behavior and nucleation of LDPE/Al Nano- and Microcomposites. In *Polym. Eng. Sci.* 47 (7), pp. 1052–1061.

Hult, E.-L.; Larsson, P. T.; Iversen, T. (2001): Cellulose fibril aggregation — an inherent property of kraft pulps. In *Polymer* 42 (8), pp. 3309–3314. DOI: 10.1016/S0032-3861(00)00774-6.

Ibach, Rebecca E.; Ellis, W. Dale (2005): 15. Lumen Modifications. In Roger M. Rowell (Ed.): Handbook of Wood Chemistry and Wood Composites. Boca Raton, Florida, USA: Taylor & Francis Group (CRC Press), pp. 421–446.

Idström, Alexander; Brelid, Harald; Nydén, Magnus; Nordstierna, Lars (2013): CP/MAS ^{13}C NMR study of pulp hornification using nanocrystalline cellulose as a model system. In *Carbohydr. Polym.* 92 (1), pp. 881–884. DOI: 10.1016/j.carbpol.2012.09.097.

Ihmels, Carsten Wolfgang (2004): Metallocenkatalysierte Gasphasenpolymerisation von Ethylen in einem Minireaktor. Dissertation. Technische Universität Berlin, Berlin.

Ilvessalo-Pfäffli, Marja-Sisko (1995): Fiber Atlas. Identification of Papermaking Fibers. With 385 Figures. Berlin Heidelberg: Springer-Verlag (Springer Series in Wood Science).

Ittel, Steven D.; Johnson, Lynda K.; Brookhart, Maurice (2000): Late-Metal Catalysts for Ethylene Homo- and Copolymerization. In *Chem. Rev.* 100 (4), pp. 1169–1204. DOI: 10.1021/cr9804644.

Jiang, Feng; Hsieh, You-Lo (2014): Amphiphilic superabsorbent cellulose nanofibril aerogels. In *J. Mater. Chem. A* 2 (18), pp. 6337–6342. DOI: 10.1039/C4TA00743C.

Johannsen, Matthias (2011): Metallocen-katalysierte Synthese von polaren Olefin-basierten Makromonomeren. Dissertation. Technischen Universität Dresden, Dresden. Leibniz-Institut für Polymerforschung Dresden e.V.

Johansson, Leena-Sisko; Tammelin, Tekla; Campbell, Joseph M.; Setälä, Harri; Österberg, Monika (2011): Experimental evidence on medium driven cellulose surface adaptation demonstrated using nanofibrillated cellulose. In *Soft Matter* 7 (22), pp. 10917–10924. DOI: 10.1039/c1sm06073b.

Jousten, Karl (Ed.) (2016): Handbook of Vacuum Technology. Second, completely revised and updated edition. Weinheim, Germany: Wiley-VCH. Available online at http://onlinelibrary.wiley.com/book/10.1002/9783527688265.

Kalia, Susheel; Dufresne, Alain; Cherian, Bibin Mathew; Kaith, B. S.; Avérous, Luc; Njuguna, James; Nassiopoulos, Elias (2011): Cellulose-Based Bio- and Nanocomposites: A Review. In *Int. J. Polym. Sci.* 2011, pp. 1–35. DOI: 10.1155/2011/837875.

Kaminsky, Walter (1980): Verfahren zur Herstellung von Polymermassen aus Polyolefinen und Stärke und/oder Lignin sowie gegebenenfalls Cellulosefasern. Applied for by Maizena GmbH, 2000 Hamburg on 2/28/1980. Patent no. DE 3007433 C2.

Kaminsky, Walter (1981): Neues über Ziegler-Natta-Katalyse. In *Nachr. Chem. Tech. Lab.* 29 (6), pp. 373–377. DOI: 10.1002/nadc.19810290606.

Kaminsky, Walter (1982): Process for producing starch/polyolefin polymer composites. Applied for by CPC International Inc. on 11/12/1982. App. no. 440,789. Patent no. 4,431,788.

Kaminsky, Walter (1983): Polymerization and Copolymerization with a Highly Active, Soluble Ziegler-Natta Catalyst. In Roderic P. Quirk (Ed.): Transition Metal Catalyzed Polymerizations. Alkenes and Dienes. Part A. With assistance of Henry L. Hsieh, G. Bruce Klingensmith, Peter J. T. Tait. 11th Midland Macromolecular Metting. Michigan Molecular Institute. Chur, London, New York: Published for MMI Press by Harwood Academic Publishers, pp. 225–244.

Kaminsky, Walter (1996): New polymers by metallocene catalysis. In *Macromol. Chem. Phys.* 197, pp. 3907–3945.

Kaminsky, Walter (2004): The Discovery of Metallocene Catalysts and Their Present State of the Art. In *J. Polym. Sci. A Polym. Chem.* 42 (16), pp. 3911–3921. DOI: 10.1002/pola.20292.

Kaminsky, Walter (2014): Metallocene Based Polyolefin Nanocomposites. In *Materials* 7 (3), pp. 1995–2013. DOI: 10.3390/ma7031995.

Kaminsky, Walter; Bark, A.; Spiehl, R.; Möller-Lindenhof, N.; Niedoba, S. (1988): Isotactic Polymerization of Olefins with Homogeneous Zirconium Catalysts. In Walter Kaminsky, Hansjörg Sinn (Eds.): Transition Metals and Organometallics as Catalysts for Olefin Polymerization. Berlin, Heidelberg: Springer Berlin Heidelberg, 291-301.

Kaminsky, Walter; Funck, A.; Klinke, C. (2008): In-situ Polymerization of Olefins on Nanoparticles or Fibers by Metallocene Catalysts. In *Top. Catal.* 48 (1-4), pp. 84–90. DOI: 10.1007/s11244-008-9044-9.

Kaminsky, Walter; Miri, Massoud; Sinn, Hansjörg; Woldt, Rüdiger (1983): Bis(cyclopentadienyl)zirkon-Verbindungen und Aluminoxan als Ziegler-Katalysatoren für die Polymerisation und Copolymerisation von Olefinen. In *Makromol. Chem., Rapid Commun.* 4 (6), pp. 417–421. DOI: 10.1002/marc.1983.030040612.

Kaminsky, Walter; Sinn, Hansjörg (2013): Methylaluminoxane: Key Component for New Polymerization Catalysts. In Walter Kaminsky (Ed.): Polyolefins: 50 years after Ziegler and Natta II. Polyolefins by Metallocenes and Other Single-Site Catalysts. Berlin, Heidelberg: Springer-Verlag (Advances in Polymer Science, 258), pp. 1–28.

Kaminsky, Walter; Steiger, R. (1988): Polymerization of olefins with homogeneous zirconocene/alumoxane catalysts. In *Polyhedron* 7 (22-23), pp. 2375–2381. DOI: 10.1016/S0277-5387(00)86355-X.

Kaminsky, Walter; Zielonka, Holger (1993): Polymerization of Olefins in the Presence of Metal Powders with Homogeneous Catalysts. In *Polymer. Adv. Tech.* 4, pp. 415–422.

Karmarkar, A. (2011): Synthesis of Cellulose Filled-HDPE Composites using Polymerization Filling Technique. In : 11th International Conference on Wood and Biofiber Plastic Composites 2011. Madison, Wisconsin, USA, 16-17 May. Forest Products Society. Red Hook, NY: Curran Associates, Inc.

Käselau, Sven (2019): Development of Polyolefin Nanocomposites for Electrical Applications. Dissertation. Universität Hamburg, Hamburg. Technische und Makromolekulare Chemie.

Käselau, Sven; Scheel, Saskia; Petersson, Linnea; Ho, Chau-Hon; Luinstra, Gerrit A. (2018): Synthesis of a linear low-density polyethylene/MgO@$Mg(OH)_2$ nanocomposite using modified *in situ* polymerization. In *Polym. Int.* 67 (10), pp. 1359–1367. DOI: 10.1002/pi.5637.

Käselau, Sven; Scheel, Saskia; Petersson, Linnea; Ho, Chau-Hon; Luinstra, Gerrit A. (2019): Isotactic polypropylene metal oxide and silica nanocomposites by a two-step process comprising in situ olefin polymerization and melt compounding. In *Polym. Int.* 68 (5), pp. 946–954. DOI: 10.1002/pi.5785.

Keplinger, Tobias; Cabane, Etienne; Chanana, Munish; Hass, Philipp; Merk, Vivian Marina; Gierlinger, Notburga; Burgert, Ingo (2015): A versatile strategy for grafting polymers to wood cell walls. In *Acta Biomater.* 11, pp. 256–263. DOI: 10.1016/j.actbio.2014.09.016.

Kettunen, Marjo; Silvennoinen, Riitta J.; Houbenov, Nikolay; Nykänen, Antti; Ruokolainen, Janne; Sainio, Jani et al. (2011): Photoswitchable Superabsorbency Based on Nanocellulose Aerogels. In *Adv. Funct. Mater.* 21 (3), pp. 510–517. DOI: 10.1002/adfm.201001431.

Klyosov, Anatole A. (2007): Wood-Plastic Composites. 1st ed. Hoboken, New Jersey: Wiley-VCH.

Koch, Gerald (2006): I-2. Raw Material for Pulp. In Herbert Sixta (Ed.): Handbook of Pulp. 1st ed. Weinheim: Wiley-VCH, 21-68.

Kollmann, Franz (1951): Technologie des Holzes und der Holzwerkstoffe. 1. Teil. Anatomie und Pathologie, Chemie, Physik, Elastizität und Festigkeit. 2nd ed. Berlin Göttingen Heidelberg: Springer-Verlag (1).

Kollmann, Franz (1972): Persönliches. Prof. Dr. Alfred J. Stamm 75 Jahre. In *Eur. J. Wood Wood Prod.* 30 (12).

Kollmann, Franz; Höckele, Günther (1962): Kritischer Vergleich einiger Bestimmungsverfahren der Holzfeuchtigkeit. In *Eur. J. Wood Wood Prod.* 20 (12), pp. 461–473. DOI: 10.1007/BF02619168.

Koltzenburg, Sebastian; Maskos, Michael; Nuyken, Oskar (2014): Polymere: Synthese, Eigenschaften und Anwendungen. Berlin, Heidelberg: Springer-Verlag.

Köppl, Alexander; Alt, Helmut G.; Palackal, Syriac J.; Welch, M. Bruce (1997): Polymerization catalyst system their preparation, and use on 10/21/1997. App. no. 08/955,219. Patent no. 5,990,035.

Korhonen, Juuso T.; Kettunen, Marjo; Ras, Robin H. A.; Ikkala, Olli (2011): Hydrophobic Nanocellulose Aerogels as Floating, Sustainable, Reusable, and Recyclable Oil Absorbents. In *ACS Appl. Mater. Interfaces* 3 (6), pp. 1813–1816. DOI: 10.1021/am200475b.

Koshijima, T.; Watanabe, T.; Yaku, F. (1989): Structure and Properties of the Lignin-Carbohydrate Complex Polymer as an Amphipathic Substance. In Wolfgang G. Glasser (Ed.): Lignin. Properties and materials, vol. 397. 2.th ed. Washington, DC: American Chemical Society (ACS Symposium Series, 397), pp. 11–28.

Koumoutsakos, Anastasios; Avramidis, Stavros; Hatzikiriakos, Savvas G. (2001): Radio frequency vacuum drying of wood. I. Mathematical model. In *Dry. Technol.* 19 (1), pp. 65–84. DOI: 10.1081/DRT-100001352.

Krässig, Hans A (1993): Cellulose. Structure, Accessibility and Reactivity. With assistance of Malcom B Huglin. Yverdon, Switzerland: Gordon and Breach Science Publishers (Polymer Monographs, 11).

Kruse, Uno (1967): Process of Forming a Polyethylene Coating Using a Vanadium Compound as the Catalyst. Applied for by National Lead Company on 11/15/1967. App. no. 683,124. Patent no. 3,503,785.

Kurtz, Steven M. (2016): 2. From Ethylene Gas to UHMWPE Component: The Process of Producing Orthopedic Implants. In Steven M. Kurtz (Ed.): UHMWPE Biomaterials Handbook. Ultra-High Molecular Weight Polyethylene in Total Joint Replacement and Medical Devices. Third edition. Oxford: William Andrew is an imprint of Elsevier, pp. 7–20.

Laivins, G. V.; Scallan, A. M. (1996): The Influence of Drying and Beating on the Swelling of Fines. In *J. Pulp Pap. Sci.* 22 (5).

Lampke, Thomas (2001): Beitrag zur Charakterisierung naturfaserverstärkter Verbundwerkstoffe mit hochpolymerer Matrix. Dissertation. Technischen Universität Chemnitz, Chemnitz. Fakultät für Maschinenbau und Verfahrenstechnik.

Larkin, Peter J. (2011): IR and Raman Spectroscopy. Principles and Spectral Interpretation: Elsevier.

Lebow, Stan T. (2010): Chapter 15. Wood Preservation. In Robert J. Ross (Ed.): Wood Handbook. Wood as an Engineering Material. Madison, Wisconsin: U.S. Department of Agriculture, Forest Service, Forest Products Laboratory.

Lee, Dong-Ho; Yoon, Keun-Byoung (1995): Metallocene / MAO polymerization catalysts supported on cyclodextrin. In *Macromol. Symp.* 97 (1), pp. 185–193. DOI: 10.1002/masy.19950970119.

Li, Shenghai; Xie, Haibo; Zhang, Suobo; Wang, Xianhong (2007): Facile transformation of hydrophilic cellulose into superhydrophobic cellulose. In *ChemComm* (46), pp. 4857–4859. DOI: 10.1039/b712056g.

Li, Yongfeng; Wu, Qinglin; Li, Jian; Liu, Yixing; Wang, Xiang-Ming; Liu, Zhenbo (2012): Improvement of dimensional stability of wood via combination treatment: swelling with maleic anhydride and grafting with glycidyl methacrylate and methyl methacrylate. In *Holzforschung* 66 (1), pp. 59–66. DOI: 10.1515/HF.2011.123.

Li, Yuanyuan; Fu, Qiliang; Yang, Xuan; Berglund, Lars (2018): Transparent wood for functional and structural applications. In *Philos. Trans. R. Soc. A* 376 (2112). DOI: 10.1098/rsta.2017.0182.

Lin, Stephen Y.; Dence, Carlton W. (Eds.) (1992): Methods in Lignin Chemistry. Berlin, Heidelberg: Springer-Verlag (Springer Series in Wood Science).

Lindman, Björn; Karlström, Gunnar; Stigsson, Lars (2010): On the mechanism of dissolution of cellulose. In *J. Mol. Liq.* 156 (1), pp. 76–81. DOI: 10.1016/j.molliq.2010.04.016.

Liu, Honghai; Yang, Lin; Cai, Yingchun; Sugimori, Masatoshi; Hayashi, Kazuo (2010a): Effect of ambient pressure on equilibrium moisture content of wood. In *Wood Fiber Sci.* 42 (3), pp. 346–351.

Liu, Honghai; Yang, Lin; Cai, Yingchun; Sugimori, Masatoshi; Hayashi, Kazuo (2010b): Effect of EMC and air in wood on the new in-process moisture content monitoring concept under radiofrequency/vacuum (RF/V) drying. In *J. Wood Sci.* 56 (2), pp. 95–99. DOI: 10.1007/s10086-009-1079-4.

Liu, Honghai; Yang, Lin; Xu, Wei; Wu, Zhihui; Hayashi, Kazuo; Huang, Qiongtao (2015): Equilibrium moisture content under vacuum conditions. In *Wood Fiber Sci.* 47 (4), pp. 345–354.

Long, Wendell P. (1959): Complexes of Aluminum Chloride and Methylaluminum Dichloride with Bis-(cyclopentadienyl)-titanium Dichloride as Catalysts for the Polymerization of Ethylene. In *J. Am. Chem. Soc.* 81 (20), pp. 5312–5316. DOI: 10.1021/ja01529a017.

Long, Wendell P.; Breslow, David S. (1975): Der Einfluß von Wasser auf die katalytische Aktivität von Bis(π-cyclopentadienyl)titandichlorid-Dimethylaluminiumchlorid zur Polymerisation von Äthylen. In *Liebigs Ann. Chem.*, pp. 463–469. DOI: 10.1002/jlac.197519750310.

Lu, Xi; Hu, Yingcheng (2016): Layer-by-layer Deposition of TiO_2 Nanoparticles in the Wood Surface and its Superhydrophobic Performance. In *Bioresources* 11 (2).

Luo, Chao; Zhu, Hongli; Luo, Wei; Shen, Fei; Fan, Xiulin; Dai, Jiaqi et al. (2017): Atomic-Layer-Deposition Functionalized Carbonized Mesoporous Wood Fiber for High Sulfur Loading Lithium Sulfur Batteries. In *ACS Appl. Mater. Interfaces* 9 (17), pp. 14801–14807. DOI: 10.1021/acsami.7b01205.

Mädler, Hartmut (1981): Modifizierung von Cellulose und Stärke durch Aufpolymerisieren von Olefinen mit halogenfreien Ziegler-Katalysatoren. Diploma. Universität Hamburg, Hamburg. Institut für Anorganische und Angewandte Chemie.

Mädler, Hartmut (1987): Ziegler-Natta-Polymerisation unter Verwendung von Stärke und Stärkeabbauprodukten als Füllstoff- bzw. Cokatalysatorkomponente. Dissertation. Universität Hamburg, Hamburg. Technische und Makromolekulare Chemie.

Mantanis, George I.; Young, Raymond A.; Rowell, Roger M. (1994): Swelling of Wood. Part II. Swelling in Organic Liquids. In *Holzforschung* 48 (6), pp. 480–490. DOI: 10.1515/hfsg.1994.48.6.480.

Mantau, Udo; Döring, Przemko; Weimar, Holger; Glasenapp, Sebastian (2018): Rohstoffmonitoring Holz. Mengenmäßige Erfassung und Bilanzierung der Holzverwendung in Deutschland : Verbundvorhaben Rohstoffmonitoring Holz : gefördert durch: Bundesministerium für Ernährung und Landwirtschaft. Gülzow-Prüzen: Fachagentur Nachwachsende Rohstoffe e.V. (FNR) (Schriftenreihe nachwachsende Rohstoffe, 38). Available online at https://edocs.tib.eu/files/e01fn18/1029673020.pdf.

Marchessault, R. H.; Fisa, B.; Revol, J. F. (1989): Nascent Polyethylene—Cellulose Composite. In Wolfgang G. Glasser (Ed.): Lignin. Properties and materials, vol. 10. 2.th ed. Washington, DC: American Chemical Society (ACS Symposium Series, 397), pp. 147–159.

McDaniel, Max P. (2010): Chapter 3. A Review of the Phillips Supported Chromium Catalyst and Its Commercial Use for Ethylene Polymerization. In Bruce Gates, Bruce C. Gates, Friederike C. Jentoft, Helmut Knözinger (Eds.): Advances in Catalysis. Volume 53, vol. 53. 1st ed. Amsterdam: Elsevier (Advances in Catalysis), pp. 123–606.

Mecking, Stefan; Claverie, Jérôme P. (2006): Transition Metal-Catalyzed Polymerization in Aqueous Systems. In Bernhard Rieger, Lisa Saunders Baugh, Smita Kacker, Susanne Striegler (Eds.): Late Transition Metal Polymerization Catalysis. Weinheim: Wiley-VCH, pp. 231–278.

Mehl, Werner (1977): Polymerholz und seine wirtschaftliche Anwendung. In *Eur. J. Wood Wood Prod.* 35 (11), pp. 431–435. DOI: 10.1007/BF02607742.

Mende, Manfred (1981): Polymerisation von Ethylen auf Stärkekörnern mit Hilfe löslicher, halogenfreier Zieglerkatalysatoren. Diploma. Universität Hamburg, Hamburg. Institut für Anorganische und Angewandte Chemie.

Menges, Georg; Haberstroh, Edmund; Michaeli, Walter; Schmachtenberg, Ernst (2011): Menges Werkstoffkunde Kunststoffe. 6th ed. München: Carl Hanser Fachbuchverlag.

Merck, Alexander (1976): Untersuchungen eines halogenfreien homogenen Ziegler-Katalysators: Abhängigkeit der Aktivität von den Versuchsbedingungen. Diploma. Universität Hamburg, Hamburg. Institut für Anorganische und Angewandte Chemie.

Merck KGaA: Bis(butylcyclopentadienyl)zirconium(IV) dichloride 97% | Sigma-Aldrich. Darmstadt, Germany. Available online at https://www.sigmaaldrich.com/catalog/product/aldrich/447862?lang=de&region=DE, checked on 1/19/2020.

Merk, Vivian; Chanana, Munish; Gierlinger, Notburga; Hirt, Ann M.; Burgert, Ingo (2014): Hybrid wood materials with magnetic anisotropy dictated by the hierarchical cell structure. In *ACS Appl. Mater. Interfaces* 6 (12), pp. 9760–9767. DOI: 10.1021/am5021793.

Merk, Vivian; Chanana, Munish; Keplinger, Tobias; Gaan, Sabyasachi; Burgert, Ingo (2015): Hybrid wood materials with improved fire retardance by bio-inspired mineralisation on the nano- and submicron level. In *Green Chem.* 17 (3), pp. 1423–1428. DOI: 10.1039/C4GC01862A.

Mertens, Oliver; Gurr, Julius; Krause, Andreas (2017): The utilization of thermomechanical pulp fibers in WPC. A review. In *J. Appl. Polym. Sci.* 134 (31), p. 45161. DOI: 10.1002/app.45161.

Meyer, K.; Reichert, K. H. (1970): Zur Bildung und Konzentration der aktiven Spezies löslicher Ziegler-Natta-Katalysatoren. In *Angew. Makromol. Chem.* 12 (157), pp. 175–183. DOI: 10.1002/apmc.1970.050120114.

Michell, Anthony J.; Vaughan, Janet E.; Willis, Donald (1976): Wood fiber-synthetic polymer composites. I. Laminates of paper and polyethylene. In *J. Polym. Sci. C Polym. Symp.* 55 (1), pp. 143–154. DOI: 10.1002/polc.5070550116.

Michler, Goerg H. (2008): Electron Microscopy of Polymers. With assistance of R. Godehardt, R. Adhikari, G.-M. Kim, S. Henning, V. Seydewitz, W. Lebek. Berlin Heidelberg: Springer-Verlag (Springer Laboratory Manuals in Polymer Science).

Militz, Holger (2020): Wood modification research in Europe. In *Holzforschung* 74 (4). Available online at https://doi.org/10.1515/hf-2020-0050.

Minh Hoang, Peter Phung; Jeremic, Dusan; Kearns, Jason Roy; McLaren Coulter, Iain; Donaldson, Robert D. (1999): "Sweet" MAO. Applied for by Nova Chemicals (International) S. A. on 12/22/1999. App. no. 09/470,569. Patent no. 6,340,771 B1.

Minh Hoang, Peter Phung; Jeremic, Dusan; Kearns, Jason Roy; McLaren Coulter, Iain; Donaldson, Robert D. (2001): Sweet MAO. Applied for by Nova Chemicals (International) S.A. on 12/4/2001. App. no. 10/004,744. Patent no. 6,750,170 B2.

Minor, James L. (1994): Hornification - Its Origin and Meaning. In *Progress in Paper Recycling* 3 (2), pp. 93–95.

Mottweiler, Renke (1975): Untersuchung der Reaktionen von Bis(cyclopentadienyl)Titan(IV)-Verbindungen mit Aluminiumalkylen, auch in Gegenwart von Äthylen. Dissertation. Universität Hamburg, Hamburg.

Müller, Fabian (2003): Polymerisationen von Ethen, Propen und 1,3-Butadien mit Metallocen/MAO-Trägerkatalysatoren. Dissertation. Universität Hamburg, Hamburg. Technische und Makromolekulare Chemie.

Navarro, Julien R. G.; Edlund, Ulrica (2017): Surface-Initiated Controlled Radical Polymerization Approach To Enhance Nanocomposite Integration of Cellulose Nanofibrils. In *Biomacromolecules* 18 (6), pp. 1947–1955. DOI: 10.1021/acs.biomac.7b00398.

Neumann, R.; Mielke, A.; Glos, P. (1993): Zur Feuchtebewegung im Holz während der konvektiven Vakuumtrocknung. In *Eur. J. Wood Wood Prod.* 51 (3), pp. 156–162. DOI: 10.1007/BF02628272.

Nopens, Martin (2019): Wood-Water-Interactions. Dissertation. Universität Hamburg, Hamburg. Institute of Wood Science.

Nopens, Martin; Riegler, Martin; Hansmann, Christian; Krause, Andreas (2019): Simultaneous change of wood mass and dimension caused by moisture dynamics. In *Sci. Rep.* 9 (1), p. 10309. DOI: 10.1038/s41598-019-46381-8.

Nopens, Martin; Sazama, Uta; König, Sandra; Kaschuro, Sergej; Krause, Andreas; Fröba, Michael (2020): Determination of mesopores in the wood cell wall at dry and wet state. In *Sci. Rep.* 10 (1), p. 9543. DOI: 10.1038/s41598-020-65066-1.

Nordin, Sören B.; Nyrén, Jan O.; Back, Ernst L. (1974): An Indication of Molten Cellulose Produced in a Laser Beam. In *Text. Res. J.* 44 (2), pp. 152–154. DOI: 10.1177/004051757404400211.

Norimoto, Misato; Gril, Joseph (1993): Structure and Properties of Chemically Treated Woods. In Nobuo Shiraishi, Hiromu Kajita, Misato Norimoto (Eds.): Recent Research on Wood and Wood-Based Materials. London, New York: Elsevier (Current Japanese Materials Research, 11), pp. 135–145.

Nuñez, Adrián J.; Kenny, José M.; Reboredo, María M.; Aranguren, Mirta I.; Marcovich, Norma E. (2002): Thermal and Dynamic Mechanical Characterization of Polypropylene-Woodflour Composites. In *Polym. Eng. Sci.* 42 (4), pp. 733–742.

Ohlberg, S. M.; Roth, J.; Raff, R. A. V. (1959): Relationship between impact strength and spherulite growth in linear polyethylene. In *J. Appl. Polym. Sci.* 1 (1), pp. 114–120. DOI: 10.1002/app.1959.070010118.

Oksman Niska, Kristiina; Sain, Mohini (Eds.) (2008): Wood–Polymer Composites. Cambridge: Woodhead Publishing Limited.

Orsino, Joseph A.; Herman, Daniel F.; Brancato, Jack J. (1959): Process of coating cellulosic particles by polymerizing a 1-olefin onto said particles; Profess of removing the cellulosic particles from the coated particles and hollow shells obtained therefrom on 11/13/1959. App. no. 852,844. Patent no. 3,121,698.

Park, Sungjin; Choi, Insung S. (2009): Production of Ultrahigh-Molecular-Weight Polyethylene/Pristine MWCNT Composites by Half-Titanocene Catalysts. In *Adv. Mater.* 21 (8), pp. 902–905. DOI: 10.1002/adma.200801674.

Patat, F.; Sinn, Hansjörg (1958): Zum Ablauf der Niederdruckpolymerisation der α-Olefine. Komplexpolymerisation I. In *Angew. Chem.* 70 (16), pp. 496–500. DOI: 10.1002/ange.19580701603.

Pechmann, Hans von (1898): Ueber Diazomethan und Nitrosoacylamine. In *Ber. Dtsch. Chem. Ges.* 31 (3), pp. 2640–2646. DOI: 10.1002/cber.18980310314.

Pettijohn, Ted M. (1989): Use of starch in the preparation of polymers. Applied for by Phillips Petroleum Company on 11/30/1989. App. no. 443,545.

PlasticsEurope AISBL (2019): Plastics – the Facts 2019. An analysis of European plastics production, demand and waste data. Brussels, Belgium. Available online at https://www.plasticseurope.org/download_file/force/3183/181, checked on 3/3/2020.

Poltimäe, Triinu; Tarasova, Elvira; Krumme, Andres; Roots, Jaan; Viikna, Anti (2011): Thermal Analyses of Blends of Hyperbranched Linear Low-density Polyethylene (LLDPE) with High-density Polyethylene and LLDPE Prepared by Dissolving Method. In *Material Science (Medžiagotyra)* 17 (3). DOI: 10.5755/j01.ms.17.3.589.

Prahl, Helmut F.; Hart, Frederick M. (1970): Polyolefin-Starch. Applied for by Dynatron Research Corporation on 10/29/1970. App. no. 85,041. Patent no. 3,704,271.

Deutsches Institut für Normung DIN 52184:1979-05: Prüfung von Holz - Bestimmung der Quellung und Schwindung.

Deutsches Institut für Normung DIN 52182:1976-09: Prüfung von Holz - Bestimmung der Rohdichte.

Radovanovic, Itana (2007): Verarbeitung und Optimierung der Rezeptur von Wood Plastic Composites (WPC). Dissertation. Universität Osnabrück, Osnabrück.

Ralph, John; Lapierre, Catherine; Boerjan, Wout (2019): Lignin structure and its engineering. In *Curr. Opin. Biotechnol.* 56, pp. 240–249. DOI: 10.1016/j.copbio.2019.02.019.

Reichert, K. H.; Meyer, K. R. (1973): Zur Kinetik der Niederdruckpolymerisation von Äthylen mit löslichen Ziegler-Katalysatoren. In *Macromol. Chem. Phys.* 169 (1), pp. 163–176. DOI: 10.1002/macp.1973.021690116.

Reinprecht, Ladislav; Pánek, Miloš; Daňková, Jana; Murínová, Tereza; Mec, Pavel; Plevová, Lenka (2013): Performance of methyltripotassiumsilanol treated wood against swelling in water, decay fungi and moulds. In *Wood Res.* 58 (4), pp. 511–520.

Ren, YongLin; O'Brien, G.; Desmarchelier, J. M. (1997): Improved Methodology for Studying Diffusion, Sorption and Desorption in Timber Fumigation. In *J. Stored Prod. Res.* 33 (3).

Richardson, Barry A. (2001): Wood preservation. 2nd ed. London: E & FN Spon.

Rijckaert, V.; Stevens, M.; van Acker, J.; Meijer, M. de; Militz, Holger (2001): Quantitative assessment of the penetration of water-borne and solvent-borne wood coatings in Scots pine sapwood. In *Eur. J. Wood Wood Prod.* 59 (4), pp. 278–287. DOI: 10.1007/s001070100208.

Rosehr, Andre; Luinstra, Gerrit A. (2017): Polypropylene composites with finely dispersed multi-walled carbon nanotubes covered with an aluminum oxide shell. In *Polymer* 120, pp. 164–175. DOI: 10.1016/j.polymer.2017.05.045.

Rosehr, André (2012): Synthese und Untersuchung von Polypropylen/MWCNT Nanocomposites. Diploma. Universität Hamburg, Hamburg. Technical and Macromolecular Chemistry.

Rosehr, André (2019): Synthese und Charakterisierung von Polypropylen Kohlenstoff-Nanocomposites. Dissertation. Universität Hamburg, Hamburg.

Ross, Robert J. (Ed.) (2010): Wood Handbook. Wood as an Engineering Material. USDA Forest Service. Madison, Wisconsin: U.S. Department of Agriculture, Forest Service, Forest Products Laboratory.

Rowell, Roger M. (1984): The Chemistry of Solid Wood. Washington D.C.: American Chemical Society (Advances in Chemistry Series, 207).

Rowell, Roger M. (2005): 14. Chemical Modification of Wood. In Roger M. Rowell (Ed.): Handbook of Wood Chemistry and Wood Composites. Boca Raton, Florida, USA: Taylor & Francis Group (CRC Press), 381-420.

Rowell, Roger M. (2016): Definition of wood. Conversation to Julius Gurr. Östad, Sweeden, 5/10/2016.

Rowell, Roger M.; LeVan-Green, Susan L. (2005): 6. Thermal Properties. In Roger M. Rowell (Ed.): Handbook of Wood Chemistry and Wood Composites. Boca Raton, Florida, USA: Taylor & Francis Group (CRC Press).

Rowell, Roger M.; Pettersen, Roger; Han, James S.; Rowell, Jeffrey S.; Tshabalala, Mandla A. (2005): 3. Cell Wall Chemistry. In Roger M. Rowell (Ed.): Handbook of Wood Chemistry and Wood Composites. Boca Raton, Florida, USA: Taylor & Francis Group (CRC Press).

Sakharovskaya, G. B.; Korneev, N. N.; Popov, A. F.; Larikov, E. I.; Zhigach, A. F. (1964): Reaction of Aluminium Trialkyls with Water. In *Zhurnal Obshchei Khimii* 34 (10), pp. 3478–3480.

Sandberg, Dick; Kutnar, Andreja; Mantanis, George (2017): Wood modification technologies - a review. In *Iforest* 10 (6), pp. 895–908. DOI: 10.3832/ifor2380-010.

Sandquist, David (2013): New horizons for microfibrillated cellulose. In *Appita J.* 66 (2), pp. 156–162.

Santos, João Henrique Zimnoch dos; Larentis, Ariane; da Rosa, Marcelo Barbosa; Krug, Cristiano; Baumvol, Israel Jacob Rabin; Dupont, Jaïrton et al. (1999): Optimization of a silica supported bis(butylcyclopentadienyl)-zirconium dichloride catalyst for ethylene polymerization. In *Macromol. Chem. Phys.* 200 (4), pp. 751–757. DOI: 10.1002/(SICI)1521-3935(19990401)200:4<751::AID-MACP751>3.3.CO;2-U.

Sato, Harumi; Shimoyama, Masahiko; Kamiya, Taeko; Amari, Toru; Sasic, Slobodan; Ninomiya, Toshio et al. (2002): Raman Spectra of High-Density, Low-Density, and Linear Low-Density Polyethylene Pellets and Prediction of Their Physical Properties by Multivariate Data Analysis. In *J. Appl. Polym. Sci.* 86 (2), pp. 443–448. DOI: 10.1002/app.10999.

Scheel, Saskia (2014): Synthese und Charakterisierung von Polyolefin-Nanocomposites via *in situ* Polymerisation. Dissertation. Universität Hamburg, Hamburg. Institute of Technical and Macromolecular Chemistry.

Scheffrahn, Rudolf H.; Su, Nan-Yao; Hsu, Ruei-Ching (1992): Diffusion of methyl bromide and sulfuryl fluoride through selected structural Wood matrices during fumigation. In *Material und Organismen* 27 (2), pp. 147–155.

Schimpf, Ulrike (2014): Enzymatischer Abbau des Lignocellulosekomplexes in Energiepflanzen unter besonderer Berücksichtigung der Silierung und der Biogasproduktion. Dissertation. Humboldt-Universität zu Berlin, Berlin. Mathematisch-Naturwissenschaftliche Fakultät I.

Schmidt, Olaf (2006): Wood and Tree Fungi. Biology, Damage, Protection, and Use. Berlin, Heidelberg: Springer-Verlag Berlin Heidelberg.

Schoeneberger, Elsa (2016): Kinetische Untersuchungen zur Ethenpolymerisation mit einem Eisen-Bis(imino)pyridin-Katalysator. Kinetic study of ethylene polymerization by a bis(imino)pyridyl-iron (II)-catalyst. Master Thesis. Universität Hamburg, Hamburg. Institute of Technical and Macromolecular Chemistry.

Scholz, G.; Krause, A.; Militz, H. (2010a): Exploratory study on the impregnation of Scots pine sapwood (*Pinus sylvestris L.*) and European beech (*Fagus sylvatica L.*) with different hot melting waxes. In *Wood Sci. Technol.* 44 (3), pp. 379–388. DOI: 10.1007/s00226-010-0353-3.

Scholz, G.; Krause, Andreas; Militz, Holger (2010b): Beeinflussung der Holzfestigkeit durch Wachstränkung. In *holztechnologie* 51 (3).

Scholz, G.; Krause, Andreas; Militz, Holger (2012): Volltränkung modifizierten Holzes mit Wachs. In *Eur. J. Wood Wood Prod.* 70 (1-3), pp. 91–98. DOI: 10.1007/s00107-010-0485-z.

Scholz, Gunthard; van den Bulcke, Jan; Boone, Matthieu; Zauer, Mario; Bäucker, Ernst; van Acker, Joris; Militz, Holger (2010c): Investigation on wax-impregnated wood. Part 1: Microscopic observations and 2D X-ray imaging of distinct wax types. In *Holzforschung* 64 (5). DOI: 10.1515/hf.2010.091.

Scholz, Gunthard; Zauer, Mario; van den Bulcke, Jan; van Loo, Denis; Pfriem, Alexander; van Acker, Joris; Militz, Holger (2010d): Investigation on wax-impregnated wood. Part 2: Study of void spaces filled with air by He pycnometry, Hg intrusion porosimetry, and 3D X-ray imaging. In *Holzforschung* 64 (5). DOI: 10.1515/hf.2010.090.

Schroeter, Johannes; Felix, Florian (2005): Melting cellulose. In *Cellulose* 12 (2), pp. 159–165. DOI: 10.1007/s10570-004-0344-3.

Schulz, H. (1993): Entwicklung der Holzverwendung im 19., 20. und 21. Jahrhundert. In *Eur. J. Wood Wood Prod.* 51 (2), pp. 75–82. DOI: 10.1007/BF03325368.

Sell, Jürgen (1977): Hydrophobierende Holzimprägnierung – Wirkungsweise, Eigenschaften, Anwendungsmöglichkeiten. In *Eur. J. Wood Wood Prod.* 35, pp. 75–78.

Sernek, Milan (2002): Comparative Analysis of Inactivated Wood Surfaces. Dissertation. Virginia Polytechnic Institute and State University, Blacksburg, Virginia, USA. Wood Science and Forest Products.

Severn, John R.; Chadwick, John C.; Duchateau, Robbert; Friederichs, Nic (2005): "Bound but Not Gagged"–Immobilizing Single-Site α-Olefin Polymerization Catalysts. In *Chem. Rev.* 105 (11), pp. 4073–4147. DOI: 10.1021/cr040670d.

Siau, John F. (1984): Transport Processes in Wood. Berlin Heidelberg: Springer-Verlag (Springer Series in Wood Science).

Siau, John F. (1995): Wood: Influences of Moisture on Physical Properties. Blacksburg, Virginia, USA: Department of Wood Science and Forest Products,

Sinn, Hansjörg (1963): Die Wirkungsweise metallorganischer Polyreaktions-Katalysatoren. Habilitation. Technische Universität München, München.

Sinn, Hansjörg (1995): Proposals for structure and effect of methylalumoxane based on mass balances and phase separation experiments. In *Macromol. Symp.* 97 (1), pp. 27–52. DOI: 10.1002/masy.19950970105.

Sinn, Hansjörg; Kaminsky, Walter; Vollmer, Hans-Jürgen; Woldt, Rüdiger (1980a): „Lebende Polymere" bei Ziegler-Katalysatoren extremer Produktivität. In *Angew. Chem.* 92 (5), pp. 396–402. DOI: 10.1002/ange.19800920517.

Sinn, Hansjörg; Kaminsky, Walter; Vollmer, Hans-Jürgen; Woldt, Rüdiger (1980b): Verfahren zur Herstellung von Polyethylen, Polypropylen und Copolymeren. Applied for by Sinn, Hansjörg, Prog. Dr., 2000 Hamburg on 2/29/1980. Patent no. DE 3007725 A1.

Sishta, Chand; Hathorn, Robin M.; Marks, Tobin J. (1992): Group 4 metallocene–alumoxane olefin polymerization catalysts. CPMAS–NMR spectroscopic observation of cation-like zirconocene alkyls. In *J. Am. Chem. Soc.* 114 (3), pp. 1112–1114. DOI: 10.1021/ja00029a063.

Sixta, Herbert (Ed.) (2006): Handbook of Pulp. 1st ed. Weinheim: Wiley-VCH.

Skaar, Christen (1988): Wood-Water Relations. Berlin Heidelberg: Springer-Verlag (Springer Series in Wood Science).

Sonnewald, Uwe (2014): 19 Stoffwechselphysiologie. In Joachim W. Kadereit, Christian Körner, Benedikt Kost, Uwe Sonnewald (Eds.): Strasburger. Lehrbuch der Pflanzenwissenschaften. 37th ed. Berlin Heidelberg: Springer, 339-446.

Spiegelberg, Stephen; Kozak, Adam; Braithwaite, Gavin (2016): 29. Characterization of Physical, Chemical, and Mechanical Properties of UHMWPE. In Steven M. Kurtz (Ed.): UHMWPE Biomaterials Handbook. Ultra-High Molecular Weight Polyethylene in Total Joint Replacement and Medical Devices. Third edition. Oxford: William Andrew is an imprint of Elsevier, pp. 531–552.

Spiehl, Regina (1984): Polymerisation von Ethen in Gegenwart von Holz als Füllstoff mit einem löslichen Ziegler-Katalysator bestehend aus Biscyclopentadienylzirkondichlorid und Methylaluminoxan. Diploma. Universität Hamburg, Hamburg. Institut für Anorganische und Angewandte Chemie.

Spottog, Carmen (pending): Advanced Wood Plastic Composite Materials by *in situ* Polymerization. Dissertation. Universität Hamburg, Hamburg. Institute of Technical and Macromolecular Chemistry.

Spurr, Arthur R. (1969): A Low-Viscosity Epoxy Resin Embedding Medium for Electron Microscopy. In *J. Ultrastruct. Res.* 26 (1-2), pp. 31–43. DOI: 10.1016/S0022-5320(69)90033-1.

Stamm, Alfred J. (1967a): Movement of Fluids in Wood - Part I: Flow of Fluids in Wood. In *Wood Sci. Technol.* 1, pp. 122–141.

Stamm, Alfred J. (1967b): Movement of Fluids in Wood - Part II: Diffusion. In *Wood Sci. Technol.* 1, pp. 205–230.

Stark, Nicole M.; Cai, Zhiyong; Carll, Charles (2010): Chapter 11. Wood-Based Composite Materials. Panel Products, Glued-Laminated Timber, Structural Composite Lumber, and Wood–Nonwood Composite Materials. In Robert J. Ross (Ed.): Wood Handbook. Wood as an Engineering Material. Madison, Wisconsin: U.S. Department of Agriculture, Forest Service, Forest Products Laboratory.

Starzewski, Aleksander Ostoja (2006): Nickel Polymerization Catalysts with Ylide Steering Ligands. In Bernhard Rieger, Lisa Saunders Baugh, Smita Kacker, Susanne Striegler (Eds.): Late Transition Metal Polymerization Catalysis. Weinheim: Wiley-VCH, pp. 1–26.

Starzewski, Aleksander Ostoja; Josef, Witte (1982): Nickel-Ylid-Komplexe, deren Herstellung und Verwendung als Katalysatoren bei der Polymerisation von Olefinen. Applied for by Bayer AG, 5090 Leverkusen on 8/3/1982. Patent no. DE 32 28 865 A1.

Staudinger, Herman; Fritschi, J. (1922): Über Isopren und Kautschuk. 5. Mitteilung. Über die Hydrierung des Kautschuks und über seine Konstitution. In *Helv. Chim. Acta* 5 (5), pp. 785–806. DOI: 10.1002/hlca.19220050517.

Stürzel, Markus; Kurek, Alexander; Anselm, Melanie; Halbach, Tobias; Mülhaupt, Rolf (2013): Polyolefin Nanocomposites and Hybrid Catalysts. In Walter Kaminsky (Ed.): Polyolefins: 50 years after Ziegler and Natta II. Polyolefins by Metallocenes and Other Single-Site Catalysts. Berlin, Heidelberg: Springer-Verlag (Advances in Polymer Science, 258), pp. 279–309.

Tajima, Keisuke; Ogawa, Gen; Aida, Takuzo (2000): Novel Molecularly Hybridized Polyethylene/Silica Composite Materials: Polymerization of Ethylene with Supported Titanocenes by Mesoporous Silicates. In *J. Polym. Sci. A Polym. Chem.* 38, pp. 4821–4825.

Thielen, Michael (2018): Biokunststoffe. Pflanzen Rohstoffe Produkte. 5th ed. Gülzow-Prüzen: Fachagentur Nachwachsende Rohstoffe e. V. (FNR). Available online at https://www.fnr.de/fileadmin/allgemein/pdf/broschueren/WEB_Biokunststoffe_2018_2.pdf, checked on 10/30/2020.

Thybring, Emil Engelund; Kymäläinen, Maija; Rautkari, Lauri (2018): Experimental techniques for characterising water in wood covering the range from dry to fully water-saturated. In *Wood Sci. Technol.* 52 (2), pp. 297–329. DOI: 10.1007/s00226-017-0977-7.

Thybring, Emil Engelund; Thygesen, Lisbeth Garbrecht; Burgert, Ingo (2017): Hydroxyl accessibility in wood cell walls as affected by drying and re-wetting procedures. In *Cellulose* 24 (6), pp. 2375–2384. DOI: 10.1007/s10570-017-1278-x.

Tiemann, Harry Donald (1906): Effect of moisture upon the strength and stiffness of wood. Washington, D.C.: U.S. Department of Agriculture (Bulletin, 70).

Trache, Djalal; Hussin, M. Hazwan; Hui Chuin, Caryn Tan; Sabar, Sumiyyah; Fazita, M. R. Nurul; Taiwo, Owolabi F. A. et al. (2016): Microcrystalline cellulose: Isolation, characterization and bio-composites application–A review. In *Int. J. Biol. Macromol.* 93 (Pt A), pp. 789–804. DOI: 10.1016/j.ijbiomac.2016.09.056.

Trübswetter, Thomas (2006): Holztrocknung. Verfahren zur Trocknung von Schnittholz - Planung von Trockenanlagen. Leipzig: Fachbuchverlag Leipzig.

Unger, Achim; Schniewind, Arno P.; Unger, Wibke (2001): Conservation of Wood Artifacts. A Handbook. Berlin, Heidelberg: Springer (Natural Science in Archaeology).

Uraki, Yasumitsu; Usukura, Yuriko; Kishimoto, Takao; Ubukata, Makoto (2006): Amphiphilicity of a lignin-carbohydrate complex. In *Holzforschung* 60 (6), pp. 659–664. DOI: 10.1515/HF.2006.111.

van Grieken, R.; Carrero, A.; Suarez, I.; Paredes, B. (2007): Ethylene polymerization over supported MAO/(*n*BuCp)$_2$ZrCl$_2$ catalysts: Influence of support properties. In *Eur. Polym. J.* 43, pp. 1267–1277.

van Opdenbosch, Daniel; Dörrstein, Jörg; Klaithong, Somruedee; Kornprobst, Tobias; Plank, Johann; Hietala, Sami; Zollfrank, Cordt (2013): Chemistry and water-repelling properties of phenyl-incorporating wood composites. In *Holzforschung* 67 (8), pp. 931–940. DOI: 10.1515/hf-2013-0011.

Vasile, Cornelia; Pascu, Mihaela (2005): Practical Guide to Polyethylene. Shawbury, Shrewsbury, Shropshire, UK.

Verein Deutscher Ingenieure e.V. VDI 4630, 04/2006: Vergärung organischer Stoffe - Substratcharakterisierung, Probenahme, Stoffdatenerhebung, Gärversuche.

Vogt, Dominik; Karus, Michael; Ortmann, Sven; Schmidt, Christin; Gahle, Christian (2006): Wood-Plastic-Composites (WPC). Märkte in Nordamerika, Japan und Europa mit Schwerpunkt auf Deutschland. nova-Institut für politische und ökologische Innovation GmbH.

Wagenführ, Rudi (2006): Holzatlas. 6th ed. Leipzig: Fachbuchverlag Leipzig.

Walker, John C. F. (2006): Primary Wood Processing. Principles and Practice. 2nd ed. Dordrecht The Netherlands: Springer.

Watt, I. C.; Kabir, M. (1975): Sorption of Water Vapor in Jute Fibers. In *Text. Res. J.* 45 (1), pp. 42–48. DOI: 10.1177/004051757504500108.

Watt, I. C.; Kennett, R. H. (1960): Variations in the Equilibrium Weight of Wool at Zero Humidity. In *Text. Res. J.* 30 (7), pp. 489–494. DOI: 10.1177/004051756003000703.

Wegner, Marcus Martin (2009): Gasphasenpolymerisation von Ethylen mit neuen, heterogenisierten α-Diimin-Ni(II)-Komplexen. Dissertation. Technische Universität München, München. Makromolekulare Chemie.

Williams, R. S. (2005): 7. Weathering of Wood. In Roger M. Rowell (Ed.): Handbook of Wood Chemistry and Wood Composites. Boca Raton, Florida, USA: Taylor & Francis Group (CRC Press).

Woelk, H. U. (1981): Stärke als Chemierohstoff — Möglichkeiten und Grenzen. In *Starch* 33 (12), pp. 397–408. DOI: 10.1002/star.19810331202.

Wolfmeier, Uwe; Schmidt, Hans; Heinrichs, Franz Leo; Michalczyk, Georg; Payer, Wolfgang; Dietsche, Wolfram et al. (2011): Waxes. In Barbara Elvers (Ed.): Ullmann's Encyclopedia of Industrial Chemistry, vol. 39. With assistance of Giuseppe Bellussi, Uwe Karst, Kai Sundmacher, Matthias Bohnet, Axel Kleemann, Roland Ulber et al. 7th ed. 40 volumes. Weinheim: Wiley-VCH Verlag GmbH, pp. 111–172.

Worden, Chauncey Edward (1911): Nitrocellulose industry. 2 volumes. London, United Kingdom: Constable and Company LTD (2).

WRAP (2003): Wood Plastic Composites Study - Technologies and UK Market Opportunities. The Waste and Resources Action Programme. Banbury, UK.

Xie, L. X.; Li, K. Y. R.; Tjong, C. S.; Mai, Y.-W. (2002): Structural Properties and Mechanical Behavior of Injection Molded Composites of Polypropylene and Sisal Fiber. In *Polym. Compos.* 23 (3), pp. 319–328.

Yang, Rui; Liang, Yunyi; Hong, Shu; Zuo, Shida; Wu, Yingji; Shi, Jiangtao et al. (2020): Novel Low-Temperature Chemical Vapor Deposition of Hydrothermal Delignified Wood for Hydrophobic Property. In *Polymers* 12 (8). DOI: 10.3390/polym12081757.

Yanulis, M. J. (1965): Polyethylene Encapsuled Fibers: Converting and Properties. In *TAPPI J.* 48 (9).

Yi, Song-lin; Zhou, Yong-dong; Liu, Yu-rong; Zhang, Bi-guang; Feng, Xiao-jiang (2008): Experimental equilibrium moisture content of wood under vacuum. In *Wood Fiber Sci.* 40 (3).

YongFeng, Li; XiaoYing, Dong; ZeGuang, Lu; WanDa, Jia; YiXing, Liu (2013): Effect of Polymer *In Situ* Synthesized from Methyl Methacrylate and Styrene on the Morphology, Thermal Behavior, and Durability of Wood. In *J. Appl. Polym. Sci.* 128 (1), pp. 13–20. DOI: 10.1002/app.38099.

Younkin; Connor; Henderson; Friedrich; Grubbs; Bansleben (2000): Neutral, Single-Component Nickel (II) Polyolefin Catalysts That Tolerate Heteroatoms. In *Science* 287 (5452), pp. 460–462. DOI: 10.1126/science.287.5452.460.

Zelinka, Samuel L.; Glass, Samuel V.; Thybring, Emil Engelund (2020): Evaluation of previous measurements of water vapor sorption in wood at multiple temperatures. In *Wood Sci. Technol.* 54 (4), pp. 769–786. DOI: 10.1007/s00226-020-01195-0.

Zhu, Mingwei; Song, Jianwei; Li, Tian; Gong, Amy; Wang, Yanbin; Dai, Jiaqi et al. (2016): Highly Anisotropic, Highly Transparent Wood Composites. In *Adv. Mater.* 28 (26), pp. 5181–5187. DOI: 10.1002/adma.201600427.

Zijlstra, Harmen S.; Harder, Sjoerd (2015): Methylalumoxane - History, Production, Properties, and Applications. In *Eur. J. Inorg. Chem.*, pp. 19–43. DOI: 10.1002/ejic.201402978.

Zimmermann, Lisa; Dierkes, Georg; Ternes, Thomas A.; Völker, Carolin; Wagner, Martin (2019): Benchmarking the in Vitro Toxicity and Chemical Composition of Plastic Consumer Products. In *Environ. Sci. Technol.* 53 (19), pp. 11467–11477. DOI: 10.1021/acs.est.9b02293.

Zimmermann, Lisa; Dombrowski, Andrea; Völker, Carolin; Wagner, Martin (2020): Are bioplastics and plant-based materials safer than conventional plastics? *In vitro* toxicity and chemical composition. In *Environ. Int.*, p. 106066. DOI: 10.1016/j.envint.2020.106066.

Eidesstattliche Erklärung

Hiermit erkläre ich an Eides statt, dass ich die vorliegende Dissertationsschrift selbst verfasst und keine anderen als die angegebenen Quellen und Hilfsmittel benutzt habe.

Hamburg, 20.12.2020